VERSATILE ROUTES TO PHOTO-RESPONSIVE POLYESTERS FOR DUAL AND TRIPLE SHAPE MEMORY BIOMATERIALS

Jason Michael Rochette

A dissertation submitted to the faculty of the University of North Carolina at Chapel Hill in partial fulfillment of the requirements for the degree of Doctor of Philosophy in the Department of Chemistry.

Chapel Hill
2012

Approved by
Dr. Valerie Sheares Ashby
Dr. Wei You
Dr. James Cahoon
Dr. Joseph Templeton
Dr. Mark Schoenfisch

ABSTRACT

JASON M. ROCHETTE: VERSATILE ROUTES TO PHOTO-RESPONSIVE POLYESTERS FOR DUAL AND TRIPLE SHAPE MEMORY BIOMATERIALS
(Under the direction of Dr. Valerie S. Ashby)

Shape memory polymers are promising materials for smart biomedical devices and applications, however, thermal systems are limited by a narrow applicable temperature range. Light-induced shape memory (LSM) circumvents this limitation by using a mechanism independent of heat that can be remotely triggered. This work presents the synthesis and characterization of multiple photo-responsive polyester platforms which contain regularly repeating pendant cinnamic acid derivatives. Elastomeric thermoset poly(ester urethane)s (P-PEUs) synthesized by step-growth polymerization of novel bifunctional monomers possessed a range of thermal and mechanical properties that likened them to a variety of soft tissues found in the body, as well as boasted negligible cytotoxicity and physiological degradation. All P-PEUs displayed LSM, with those in the DCA series also exhibiting thermal shape memory which afforded two independent triggers which when combined allowed for the programming and recovery of a novel multifunctional triple shape material, capable of switching on macroscopic and microscopic scales. Photo-responsive poly(β-amino ester)s (PBAEs) were synthesized by functional monomer or post-polymerization route to give soft elastomeric materials containing photo-groups as well as additional reactive functionality to be used for further modification of chemical and physical properties. All materials were characterized by ^{1}H-NMR, GPC, TGA, DSC, DMA, and Instron.

This work is dedicated to my family, Susan Rochette, Neil Rochette, Dr. Jennifer Rochette, and David Rochette for their love, support, and motivation, as well as my colleagues and friends, Dr. Hayden Black, Dr. Duy Le, Sarah Brosnan, Annie Jackson, Dr. Peter Uthe, Dr. Benjamin Pierce, Dr. Tim Merkel, Dr. Bryan Frauhiger, and Stuart Dunn for their advice, intellectual discussions, and friendships. I would like to thank my advisor, Dr. Valerie S. Ashby for her direction, encouragement, and trust. I would also like to thank my friends, Landon Simmons, Mike Vysocka, Mike Hargrove, Matt Rivenbark, Antoine Moore, and Michael Downer for their lasting friendships, support, and diversions from work needed periodically. Most importantly I would like to thank and dedicate this work to Amber Baxley for standing by me throughout my graduate career amidst the long nights and weekends in lab, the grumpy moods when experiments weren't working, acting as my one-woman audience as I prepared for presentations and interviews, and for her endless love and encouragement.

TABLE OF CONTENTS

LIST OF TABLES

Table

LIST OF FIGURES

Figure

LIST OF ABBREVIATIONS

AA	Adipic Acid
AIBN	2,2'-Azobis(2-methylpropionitrile)
BC	Butyl cinnamate
BD	1,4-Butanediol diacrylate
BDO	1,4-Butanediol
BO	Butanolamine
CA	Cinnamate
CAD	N,N-bis(2-hydroxyethyl)cinnamamide
CHDCA	1,4-Cyclohexane dicarboxylic acid
CHDM	1,4-Cylcohexanedimethanol
CNT	Carbon nanotube
DA	Diacrylate
DBU	1,8-Diazabicylo[5.4.0]undec-7-ene
DCA	Diethyl 2,2'-(cinnamoylazanediyl) diacetate
DCE	Diethyl 3-(cinnamoyloxy)pentanedioate
DCM	Dichloromethane
DI	Deionized
DMA	Dynamic mechanical analysis
DMF	Dimethylformamide
DP	Degree of polymerization
DSC	Differential scanning calorimetry

EC	Ethyl cinnamate
EO	Ethanolamine
Et_2O	Diethyl ether
Et_3N	Triethylamine
EtOAc	Ethyl acetate
Fmoc	9-Fluorenylmethoxycarbonyl
GPC	Gel permeation chromatography
HD	1,6-hexanediol diacrylate
IR	Infrared
LC	Liquid crystalline
LCE	Liquid crystalline elastomer
LSM	Light-induced shape memory
MA	Methyl acrylate
MDI	4,4'-diphenylmethane diisocyanate
MeOH	Methanol
ML	Mass loss
MMA	Methyl methacrylate
MSA	Mercaptosuccinic acid
MW	Molecular weight
MWNT	Multi-walled carbon nanotube
NiPAAm	Poly(N-isopropylacrylamide)
NMR	Nuclear magnetic resonance
OD	1,8-octanediol

PBAE	Poly(β–amino ester)
PBS	Phosphate buffered saline
PCHMA	Poly(cyclohexyl methacrylate)
PCL	Polycaprolactone
PDI	Polydispersity index
PE	Polyethylene
PEG	Poly(ethylene glycol)
PEO	Poly(ethylene oxide)
PET	Polyethylene terephthalate
PEU	Poly(ester urethane)
PFPE	Perfluoropolyether
PGA	Polyglycolide
PLA	Poly(lactic acid)
PLLA	Poly(*L*-lactide)
PMMA	Poly(methyl methacrylate)
P-PEU	Photo-responsive poly(ester urethane)s
PRINT	Particle replication in non-wetting templates
PS	Polystyrene
PU	Polyurethane
PVA	Polyvinyl alcohol
PVAc	Poly(vinyl acetate)
PVC	Polyvinyl chloride
PVDF	Poly(vinylidene fluoride)

$Sc(OTf)_3$	Scandium trifluoromethanesulfonate
SCF	Short carbon fiber
SCP	Shape changing polymer
SMA	Shape memory alloy
SME	Shape memory effect
SMP	Shape memory polymer
SnOct	Tin (II) ethylhexanoate
SSM	Surface shape memory
TGA	Thermogravimetric analysis
THF	Tetrahydrofuran
TPE	Thiol pendant copolyesters
TSM	Triple shape memory
TSP	Triple shape polymer
UV	Ultraviolet
WU	Water uptake

LIST OF SYMBOLS

R_f	Strain fixity
R_r	Strain recovery
ε_u	Temporary relaxed strain
ε_m	Maximum deformation strain
ε_p	Residual strain after recovery
ε_{max}	Maximum deformation
T_{trans}	Transition temperature
T_m	Melting temperature
T_g	Glass transition temperature
T_h	Higher temperature
T_l	Lower temperature
M_n	Number average molecular weight
M_w	Weight average molecular weight
G	Young's modulus
δ	NMR shift
λ	Wavelength
Δ	Heat

Chapter I

LITERATURE REVIEW OF SHAPE MEMORY MATERIALS

1.1 The Shape Memory Effect

Shape memory behavior is defined as the capability to change shapes upon application of an external stimulus.[1] As such shape memory materials are smart materials with a wide range of applications including biomedical devices[2,3,4,5], sensors[6,7,8], aerospace equipment[9,10,11], and textiles[12,13]. The material in its permanent form is packaged or programmed into a predetermined temporary shape by a stress or force and fixed in this state. Recovery occurs in response to the external stimulus or switch that actuates return of the material to the original shape (Figure 1.1). In order for a polymeric material to possess the shape memory effect (SME), the system is required to contain netpoints and molecular switches (switching segments or groups).[14] Netpoints, whether physical or chemical

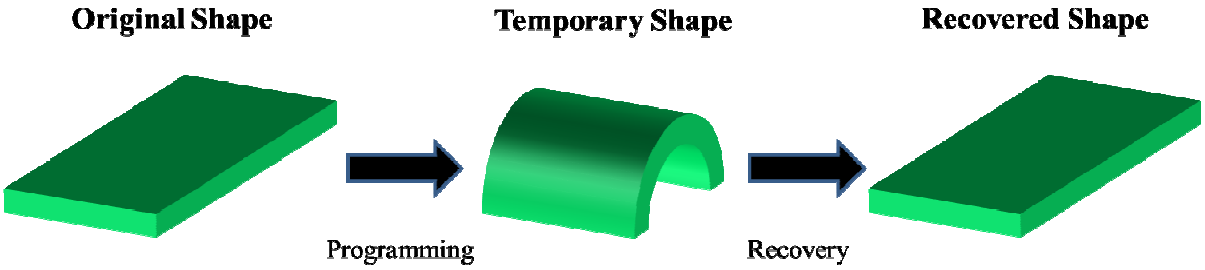

Figure 1.1 Programming and recovery of a general shape memory polymer.

crosslinks, determine the permanent shape and allow for the memory of the original form. Between these netpoints are chain segments which act as molecular switches in response to specific stimuli that reversibly fix the temporary shape. Reversible fixing is possible through vitrification, crystallization, or formation of temporary covalent bonds.

The polymer segments must also have the ability to assume a variety of conformations to allow deformation of the system in the programming process. In the fixed temporary shape the access to different conformations in the switching segments is limited creating a highly unfavorable entropic state. When the stimulus is applied, the fixation of the chain segments is reversed and reconfiguration to the maximum state of entropy drives the recovery of the original shape.[15] The SME is quantified by the strain fixity ratio (R_f) and strain recovery ratio (R_r) (Figure 1.2), which evaluates the fixation of the temporary shape and the recovery of the original shape, respectively. R_f measures the ratio of strain in the relaxed temporary state (after unloading) (ε_u) to the maximum deformation (before unloading) (ε_m) of the applied stress in programming. R_r measures the ratio of strain released during the recovery process (ε_u-ε_p) compared to the strain held in the packaged state (ε_u).[16]

Shape memory polymers (SMPs) should not be confused with another class of stimuli-responsive materials known as shape changing polymers (SCPs). SCPs differ from SMPs in two ways; first the temporary shape change in SCPs is a response to a stimulus

$$R_f(N) = \frac{\varepsilon_u(N)}{\varepsilon_m(N)} \times 100 \qquad R_r(N) = \frac{\varepsilon_u(N) - \varepsilon_p(N)}{\varepsilon_u(N) - \varepsilon_p(N-1)} \times 100$$

Figure 1.2. Strain fixty ratio (R_f) and strain recovery ratio (R_r).

whereas the temporary shape in SMPs must be programmed by an external force or stress. Secondly, in SCPs exposure to the stimulus is required to keep the temporary shape change; once the stimulus is removed, the system returns to the original form.[14] In SMPs the programmed temporary shape is persistent until reapplication of the stimulus triggers the controlled recovery of the original shape.

1.2 Shape Memory Materials

The shape memory effect was first observed in metal alloys in the early 1950s with the study of plastic deformation and diffusionless phase changes in gold-cadmium alloys in response to a thermal stimulus.[17] Other alloys such as Ni-Ti, Cu-Zn-Al, and Fe-Mn-Si have found technical application as shape memory materials for biomedical devices, electrical devices, and construction materials, respectively. While some possess the SME, shape memory alloys (SMAs) lack an elastic nature which limits the deformations (ε_{max} = 8%) and shapes available for a given application.

The extension of the SME into polymeric materials such as thermoplastic or thermoset elastomers has not only expanded the accessible shapes/deformations, but has also led to the development of diverse chemical and physical material property combinations, various external triggers, and expansive applications.[18] The first example of a polymer system possessing the SME was crosslinked polyethylene (PE) via ionizing radiation, which came to be known as "heat-shrinkable tubing" in the 1960s.[19,20] Since that time different polymers, copolymers, architectures, and composites have been utilized.

1.2.1 Thermoplastic Shape Memory Polymers

One of the most studied families of shape memory polymers is thermoplastic elastomers, specifically polyurethane (PU) based elastomers.[21-25] Thermoplastic SMPs are

designated by the nature of the netpoints within the system which are physical crosslinks. PU SMPs are a two phase system consisting of hard and soft segments. In order to possess the SME, the hard segments must aggregate to form physical crosslinks which hold the permanent shape, while the soft segments act as switching segments. Hard segments are usually created from diisocyanates and chain extenders or from a macro-diol with a higher thermal transition.[26] Soft segments can be low molecular weight diols, hydroxyl terminated oligomeric esters, or hydroxyl terminated oligomeric ethers. An example of such a combination is a polyesterurethane (PEU) where oligourethane units act as the hard segment and polyesters as the soft segment. Kim and coworkers synthesized a series of polycaprolactone (PCL) based PEUs with 4,4'-diphenylmethane diisocyanate (MDI) and 1,4-butanediol (BDO) to study the influence of the length and content of the PCL macrodiol on

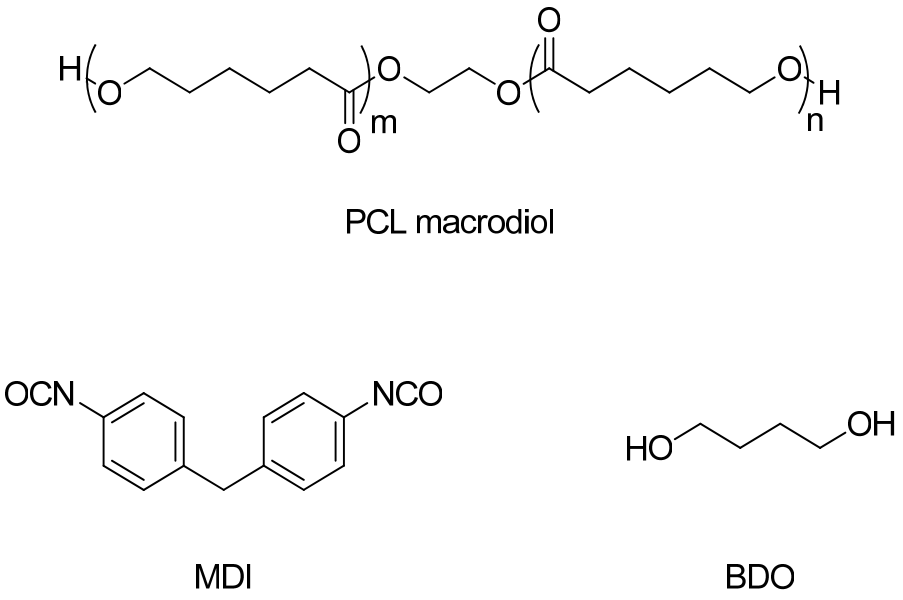

Figure 1.3 Components for segmented PCL based PEU SMP.

shape memory properties (Figure 1.3).[27] They showed there was a lower limit of PCL molecular weight (MW) for crystallization to occur when in the segmented PU, which in turn allowed for the SME of the system.

Other linear block copolymers have also been studied as thermoplastic elastomers such as styrene-*trans*-butadiene-styrene triblocks[28], poly(norbornene)-*b*-poly(norbornenyl-polyhedral oligosilsesquioxane)[29], and polyethylene terephthalate-*b*-polyethylene oxide (PET-PEO)[30]. Miscible polymer blends such as poly(lactic acid)/poly(vinyl acetate) (PLA/PVAc) and poly(methyl methacrylate)/poly(vinylidene fluoride) (PMMA/PVDF) also possess the SME due to one polymer imparting a hard phase and the other a soft phase.[31] Ultra high MW polymers can also function as physically crosslinked materials when the entanglements act to hold the permanent shape.[32] Although block copolymers, blends, and high MW polymers demonstrate the shape memory effect, the thermoplastic elastomer PU SMPs have the highest shape recoverability, a wider range of transition temperatures, better processing ability, and better biocompatibility depending on composition.[33,34] One limitation of thermoplastic SMPs is their susceptibility to irreversible deformation and creep during the programming process.

1.2.2 Thermoset Shape Memory Polymers

Thermoset elastomers have an advantage over thermoplastic elastomers because the chemical netpoints prevent creep or chain slippage during the programming process. This leads to better fidelity in several shape memory cycles, as well as the chemical crosslinked materials tend to have improved thermal, mechanical, chemical, and shape memory

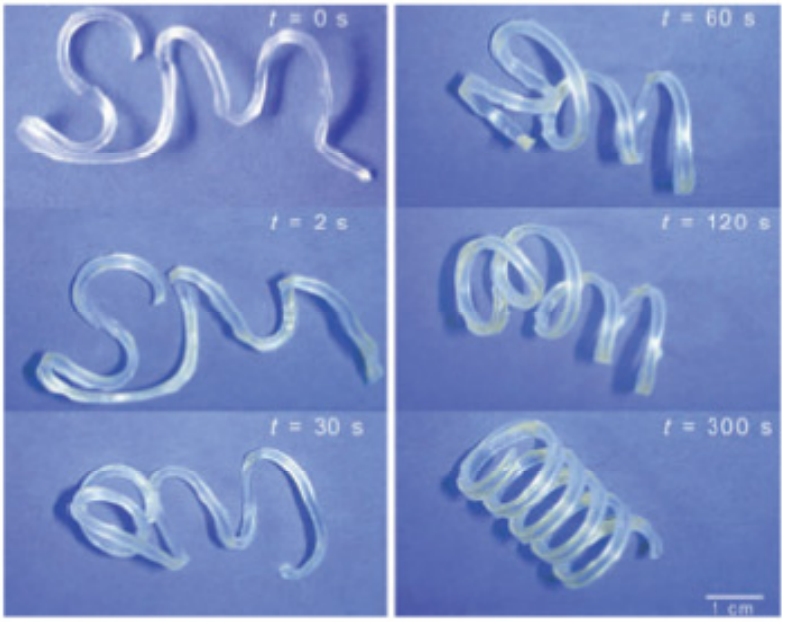

Figure 1.4 Amorphous thermoset copolyester urethane SMP.

properties.[35] The covalent network of thermoset elastomers can be achieved by crosslinking of linear or branched prepolymers, or polymerization in the presence of at least one trifunctional or greater monomer.[36-38] As mentioned earlier, the first example of this type of system was crosslinked PE, but other homopolymers, copolymers, and blends also show the SME when crosslinked such as PE/poly(vinyl alcohol) (PVA)[36], poly(vinyl chloride) (PVC)[38], PCL[39], PS[40], and PEO-PET[41]. Thermoplastic PU and PEU SMPs (Figure 1.4) have also been improved by introducing covalent crosslinks via incorporation of a trifunctional diol as a chain extender or by end-functionalizing a precursor with crosslinkable end groups.[42,43,44] Using the same components as the previously mentioned PU SMP (Figure 1.3) plus the addition of glycerin, Zouohong *et al.* saw an increase in storage modulus and in tensile strength, as well as in R_f and R_r after the fifth shape memory cycle (Table 1.1).[45]

Table 1.1 Effect of crosslinking on mechanical and shape memory properties of crosslinked PUs.[45,42]

Hard Phase	Soft phase	Crosslinker	E' GPa	σ MPa	T_m* °C	R_f (5) %	R_r (5) %
MDI,1,4-BD, DMPA	PCL M_n ~4000	None	0.2	18	50.3	80	75
MDI,1,4-BD, DMPA	PCL M_n ~4000	Glycerin 6 wt%	0.5	40	46.9	90	88

*melting transition of soft phase

1.2.3 Composites and Liquid Crystalline Shape Memory Polymers

Besides thermoplastic and thermoset polymers/copolymers, there has also been the development of liquid crystalline SMPs and composite SMPs to diversify the possible applications. Incorporation of fillers into SMPs is utilized to reinforce material strength, improve mechanical properties, create conductive composites, and diversify triggering methods.[35,46,47] Fillers in these composites include fibers[48-50], glass[51], carbon black[52], silicon carbide[53,5], carbon nanotubes (CNTs)[54-63], or metallic particles[64-68]. Distinct fabrication methods can also be employed to produce SMP composites made from only polymer material. Mather *et al.* used electrospinning to create a nonwoven fiber mat of PCL within a silicon rubber matrix[16] (Figure 1.5).

Liquid crystalline elastomers (LCEs) have been investigated as shape memory materials due to their fast actuation speed and mechanical properties.[69,70] LCEs also show the potential for reversible two-way shape memory which could be used for reversible actuators such as artificial muscles.[71,72] The mechanism of this reversible effect is due to the change in direction of the polymer chains as they transition between crystalline phases.[73]

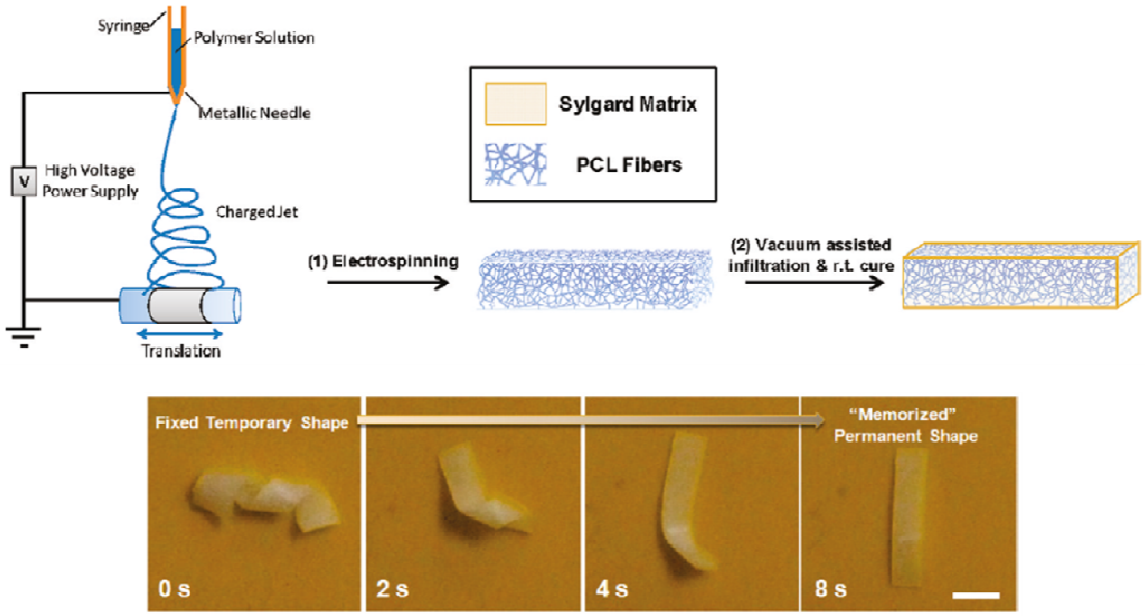

Figure 1.5 SMP composite made by electrospun PCL fibers in Sylgard 184 matrix (top). Recovery of programmed temporary shape over 8 seconds at 80 ^{o}C (photos, bottom).[16]

1.2.4 Shape Memory Biomaterials

SMPs span a wide range of potential applications, however biomedical applications has been an area of considerable research interest.[74-76] This began with the development of a PCL-based biodegradable thermoplastic SMP that could be targeted for specific switching temperatures by controlling the PCL molecular weight and hard/soft phase compositions.[77] SMA had found application for self-deploying stents, but the introduction of synthetic SMPs that could be comprised of PCL, polyglycolide (PGA), poly(L-lactide) (PLLA) or different combinations allowed for degradable devices that required no removal.[78,79] The addition of polyethylene glycol (PEG) to the composition improved properties such as increased hydrophilicity, permeability, and degradability.[80,81] Crystalline and amorphous materials have been used for biodegradable SMPs, depending on the target application. For example, thermoplastic and thermoset SMPs using a T_m switch are semi-crystalline and therefore are normally more opaque. Fully amorphous SMPs, on the other hand, are transparent and can

meet the requirements for ocular tissue transplants.[82,83] Degradation rates can also be tailored depending on the monomers incorporated. PCL materials alone have a low biodegradation rate, but as mentioned previously incorporation of PEG can increase the rate. PLA based materials also show faster degradation, however, the thermal transition cannot be targeted to temperatures close to body temperature (37 ^{o}C), which is necessary for SMP activation in biomedical devices.[84]

1.3 External Stimuli

To this point nearly all examples of SMPs discussed possess thermal shape memory that is triggered by heating, however there are a variety of other triggers or external stimuli that can be used to switch a packaged shape to the original shape including magnetic, electric, solvent, and light stimuli.

1.3.1 Thermal Triggering

The most common and extensively studied SMP mechanism is based on thermal transitions where a material is heated above a transition temperature (T_{trans}) actuating a shape change from temporary to permanent. The specific mechanism for thermal shape memory is dependent on the type of material (thermoplastic or thermoset) and the thermal transition (melting transition, T_m, or glass transition, T_g).

Thermoplastic SMPs as mentioned earlier are held by physical crosslinks or netpoints due to hard segments or segments with high thermal transitions. The switching segments are soft phases, meaning they possess lower thermal transitions, in between the hard segments that can be deformed when above the T_{trans}. T_{trans} can be either the T_m or T_g of the soft segment and must be distinct from the higher thermal transition (T_h, usually a T_m) of the hard segment otherwise the permanent network is lost when heated above T_h. In the case of a T_m

based thermoplastic SMP, the system is heated above T_{trans} (< T_h) and deformed by an external force. In this deformed state, the soft segment polymer chains have been reassembled into an entropically less favorable conformation and upon cooling below T_{trans} the soft segments recrystallize, confining the polymer chains in this entropically strained position and fixing the temporary shape. When heated above T_{trans} again, the newly arranged crystallites of the soft phases melt and the physical netpoints of the hard segment recover to the original position.

For thermoplastic SMP systems based on T_g switches, the above mechanism is followed, instead of the soft segments crystallizing to hold the entropic strain, they vitrify which can lead to a small decrease in strain fixity. The recovery rate can also be slower for T_g based materials due to the broad thermal transition compared to the sharp melting transition of a semicrystalline soft segment.

Thermoset SMPs on the other hand do not require multiple phases in order to possess a thermal SME, however multiphase compositions like thermoset PEUs are still applicable. In either case chemical crosslinks hold the permanent network so T_{trans} can be the highest thermal transition in the system without losing the original shape. Systems based on a T_m or T_g behave in the same manner as thermoplastic SMPs with either reversible crystallization or vitrification to fix the temporary shape after physical deformation while heated above T_{trans} followed by cooling.

1.3.2 Indirect Thermal Actuation

While direct heating is the most common trigger for thermal SMPs and SMPs in general, there have also been various methods of indirect thermal actuation to trigger recovery or utilize other stimuli, in some cases allowing for remote activation.[14] Magnetic

fields[85,86], electrical current[87,88], infrared (IR) irradiation[3,89], and water/solvent interactions[90-93] are able to trigger a thermal mechanism in specifically designed SMP materials and composites. As mentioned earlier, composites can contain an assortment of fillers, and it is this availability of various fillers in SMP composites that accounts for the variety of stimuli which can be utilized.

Electro-responsive SMP composites can be filled with conductive materials such as carbon nanotubes[94-96], carbon particles (carbon black)[97,52], Ni powder[98], and short carbon fibers (SCF)[99-100]. When a voltage is applied the conducting materials will produce resistive heating and the surrounding SMP material will be thermally actuated.[35] Goo *et al*. reinforced a shape memory PU system with multi-walled carbon nanotubes (MWNTs) and showed electro-active shape recovery with 10.4 % energy conversion efficiency, as well as recovery rates as fast as 10 seconds for macroscopic shape changes when a constant voltage was applied (Figure 1.6).[101] Magnetic-responsive composites demonstrate similar recovery when placed within an alternating magnetic field, triggering inductive heating.[102] The composite fillers in these cases are magnetic iron oxide particles (Fe_2O_3 or Fe_3O_4)

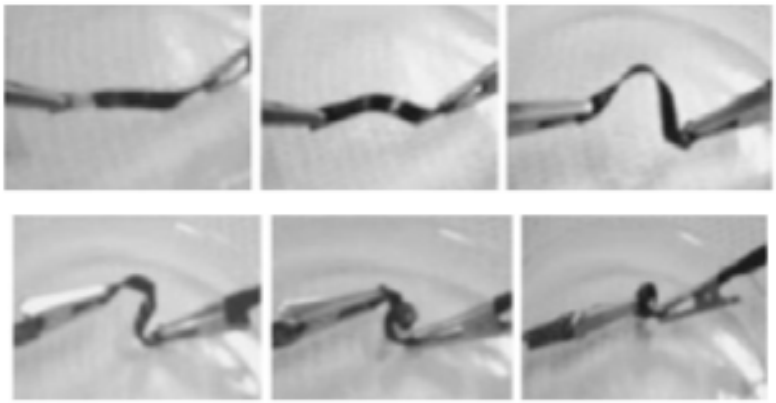

Figure 1.6 Electro-active shape memory polymer recovering from temporary unwound form to curled shape when voltage applied.[35]

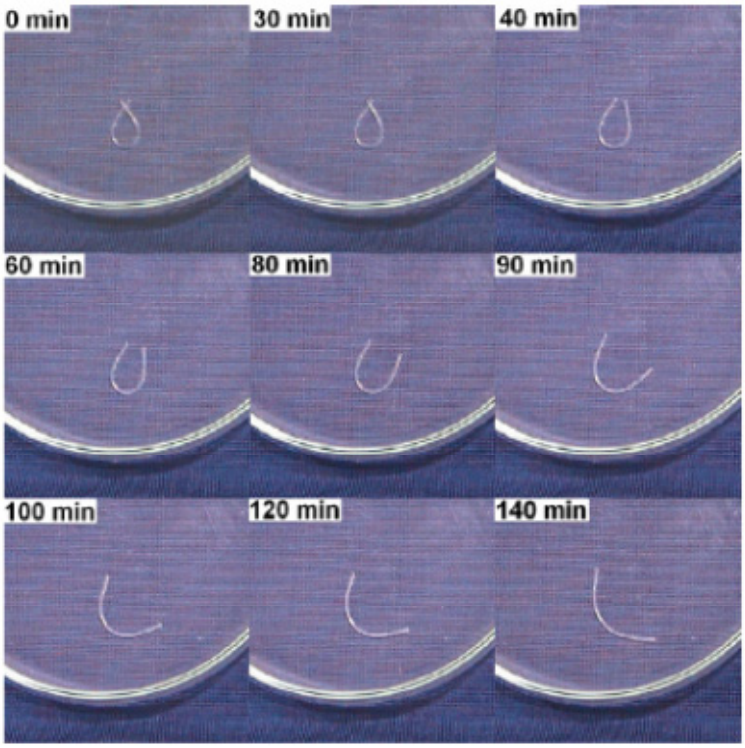

Figure 1.7 Shape memory PU immersed in water to trigger recovery by plasticization effect of water molecules.[91]

homogenously distributed throughout the polymer matrix.[85,103] Shape memory composites impregnated with tuned gold nanoparticles can also be actuated via IR laser irradiation at specific wavelengths.[104]

Other methods of indirect thermal actuation can be achieved in non-composite materials, however in some cases the addition of fillers will enhance the response rate. IR irradiation can be used as a source of radiant thermal energy when a SMP is illuminated with an IR laser or optical fiber[105], and the addition of carbon black to SMPs increases the absorption of this energy and increases the heat transfer throughout the system.[106] Solution interactions can also induce a thermal trigger by creating a plasticizing effect within a shape memory network.[107,108] Molecules of solvent, water, or mixtures penetrate the material network and increase the flexibility of the polymer chains, which in turn decreases the T_{trans}.

When the effect is pronounced enough to lower T_{trans} below the ambient temperature as in the case of PU in water[91] (Fiugre 1.7) or styrene –based SMPs in DMF[109] or toluene, recovery begins to occur albeit at a slow rate depending on the rate of solution penetration in the material.

Recently, polymer networks containing metal-ligand coordination complexes have been studied as responsive metallo-supramolecular materials, which can be triggered with heat, light, or chemical triggers.[110] The materials are based on a crosslinked poly(butadiene) network endcapped with ligands, which when in the presence of metal salts will form supramolecular reversible crosslinks. Heating of the metal-ligand coordination bonds decomplexes the metal center and cleaves the reversible crosslinks. The combination of triggers that can activate this system are related to different methods mentioned previously: normal heating, UV light absorption leading to localized heating, and chemical/solvent interactions interfering with the thermal stability of the material via plasticization or decomplexation.

1.4 Light-Responsive Polymers

Triggering methods free of a heat are limited to photo-responsive systems that undergo a photochemical reaction. Unlike previously mentioned methods where light (UV, IR) are utilized for localized heating through energy absorption, the intrinsically light-induced shape memory effect is independent of any thermal mechanism. Light can be applied as a precise stimulus through selection of wavelengths, intensity, and polarization angle for the remote activation of a variety of changes to the chemical and physical properties of a polymer material.[111]

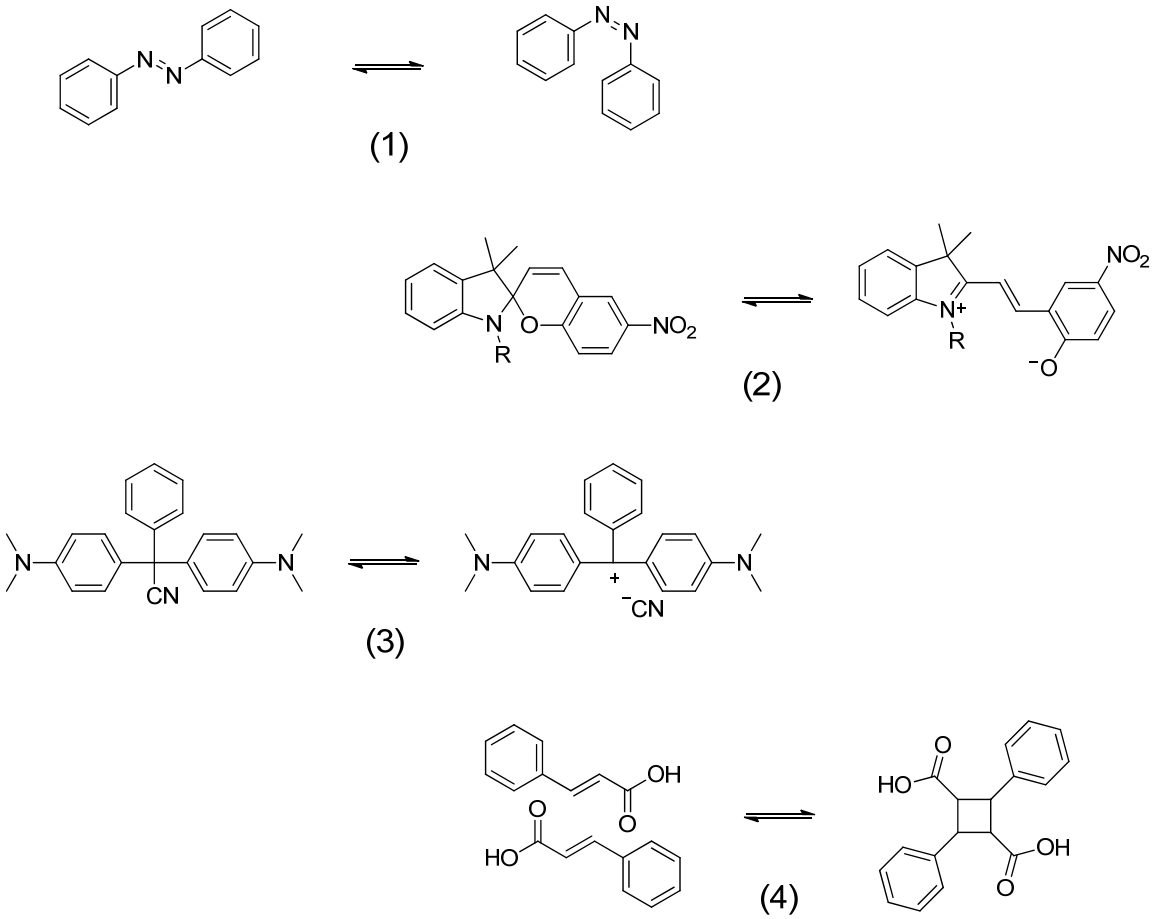

Scheme 1.1 Photochromic molecules: azobenzene (1) spirobenzopyran (2) triphenylmethane leuconitrile (3) cinnamic acid (4).

1.4.1 Photochromic Molecules and Photo-isomerization

Various light-responsive polymer systems have been developed and studied as materials that can reversibly change conformation, shape, surface wettability, permeability, solubility, sol-gel transition temperature, and color when irradiated.[112] The chemical basis of these materials are photochromic groups that undergo isomerizations when irradiated with light which are then reversible either thermally or photochemically[113] including *trans-cis* isomerization[114,115], ion formation[116], radical formation, ionic dissociation[117], and ring formation/cleavage. Photochromic groups (Scheme 1.1) attributed to these

photoisomerizations include azobenzene(1)[118-120], stilbene[121], triphenylmethane leucoderivatives(2)[116], spirobenzopyrans (3)[122], hydroxytriphenylmethanol[117], coumarin, and cinnamic acid (4).

1.4.2 Light-Induced Shape Changing

Extension of the molecular changes induced by photoisomerization to a macroscopic level leads to light-induced shape changes in polymers and gels such as bending[123-125], contraction[126,127], and volume change[128-131] in isolated materials under no force of

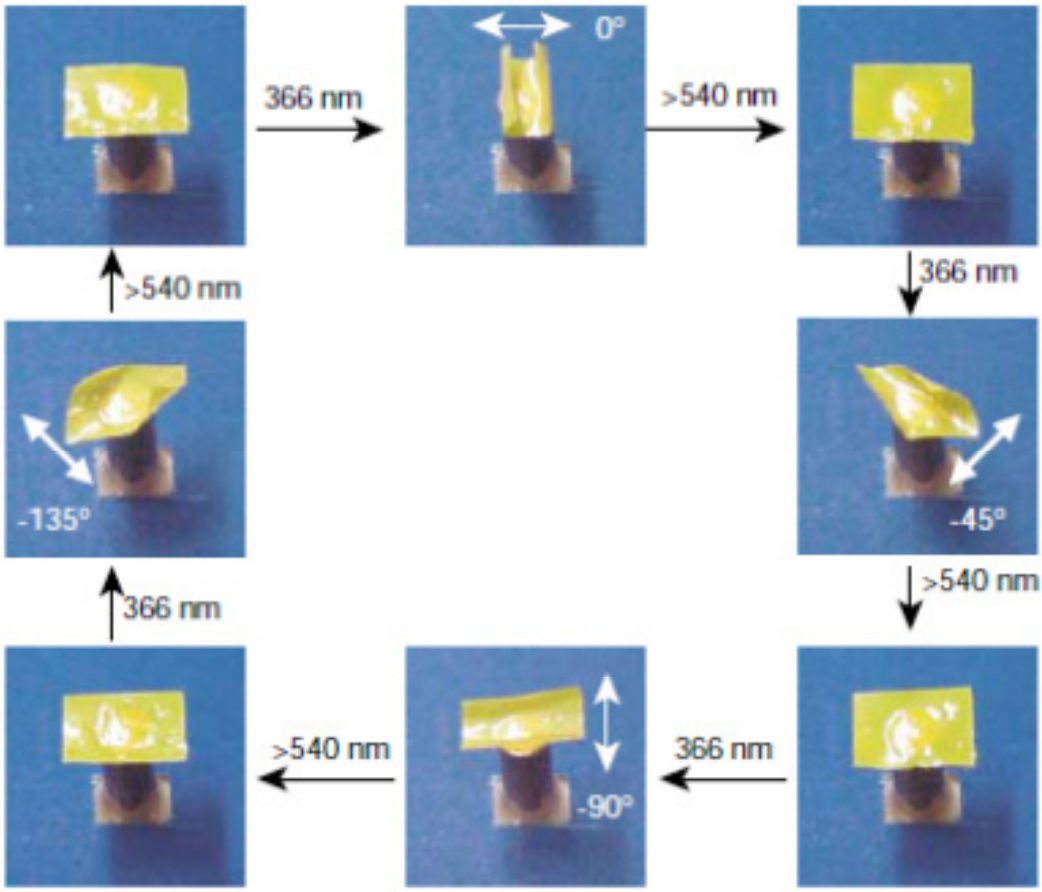

Figure 1.8 Directed bending by linear polarized light irradiation of azobenzene LCEs at different angles.

deformation when under light irradiation. When the light source is removed, the shape change generally reverses.[123-127,132-134] Polymer gels with triphenylmethane leucoderivatives incorporated swelled in the presence of UV light due to the formation of cyanide ions creating an osmotic pressure change, and when the light was removed, the gel shrank.[129] The dissociation into ions also creates an electrostatic repulsion effect. Photo-responsive elastomers containing azobenzene in the polymer backbone or side chains can reversibly contract and expanded based on the light-induced *cis-trans* isomerization under two different UV wavelengths.[112,135,136] The development of azobenzene LCEs has led to larger macroscopic changes such as bending due to the ordered nature of the materials[125,133,137,138], which also allows for direction-controlled bending[123] using linear polarized light at different angles (Figure 1.8).

1.4.3 Light-Induced Shape Memory

The controlled bending of azobenzene LCEs in one of the few examples of somewhat of a predetermined shape change for light-induced shape changing polymers, however as mentioned previously, the removal of the light source recovers the original form. In order to allow programming of a predetermined temporary shape and triggered recovery, a mechanism to fix the material based on a photoisomerization is necessary. Recently, White *et al*. demonstrated a light-induced shape memory effect in azobenzene LCEs by programming with circular polarized light.[139] The angle of polarized light allows for controlled bending angle of the polymer film, but when the light source is removed the bend is held until recovered either thermally or photochemically. The fixation of the photo-induced bend does make this system an example of a light-induced SMP, however a

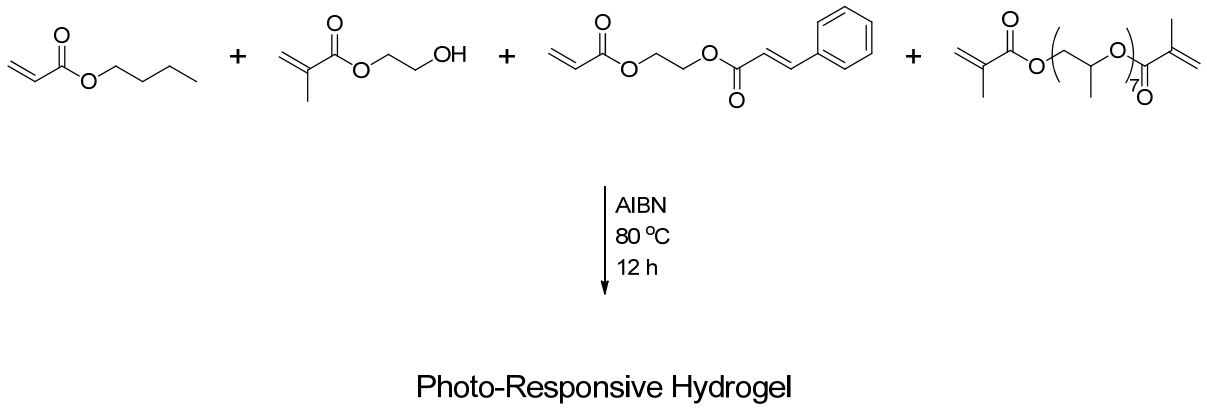

Scheme 1.2 Light-induced SMP synthesized by Lendlein *et al*.

limitation on the temporary programming available remains because temporary shapes are restricted to bending at angles between -25° – 25°. The first light-induced SMPs were developed by Lendlein *et al.*, which could be physically deformed and fixed into a variety of shapes (comparative to thermal SMPs), based on photoreactive cinnamate groups which undergo reversible photo-induced [2+2] cycloaddition.[140] The material was a thermoset hydrogel synthesized by the radical-initiated polymerization of various acrylate and methacrylate monomers, one of which was functionalized with a cinnamate moiety and one of which was bifunctional to act as a crosslinking agent (Scheme 1.2). The mechanism that produces the SME (Figure 1.9) is the reversible dimerization of cinnamate groups when irradiated with UV light (λ > 260 nm) while the material is under a physical stress to form temporary crosslinks within the already chemically crosslinked network. The increased crosslink density holds the material in a deformed shape until irradiation with UV light (λ < 260 nm) cleaves the cyclobutane ring formed between two cinnamate groups and recovers the original shape. Unlike thermal SMPs, the strain fixity of light-induced SMPs relies on the ability of the temporary crosslinks to hold the polymer chains in the deformed state. Once the stress is removed in the programming process, chain segments in between temporary

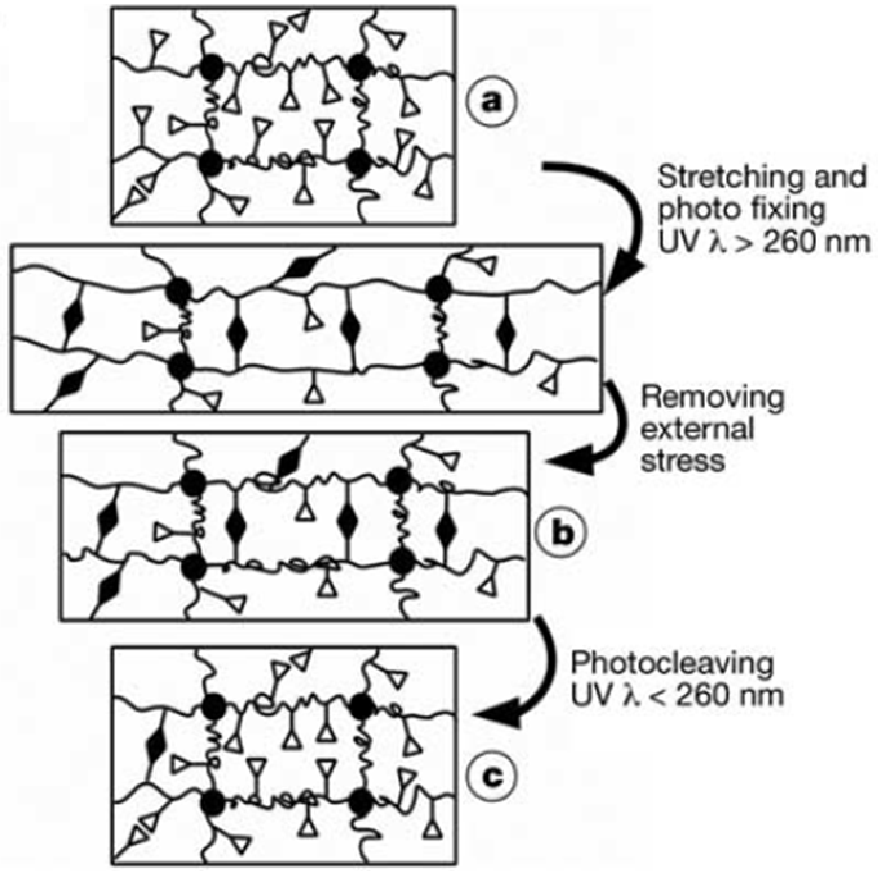

Figure 1.9 Light-induced shape memory mechanism for crosslinked network possessing photoreactive cinnamate groups.

netpoints will relax to the point at which they are held, whereas switching segments are locked out from relaxation by crystallization or vitrification in thermal SMPs. This relaxation leads to strain fixity values of 20-50% in light-induced SMP systems irradiated for up to 60 min. Strain recovery is comparable to thermal SMPs, although not all temporary crosslinks are cleaved during irradiation with the higher energy wavelength of light.

As is the case with all types of SMPs, a major application field of interest for light-induced SMPs is biomedical devices, given that light-induced triggering can be performed remotely at ambient temperatures.[140] Recently, Wu *et al.* synthesized a thermoplastic

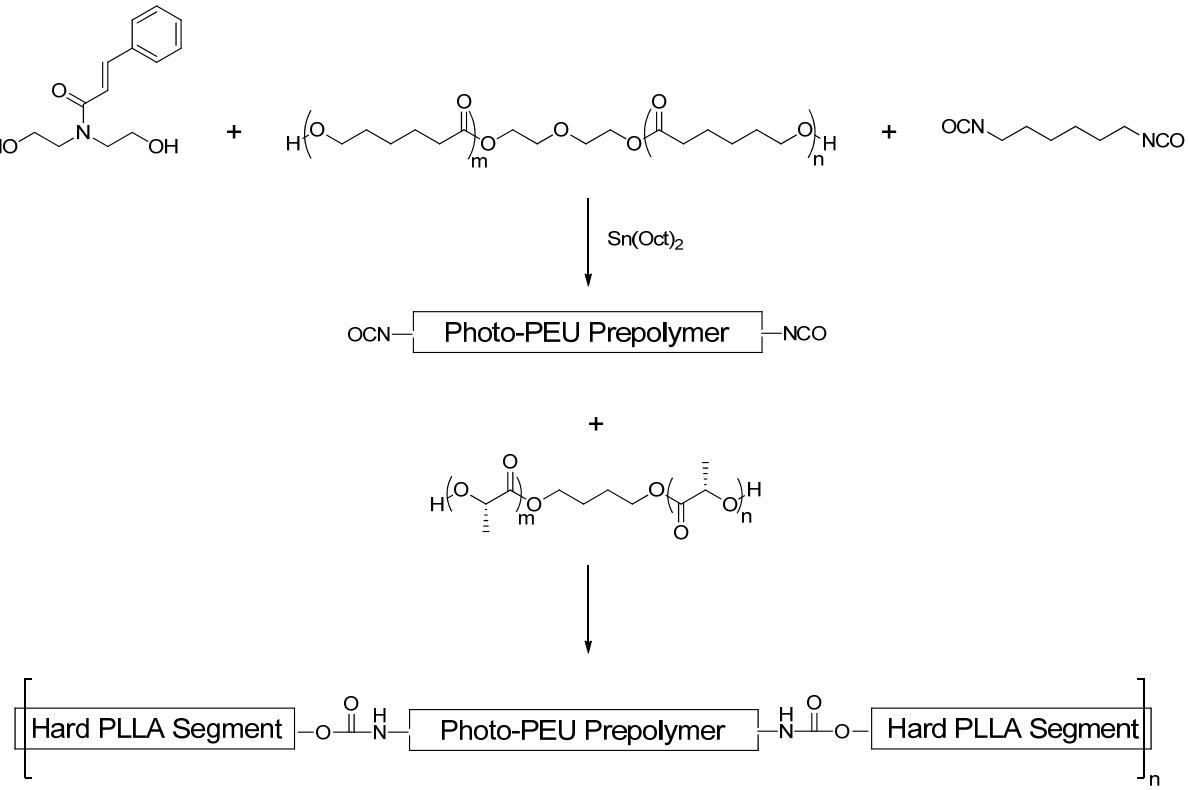

Scheme 1.3 Light-induced thermoplastic PEU SMP synthesized by Wu *et al*.

poly(ester urethane) copolymer containing cinnamamide functional groups (Scheme 1.3) as the first example of a biodegradable light-induced SMP.[141] The original network was formed via physical crosslinks due to the hard PLLA based segments (T_m = 147 – 164 ^oC), while soft PCL based segments (T_m = 31 – 37 ^oC) possessed randomly distributed photogroups. In addition both the PLLA and PCL segments provide degradable polymer backbones. The crystallinity of the PCL segments was not observed within the copolymer network, however the high T_g of PLLA (54 ^oC) required the heating of the system to increase the extent of deformation possible. The nature of the thermoplastic PEU system resulted in good mechanical properties with tensile modulus ranging from 20 to 230 MPa, however this is outside the range of soft tissue in the body which could signal negative immune responses or rejection of devices when placed in contact with tissue.

1.5 Triple Shape Memory

The SME can be extended from dual to triple shape memory (TSM) allowing for more complex movement. TSM systems possess two independent transitions (T_h, T_l), so when programmed in a multi-step process the material can hold two temporary shapes, with triggering recovery resulting in the original shape from the second temporary shape through the first temporary shape.[142] Most TSM systems possess two phase-separated domains within the same network, each contributing an independent thermal transition.[143] The thermal switches can be a combination of two melting and/or glass transition temperatures in the different phases[144-146], or it has also been shown that programming at different temperatures within a broad transition can also result in independent switching.[147]

The first triple shape polymers (TSPs) were developed by Lendlein *et al.* using two different polymer architectures.[143] The first contained PCL and poly(cyclohexyl methacrylate) (PCHMA) segments as a random copolymer network (MACL), the second was a PCL network with PEG side chains (CLEG) giving rise to a T_m/T_g and T_m/T_m system, respectively. Figure 1.10 shows an example of the CLEG material which has been

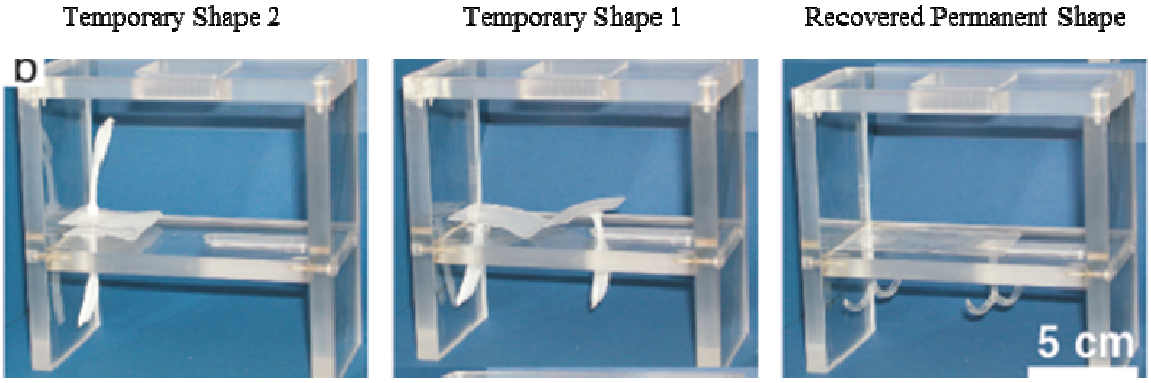

Figure 1.10 Recovery of triple shape polymer network by heating to 40 °C and 60 °C sequentially.

programmed in two steps. When triggered by heating above T_1 (40 ^oC) it unfolds to recover the 1st temporary shape and upon heating above T_2 (60 ^oC) reforms hanging anchors of the original shape. Similar to dual shape memory development, TSPs have also been made to utilize indirect thermal actuation through nanocomposites containing iron (III) oxide.[148] TSM is also present in some LCE systems which also possess shape changing ability through different LC transitions.[142]

1.6 Conclusions

The previous sections described the current state of SMPs, specifically the extension of triggering to various external stimuli and the development of multifunctional triple shape materials. As discussed, the use of light as a trigger independent of thermal mechanisms is advantageous for biomaterials allowing for remote triggering at ambient temperatures. Although multiple LSMPs have been demonstrated, there are still areas that need to be addressed including uniformity, elasticity, tailoring of properties, cytotoxicity, and extension into multifunctional biomaterials. The following chapters describe in detail efforts to produce materials with a range of properties which embody the characteristics of degradable, biocompatible, tunable, multifunctional, and responsive systems.

1.7 Dissertation Organization

This dissertation is organized into five parts. Chapter I is a general discussion of shape memory materials and their recent advances in the areas of triggering, biomaterial applications, and triple shape memory. Chapter II discusses the synthesis and characterization of novel photo-responsive poly(ester urethane)s and the resulting thermoset elastomer networks. Chapter III discusses the development of novel multifunctional triple shape biomaterials using light and thermal transitions in combination to perform macroscopic

and microscopic shape memory. Chapter IV describes the synthesis and characterization of functional photo-responsive poly(β-amino ester)s via two methods: functional monomers and post-functionaliztion. Chapter V discusses continuing experiments and future research directions. Supplemental data for Chapter II – IV is presented in the appendices along with initial synthesis and characterization of thiol pendant copolyesters for functional thermal SMPs in Appendix D. The material in Chapter II and Chapter III, as well as Appendix D, will be submitted for publication.

References

1.) Yoshihito, O.; Matsuda, A. *Nature*, 1995, *376*, 219.

2.) Wache, H.; Hentrich, D.; Wagner, M. *J. Mater. Sci.* 2003, *14*, 109.

3.) Maitland, J.; Metzeger, F.; Schumann, D.; Lee, A.; Wilson, S. *Laser Surg. Med.* 2002, *30*, 1.

4.) Langer, R.; Lendlein, A. World Patent WO 2003088818 A2, 2003.

5.) Gall, K.; Yakacki, C.; Liu, Y.; Shandas, R.; Willett, N.; Anseth, K. *J. Biomed. Mater. Res., Part A* 2005, *73*, 339

6.) Adachi,H.; Yokoi, T.; Hatori, T.; Morishita, K.; Sakashita, K.; Kaiya, H.; Inoue, K.; Ueda, Y.; Nakamura, T.; Yamaguchi, S. Japan Patent 02124438, 1990.

7.) Kobayashi, K.; Hayashi, S. Japan Patent 02183132, 1990.

8.) Kondo, S.; Hayashi, S. Japan Patent 03183920, 1991.

9.) Lan X, Liu, Y.; Lv, H.; Wang, X.; Leng, J.; Du, S. *Smart Mater Struct* 2009, *18*, 240021.

10) Arzberger SC, Munshia NA, Lakea MS, Wintergerst J, Varlese S, Ulmer MP. *Optical Materials and Structural Technologies Proceedings of SPIE* 2003, *5179*, 143.

11.) Benett WJ, Krulevitch PA, Lee AP, Northrup MA, Folta JA.United States Patent 5609, 608, 1997.

12.) Kobayashi K, Hayashi S. United States Patent 5098776; 1992.

13.) Ji F, Zhu Y, Hu J, Liu Y, Yeung L, Ye G. *Smart Mater Struct* 2006, *15*, 1547.

14.) Behl, M.; Zotzmann, J.; Lendlein, A. *Adv Polym Sci* 2010, *226*, 1.

15.) Lendlein, A. Kelch, S. *Angew Chem Int* 2002, *41*, 2034.

16.) Luo X.; Mather P.T. *Macromoleucles* 2009, *42*, 7251.

17.) Chang, L.C.; Read, T.A. *J Metals* 1951, *191*, 47.

18.) Liu, C.; Qin, H.; Mather, P.T. *J Mater Chem* 2007, *17*, 1543.

19.) Charlesby, A. *Atomic Radiation and Polymers*, Pergamon Press, Oxford, 1960, 842.

20.) Ota, S. *Radiat Phys Chem* 1981, *18*, 81.

21.) Mondal, S.; Hu, J.L. *J Elastom Plast* 2007, *39*, 81.

22.) Chen, S.; Hu, J.; Liu, Y.; Liem, H.; Zhu, Y.; Liu, Y. *J Polym Sci Part B, Polymer Physics* 2007, *45*, 444.

23.) Cao, Q.; Liu, P. *Polym Bull* 2006, *57*, 889.

24.) Lin, J.R.; Chen, L.W. *J Appl Polym Sci* 1998, *69*, 1563.

25.) Lin, J.R.; Chen, L.W. *J Appl Polym Sci* 1998, *69*, 1575.

26.) Jiangand, H.Y.; Schmidt, A.M. In: Shape-memory polymers and multifunctional composites, CRC Press LLC, 2010, p. 21-63.

27.) Li, F.; Hou, J.; Zhu, W.; Zhang, X.; Xu, M.; Luo, X.; Ma, D.; Kim, B.K. *J Appl Polym Sci* 1996, *62*, 631.

28.) Ikematsu, T.; Kishimoto, Y.; Karaushi, M. Japan Patent 02022355, 1990.

29.) Jeon, H.G.; Mather, P.T.; Haddad, T.S. *Polym Int* 2009, *49*, 453.

30.) Luo, X.; Zhang, X.; Wang, M.; Ma, D.; Xu, M.; Li, F. *J Appl Polym Sci* 1997*, 64*, 2433.

31.) Kraft, A.; Rabani, G.; Schuh, C.; Mueller, K.; Lechmann, M.C. *Polym Mater Sci Eng* 2005, *93*, 935.

32.) Hu JL. In: Characterization of shape memory properties in polymers. CRC Press LLC, 2007. p. 197–225.

33.) Yakacki CM, Willis S, Luders C, Gall K. *Adv Eng Mater* 2008, *10*, 112.

34.) Kim BK, Lee SY, Lee JS, Baek SH, Choi YJ, Lee JO, *et al*. *Polymer* 1998, *39*, 2803.

35.) Leng, J.; Lan, X.; Liu, Y.; Du, S. *Prog Mater Sci* 2011, *56*, 1077

36.) Li, F.; Zhu, W.; Zhang, X.; Zhao C.; Xu, M. *J Appl Polym Sci* 1999, *71*, 1063.

37.) Skakalova, V.; Lukes, V.; Breza, M. *Macromol Chem Phys* 1997, *198*, 3161.

38.) Hu, Z.; Zhang, X.; Li, Y. *Science* 1995, *269*, 525.

39) Zhu, G.; Liang, G.; Xu, Q.; Yu, Q. *J Appl Polym Sci* 2003, *90*, 1589.

40.) Zhang, D.; Lan, X. Liu, Y.; Leng, J. In: Behavior and mechanics of multifunctional and composite materials, Proc. SPIE 6526, 2007.

41.) Park, C.; Lee, J.Y.; Chun, B.C.; Chung, Y.C.; Cho, J.W.; Cho, B.G. *J Appl Polym Sci* 2004, *94*, 308.

42.) Hu, J.; Yang, Z.; Yeung, L.; Ji, F.; Liu, Y. *Polym Int* 2005, *54*, 854.

43.) Lee, S.H.; Kim, J.W.; Kim, B.K. *Smart Mater Struc* 2004, *13*, 1345.

44.) Alteheld, A.; Feng, Y.; Kelch, S.; Lendlein, A. *Angew Chem Int Ed* 2005, *44*, 1188.

45.) Yang, Z.; Hu, J.; Liu, Y.; Yeung, L. *Mater Chem Phys* 2006, *98*, 368.

46.) Balazs, A.; Emrick, T.; Russell, T.P. *Science* 2006, *314*, 1107.

47) Manias, E. *Nat Mater* 2007, *6*, 9.

48) Manpreet S. Thermal characterization of nanocomposite shape memory polymer for their mechanical and thermal properties. Thesis of graduate studies, Lamar University. UMI Number 1429868.

49) Ohki, T.; Ni, Q.Q.; Iwamoto, M. *Sci Eng Compos Mater* 2004, *11*, 137.

50) Zhang, C.S.; Ni, Q.Q. *Compos Struct* 2007, *78*, 153.

51) Liang, C.; Rogers, C.A.; Malafeew, E. *J Intelligent Mater Syst Struct* 2000, *11*, 877.

52) Lan, X.; Huang, W.M.; Leng, J.S.; Liu, Y.J.; Du, S.Y. *Adv Mater Res* 2008, *47*, 714.

53) Wornyo, E.; Gall, K.; Yang, F.; King, W. *Polymer* 2007, *48*, 3213.

54) Sahoo, N.G.; Jung, Y.C.; Yoo, H.J.; Cho, J.W. *Compos Sci Technol* 2007, *67*, 1920.

55) Bhattacharyya, A.R.; Sreekumar, T.V.; Liu, T.; Kumar, S.; Ericson, L.M.; Hauge, R.H. *Polymer* 2003, *44*, 2373.

56) Assouline, E.; Lustiger, A.; Barber, A.H.; Cooper, C.A.; Klein, E.; Wachtel, E. *J Polym Sci Part B* 2003, *41*, 520.

57) Seoul, C.; Kim, Y.T.; Baek, C.K. *J Polym Sci Part B Polym Phys* 2003, *41*, 1572.

58) Liu, T.; Phang, I.Y.; Shen, L.; Chow, S.Y.; Zhang, W.D. *Macromolecules* 2004, *37*, 7214.

59) Lou, X.; Detrembleur, C.; Sciannamea, V.; Pagnoulle, C.; Jerome, R. *Polymer* 2004, *45*, 6097.

60) Wong, M.; Paramsothy, M.; Xu, X.J.; Ren, Y.; Li, S.; Liao, K. *Polymer* 2003, *44*, 7757.

61) Gojny, F.H.; Schulte, K. *Compos Sci Technol* 2004, *64*, 2303.

62) Sandler, J.K.W.; Kirk, J.E.; Kinloch, I.A.; Shaffer, M.S.P.; Windle, A.H. *Polymer* 2003, *44*, 5893.

63) Shaffer, M.S.P.; Windle, A.H. *Adv Mater* 1999,*11*, 937.

64) Buckley, P.R.; McKinley, G.H.; Wilson, T.S.; Small, W.; Benett, W.J.; Bearinger, J.P. *IEEE Trans Biomed Eng* 2006, *53*, 2075.

65) Razzaq, M.Y.; Anhalt, M.; Frormann, L.; Weidenfeller, B. *Mater Sci Eng A – Struct Mater Prop Microstruct Process* 2007, *471*, 57.

66) Yakacki, C.M.; Satarkar, N.S.; Gall, K.; Likos, R.; Hilt, J.Z. *J Appl Polym Sci* 2009, *112*, 3166.

67) Hazelton, C.S.; Arzberger, S.C.; Lake, M.S.; Munshi, N.A. *J Adv Mater* 2007, *39*, 35.

68) Vaia, R. *Nat Mater* 2005, *4*, 429.

69) Rousseau, I.A.; Mather, P.T. *J Am Chem Soc* 2003, *125*, 15300.

70) Rousseau, I.A.; Qin, H.H.; Mather, P.T. *Macromolecules* 2005, *38*, 4103.

71) Zhang, Q.M.; Li, H.; Poh, M.; Xia, F.; Cheng, Z.Y.; Xu, H.; Huang, C. *Nature* 2002, *419*, 284.

72) Hiraoka, K.; Sagano, W.; Nose, T.; Finkelmann, H. *Macromolecules*, 2005, *38*, 7352.

73) M. Warner and E. M. Terentjev, *Liquid Crystalline Elastomers*, Oxford University Press, Oxford, UK, 2003.

74) Lendlein, A.; Schmidt, A.M.; Langer, R. *Proc Natl Acad Sci* 2001, *98*, 842.

75) Brennan, M. *Chem Eng News* 2001, *79(6)*, 5.

76) Ashley, S. *Sci Am* 2001, No. 5.

77) Lendlein, A.; Langer, R. *Science* 2002, *296*, 1673.

78) Laurencin, C.T.; Sobrasua, I.E.M.; Langer, R.S. in *Biomedical Applications of Synthetic Biodegradable Polymers*, CRC Press, Boca Raton, 1995.

79) J.D. Bronzino *The Biodmedical Engineering Handbook*, CRC Press, Boca Raton, 1995.

80) Petrova, P.S.; Manolova, N.; Rashkov, I.; Li, S.; Vert, M. *Polym Int* 1998, *45*, 419.

81) Cohn, D.; Stern, T.; Gonzalez, F.; Epstein, J. *J Biomed Mater Res* 2002, *59*, 273.

82) Liu, L.; Sheardown, H. *Biomaterials* 2005, *26*, 233.

83) Williams, D.F. *Sadhana* 2003, *28*, 563.

84) Wang, W.; Ping, P.; Chen, X.; Jing, X. *Eur Polym J* 2006, *42*, 1240.

85) Mohr, R.; Kratz, K.; Weigel, T.; Lucka-Gabor, M.; Moneke, M.; Lendlein, A. *Proc Natl Acad Sci USA* 2006, *103*, 3540.

86) Weigel, T.; Mohr, R.; Lendlein, A. *Smart Mater Struct* 2009, *18*, 025011.

87) Koerner, H.; Price, G.; Pearce, N.A.; Alexander, M.; Vaia, R.A. *Nat Mater* 2004, *3*, 115.

88) Liu, Y.; Lv, H.; Lan, X.; Leng, J.; Du, S. *Compos Sci Technol* 2009, *69*, 2064.

89) Small, W.; Wilson, T.S.; Benett, W.J.; Loge, J.M.; Maitland, D.J. *Opt Express* 2005, *13*, 8204.

90) Yang, B.; Huang, W.M.; Li, C.; Lee, C.M.; Li, L. *Smart Mater Struct* 2004, *13*, 191.

91) Huang, W.M.; Yang, B.; An, L.; Li, C.; Chan, Y.S. *Appl Phys Lett* 2005, *86*, 114105.

92) Yang, B.; Huang, W.M.; Li, C.; Li, L. *Polymer* 2006, *47*, 1348.

93) Yang, B.; Huang, W.M.; Li, C.; Li, L.; Chor, J.H. *Scr Mater* 2005, *53*, 105

94) Biercuk, M.J.; Llaguno, M.C.; Radosavljevic, M.; Hyun, J.K.; Johnson, A.T.; Fischer, J.E. *Appl. Phys. Lett*. 2002, *80*, 2767.

95) Chang, T.E.; Jensen, L.R.; Kisliuk, A.; Pipes, R.B.; Pyrz, R.; Sokolov, A.P. *Polymer* 2005, *46*, 439.

96) Gall, K.; Dunn, M.L.; Liu, Y; Finch, D.; Lake, M.; Munshi, N.A. *Acta Mater* 2002, *50*, 5115.

97) Leng, J.S.; Lan, X.; Liu, Y.J.; Du, S.Y. *Smart Mater Struct 2009*, 18, 074003.

98) Leng, J.S.; Lan, X.; Liu, Y.J.; Du, S.Y.; Huang, W.M.; Liu, N. *Appl Phys Lett* 2008, *92*, 014104.

99) Leng, J.S.; Lv, H.B.; Liu, Y.J.; Du, S.Y. *Appl Phys Lett* 2007, *91*, 144105.

100) Leng, J.S.; Lv, H.B.; Liu, Y.J.; Du, S.Y. *J Appl Phys* 2008, *104*, 104917.

101) Cho, J.W.; Kim, J.W.; Jung, Y.C.; Goo, N.S. *Macromol Rapid Commun* 2005, *26*, 412.

102) Razzaq, M.Y.; Anhalt, M.; Frormann, L.; Weidenfeller, B. *Mater Sci Eng A – Struct Mater Prop Microstruct Process* 2007, *444*, 227.

103) Schmidt, A.M. *Macromol Rapid Commun* 2006, *27*, 1168.

104) Zhang, H.; Xia, H.; Zhao, Y. *J Mater Chem* 2012, *22*, 845.

105) Leng, J.; Zhang, D.; Liu, Y.; Yu, K.; Lan, X. *Appl Phys Lett* 2010, *96*, 111905.

106) Leng JS, Wu XL, Liu YJ. Appl Polym Sci 2009, *114*, 2455.

107) Behl, M.; Lendlein, A. *Mater Today* 2007, *10*, 20.

108) Leng, J.S.; Lv, H.B.; Liu, Y.J.; Du, S.Y. *Appl Phys Lett* 2008, *92*, 206105.

109) Lv, H.B.; Leng, J.S.; Liu, Y.J.; Du, S.Y. *Adv Eng Mater* 2008, *10*, 592.

110) Kumpfer, J.R.; Rowan, S.J. *J Am Chem Soc* 2011, *133*, 12866.

111) Jiang, H.Y.; Kelch, S.; Lendlein, A. *Adv Mater* 2006, *18(11)*, 1471.

112) Irie, M. *Adv Polym Sci* 1990, *94*, 27.

113) Brown, G.H. *Photochromism* 1971, Wiley-Interscience.

114) Lovrien, R. *PNAS* 1967, *57*, 236.

115) Irie, M.; Suzuki, T. *Macromol Chem Rapid Commun* 1981, *8*, 607.

116) Irie, M.; Hosoda, M. *Macromol Chem Rapid Commun* 1985, *6*, 533.

117) Irie, M.; Iga, R. *Macromol Chem Rapid Commun* 1987, *8*, 569.

118) Kumar, G.S.; DePra, P.; Neckers, D.C. *Macromolecules* 1984, *17*, 1912.

119) Kumar, G.S.; DePra, P.; Zhang, K.; Neckers, D.C. *Macromolecules* 1984, *17*, 2463.

120) Kumar, G.S.; Savariar, C.; Sattran, M.; Neckers, D.C. *Macromolecules* 1985, *18*, 1525.

121) Zimmerman, E.K.; Stille, J.K. *Macromolecules*, 1985, *14*, 1246.

122) Irie, M.; Menju, A.; Hayashi, K. *Macromolecules*, 1981, *12*, 1176.

123) Yu, Y.L.; Nakano, M.; Ikeda, T. *Nature* 2003, *425*, 145.

124) Camacho-Lopez, M.; Finkelmann, H.; Palffy-Muhoray, P.; Shelley, M. *Nat Mater* 2004, *3*, 307.

125) Ikeda, T.; Nakano, M.; Lei, Y.Y.; Tsutsumi, O.; Kanazawa, A. *Adv Mater* 2003, *15*, 307.

126) Finkelmann, H.; Nishikawa, E.; Pereira, G.G.; Warner, M. *Phys Rev Lett* 2001, *87*, 015501.

127) Li, M.H.; Keller, P.; Li, B.; Wang, X.G.; Bruner, M. *Adv Mater* 2003, *15*, 569.

128) Irie, M.; Kunwatchakun, D. *Macromolecules* 1986, *19*, 2476.

129) Mamada, A.; Tanaka, T.; Kunwatchakun, D.; Irie, M. *Macromolecules* 1990, *23*, 1517.

130) Suzuki, A.; Tanaka, T. *Nature* 1990, *346*, 345.

131) Juodkazis, S.; Mukai, N.; Wakaki, R.; Yamaguchi, A.; Matsuo, S.; Misawa, H. *Nature* 2000, *408*, 178.

132) Hogan, P.M.; Tajbakhsh, A.R.; Terentjev, E.M. *Phys Rev E: Stat Nonlinear Soft Matter Phys* 2002, *65*, 041720.

133) Yu, Y.L.; Nakano, M.; Shishido, A.; Shiono, T.; Ikeda, T. *Chem Mater* 2004, *16*, 1637.

134) Yu, Y.L.; Ikeda, T. *Macromol Chem Phys Suppl* 2005, *206*, 1705.

135) Kumar, G.S.; Neckers, D.C. *Chem Rev* 1989, *89*, 1915.

136) Kinoshita, T. *J Photochem Photobiol B: Biol* 1998, *42*, 19.

137) Nakano, M.; Yu, Y.; Shishido, A.; Tsutsumi, O.; Kanazawa, A.; Shiono, T.; Ikeda, T. *Mol Cryst Liq Cryst* 2003, *398*, 1.

138) Yu, Y.; Nakano, M.; Ikeda, T. *Pure Appl Chem* 2004, *76*, 1435.

139) Lee, K.M.; Koerner, H.; Vaia, R.A.; Bunning, T.J.; White, T.J. *Soft Matter* 2011, *7*, 4318.

140) Lendlein, A.; Jiang, H.Y.; Junger, O.; Langer, R. *Nature* 2005, *434*, 879.

141) Wu, L.; Jin, C.; Sun, X. *Biomacromolecules* 2011, *12*, 235.

142) Behl, M.; Lendlein, A. *J. Mater. Chem.* 2010, *20*, 3335.

143) Bellin, I.; Kelch, S.; Langer, R.; Lendlein, A. *Proc Natl Acad Sci* 2006, *103(48)*, 18043.

144) Pretsch, T. *Smart Mater. Struct.* 2010, *19*, 1.

145) Chen, S.; Hu, J.; Yuen, C.H.; Chan, L.; Zhuo, H. *Polym Adv Technol* 2010, *21*, 377.

146) Behl, M.; Bellin, I.; Kelch, S.; Wagermaier, W.; Lendlein, A. *Adv. Funct. Mater.* 2009,*19*,102.

147) Xie, T. *Nature Letters* 2010, *464*, 267.

148) Narendra, U.K.; Kratz, K.; Behl, M.; Lendlein, A. in *Active Polymers, Materials Research Society Symposium Proceedings*, ed. A. Lendlein, V.P. Shastri, K. Gall. Materials Research Society, Warrendale, PA, 2009, Vol. 1190.

Chapter II

PHOTO-RESPONSIVE POLY(ESTER URETHANE)S FOR DUAL SHAPE MEMORY BIOMATERIALS

2.1 Introduction

Shape memory polymers (SMPs) are proving to be promising enabling materials in the field of minimally invasive implants and smart biomedical devices.[1,2] SMPs are programmed into a temporary state by an external force and will recover the original shape when exposed to an external stimulus. The ability to change shape in a predetermined manner upon exposure of a given stimulus has led to the development of smart polymeric stents, sutures, scaffolds, and other devices.[3,4] Recovery of the permanent shape is typically triggered thermally by passing through a transition temperature (T_{trans}), although for dual shape memory it has also been induced electrically[5] , magnetically[6], electromagnetically[7], or by solvent interactions[8]. Each of these varying stimuli acts to indirectly actuate a thermal mechanism in the polymer system. There have been several examples of dual (one temporary shape) and triple shape memory[9] (two temporary shapes). The shape memory effect (SME) is gauged by the strain fixity ratio (R_f) and strain recovery ratio (R_r), which evaluates the fixation of the temporary shape and the recovery of the original shape, respectively.

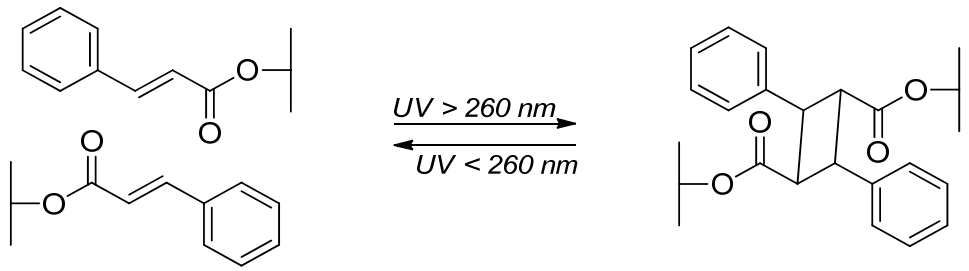

Scheme 2.1 Photo-induced reversible [2+2] cycloaddition of two cinnamate functional groups.

Several researchers have described shape changes induced by light that are independent of heat,[10,11,12] however, the most closely related to the present work is based on moieties which undergo a reversible UV induced [2+2] cycloaddition (Scheme 2.1). Lendlein *et al.* programmed an acrylate-based hydrogel containing cinnamate groups into fixed shapes by ultraviolet light illumination ($\lambda > 260$ nm). When exposed a second time to a higher energy ultraviolet light ($\lambda < 260$ nm), newly formed temporary crosslinks were cleaved and the polymer network recovered its original shape, demonstrating that remote light activation at ambient temperatures was possible.[13] Figure 2.1 shows an illustration of this programming and recovery process. More recently, Wu *et al*. utilized polyester segments functionalized with similar photo-responsive groups randomly distributed them in a thermoplastic polyurethane system to create materials that were hydrolytically degradable.[14] For such materials the strain fixity is much lower when compared with thermal shape memory materials due to the ability of the chains between the temporary crosslinks to relax to a more entropically favored position when external force is released. This requires over programming a material in order to fix the desired temporary shape. The

SME has also been shown in systems based on the photochromic reaction of azobenzene[15], however, these materials lack a degradable backbone and other properties advantageous for biomaterials.

For shape memory materials in biomedical applications, targeting thermal transitions can be challenging, and little flexibility for tailoring other properties remains once T_{trans} has been set. The use of a light-induced mechanism removes dependence on a thermal transition and allows switching at ambient temperatures. Herein, we present the synthesis and characterization of a library of biodegradable amorphous poly(ester urethane) prepolymers which are functionalized with a photo-responsive group in each repeat unit to give a uniform

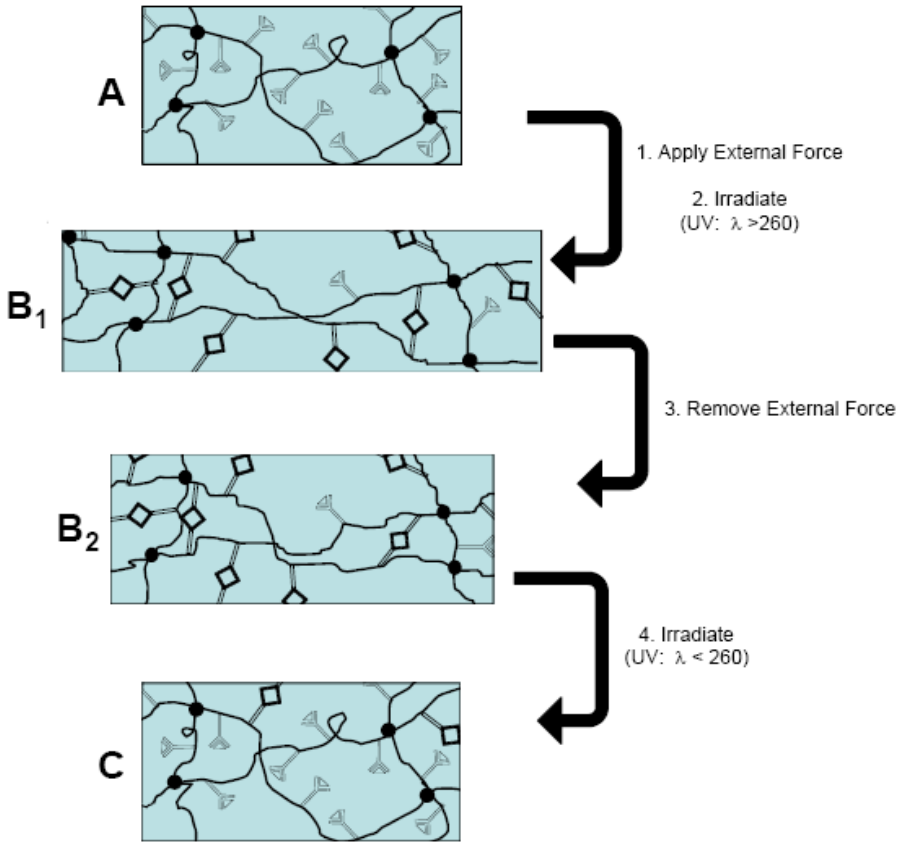

Figure 2.1 Light-induced shape memory mechanism.

distribution along the polymer backbone. The thermoset networks that result from thermal curing possess a range of thermal and mechanical properties as well as the ability to undergo light induced shape memory.

2.2 Experimental Section

2.2.1 Materials

All reagents were purchased from Sigma-Aldrich and used without further purification unless otherwise noted. Dichloromethane was dried by distilling from $CaSO_4$. Triethylamine and pyridine were dried by distilling from CaH_2. 1,8-octanediol was recrystallized from THF.

2.2.2 Instrumentation.

Gel permeation chromatography was used to determine molecular weights and molecular weight distributions, M_w/M_n, of polymer samples using a Waters Alliance 2695 and Waters 2414 Refractive Index detector. Molecular weights were calculated using a calibration plot constructed from polystyrene standards (Polyscience Corp.). The measurements were taken at 35 °C with THF as the mobile phase on three columns (Waters Styragel HR5, HR4, and HR2). ^{1}H NMR spectra of the monomers and polymers were obtained on a Bruker 400 ADVANCE spectrometer. Thermal transitions were analyzed using TA Differential Scanning Calorimeter Q200 with liquid N_2 cooling unit at a cooling rate of 5 ^{o}C/min and heating rate of 10 ^{o}C/min. A Pyris I Thermogravimetric Analyzer was used to collect 5% and 10% decomposition temperature data from 25 ^{o}C to 500 ^{o}C at a heating rate of 20 ^{o}C/min in N_2 atmosphere. Mechanical analysis was conducted on an Instron 5566 at a crosshead speed of 10 mm/min at 25 °C. The Young's modulus (*G*) was calculated using the initial linear portion of the stress/strain curve (0 – 5 % strain).

2.2.3 Monomer Synthesis

*Synthesis of Diethyl 2,2'-(Cinnamoylazanediyl)diacetate (DCA) (**1**)*. A solution of cinnamoyl chloride (4.165 g, 25.0 mmol) in dry CH_2Cl_2 was added dropwise into a stirring solution of diethyl iminodiacetate (4.57 mL, 25.5 mmol), triethylamine (7.02 mL, 50.5 mmol) and dry CH_2Cl_2 (115 mL) at 0 ^oC. The reaction solution was allowed to stir for 30 minutes at 0 ^oC and then warmed to room temperature and left stirring for 12 h. The precipitant was removed by gravity filtration and the solution was washed sequentially with 1.0 M HCl, saturated $NaHCO_3$, and DI H_2O. The organic layer was dried over $MgSO_4$, filtered, and excess solvent was removed under reduced pressure. The crude product was recrystallized from hot CH_2Cl_2/hexanes and dried under vacuum to afford a white solid in 93% yield. ^{1}H-NMR: δ (ppm) = 7.67 (m, 2H), 7.64 (d, 1H, J = 15.3 Hz), 7.41 (m, 3H), 7.14 (d, 1H, J = 15.6 Hz), 4.55 (s, 2H), 4.28 (s, 2H), 4.20 (q, 2H, J = 7.1 Hz), 4.16 (q, 2H, J = 7.1 Hz), 1.25 (t, 6H, J = 7.2 Hz).

*Synthesis of Diethyl 3-(Cinnamoyloxy)pentanedioate (DCE) (**2**)*. A solution of cinnamoyl chloride (10 g, 60 mmol) in dry CH_2Cl_2 was added dropwise into a stirring solution of diethyl 3-hydroxygluturate (10.21 g, 50 mmol) and dry CH_2Cl_2 (100 mL) at 0 ^oC. After the addition was complete, pyridine (4.83 mL, 60 mmol) was added dropwise. The reaction solution was allowed to stir for 30 minutes at 0 ^oC and then warmed to room temperature for 12 h. The precipitant was removed by gravity filtration and the solution was washed sequentially with 1.0 M HCl, saturated $NaHCO_3$, and DI H_2O. The organic layer was dried over $MgSO_4$, filtered, and product was concentrated under reduced pressure. Purification by column chromatography (CH_2Cl_2/EtOAc 9:1) resulted in an oil in 62% yield. ^{1}H-NMR: δ (ppm) = 7.69 (m, 2H), 7.67 (d, 1H, J = 11.2 Hz), 7.44 (m, 3H), 6.51 (d, 1H, J =

16 Hz), 5.62 (qn, 1H, J = 6.0 Hz) 4.11 (q, 4H. J = 7.3 Hz), 2.80 (dd, 4H, J_1 = 3.8 Hz, J_2 = 4.4 Hz) 1.21 (t, 6H, J = 6.0 Hz).

*Synthesis of N,N-bis(2-hydroxyethyl)cinnamamide (CAD) (**3**).* A solution of diethanolamine (2.00 g, 19 mmol) and Et_3N (9.31 mL, 67 mmol) in dry CH_2Cl_2 under N_2 atmosphere was cooled to 0 ^oC in an ice bath. To this mixture a solution of cinnamoyl chloride (9.51 g, 57 mmol) in dry CH_2Cl_2 was added dropwise over a period of 20 min. After complete addition the reaction was allowed to stir for 1 h before removal of the ice bath and returning the reaction to room temperature to stir overnight. The solvent was then removed by rotary evaporation and methanol was added to dilute the residue. Saturated Na_2CO_3 was added and the solution was stirred for 3 h before being diluted with DI water. After an extraction with CH_2Cl_2, the organic layer was dried over $MgSO_4$ and the product was concentrated by vacuum evaporation. Flash chromatography (10:1 $CHCl_3$/MeOH) followed by vacuum drying resulted in a white powder in 68% yield. ^{1}H-NMR: δ (ppm) = 7.66 (d, 1H, J = 16 Hz), 7.50 (m, 2H), 7.35 (m, 3H), 6.94 (d, 1H, J = 16 Hz), 3.88 (dt, 4H, J_1 = 6 Hz, J_2 = 16 Hz) 3.70 (bs, OH), 3.66 (q, 4H, J = 5.3 Hz).

2.2.4 Polyester Prepolymer Synthesis

*Polymerization with DCA Monomer (**4, 5**).* Prepolymers were synthesized with either 1,8-octanediol or 1,4-cyclohexanedimethanol for both monomer **1** and **2**. An example of a typical polymerization with the DCA monomer is given. A three-necked round bottom flask was charged with monomer **1** (2.500 g, 7.83 mmol) and 1,8-octanediol (1.244 g, 8.51 mmol), evacuated and filled with N_2. The mixture of monomers was heated to a melt at 90 ^oC for 20 minutes. Tin (II) 2-ethylhexanoate (27.5 μL, 1 mol% of diol) was syringed into the flask, the heat was increased to 125 ^oC, and the melt was stirred. After 1 hour the pressure was slowly

reduced to 40 torr, after another 5 hours the pressure reduced to 20 torr, and after 18 hours the pressure was reduced to 0.1 torr. The mixture continued to stir under reduced pressure for another 24 hours, to give a total of 48 hours reaction time. The reaction was removed from heat and atmospheric pressure was re-established. The polymer was dissolved in 5 mL of chloroform and precipitated into cold stirring methanol (-78 ^{o}C). The polymer was then dried under vacuum for 24 hours. ^{1}H-NMR: δ (ppm) = 7.66 (m, 2H), 7.65 (d, 1H, *J* = 15.2 Hz), 7.40 (m, 3H), 7.14 (d, 1H, *J* = 15.2 Hz), 4.56 (s, 2H) 4.29 (s, 2H) 4.13 (t, 2H, *J* = 5.4 Hz), 4.10 (t, 2H *J* = 5.4 Hz), 3.52 (t, 0.08H, *J* = 5.8 Hz) 1.61 (m, 4H) 1.29 (m, 8H).

Polymerization with DCE Monomer (6, 7). An example of a typical polymerization with the DCE monomer is given. A three-necked round bottom flask was charged with monomer 2 (1.663 g, 4.97 mmol), 1,8-octanediol (0.733 g, 5.01 mmol), and Lipase acrylic resin catalyst (240 mg, 10 wt% monomers), evacuated and filled with N_2. The mixture of monomers and catalyst is heated to 80 ^{o}C to form a melt and stirring is begun. After 2 hours, pressure is slowly reduced to 40 torr for 12 hours, then reduced to 20 torr for 24 hours, and finally reduced to 0.1 torr for a final 12 hours. Heat is removed and atmospheric pressure restored, followed by the polymer being dissolved in 5 mL of chloroform and precipitated into cold stirring methanol (-78 ^{o}C). The polymer was collected and dried under vacuum for 24 hours. ^{1}H-NMR: δ (ppm) = 7.66 (d, 1H, *J* = 16.0 Hz), 7.50 (m, 2H), 7.38 (m, 3H), 6.38 (d, 1H, *J* = 16.0 Hz), 5.64 (qn, 1H, *J* = 6.0 Hz), 4.05 (m, 4H), 3.74 (m, endgroup), 2.79 (d, 4H, *J* = 4.0 Hz), 1.85 (m, endgroup), 1.57 (m, 4H), 1.23 (m, 8H).

Polymerization with CAD Monomer (8). Polymerization with diol monomer 3 required the use of either a complementary diacid or diester, therefore, 1,4-cyclohexanedicarboxylic acid was employed. A typical polymerization is given. A flame

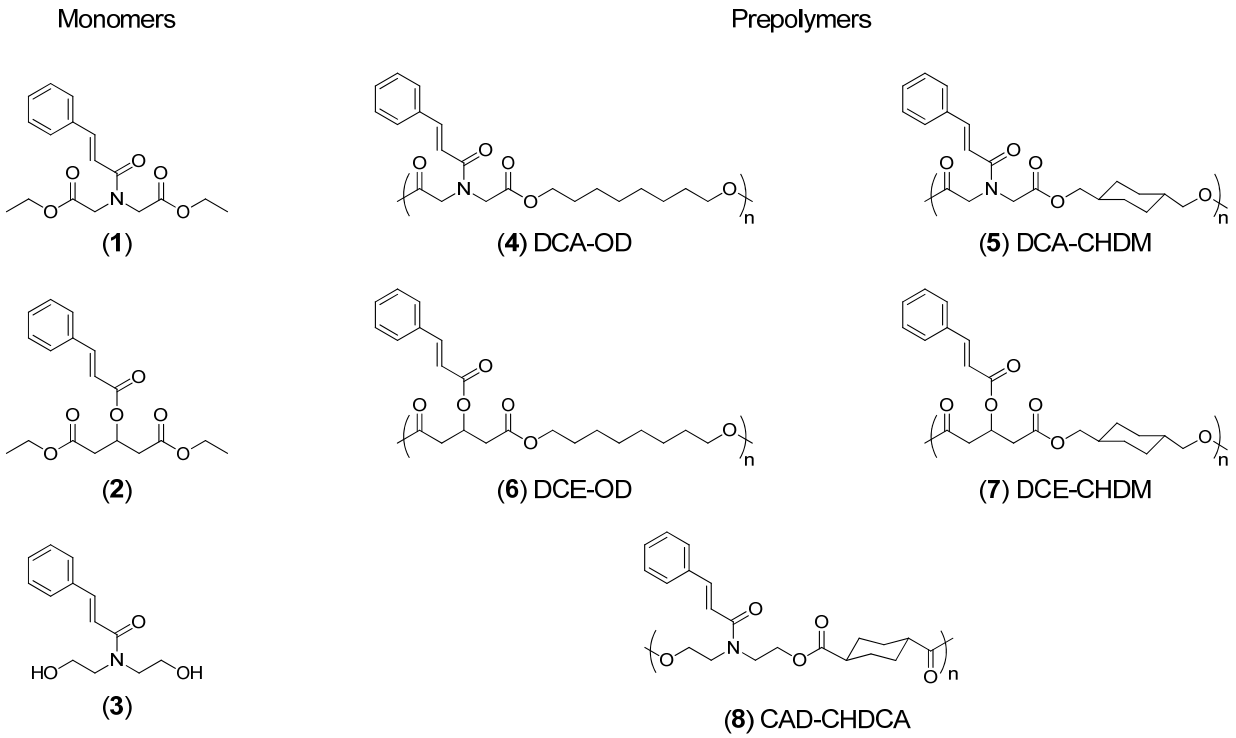

Figure 2.2 Bifunctional monomers DCA, DCE, CAD and resulting prepolymers from polycondensation with complementary monomers.

dried round bottom flask was charged with monomer 3 (3.13 g, 13.3 mmol) and 1,4-cyclohexanedicarboxylic acid (2.22 g, 12.9 mmol). After purging with nitrogen for several minutes, the vessel was heated to 125 ^{o}C to form a melt solution, afterwhich tin (II) ethylhexanoate catalyst (100 μL, 0.3 mmol) was added. The reaction was allowed to stir under nitrogen atmosphere at 125 ^{o}C for 2 h after which the pressure was slowly reduced to 0.1 torr for a total reaction time for 50 h. After returning to atmospheric pressure and removing from heat, the crude polymer was dissolved in $CHCl_3$ and precipitated into cold stirring diethyl ether. The purified polymer was collected and dried under vacuum overnight. ^{1}H-NMR: δ (ppm) = 7.72 (d, 1H, J = 12 Hz), 7.54 (m, 2H), 7.37 (m, 3H), 6.95 (d, 1H, J = 12

Hz), 4.28 (m, 4H), 3.76 (m, 4H), 2.48 (s, 2H), 2.25 (s, 2H), 2.04 (m, 4H), 1.86 (m, 4H), 1.61 (m, 4H), 1.44 (m, 4H).

2.2.5 Thermoset Network Formation

Prepolymer end-functionalization. Hydroxy-terminated polymer of known $\overline{M}_n$ (43 mg, 6.78 x 10^{-3} mmol) was dissolved in CH_2Cl_2 (2.0 mL). The solution was heated to reflux at 60 ^oC, then 2-isocyanatoethyl methacrylate (5 μL, 0.035 mmol) was added by syringe. One drop of stannous octoate was also added to help catalyze the reaction. The solution was left under reflux for 2 h, excess solvent was removed under reduced pressure, and the concentrated solution was precipitated in cold stirring methanol (-78 ^oC). The resulting polymer was transferred and dried under vacuum for 1 day. Example for DCA-OD prepolymer, ^{1}H-NMR: δ (ppm) = 7.65 (m, 2H), 7.64 (d, 1H, *J* = 15.2 Hz), 7.39 (m, 3H), 7.13 (d, 1H, *J* = 15.6 Hz), 6.09 (s), 4.55 (s, 2H), 4.28 (s, 2H), 4.11 (m, 4H), 3.97 (q), 3.43 (q), 1.90 (s), 1.60 (m, 4H), 1.28 (m, 8H).

Crosslinking. Prepolymers with crosslinkable endgroups were thermally cured by two methods. The first method employed AIBN as a radical initator. To a 50% polymer solution in chloroform was added AIBN (1.0 mol %) and the mixture was stirred for 5 minutes to ensure full distribution of initiator before filling a Teflon mold or casting on a glass slide. The solvent was completely evaporated, and the mold/slide was placed in an oven at 80 ^oC for 6 h. The second method utilized a thermally initiated thiol-ene reaction in the presence of an amine catalyst. To a prepolymer solution was added trimethyloylpropane tris(3-mercaptopropionate) (2.0 mol equiv.) and amine catalyst (0.95 wt %). Two amine compounds were used: *n*-hexyl amine or 1,8-diazabicyclo[5.4.0]undec-7-ene (DBU). After

stirring for 5 minutes, the solution was cast in the mold or on the glass slide, solvent evaporated, and placed in the oven at 80 ^{o}C overnight.

2.2.6 Characterization

2.2.6.1 Light-induced Shape Memory (LSM)

Films of 0.5-2.0 mm thickness were placed in a specially designed vise apparatus to stretch and hold the sample in a stressed state while irradiating with UV light. Film samples were elongated to a specified length and the entire apparatus placed in a UVP CL 1000 Crosslinker with five 8 watt mercury bulbs (302 nm) at a distance of ~3 cm for a prescribed time. After UV fixing the film sample was removed from the vise to give the temporary shape. The film sample was then irradiated for a prescribed time in the UV chamber with 254 nm bulbs for a prescribed time under no external force. Dimension measurements before stress was applied, in the stressed state, after fixing, and after recovery were taken with a Mitutoyo ABSOLUTE Digimatic 500 Series caliper in triplicate. Strain fixity (R_f) and strain recovery (R_r) were calculated using the following equations,

$$R_f = \frac{\varepsilon_u(N)}{\varepsilon_m} = \frac{l_f - l_i}{l_p - l_i} \times 100 \qquad R_r = \frac{\varepsilon_m - \varepsilon_p(N)}{\varepsilon_m - \varepsilon_p(N-1)} = \frac{l_p - l_r}{l_p - l_i} \times 100$$

2.2.6.2 Physiological Degradation and Water Uptake

Degradation studies were performed for the DCA-OD and DCE-CHDM series. Elastomer films of known weight (30-50 mg) were placed in 1 mL of 0.01 M pH 7.4 phosphate buffered saline (PBS) solution at 37 °C. The films were removed from the buffer solution at the prescribed intervals and dried under vacuum for 24 h before their masses were

measured. Each measurement was performed on three separate samples. Mass loss (ML) was calculated according to the following equation,

$$ML = \frac{m_i - m_f}{m_i} \times 100$$

Water uptake (WU) was measured for elastomer films placed in 0.01 M pH 7.4 PBS solution at 37 ^{o}C for prescribed intervals using the equations,

$$WU = \frac{m_{sw} - m_d}{m_d} \times 100 \qquad WU(Abs) = \frac{m_{sw} - m_i}{m_i} \times 100$$

where m_{sw}, m_d, and m_i represent the swollen mass, the dry mass, and the initial mass, respectively. Film samples of known weight were removed from PBS and blotted dry before weighing swollen mass, followed by drying under vacuum for 1 day to obtain the dry mass.

2.2.6.3 Cytotoxicity Studies

Initial cytotoxicity studies were performed by ATP assay using the HeLa cell line. Polymer material was placed in well plates containing cells and cell medium. Plates were incubated at 37 ^{o}C in the dark for 3 days, after which the percent viability was found using a CellTiter-Glo® luminescent cell viability kit which determined the amount of bioluminescent ATP present in cells. Each measurement was done in triplicate for crosslinked DCA-OD materials.

2.3 Results and Discussion

2.3.1 Monomer Synthesis

The successful synthesis of both diester monomers (DCA, DCE) and diol monomer (CAD) was achieved by reacting the acyl chloride derivative of cinnamic acid, with diethyl iminodiacetate, 3-hydroxygluturate, or diethanolamine at low temperatures (0 ^{o}C) (Scheme 2.2). Due to the high reactivity of acid chlorides, low temperatures were used in order to decrease reactivity and to control the heat generated. Triethylamine (Et_3N) was employed for the synthesis of DCA (**1**) and CAD (**3)** but could not be used for the DCE (**2)** synthesis due to the difference in nucleophilicity of the 2° amine and the 1° alcohol. Due to the nature of the less nucleophilic alcohol, Et_3N inhibits the reaction with cinnamoyl chloride because in the reaction mixture it is the most nucleophilic species. Pyridine, whose stabilized ring structure decreases its nucleophilicity, was employed instead.

The synthesis of multiple monomers allowed for the study of structure property relationships of the two linkage chemistries. The barrier of rotation around the amide or the ester linkage, as well as the position in the resulting polymer (the amide bond lies in the backbone, while the ester is one atom removed), was expected to affect the ability of intermolecular temporary crosslinks to be formed between two photo crosslinkable groups. The H^1-NMR of Monomer **1** (Figure 2.3, top) shows two shifts for the α-methylene peaks of the carbonyl groups (c_1 and c_2). The two inequivalent α-methylene groups are characteristic of an amide bond. Best represented in a resonance structure, the amide linkage leads to restricted rotation around the C-N bond. Depending on the magnitude of this rotational barrier, the two methylene groups can feel different magnetic environments at NMR pulse time scales shorter than the rotational rate. This gives rise to the two signals, one

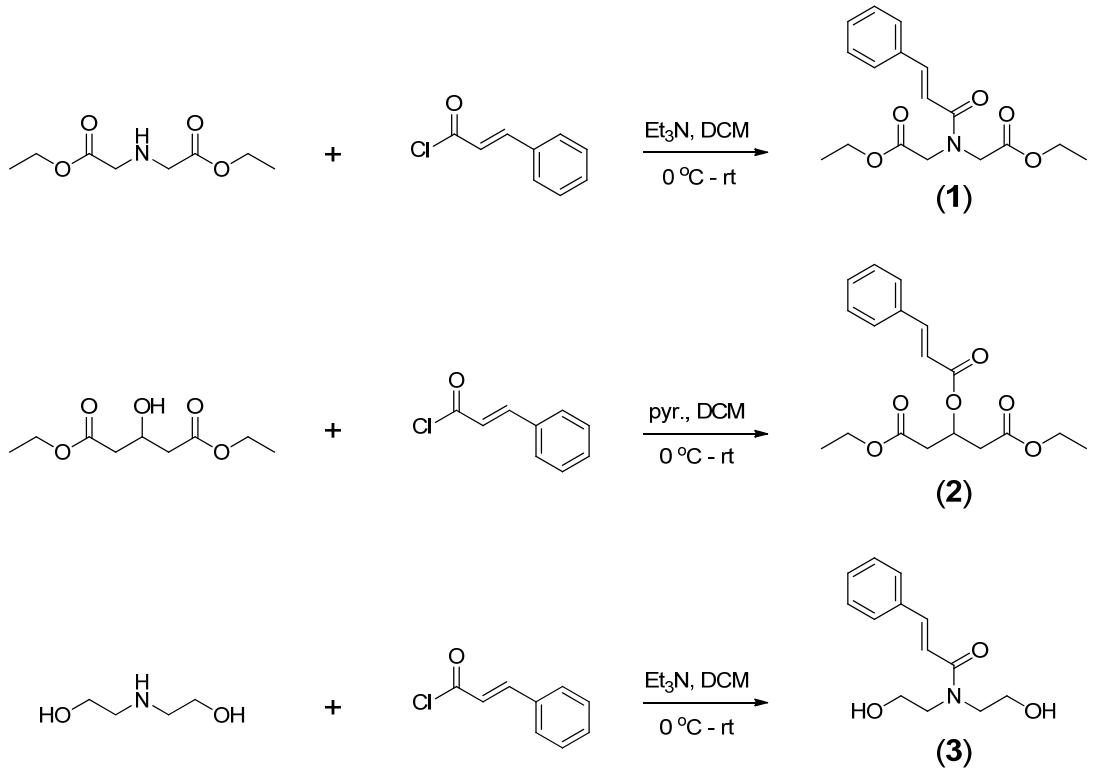

Scheme 2.2 Bifunctional photo-monomer synthesis.

corresponding to the *cis*-methylene and one to the *trans*-methylene with respect to the carbonyl. The restricted rotation is also evident in the overlapping of the other two methylene signals. Although these protons are not adjacent to the amide bond, they still encounter different magnetic environments. The same inequivalence can be seen in the ^{1}H-NMR of CAD (**3**), however, it is not as substantial due to the lower molecular weight of the substituents on the amine of the amide bond.

In DCE (**2**) the rotational barrier around the ester linkage is much smaller in magnitude. ^{1}H-NMR shows equivalent shifts for methylene protons unlike in DCA (Figure 2.3, bottom). The low barrier of rotation in DCE is also evidenced by its physical state; DCE is a viscous oil while DCA is a solid. It was expected that this extra freedom of movement

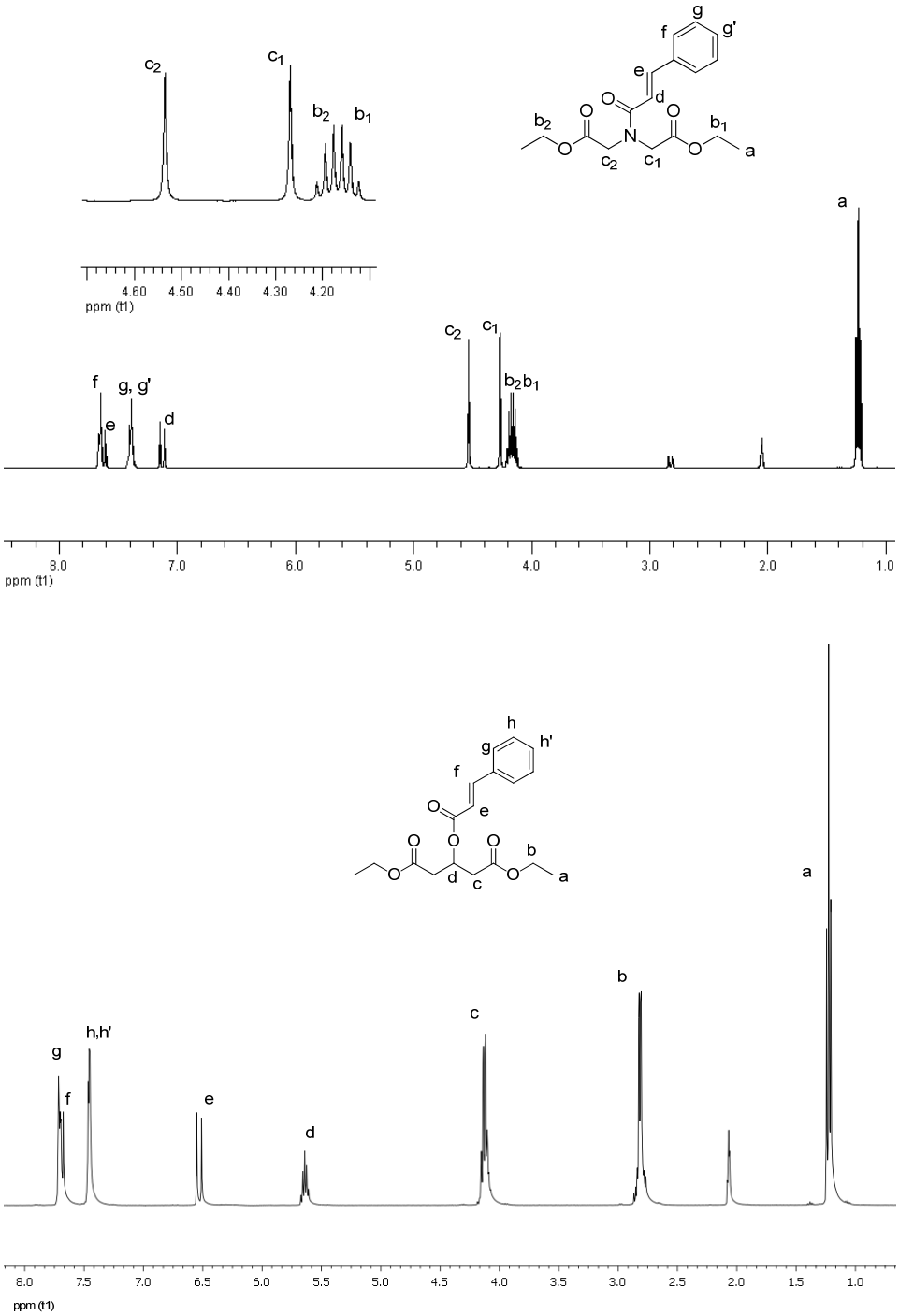

Figure 2.3 ^{1}H-NMR spectra of DCA (top) and DCE (bottom) with assignments. Expansion of α–methylene region for DCA inset.

will help increase the probability of cinnamate groups interacting in the solid state network in order to undergo the photo induced [2+2] cycloaddition.

2.3.2 Polymer Synthesis

The successful polycondensation of DCA with various diols was achieved by bulk melt polymerization with tin octoate catalyst, high temperatures (130 ^{o}C), and reduced pressures (0.1 atm). Scheme 2.3 (top) shows the reaction of DCA with 1,8-octanediol. The high reaction temperatures and reduced pressure was utilized to remove the ethanol condensate which is necessary to push the reaction to high conversion. The high temperature was also necessary to activate the catalyst. Tin octanoate (SnOct) in turn activates the ester group of the monomer for transesterification through coordination. Tin catalyzed polycondensation of DCE was not successful due to the transesterification of the cinnamate group during polymerization, which led to branching and loss of photo-groups. An enzymatic catalyst (Novozym 435-Lipase) was used instead for all polymerizations involving DCE. Novozym 435-Lipase catalyst is known to be directed towards primary alcohols or esters, thereby not affecting the photo-groups, and leading to linear polymer with no cleavage of photo groups. Scheme 2.3 (middle) shows the reaction of DCE with 1,4-cyclohexanedimethanol.

The diols utilized in reactions with the DCA and DCE monomers were 1,8-octanediol and 1,4-cyclohexanedimethanol, which were chosen due to the similarity in molecular weight and very different molecular structure. This allowed for the elucidation of structure/property relationships independent of molecular weight considerations. Polymerizations with the diol monomer CAD (**3**) and 1,4-cyclohexanedicarboxylic acid (Scheme 2.3, bottom) utilized the same conditions as polymerizations of DCA. The stoichiometry of the monomer feed was

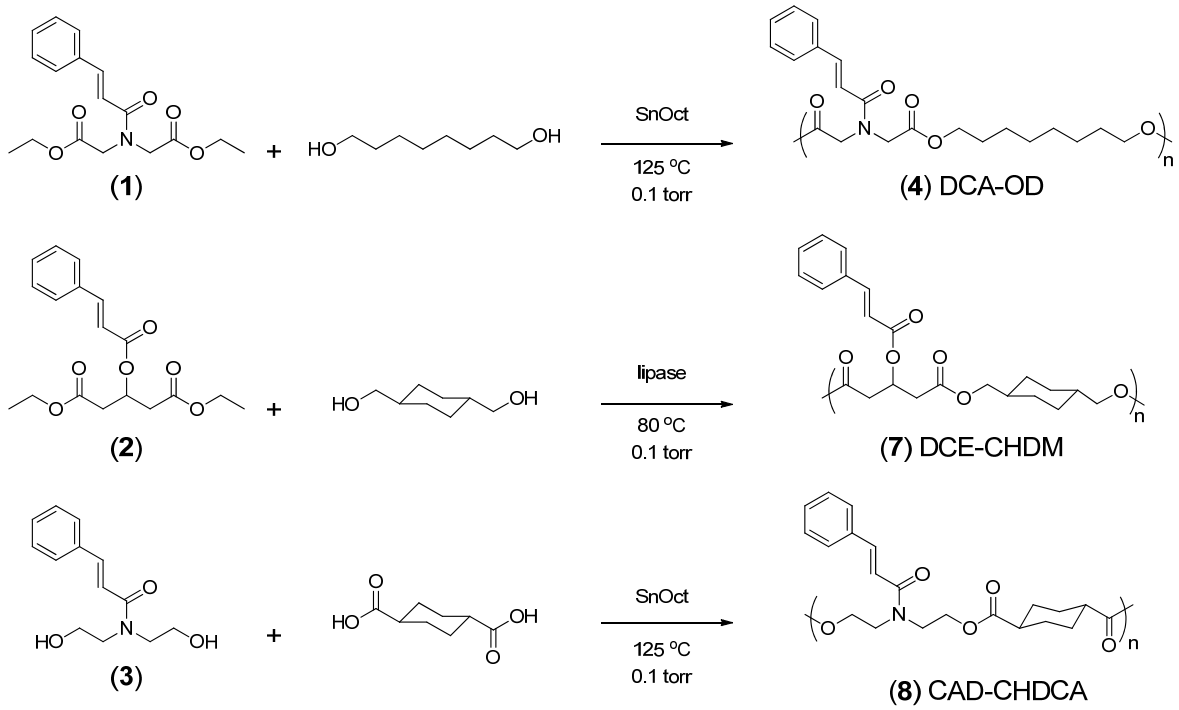

Scheme 2.3 Polymerization of polyester prepolymers.

used to target molecular weights based on a calculated imbalance. This imbalance uses the diol in excess, thereby controlling the chain ends and giving hydroxyl-terminated polymers.

Unsaturated endgroups were successfully added to the polymer chain ends via the reaction of hydroxyl-terminated polyesters with 2-isocyanatoethyl methacrylate in CH_2Cl_2 at reflux for 2 h. These cross-linkable unsaturated ends can be thermally initiated by a free radical initiator AIBN, reacted with a thiol crosslinker through a thiol-ene method, or photo-initiated, however, there is the likelihood of the latter affecting the photo-responsive moieties in an undesired manner. Therefore only the two thermal methods were utilized to form thermoset networks.

2.3.3 Thermal and Mechanical Analysis

The results of molecular weight analysis and thermal characterization for photo-responsive prepolymers can be found in Table 2.1. Molecular weights measured by gel

permeation chromatography show good correlation with stoichiometric imbalance to target polymer chain length and endgroups. A wide range of glass transition temperatures (T_g) for the completely amorphous prepolymers were seen, with the cyclic diol monomer restricting rotation and giving rise to higher glass transitions (~30 ^oC higher T_g than DCA-OD). The linkage chemistry between the polymer backbone and the pendant photo-group also affected the thermal properties. Comparing prepolymers containing the same diol monomer (linear or cyclic), those possessing cinnamamide linkages generally saw an increase of T_g by ~40 ^oC over those with cinnamate linkages. This is again associated with the rotational barriers around the different linkage bonds. Higher thermal decomposition temperatures were also

Table 2.1 Molecular weight and thermal characterization of photo-responsive prepolymers.

Polymer Sample	$\overline{M}_n$ [a] (g/mol x 10^-	$\overline{M}_w / \overline{M}_n$ [a]	Decomposition Temp.[b] 5% (^oC)	10% (^oC)	T_g (^oC)[c]
DCA-OD-5	5.4	1.6	301	319	4
DCA-OD-8	7.9	1.8	371	395	6
DCA-CHDM-5	4.9	1.9	365	382	35
DCA-CHDM-8	7.2	1.4	343	414	43
DCE-OD	1.9	2.1	248	268	-34
DCE-CHDM	2.7	1.6	293	306	-7
CAD-CHDCA	4.0	1.8	306	338	15

[a]GPC- PS Stds. [b]TGA. [c]DSC.

Table 2.2 Thermal and mechanical properties of photo-responsive thermoset networks.

Series	Prepoly MW (g/mol)[a]	Decomposition 5% (°C)	Decomposition 10% (°C)	T_g (°C)[c]	*G* (MPa)[d]	Break[d]
DCA-CHDM	7000	322	355	52	61.0	5 %
DCA-OD	8000	366	392	20	28.0	32 %
DCE-CHDM	3000	300	319	7	15.7	90 %
DCE-OD	2000	267	340	-13	0.4	330 %

[a]GPC- PS Stds, [b]TGA, [c]DSC, [d]Instron (23 °C)

seen for amide containing prepolymers synthesized with either DCA or CAD monomers. Having these two handles to alter thermal properties, as well as the impact of varying molecular weights, allows for the creation of a range of material properties.

The amorphous nature of the prepolymers made for easier processing to form permanent networks of desired size and shape by molding or solvent casting. Table 2.2 shows the thermal and mechanical properties of the resulting thermoset networks. As was expected the T_g increased from prepolymer to thermoset network by about 15 °C and again, a large range of glass transition temperatures is seen which in turn produces a range of mechanical properties as characterized by Instron at room temperature (23 °C). DCA-CHDM

exhibited the highest Young's modulus (61 MPa) with very small elongation (5%) demonstrating its brittle nature at room temperature due to a higher T_g (52 °C). Within the same photo monomer series, DCA-OD possesses a lower modulus (28 MPa) relative to the cyclic series due to the lower glass transition but still displays some rigidity due to the T_g

being in proximity to room temperature. On the other hand, the two DCE series are softer materials with DCE-OD having a modulus two orders of magnitude lower than the other series (0.4 MPa). This range of moduli allows matching of different tissues in the body such as blood vessels, muscles, tendons, and cartilage which is known to be advantageous for applications where devices are in direct contact with tissue.[16,17]

2.3.4 Degradation and Cytotoxicity

Physiological degradation studies were performed to determine the hydrolytic degradation properties of representative systems for both diester photo-monomers. Samples of DCA-OD and DCE-CHDM were weighed and then placed in PBS solution with pH = 7.4 at 37 ^{o}C in order to mimic physiological conditions. The samples were removed, dried, and

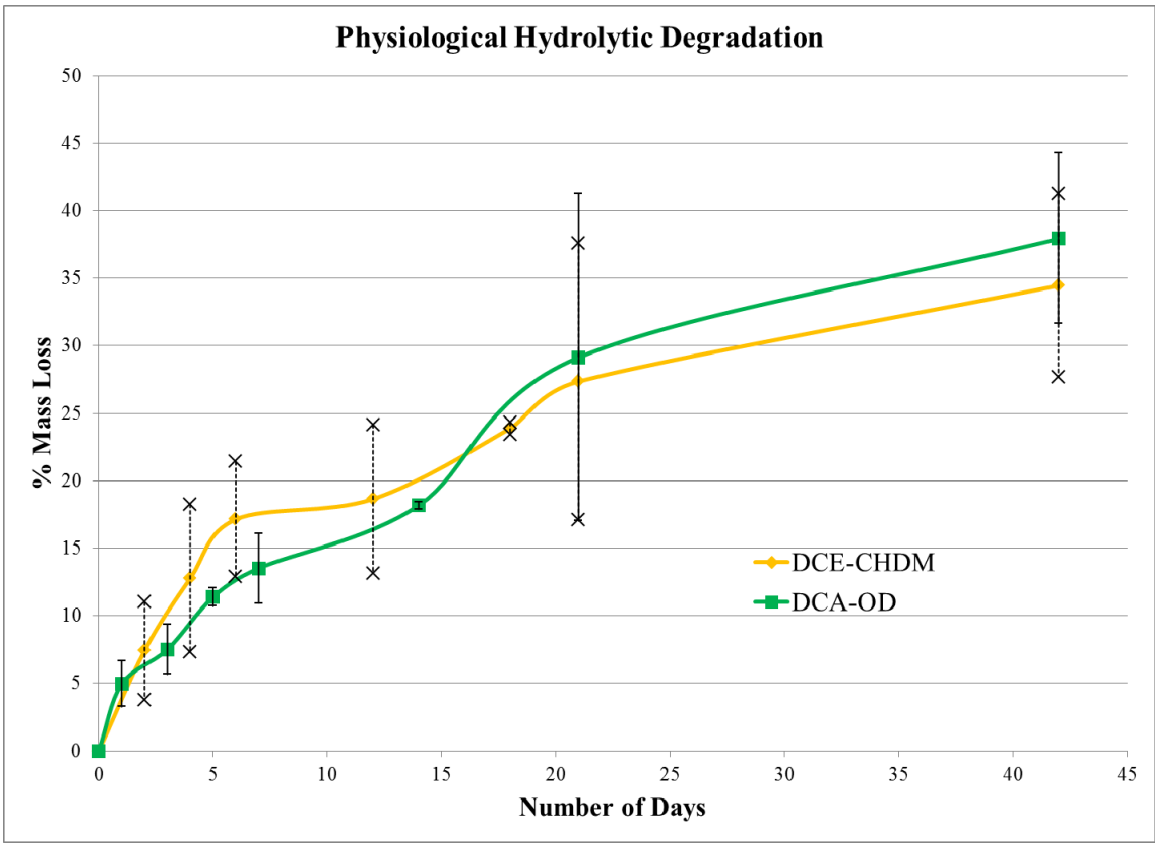

Figure 2.4 Physiological hydrolytic degradation of DCA-OD and DCE-CHDM in PBS (pH = 7.4) at 37 ^{o}C.

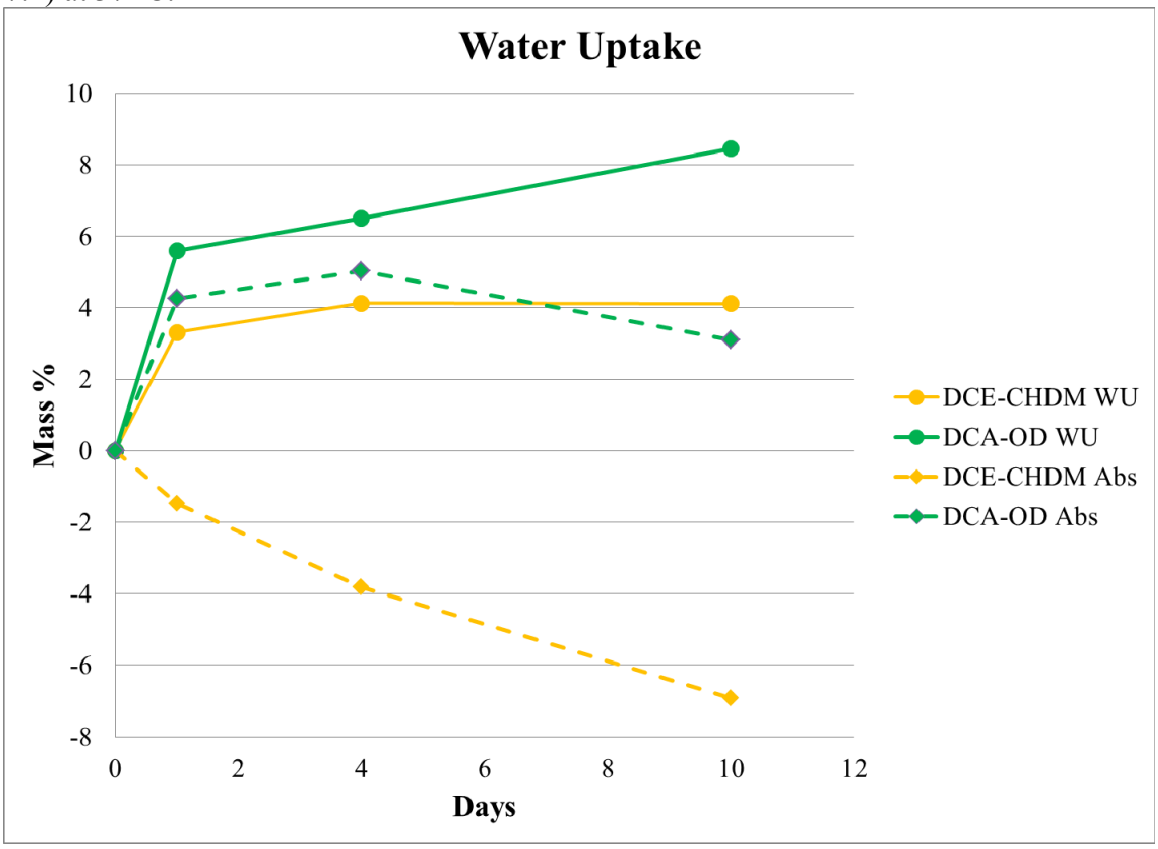

Figure 2.5 Water uptake for DCA-OD and DCE-CHDM.

weighed after different periods of time up to 42 days for initial studies. The results for both series can be seen in Figure 2.4 as the percent mass loss after the prescribed time intervals. It was expected there would be a difference seen in the rates of degradation between the DCA and DCE series due to the chemical nature of the pendant groups. The amide linkages in DCA are not susceptible to hydrolytic degradation in comparison to the ester linkages of the DCE system as well as the polymer backbone linkages of both series, however the amide linkage is more hydrophilic then an ester linkage. As can be seen in Figure 2.4, during the initial period of degradation (10-15 days) a larger percentage of mass loss is seen in the DCE

system which can attributed to hydrolytic degradation of both pendant and backbone linkages near the surface of the bulk material. At longer periods of time the DCA system shows slightly greater mass loss and it is believed to be due to the ability for water to penetrate

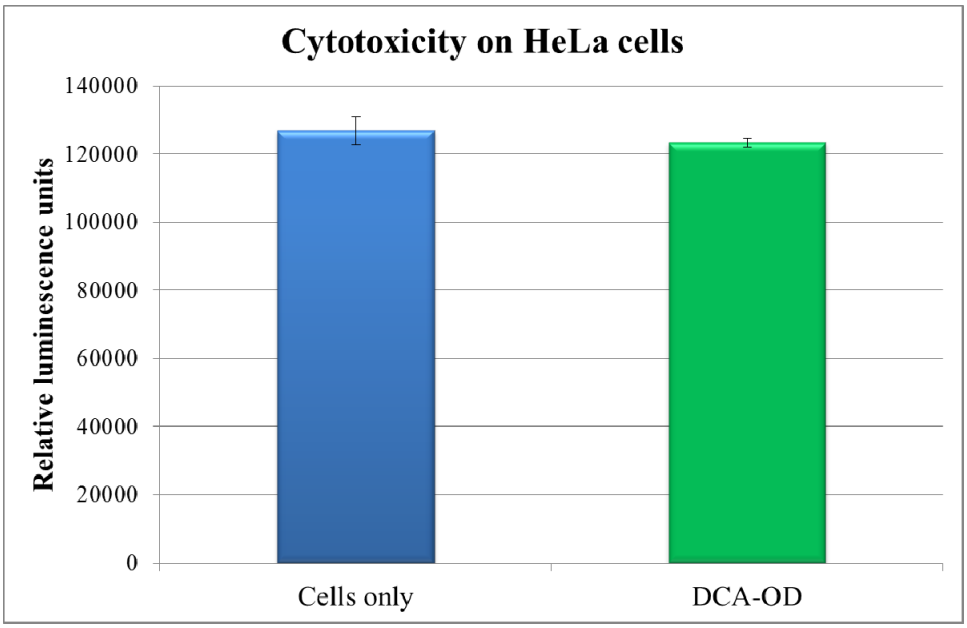

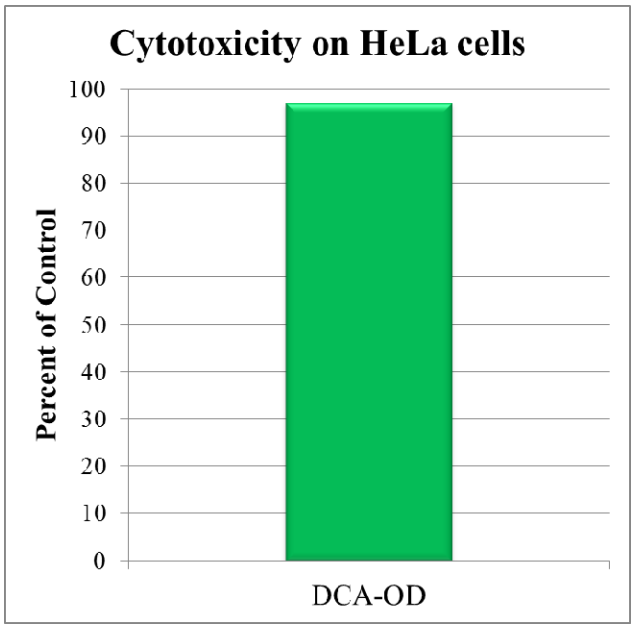

Figure 2.6 Cell viability measured by CellTiter-Glo® ATP luminescence assay. Relative luminescence count (top), percent of control count (bottom).

further into the bulk material after a period of time due to the more hydrophilic nature of the amide linkages. The water uptake study performed verified this assumption (Figure 2.5), with the DCA-OD series (solid green) absorbing a larger weight % of water compared to the DCE-CHDM series (solid orange). The absolute change in mass, taking into account degradation and water uptake was also measured for both systems and as can be seen in Figure 2.5 for the DCE-CHDM (dashed orange) series, the mass loss from degradation negates any mass gained by water uptake to give a negative weight % even after 1 day. The DCA-OD series (dashed green) on the other hand does not see a loss in total mass until the 10 day mark when the loss by degradation is larger than the mass added by water swelling.

Preliminary cytotoxicity studies of the DCA-OD system determined using an ATP bioluminescence assay showed minimal to no cytotoxicity in the HeLa cell line (Figure 2.6). Materials were plated in cell medium but not in direct contact of cells in the well. After 3 days of incubation at 37 ^{o}C, where any matter eluted from the polymer material was able to interact with the cells, the percent viability was quantified using a CellTiter-Glo® assay kit. Compared to control wells containing only cells in medium, there was only a small decrease in the relative luminescence count when in the presence of one unit of polymer material (97% viability).

2.3.5 Light-induced Shape Memory

Film samples were deformed and irradiation with UV light (λ = 302 nm) was used to temporarily crosslink samples in the programmed state by inducing an increase in crosslink density due to the temporary netpoints. Release of the stress did allow the system to relax to the point at which the temporary netpoints held the strain, meaning a decrease in the strain fixity of the system. Irradiation with UV light (λ = 254 nm) cleaved a percentage of the

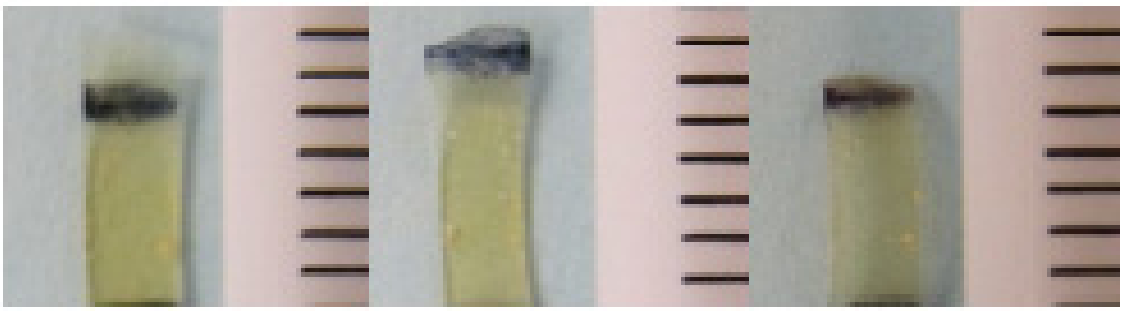

Figure 2.7 Macroscopic light-induced shape memory of DCA-OD network.

temporary crosslinks and the system recovered. Table 3 shows the values for strain fixity and strain recovery for the DCA-OD and DCE-CHDM series. In order to deform the material it must be in a rubbery state so the DCA-OD system was heated above the T_g the process to allow deformation and remove any thermal effects.

The examination of macroscopic light-induced shape memory properties focused on a uniaxial force of stretching to a specified percent elongation (Figure 2.7), however bending deformations can be programmed as well as induced. By stretching a film sample and irradiating only one side of the film during the UV fixing step (λ = 302 nm), removal of the stress allows the opposite side to relax and bend the film.

The amide-containing system showed strain fixity and strain recovery consistent with previously published materials ($R_f \approx 50\%$, $R_r \approx 90$ %). On the other hand, the DCE-CHDM system that possesses the ester linkage between the polymer backbone and the pendant photo-groups saw an increase in fixity (70-85%) however a decrease in recovery (40-70%). This suggests that the uniform distribution of the more mobile ester linked cinnamates allowed for a higher temporary crosslink density which inhibits large relaxations of the polymer chains between netpoints. The decrease in recovery can be attributed to the

incomplete cleavage of the temporary network which is known to occur during irradiation with UV light (λ = 254 nm).[18]

Different percentages of elongation were employed to study the effect of amount of strain on the fixity and recovery in the DCA-OD system. Shown in Table 3 are the values for 20%, 30%, and 40% elongation. As strain is increased from 20% to 30% there is a slight increase in R_f and a large increase in R_r. The change in the recovery of the system was expected because with larger fixed strains, it was presumed the larger relaxation of the polymer chains when temporary crosslinks were cleaved. It is also known that not all temporary crosslinks are cleaved during the recovery process, so at higher strains ($\geq$ 40%), there is a decrease in recovery as well as fixity indicating the shortcomings of LSM for larger deformations.

Table 2.3 Characterization of light-induced shape memory in DCA-OD and DCE-CHDM series.

				Irradiation Time	
Series	Elongation %	R_f (%)	R_r (%)	Fixing (min)	Cleaving (min)
	20	47	76	60	90
DCA-OD	30	50	91	60	90
	40	42	88	60	90
	30	69	73	60	60
DCE-CHDM	30	76	67	90	90
	30	86	42	150	150

The irradiation time for each step of the programming and recovery process was also varied to study the effect on R_f and R_r using the DCE-CHDM system. An equivalent percent elongation was used for each sample (30%) while varying the irradiation time for fixing and cleavage from 60 to 150 min. As would be expected, the R_f increased with longer irradiation time during the programming process, but as noted previously R_r saw a decrease in comparison to the DCA-OD system even with longer irradiation times during the recovery process. Longer irradiation during fixation results in higher crosslink density, or greater concentration of dimerized photo-groups. During recovery, partial cleavage leaves the system with more netpoints than in the original state. For samples programmed for longer time periods, the residual netpoints after recovery inhibit relaxation of the polymer chains to their most entropically favorable conformation.

2.4 General Conclusions

The synthesis of a library of poly(ester urethane)s (PEUs) containing pendant photo-responsive moieties afforded through the incorporation of one of three bifunctional monomers, DCA and DCE being novel monomers, results in uniform degradable materials. By interchanging the two diester photo-monomers and cyclic/linear diols, a range of thermal and mechanical properties were realized; glass transition temperatures ranged from -10 – 50 ^{o}C and Young's modulus ranging 0.4 – 60 MPa. Utilizing light irradiation, macroscopic temporary shapes can be fixed by increasing the crosslink density of a thermoset network via photo-induced reversible [2+2] cycloaddition of cinnamamide or cinnamate pendant groups under UV light (λ = 302 nm), and irradiation with UV light (λ = 254 nm) **cleaves** the temporary crosslinks and recovers the original shape. Possessing an ambient temperature

switch allows triggering to be more discriminate and the limitation of a narrow temperature range for biomedical applications is avoided making our system advantageous.

2.5 Acknowledgements

The authors would like to thank Christopher Luft for help with cell work and cytotoxicity assays. This research was funded by the National Science Foundation (Department of Materials Research) under Grant 0418499.

References

1) Neuss, S.; Blomenkamp, I.; Stainforth, R.; Boltersdorf, D.; Jansen, M.; Butz, N.; Perez-Bouza, A.; Knuchel, R. *Biomaterials* 2009, *30*, 1697.

2) Mather, P.T.; Luo, X.; Rousseau, I.A. *Annual Review of Materials Research* 2009, *39*, 445.

3) Raymond, L. *Journal of Biomedical Materials* 2007, *2*, 23.

4) Gunes, I.S.; Jana, S.C. *Journal of Nanoscience and Nanotechnology* 2008, *8*, 1616.

5) Baer, G.M.; Small, W.; Wilson, T.S.; Benett, W.J.; Matthews, D.L. *Biomedical Engineering Online* 2007, *54*, 1657.

6) Vaia, R. *Nature Materials* 2005, *4*, 429.

7) Razzaq, M.Y.; Anhalt, M.; Frormann, L.; Weidenfeller, B. *Materials Science and Engineering A* 2007, *444*, 227.

8) Huang ,W.M.; Yang, B.; An, L.; Li, C.; Chan, Y.S. *Appl. Phys. Lett.* 2005, *86*, 114105.

9) Behl, M.; Lendlein, A. *J. Materials Chem.* 2010. *20*, 3335.

10) Maitland, D.J.; Metzger, M.F.; Schumann, D.; Lee, A.; Wilson, T.S. *Lasers in Surgery and Medicine* 2002, *30*, 1.

11) Li, M.H.; Keller, P.; Li, B.; Wang, X.; Brunet, M. *Adv. Mater.* 2003, *15*, 569.

12) Yu, Y. L., Nakano, M. & Ikeda, T. *Nature* 2003, *425*, 145.

13) Lendlein, A.; Jiang, H.Y.; Junger, O.; Langer, R. *Nature* 2005, *434*, 879.

14) Wu, L.; Jin, C.; Sun, X. *Biomacromolecules* 2011, *12*, 235.

15) Lee, K.M.; Koerner, H.; Vaia, R.A.; Bunning, T.J.; White, T.J. *Soft Matter* 2011, *7*, 4318.

16) Engler, A.J.; Sen, S.; Sweeney, H.L.; Discher, D.E. *Cell* 2006, *126*, 677.

17) Discher, D.E.; Janmey, P.; Wang, Y. *Science* 2005, *310*, 1139.

18) Jin, C.; Sun, X.; Wu, L. *Des Monomers Polym*. 2011, *14*, 47.

Chapter III

MULTIFUNCTIONAL TRIPLE SHAPE MATERIALS: COMBINATION OF LIGHT AND THERMAL ACTUATION

3.1 Introduction

The extension of the shape memory phenomenon from dual to triple shape memory allows for more complex movement. Triple shape memory (TSM) systems possess two independent transitions, so when programmed accordingly the material can retain two temporary shapes and upon actuation recover the original shape through a multipart motion (Figure 3.1).[1] To date, most TSM systems rely on multiphase polymer networks that possess two phase-separated domains, each associated with independent thermal transitions.[2] The

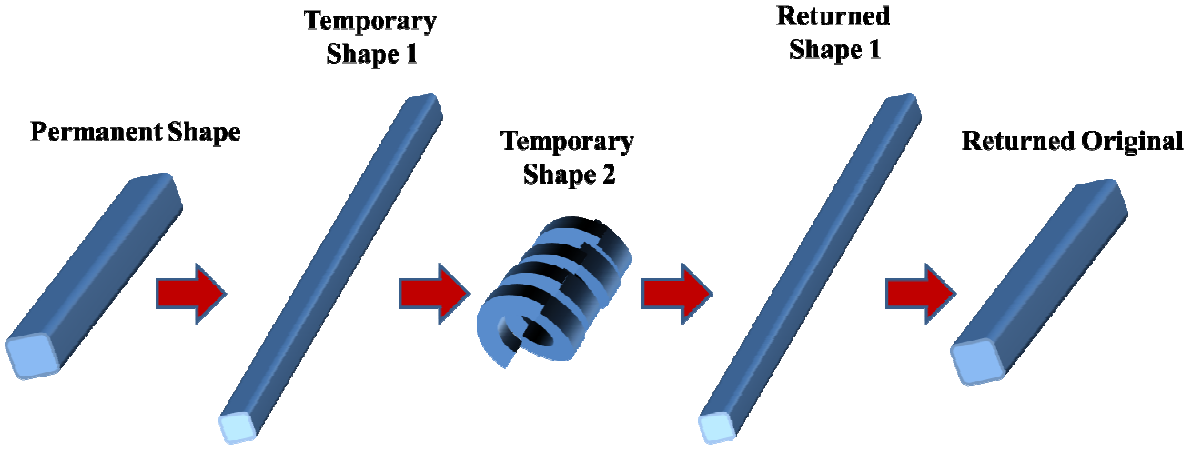

Figure 3.1 Triple shape memory cycle.

triggers can be a combination of two melting and/or glass transition temperatures in the different phases[3,4,5], or it has also been shown that programming at different temperatures within a broad transition can also result in independent switching.[6]

For both dual and triple shape materials in biomedical applications, targeting thermal transitions can be challenging and little flexibility for tailoring other properties remains once T_{trans} has been set. This obstacle is even more pronounced for TSM where targeting two distinct transitions within a small window of temperatures suitable for organs and other areas of the body while also keeping in mind the requirements of a biomaterial is difficult.

Triple shape systems require a specific programming method to induce two temporary shape changes. These methods can focus on either macroscopic changes or microscopic changes, with the latter being of great interest for applications such as adhesion and cell study.[7] SMPs have been employed that possess surface shape memory (SSM) by processing temporary topography switching. This is possible by embossing the surface of a polymer substrate, resulting in the negative of the pattern used to deform the surface. Surface features on the micro and nanoscales have been programmed as temporary shapes which can be erased by triggering recovery of the original flat surface.[8,9] It is also possible to form permanent networks with surface arrays, that can then be programmed with a second pattern in the temporary shape in order to switch between surface features of different shape, size, aspect ratio.[10] Recently, SSM was extended into a multiple shape memory system, where two or three temporary shapes were programmed, all different nanoscale patterns, using a broad T_g.[11] Dual and multishape SSM creates a dynamic surface with micro-patterned arrays which can be used to control surface properties such as adhesion and

wetting, as well as use topography on micro/nano scales to influence cell responses through surface interations.[12,13,14]

Herein we present the characterization of a series of biodegradable amorphous poly(ester urethane) prepolymers which are functionalized with photo-responsive pendant groups uniformly distributed along the polymer backbone that possess both light-induced and thermal dual shape memory. Furthermore, by combining the independent photo switch with the thermal transition in the same network we have developed a novel biomaterial that boasts the triple shape memory effect with only one targeted T_{trans} necessary. The result is a triple shape polymer network where triggering is more discriminate compared to those systems that rely solely on thermal transitions. In addition, by utilizing soft lithography in our thermal programming method we have developed the first example of a multifunctional material that can independently switch on macroscopic and microscopic levels.

3.2 Experimental Section

3.2.1 Materials

All materials were purchased from Sigma Aldrich unless otherwise noted. Thermoset networks (DCA-OD, DCA-CHDM) analyzed within are from Chapter II. PRINT™ molds for surface embossing were provided by the DeSimone group.

3.2.2 Instrumentation

Thermal transitions were analyzed using TA Differential Scanning Calorimeter Q200. Stress-strain data for thermal shape memory transitions was collected on a Pyris Diamond Dynamic Mechanical Analyzer with liquid N_2 cooling unit.

3.2.3 Light-induced Shape Memory Characterization

Characterization of light-induced shape memory properties followed the same method as found in Chapter II.

3.2.4 Thermal Shape Memory Characterization

3.2.4.1 Macroscale Shape Memory

Dynamic mechanical analysis (DMA) was used to measure strain fixity and strain recovery for macroscopic thermal shape memory. The DMA programming/recovery cycle method was as follows: sample was heated to 20 ^{o}C above T_g at a rate of 5 ^{o}C/min; stress was applied to the prescribed magnitude of force at a rate of 100 mN/min; sample under stress was cooled below 0 ^{o}C at a rate of 20 ^{o}C/min; stress was removed; sample was heated to 20 ^{o}C above T_g at a rate of 5 ^{o}C/min. Using the resulting data, the strain fixity (R_f) and strain recovery (R_r) were calculated.

For programming a variety of shapes (bending, twisting, coiling) the following general procedure was used. Samples were heated in an oven at 20 ^{o}C above the T_g for ~15 min and then deformed and cooled to 2 ^{o}C to fix the temporary shape. Temporary shapes were persistent at room temperature and recovery occurred when placing the temporary shape into an oven or water bath above T_{trans}.

3.2.4.2 Microscale Surface Shape Memory

Shape programming on a microscopic level was possible utilizing PRINT^{TM} (particle replication in non-wetting templates) technology[15] to emboss the surface of films using a previously determined method.[9] Polymer films are heated above T_{trans} and the PRINT^{TM} mold was placed onto the film surface, which was then placed between glass slides in a press. The press containing the molded film was placed in an oven above T_{trans} for 30 min and then

cooled at 2 ^{o}C for 1 h. Recovery of the permanent surface topography was accomplished by heating above T_{trans} for 30-60 min. Flat surfaces and embossed surfaces with microscopic features were imaged using a Zeiss Imager D.1m microscope with AxioCam. A halogen bulb source was used for brightfield imaging under 100x magnification.

3.3 Results and Discussion

3.3.1 Thermal Shape Memory

The prepolymers and resulting thermoset networks are similar to other step-growth poly(ester urethane)s synthesized in our group that possess thermal shape memory properties with either $T_{trans} = T_g$ or $T_{trans} = T_m$.[9,10] As these materials are fully amorphous, there are no melting transitions that can be used for T_{trans}, so a T_g at or above room temperature is needed to fix the temporary shape without keeping cooled. Therefore, the potential for thermal shape memory was investigated in the DCA series using the T_g as the triggering temperature, while the DCE series was excluded. In the crosslinked network state, DCE materials possess glass transition temperatures (-13 – 7 ^{o}C) below an applicable temperature for packaging to remain persistent.

3.3.1.1 Delocalized Macroscopic Shape Memory

The macroscopic SME for DCA-OD and DCA-CHDM was realized by heating films above T_{trans} (T_g = 20 ^{o}C and 52 ^{o}C, respectively) and applying a force or stress. Cooling below T_{trans} fixed the programmed shape and the original shape was recovered by again heating above T_{trans}. In the case of the DCA series, T_{trans} is the T_g of the material. As is the case with most SMPs on the macroscale, the shape change is delocalized meaning it occurs throughout the entire material when heat is applied. A cantilever-like film of DCA-OD (Figure 3.2, top-left) was heated to 40 ^{o}C and packaged into a temporary ribbon shape (Figure

3.2, top-middle) before cooling at 2 ^{o}C. Heating triggered the recovery of the permanent shape (Figure 3.2, top-right). In the case of DCA-CHDM, the permanent shape (Figure 3.2, bottom-left) was heated to 80 ^{o}C and coiled followed by cooling to form a helical temporary shape (Figure 3.2, bottom-middle). Heating above T_{trans} restores the original shape (Figure 3.2, bottom-right).

Table 3.1 Thermal shape memory characterization.

Series	T_g (^{o}C)[a]	R_f (%)[b]	R_r(%)[b]
DCA-CHDM	52	> 99	83
DCA-OD	20	92	96

[a]DSC, [b]DMA

DMA testing was used to quantify the R_f and R_r of the systems (Table 3.1) using a cyclic programming/recovery method. Both the cyclic and linear series showed strain fixity > 90% with DCA-CHDM having near quantitative fixation (>99%). Strain recovery was greater in the DCA-OD (96%) while the cyclic series showed incomplete recovery (R_r = 83 %) at heating times < 30 min. This could be due to the T_g being a broad thermal transition, which requires a longer period of time to fully complete the switch. This can be avoided by increasing the temperature at which the sample is recovered as is the case for the macroscopic example of DCA-CHDM in Figure 3.2 which was heated to 90 ^{o}C instead of T_{trans} + 20 ^{o}C (~70 ^{o}C).

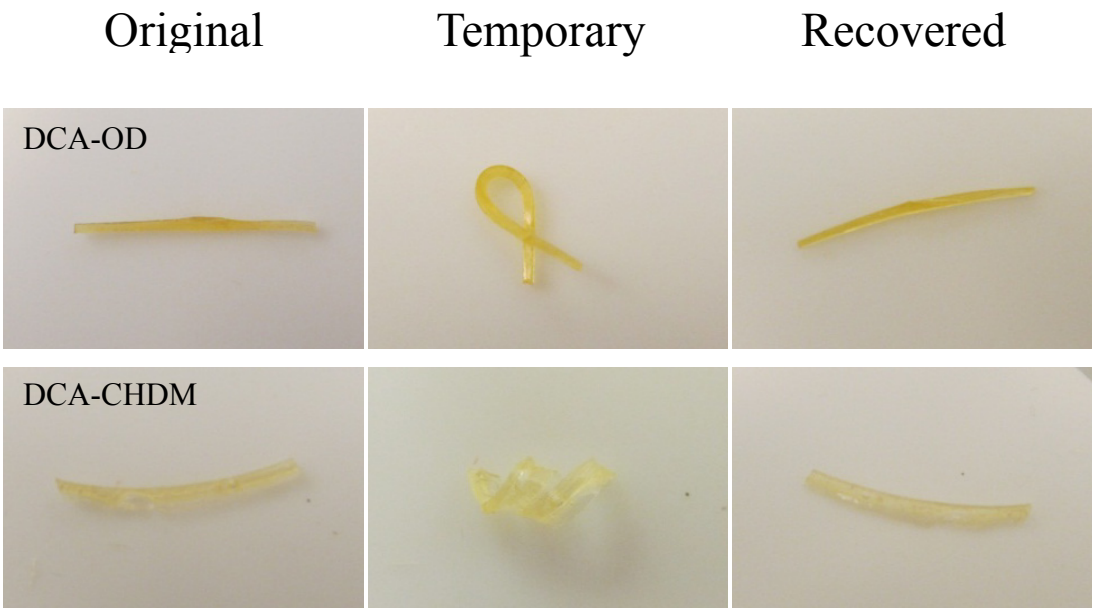

Figure 3.2 Macroscopic thermal shape memory of DCA-OD (top) and DCA-CHDM (bottom) networks.

The broad glass transition is used to our advantage for the DCA-OD system which possesses a T_g just below room temperature. Rather than targeting a higher glass transition temperature by adjusting MW or crosslink density, we are able to adjust T_{trans} by our programming method. Heating the material slightly above the T_g (T = 25 ^oC) and programming results in a temporary shape which is persistent for only 30-60 min at room temperature. However, if we program at the higher end of the broad glass transition (T = 35 ^oC), the resulting temporary shape is persistent on the order of hours at room temperature or can be recovered on the order of minutes at 40 ^oC.

3.3.1.2 Localized Surface Shape Memory

Reversible microscale surface features were successfully programmed into the surface of elastomer films using a soft lithography embossing method. A variety of shapes and sizes were patterned into the surface by heating film samples and applying a perfluoropolyether (PFPE) mold under pressure by compressing between glass slides in a

mechanical press. The elastomeric PFPE molds are replica molds of silicon master templates used to create reproducible pattern arrays on micro and nanoscales. The result is transfer of a repeatable surface pattern onto the surface of the polymer film. Heating is required to exceed T_{trans} and create a rubbery surface that can be deformed. A sufficient amount of consistent pressure is also needed to force the thermoset film surface into the mold. Additionally, permanent surface features can be built into the film by applying the mold in the crosslinking process. During heating of the prepolymer solution, the mold can be placed on top of the film, and capillary action allows filling of the mold. After thermosetting, removal of the mold leaves micro-features in the original shape, which can be programmed over with secondary features of different sizes and shapes, and then recover the primary pattern after triggering return.

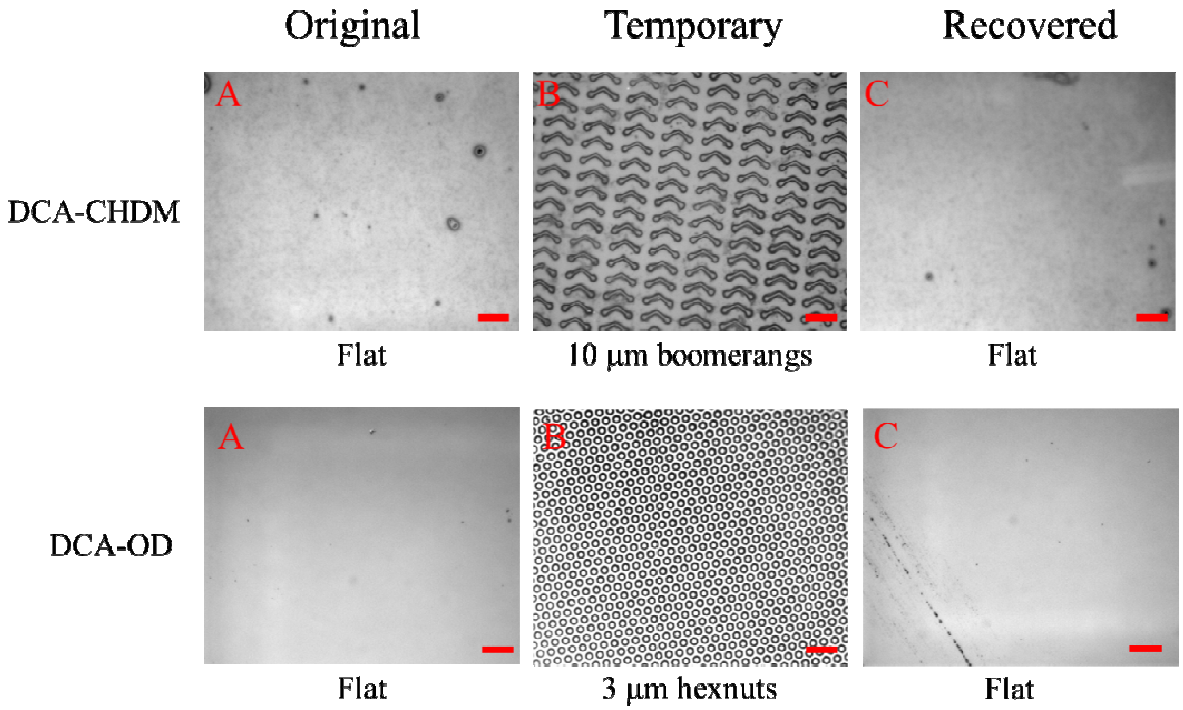

Figure 3.3 Bright-field microscope images of microscopic thermal shape memory of DCA-CHDM (top) and DCA-OD (bottom) networks, scale bar = 10 µm.

Figure 3.3 shows the original, temporary, and recovered surfaces of the DCA-OD (bottom) and DCA-CHDM (top) series. Starting with a flat surface (top left), the DCA-CHDM film was patterned with a 10 μm boomerang array (top middle) through the previously mentioned embossing method, which was persistent for the time period it was kept below T_{trans} (52 ^{o}C). Heating the film above T_{trans} erased the micropattern and returned the flat surface (top right) after 30-60 min with no noticeable change to the macroscopic dimensions of the film, showing the delocalized nature of the surface SME. Again the length of time required to recover the permanent shape is an artifact of the broad glass transition. The same temperature method used in the macroscopic shape programming for the DCA-OD system was also employed for microscale embossing in order to create a persistent temporary shape. Figure 3.3 shows the original flat surface (bottom left), the temporary patterned surface using a 3 μm hexnut mold (bottom middle), and the recovered flat topography (bottom right).

3.3.2 Triple Shape Memory

Having determined the independent thermal (3.3.1) and light-induced shape memory properties (Ch II) in the DCA materials series, we explored the potential to combine both mechanisms within the same programming method to package two temporary shapes, resulting in a triple shape material. The order in which programming occurs determines the extent with which the system can change shape from temporary shape to temporary shape. Beginning with thermal programming prevents larger deformation of the system during photo programming because it must remain below the T_g and therefore in the glassy regime. However, light irradiation after thermal programming can lead to an increase in the crosslink

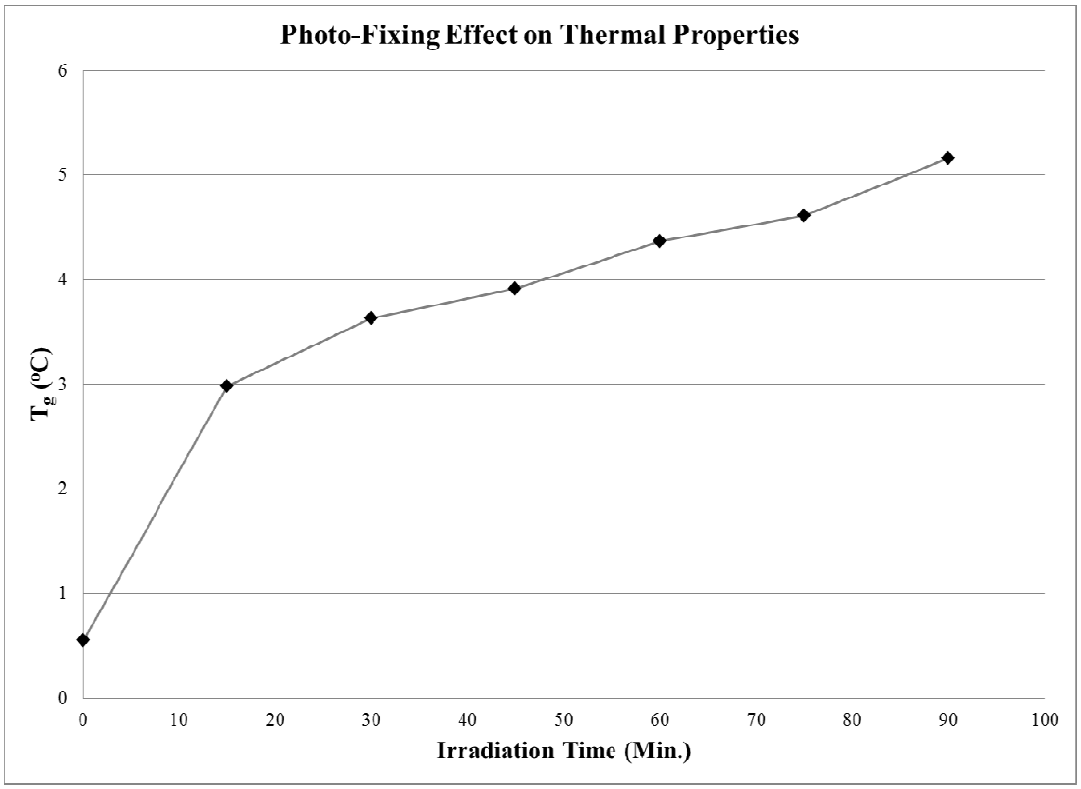

Figure 3.4 Effect of photo-fixing on the glass transition temperature of a thermoset DCE-CHDM film.

density of a system in an unstressed state which will alter the thermal and mechanical properties of the system.

A thermoset DCE-CHDM network (Initial T_g = 0.5 ^oC) prepared using a lower MW prepolymer was irradiated with UV light (λ = 302 nm) for allotted periods of time while under no external stress and then DSC was used to determine the T_g of the material. An increase in T_g can be attributed to an increase in crosslink density due to the formation of temporary netpoints and an irradiation time of 90 minutes saw an increase of nearly 5 ^oC (Figure 3.4). While not directly tested this presumably also increases the modulus of the material. On the other hand a triple shape memory programming process that begins by

photo-processing followed by thermal processing allows for the packaging of two distinct temporary shapes.

3.3.2.1 Combination Macroscopic/Macroscopic Triple Shape Memory

DCA-OD was programmed following the process illustrated in Figure 3.5 beginning with deforming the system on the macroscale and UV fixing (i) to create an elongated temporary shape. As mentioned earlier, it is necessary to heat the film above the T_g in order to deform so with continued heating, a second deformation step to bend the elongated film followed by cooling (ii) fixes the second temporary shape. Recovery of the triple shape material occurs in the opposite order whereby heating (iii) triggers the return to the first temporary shape and UV cleaving (iv) recovers the original shape. This process can be

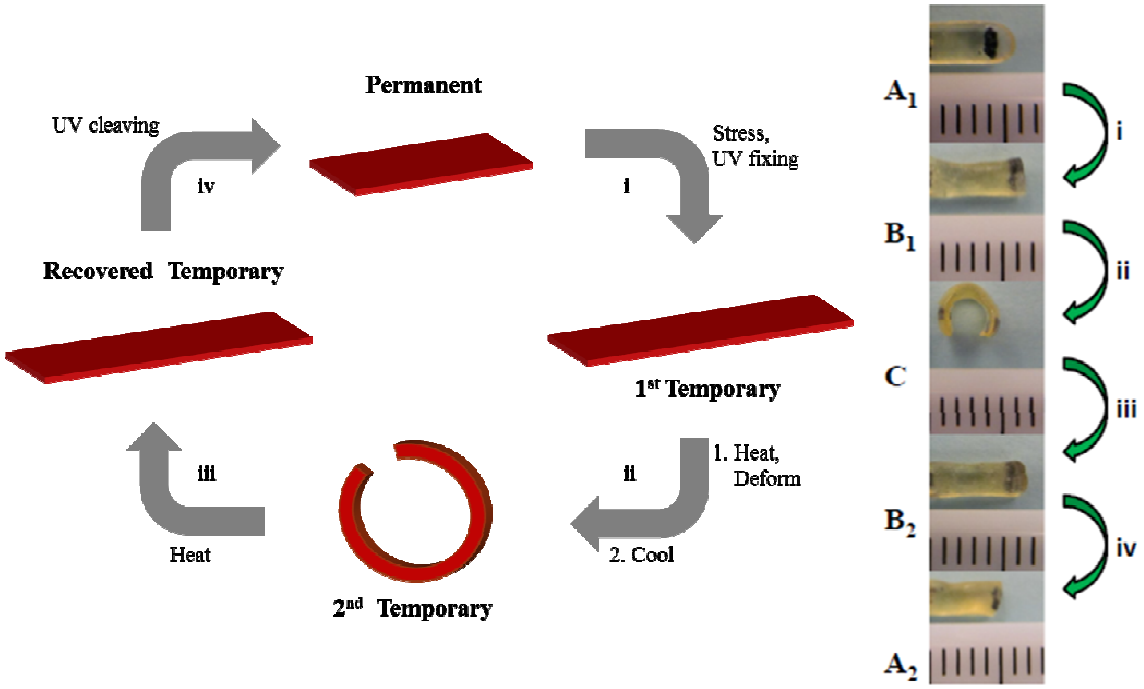

Figure 3.5 Macroscopic triple shape programming/recovery process combining light-induced shape memory and thermal shape memory (illustration, left). DCA-OD system following programming and recovery process (images, right).

observed in the images of the DCA-OD film in Figure 3.5. In this method, both programming steps change the shape on a macroscopic level, whereby visible delocalized changes in dimension and shape are observed during the recovery periods. Taking advantage of the combination of two independent triggering mechanisms within the same system, the programming of two temporary shapes through a multistep process allows for the development of a novel degradable triple shape material.

3.3.2.3 Combination Macroscopic/Microscopic Triple Shape Memory

Utilizing the embossing method previously discussed in the characterization of thermal shape memory properties in the DCA series, localized surface shape memory is combined with macroscopic shape memory to create a multifunctional triple shape material. Figure 3.6 shows a similar processing method to the previously described macroscopic/macroscopic triple shape method with an alternate thermal programming step whereby micropattern embossing creates temporary surface topography. Macroscale deformation of the DCA-OD film while heated followed by light-induced fixation (i) programs the first temporary shape. Exploiting the previously mentioned embossing method, consisting of heat, molding, compression, and cooling (ii) generates the temporary surface features while maintaining the temporary bulk dimensions programmed in the first step. Recovery is triggered by heating (iii) to remove microscopic surface features and return to the flat surface of the temporary elongated shape and UV (iv) cleaving further recovers the macroscopic dimensions of the permanent shape. The images in Figure 3.6 of the original shape (A_1) to the first temporary shape (B) and recovery of the permanent shape (A_2) follow the bulk film shape memory, while the expansion shows the surface switching from flat (B_i) to 3μm cube micropattern (B_t) back to the recovered flat topography (B_f).

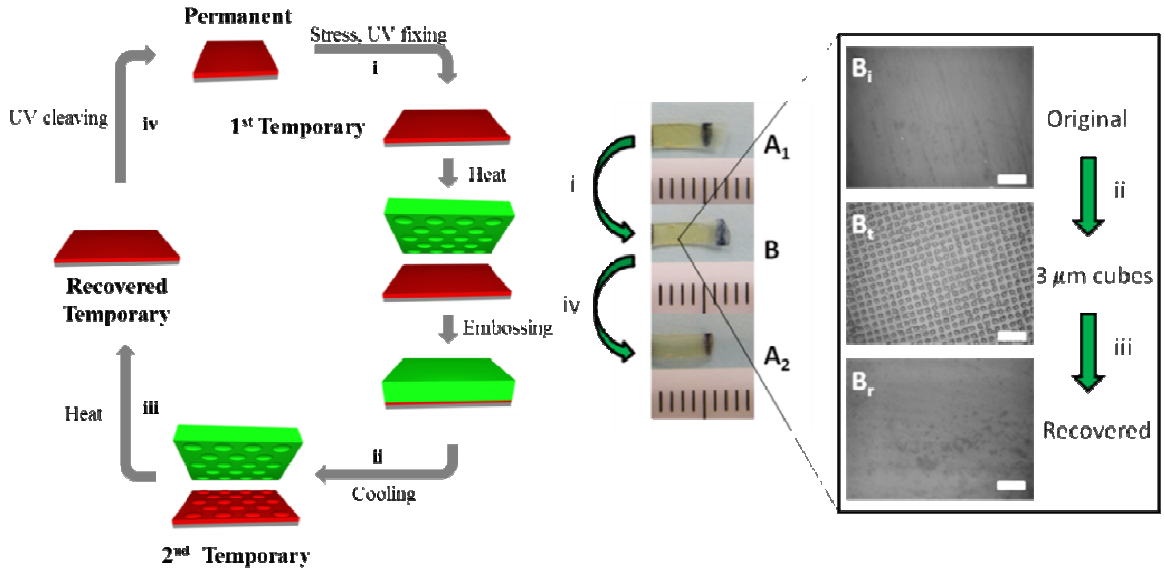

Figure 3.6 Triple shape programming/recovery process combining macroscopic and microscopic shape changes (illustration, left). DCA-OD system following programming and recovery process (images, right). Expansion: bright-field microscopic surface images, scale bar = 10 μm.

3.4 General Conclusions

The ability to discriminately trigger a macroscopic shape change via a thermal, indirect thermal, or light-induced mechanism in a biomaterial presents an interesting application in biomedical devices and materials, whereby movement and shape provide a function. Shape changes on the microscale or nanoscale are also attractive, with one motivation being the interaction of cells with surface topography to modulate cellular responses and a second the adhesive properties of the material. Combination of multiple shape changes in a triple shape material extends into more complex motion and therefore functionality, however with thermal mechanisms (direct or indirect) this is non-trivial due to the dependence on thermal transitions being distinct and within a narrow range of body temperature. The novel materials and programming methods discussed within address the

need for discrete mechanisms of triggering a triple shape effect within one temperature range and the multifunctionality of macro/micro scale shape memory in the same packaged material. The ability to change macroscopic shape or dimensions combined with dynamic surfaces make these materials advantageous for biomedical devices such as stents, sutures, and implants where function lies in structure and movement, as well as interaction with cells, surrounding tissue, and *in vivo* environment.

3.5 Acknowledgments

The authors would like to thank the DeSimone group for supplying PRINT™ molds used in surface embossing and use of the Zeiss Imager D.1m microscope. This research was funded by the National Science Foundation (Department of Materials Research) under Grant 0418499.

References

1) Behl, M.; Lendlein, A. *J. Mater. Chem.* 2010, *20*, 3335..

2) Bellin, I.; Kelch, S.; Langer, R.; Lendlein, A. *Proc. Natl. Acad. Sci.* 2006, *103(48)*, 18043.

3) Pretsch, T. *Smart Mater. Struct.* 2010, *19*, 1.

4) Chen, S.; Hu, J.; Yuen, C.H.; Chan, L.; Zhuo, H. *Polym. Adv. Technol* 2010, *21*, 377.

5) Behl, M.; Bellin, I.; Kelch, S.; Wagermaier, W.; Lendlein, A. *Adv. Funct. Mater.* 2009, *19*, 102.

6) Xie, T. *Nature Letters* 2010, *464*, 267.

7) Davis, K.A.; Luo, X.; Mather, P.T.; Henderson, J.H. *J. Vis. Exp.* (53), e2903, DOI: 10.3791/2903 (2011).

8) Ishida, K.; Hortensius, R.; Luo, X.; Mather, P.T. *J. Polym. Sci. B Polym. Phys.* 2012, *50*, 387.

9) Pierce, B.F.; Sheares, V.V. *Polymer Preprints (ACS Poly)* 2008, *49*, 1047.

10) Brosnan, S.; Brown, A.; Luft, J.C.; DeSimone, J.D.; Sheares Ashby, V. *Proc. Natl. Acad. Sci.* 2012*, Submitted 2012-05919*.

11) Wang, Z.; Hansen, C.; Ge, Q.; Maruf, S.H.; Ahn, D.U.; Qi, H.J.; Ding, Y. *Adv. Mater.* 2011, *23*, 3669.

12) Le, D.M.; Kulangara, K.; Adler, A.F.; Leong, K.W.; Ashby, V.S. *Adv. Mater.* 2011, *23*, 3278.

13) Davis, K.A.; Burke, K.A.; Mather, P.T.; Henderson, J.H. *Biomaterials* 2011, *32*, 2285.

14) Ebara, M.; Uto, K.; Idota, N.; Hoffman, J.M.; Aoygai, T. *Adv. Mater.* 2011, *24*, 273.

15) Rolland, J.P.; Maynor, B.W.; Euliss, L.E.; Exner, A.E.; Denison, G.M.; DeSimone, J.M. *J. Am. Chem. Soc.* 2005, *127*(28), 10096.

Chapter IV

PHOTO-RESPONSIVE POLY(β-AMINOESTER)S: VERSATILE ROUTES TO FUNCTIONAL SHAPE MEMORY MATERIALS

4.1 Introduction

Poly(β–aminoester)s (PBAEs) have recently gained attention as biodegradable materials utilized for various non-viral gene delivery vectors and tissue scaffolds.[1-5] The inherent tertiary amine groups found within the polymer backbone can be used to complex nucleic acids such as DNA, RNA, or si-RNA and self-assemble into nanoscale gene transfer vehicles.[6] Synthesized by 1,4 conjugate addition (Michael addition) between a diacrylate and either a primary amine or a bis-secondary amine (Scheme 4.1), the ease of polymerizing these materials as well as the commercial availability of a variety of diacrylate and amine monomers has led to the formation of various libraries of polymers for quick screening

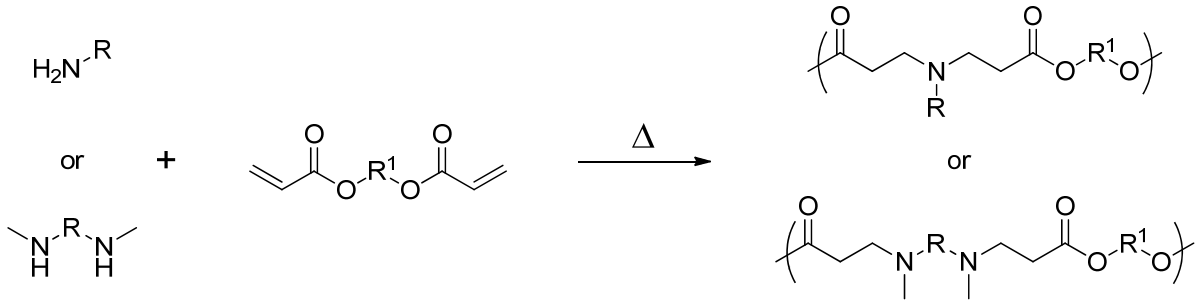

Scheme 4.1 Polymerization of PBAEs via Michael addition of diacrylate monomer and amine monomers.

techniques.[7,8] In addition there are no by-products generated during synthesis, end-group control by stoichiometry results in crosslinkable chain ends with no added synthetic steps, and the conjugate addition reaction is tolerant of other functionality including ethers, carboxylic acids, alcohols, and tertiary amines.[9] This allows easy tailoring of molecular weight (MW) and chemical structure which in turn enables the tuning of thermal and mechanical properties along with the degradation rate.

PBAEs can be copolymerized with other monomers or macromers due to the crosslinkable endgroups afforded during polymerization resulting in interesting copolymer materials. PBAE-*b*-PEG or PBAE-*g*-NIPAAm show thermo and pH-responsiveness as a result of the degree of protonation of the amino groups, and the addition of the PBAE segments also leads to degradable materials.[10,11] PBAE-*co*-MMA, PBAE-*co*-MA, and PBAE-*co*-MMA-*co*-MA were synthesized and found to be degradable thermal shape memory materials depending on the content of MMA/MA vs PBAE (9.5 - 29.5 wt % PBAE necessary).[12] The higher concentration of MMA/MA was necessary to increase the T_g of the material to an applicable temperature for thermal shape memory, while the degradation of the material was attributed to the PBAE segments. Various pendant functionality can be incorporated into PBAEs through either functional amine or diacrylate monomers. Tolerance of the resulting reactive functionality permits further modification of the polymer via post-polymerization functionalization methods.[10,13]

Herein, we introduce two versatile routes to synthesizing PBAEs with photo-responsive functional groups uniformly distributed along the polymer backbone as pendant groups. The first method utilizes the synthesis of either a functional amine monomer or functional diacrylate monomer comprising of a cinnamamide or cinnamate group, allowing

incorporation of the photo-responsive group during polymerization. Use of the functional diacrylate also affords the addition of other functionality along the polymer chain through the complimentary amine monomer to tailor properties or react further. The second method is based on the availability of reactive functionality along the polymer backbone through a post-polymerization modification of pendant alcohols to cinnamate moieties. A library of PBAEs was synthesized based on different amino-alcohol compounds and diacrylates resulting in a range of thermal and mechanical properties. Both methods result in tailorable thermoset elastomeric materials and the first example of PBAE homopolymer shape memory materials via light-induced shape memory.

4.2 Experimental Section

4.2.1 Materials

All reagents were purchased from Sigma-Aldrich and used without further purification unless otherwise noted. Dichloromethane was dried by distilling from $CaSO_4$. 1,4-butanediol diacrylate and 1,6-hexanediol diacrylate were purified by vacuum distillation in the presence of hydroquinone inhibitor followed by filtering through basic alumina.

4.2.2 Instrumentation

Gel permeation chromatography was used to determine molecular weights and molecular weight distributions, M_w/M_n, of polymer samples using a Waters Alliance 2695 and Waters 2414 Refractive Index detector. Molecular weights were calculated using a calibration plot constructed from polystyrene standards (Polyscience Corp.). The measurements were taken at 35 °C with THF as the mobile phase on three columns (Waters Styragel HR5, HR4, and HR2). ^{1}H NMR spectra of the monomers and polymers were obtained on a Bruker 400 ADVANCE spectrometer. Thermal transitions were analyzed

using TA Differential Scanning Calorimeter Q200 with liquid N_2 cooling unit at a cooling rate of 5 ^oC/min and heating rate of 10 ^oC/min. A Pyris I Thermogravimetric Analyzer was used to collect 5% and 10% decomposition temperature data from 25 ^oC to 500 ^oC at a heating rate of 20 ^oC/min in N_2 atmosphere. Mechanical analysis was conducted on an Instron 5566 at a crosshead speed of 10 mm/min at 25 °C. The Young's modulus (*G*) was calculated using the initial linear portion of the stress/strain curve (0 – 5 % strain).

4.2.3 Functional Monomer Synthesis

4.2.3.1 Functional Amine Monomer

Synthesis of (9H-fluoren-9-yl)methyl-(2-hydroxyethyl)carbamate (1). A solution of 9-fluorenylmethyl chloroformate (4.337 g, 16.8 mmol) in dry CH_2Cl_2 was added dropwise to a stirring solution of ethanolamine (2.03 mL, 33.6 mmol) in dry CH_2Cl_2 at 0 ^oC over 45 minutes. After the addition was complete, the ice bath was removed, the solution was warmed to room temperature and allowed to stir for another 1.5 h. The solution was then washed with 0.5 M HCl (3 x 100 mL), the organic layer was dried over $MgSO_4$, the solvent was removed by reduced pressure, and the solid product was dried under vacuum overnight. ^{1}H-NMR: δ (ppm) = 7.85 (d, 2H, *J* = 7.6 Hz), 7.70 (d, 2H, *J* = 7.6 Hz), 7.41 (t, 2H, *J* = 7.4 Hz), 7.32 (t, 2H, *J* = 7.2 Hz), 4.32 (d, 2H, *J* = 6.8 Hz), 4.22 (t, 1H, *J* = 7.0 Hz), 3.60 (t, 2H, *J* = 5.4 Hz), 3.26 (d, 2H, *J* = 5.6 Hz).

*Synthesis of 2-((((9H-fluoren-9-yl)methoxy)carbonyl)amino)ethyl cinnamate (**2**).* A solution of cinnamoyl chloride (0.167 g, 1 mmol) in dry CH_2Cl_2 was added dropwise into a stirring solution of the Fmoc-protected ethanolamine, compound 1 (0.284 g, 1.0 mmol), triethylamine (0.278 mL, 2 mmol) and dry CH_2Cl_2 at 0 ^oC. The reaction solution was then warmed to room temperature and stirred for 3.5 h. The precipitate was removed by gravity

filtration, and the solution was washed sequentially with 1.0 M HCl (1 x 15 mL), saturated $NaHCO_3$ (1 x 15 mL), and DI H_2O (1 x 15 mL). The organic layer was dried over $MgSO_4$, filtered, and excess solvent was removed under reduced pressure. ^{1}H-NMR: δ (ppm) = 7.87 (d, 2H, J = 7.2 Hz), 7.69 (m, 5H), 7.41 (m, 5H), 7.32 (m, 2H), 6.55 (d, 1H, J = 16 Hz), 4.36 (d, 2H, J = 6.8 Hz), 4.27 (m, 3H), 3.50 (m, 2H).

*Synthesis of 2-aminoethyl cinnamate (**3**).* Compound 2 was deprotected by stirring in a solution of 1% piperidine/acetonitrile at room temperature for 3 h. The solvent was removed under reduced pressure, and the crude product was purified by flash chromatography (15:1 CH_2Cl_2/MeOH). The solvent was removed under reduced pressure, and the solid product dried overnight. ^{1}H-NMR: δ (ppm) = 7.58 (m, 2H), 7.55 (d, 1H, J = 15.6 Hz), 7.40 (m, 3H), 6.75 (d, 1H, J = 16.0 Hz), 3.65 (q, 2H, J = 5.6 Hz), 3.43 (q, 2H, J = 5.6 Hz).

4.2.3.2 Functional Diacrylate Monomer

*Synthesis of N,N-bis(2-hydroxyethyl)cinnamamide (**4**).* A solution of diethanolamine (18.0 g, 171.2 mmol) and Et_3N (6.7g, 66.2 mmol) in dry CH_2Cl_2 under N_2 atmosphere was cooled to 0 ^oC in an ice bath. To this mixture a solution of cinnamoyl chloride (10.0 g, 60.0 mmol) in dry CH_2Cl_2 was added dropwise over a period of 20 min. After complete addition, the reaction was allowed to stir for 1 h before removal of the ice bath and returning the reaction to room temperature to stir 10 h. The organic phase was then washed with 1M HCl, saturated $NaHCO_3$, and brine (50 mL x 3 each) followed by drying over $MgSO_4$. The product was concentrated by vacuum evaporation resulting in a white powder. ^{1}H-NMR: δ (ppm) = 7.66 (d, 1H, J = 16 Hz), 7.50 (m, 2H), 7.35 (m, 3H), 6.94 (d, 1H, J = 16 Hz), 3.88 (dt, 4H, J_1 = 6 Hz, J_2 = 16 Hz) 3.70 (bs, OH), 3.66 (q, 4H, J = 5.3 Hz).

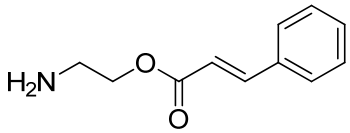

(3)

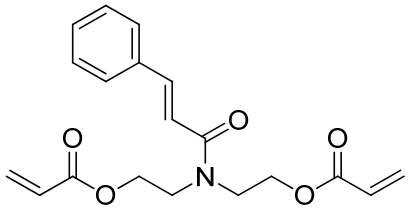

(5)

Figure 4.1 Functional monomers.

*Synthesis of (E)-(cinnamoylazanediyl)bis(ethane-2,1-diyl) diacrylate (**5**).* Compound 4 (4.02g, 17.1 mmol) was dissolved in dry CH_2Cl_2 and cooled using an ice bath. A solution of acrylol chloride (1.93 g, 21.4 mmol) in CH_2Cl_2 was added dropwise to the stirring solution of the diol over 15 minutes. The solution was allowed to stir in the ice bath for 30 minutes before dropwise addition of pyridine (1.74 g, 22.0 mmol). The reaction mixture was then warmed to room temperature and allowed to stir for an additional 8 h. The organic solution was then washed with 1M HCl, saturated $NaHCO_3$, and brine (50 mL x 3 each), followed by drying over $MgSO_4$. After filtration, the solvent was removed by rotary evaporation, resulting in a slightly yellow oil. ^{1}H-NMR: δ (ppm) = 7.68 (d, 1H, J = 16 Hz), 7.52 (m, 2H), 7.34 (m, 3H), 6.97 (d, 1H, J = 16 Hz), 6.37 (dd, 2H, J_1 = 16 Hz, J_2 = 16 Hz), 6.08 (m, 1H), 5.81 (dd, 2H, J_1 = 10, J_2 = 26), 4.37(t, 4H, J = 6 Hz), 3.80 (dt, 4H, J_1 = 4 Hz, J_2 = 24 Hz).

4.2.4 Polymer Synthesis

General Polymer Synthesis. An example of a typical polymerization is given. Amine monomer (28.5 mmol), diacrylate monomer (31.8 mmol), and $CHCl_3$ (6 mL) were added by syringe to a flame dried 50 mL Schlenk flask with stir bar and heated to 80 ^oC. The reaction was stirred for 48 hrs, and in the last hour diacrylate monomer (0.1 g, 0.5 mmol) was added to ensure crosslinkable end groups. The solution was removed from heat and precipitated into cold Et_2O (dry ice/acetone), followed by drying in a vacuum oven overnight at 40 ^oC.

This procedure was used to synthesize a library of four alcohol pendant PBAE prepolymers (6a-9a) used in the following post-polymerization functionalization method.

4.2.4.1 Post-Polymerization Route

PBAEs with pendant alcohol groups were synthesized by reacting either ethanolamine or butanolamine with 1,4-butanediol diacrylate or 1,6-hexanediol diacrylate. The resulting prepolymers are designated by four letters, the first two associated with the pendant functionality, ethanol or butanol (EO or BO), and the second two associated with the diacrylate monomer, butanediol or hexanediol (BD or HD).

EO-BD (6a) ^{1}H-NMR: δ (ppm) = 6.40 (d, endgroup 1H, J = 20 Hz), 6.11 (dd, endgroup 1H, J_1 = 10 Hz, J_2 = 18 Hz), 5.82 (d, endgroup 1H, J = 12 Hz), 4.19 (t, endgroup 2H, J = 4 Hz), 4.09 (t, 4H, J = 4 Hz), 3.57 (t, 2H, J = 6 Hz), 2.79 (t, 4H, J = 6 Hz), 2.58 (t, 2H, J = 6 Hz), 2.45 (t, 4H, J = 6 Hz), 1.69 (m, 4H).

EO-HD (7a) ^{1}H-NMR: δ (ppm) = 6.38 (d, endgroup 1H, J = 16 Hz), 6.10 (dd, endgroup 1H, J_1 = 10 Hz, J_2 = 18 Hz), 5.81 (d, endgroup 1H, J = 12 Hz), 4.05 (t, 4H, J = 4 Hz), 3.57 (t, 2H, J = 4 Hz), 2.79 (t, 4H, J = 6 Hz), 2.59 (m, 2H), 2.45 (t, 4H, J = 6 Hz), 1.62 (m, 4H), 1.37 (m, 4H).

BO-BD (8a) ^{1}H-NMR: δ (ppm) = 6.39 (d, endgroup 1H, J = 20 Hz), 6.10 (dd, endgroup 1H, J_1 = 10 Hz, J_2 = 18 Hz), 5.82 (d, endgroup 1H, J = 12 Hz), 4.08 (t, 4H, J = 6 Hz), 3.55 (t, 2H, J = 6 Hz), 2.79 (t, 4H, J = 6 Hz), 2.48 (t, 4H, J = 8 Hz), 2.44 (t, 2H, J = 6 Hz), 1.68 (m, 4H), 1.58 (m, 4H).

BO-HD (9a) ^{1}H-NMR: δ (ppm) = 6.40 (d, endgroup 1H, J = 16 Hz), 6.12 (dd, endgroup 1H, J_1 = 10 Hz, J_2 = 18 Hz), 5.82 (d, endgroup 1H, J = 8 Hz), 4.06 (t, 4H, J = 6

Hz), 3.56 (t, 2H, J = 8 Hz), 2.80 (t, 4H, J = 8 Hz), 2.49 (t, 4H, J = 8 Hz), 2.45 (t, 2H, J = 8 Hz), 1.61 (m, 6H), 1.37 (m, 6H)

Post Functionalization. EC-BD (6b), EC-HD (7b), BC-BD (8b), BC-HD (9b). Post functionalization of alcohol pendant prepolymers results in pendant cinnamate groups. The resulting prepolymers are desiginated by four letters, the first two associated with the pendant functionality, ethyl cinnamate or butyl cinnamate (EC or BC); and the second two associated with the diacrylate monomer, butanediol or hexanediol (BD or HD). A typical functionalization method is given. Alcohol functionalized PBAE of known $\overline{M}_n$ was added to a flame dried 100 mL round bottom flask with addition funnel attached and dissolved in dry CH_2Cl_2. The reaction solution was placed on ice, and after 10 min a solution of cinnamoyl chloride (1.5 mol equiv of OH groups) in dry CH_2Cl_2 was slowly dripped into the flask through the addition funnel. Once the addition was completed, pyridine (1.55 mol equiv of OH groups) was slowly dripped into the reaction which creates the precipitation of HCl salts. Once the addition of pyridine was complete, the ice bath was removed and the solution allowed to stir 12 h, at which time, the precipitate was filtered and the solution concentrated by rotary evaporation. The polymer solution was precipitated into cold methanol (dry ice/acetone) and redissolved in CH_2Cl_2. The solution was sequentially washed with 1 M HCl (1 x 100 mL), saturated $NaHCO_3$ (1 x 100 mL), and brine (1 x 100 mL). The organic phase was dried with $MgSO_4$, and the solvent was removed under reduced pressure. The resulting polymer is then redissolved in chloroform and precipitated into cold methanol (-78 ^oC). The polymer was collected and dried under vacuum for 24 hours.

(6a)

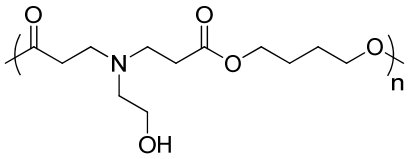

(6b)

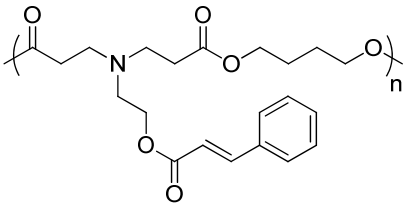

(7a)

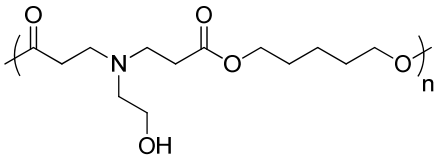

(7b)

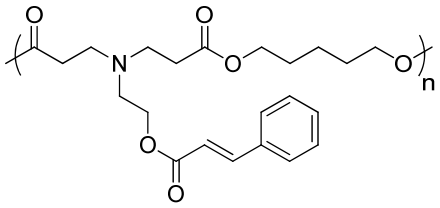

(8a)

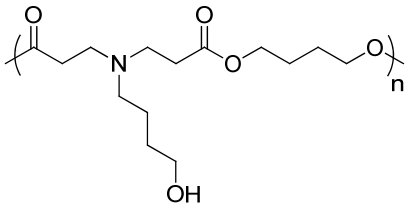

(8b)

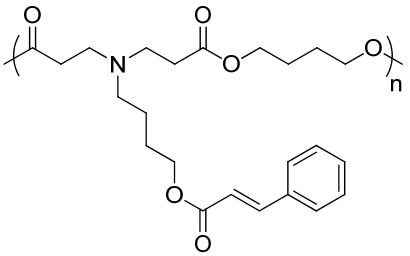

(9a)

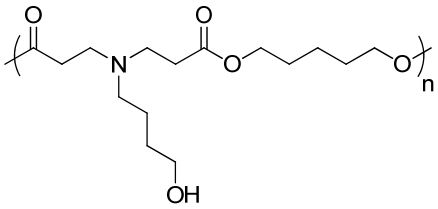

(9a)

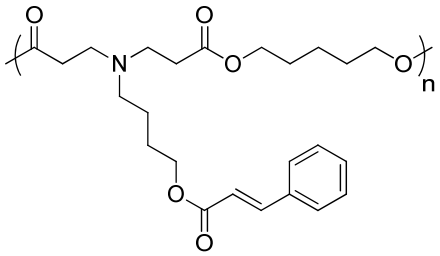

Figure 4.2 Hydroxy pendant prepolymers and cinnamate (CA) functionalized prepolymers.

EC-BD (6b) ^{1}H-NMR: δ (ppm) = 7.69 (d, 1H, J = 16 Hz), 7.67 (m, 2H), 7.42 (m, 3H), 6.54 (d, 1H, J = 16 Hz), 6.34 (d, endgroup 1H, J = 16 Hz), 6.14 (dd, endgroup 1H, J_1 = 10 Hz, J_2 = 14 Hz), 5.86 (d, endgroup 1H, J = 8 Hz), 4.24 (t, 2H, J = 6 Hz), 4.05 (m, 4H), 2.88 (t, 4H, J = 6 Hz), 2.82 (t, 2H, J = 8 Hz), 2.49 (t, 4H, J = 6 Hz), 1.66 (m, 4H)

EC-HD (7b) ^{1}H-NMR: δ (ppm) = 7.67 (d, 1H, J = 16 Hz), 7.52 (m, 2H), 7.37 (m, 3H), 6.42 (d, 1H, J = 16 Hz), 6.38 (d, endgroup 1H, J = 16 Hz), 6.10 (dd, endgroup 1H, J_1 = 12 Hz, J_2 = 16 Hz), 5.81 (d, endgroup 1H, J = 12 Hz), 4.23 (t, 2H, J = 6 Hz), 4.03 (t, 4H, J = 6 Hz), 2.86 (t, 4H, J = 6 Hz), 2.79 (t, 2H, J = 6 Hz), 2.46 (t, 4H, J = 8 Hz), 1.59 (m, 4H), 1.32 (m, 4H).

BC-BD (8b) ^{1}H-NMR: δ (ppm) = 7.65 (d, 1H, J = 16 Hz), 7.49 (m, 2H), 7.34 (m, 3H), 6.42 (d, 1H, J = 16 Hz), 6.48 (d, endgroup, J = 20 Hz), 6.09 (dd, endgroup, J_1 = 12 Hz, J_2 = 16 Hz), 5.79 (d, endgroup, J = 8 Hz), 4.17 (t, 2H, J = 6 Hz), 4.05 (m, 4H), 2.75 (t, 4H, J = 8 Hz), 2.42 (t, 6H, J = 8 Hz), 1.66 (m, 6H), 1.51 (m, 2H).

BC-HD (9b) ^{1}H-NMR: δ (ppm) = 7.69 (d, 1H, J = 20 Hz), 7.52 (m, 2H), 7.38 (m, 3H), 6.44 (d, 1H, J = 16 Hz), 6.40 (d, endgroup 1H, J = 20 Hz), 6.11 (dd, endgroup 1H, J_1 = 10 Hz, J_2 = 18 Hz), 5.81 (d, endgroup 1H, J = 8 Hz), 4.20 (t, 2H, J = 6 Hz), 4.03 (t, 4H, J = 6 Hz), 2.79 (t, 4H, J = 6 Hz), 2.48 (t, 4H, J = 6 Hz), 2.45 (t, 2H, J = 8 Hz), 1.61 (m, 6H), 1.34 (m, 6H).

4.3.4.2 Functional Monomer Route

Polymerization of CAD-OH (10). Functional diacrylate monomer CAD-DA (*5*) (0.69 g, 2.0 mmol), ethanolamine (0.12 g, 1.95 mmol), and $CHCl_3$ (1 mL) were added to a round bottom flask under N_2 and heated to 80 ^oC. The reaction mixture was allowed to stir for 24 h followed by diluting with 2 mL of $CHCl_3$. The solution was purified by

precipitation into cold diethyl ether (-78 ^{o}C), and the liquid prepolymer was collected and vacuum dried for 24 h. ^{1}H-NMR: δ (ppm) = 7.67 (d, 1H, J = 16 Hz), 7.54 (m, 2H), 7.35 (m, 3H), 6.95 (d, 1H, J = 16 Hz), 6.38 (dd, endgroup, J_1 = 18 Hz, J_2 = 18 Hz), 6.08 (m, endgroup), 5.81 (dd, endgroup, J_1 = 10, J_2 = 26), 4.24 (m, 4 H), 3.71 (m,4H), 3.52 (t, 2H, J = 16 Hz), 2.70 (t, 4H, J = 32 Hz), 2.42 (t, 6H, J = 26 Hz).

Polymerization of CAD-Alkyne (11). CAD-DA (0.64 g, 1.9 mmol), propargyl amine (0.10 g, 1.8 mmol), and $CHCl_3$ (1 mL) were added to a round bottom flask under N_2 and heated to 80 ^{o}C. The reaction mixture was allowed to stir for 24 h followed by diluting with 2 mL of $CHCl_3$. The solution was purified by precipitation into cold diethyl ether (-78 ^{o}C), and the polymer was collected and dried under vacuum. ^{1}H-NMR: δ (ppm) = 7.70 (d, 1H, J = 12 Hz), 7.54 (m, 2H), 7.36 (m, 3H), 6.96 (d, 1H, J = 12 Hz), 6.38 (dd, endgroup, J_1 = 18 Hz, J_2 = 48 Hz), 6..11 (m, endgroup), 5.68 (d, endgroup, J = 8 Hz), 4.26 (t, 4H, J = 6 Hz), 3.72 (m, 4H), 3.32 (t, 2H, J = 24 Hz), 2.76 (t, 4H, J = 26 Hz), 2.42 (t, 4H, J = 20 Hz), 2.16 (t, 1H, J = 16 Hz).

4.2.5 Thermoset Network Formation

Crosslinking. Prepolymers with crosslinkable endgroups were thermally cured by two methods. The first method employed AIBN as a radical initator. To a 50% polymer solution in chloroform was added AIBN (1.0 mol %) and the mixture was stirred for 5 minutes to ensure full distribution of initiator before filling a Teflon mold or spreading on a glass slide. The solvent was completely evaporated, and the mold/slide was placed in an oven at 80 ^{o}C for 6 h. The second method utilized a thermally initiated thiol-ene reaction in the presence of an amine catalyst. To a prepolymer solution was added trimethyloylpropane tris(3-mercaptopropionate) (2.0 mol equiv.) and amine catalyst (0.95 wt %). Two amine

compounds were used: *n*-hexyl amine or 1,8-diazabicyclo[5.4.0]undec-7-ene (DBU). After stirring for 5 minutes, the solution was cast in the mold or on the glass slide, the solvent was evaporated, and the cast film was placed in the oven at 80 ^{o}C overnight.

4.3 Results and Discussion

4.3.1 Functional Monomer Synthesis

4.3.1.1 Amine Monomer

The successful synthesis of 2-aminoethyl cinnamate (*3*) was achieved through a protection/deprotection process where the protecting group 9-fluorenylmethoxycarbonyl (Fmoc) was employed to result in a free amine containing monomer to be used for synthesis of PBAEs with a complimentary diacrylate (Scheme 4.2). Fmoc was chosen because it is labile in the presence of the weak base piperidine, whereas other protecting groups require strong acid or basic work up, which would likely degrade the cinnamate functionality. Protection was necessary due to the higher reactivity of the amino group versus the hydroxyl group of ethanolamine in the reaction with cinnamoyl chloride.

The first step of the three part synthesis was the protection of the amino group by addition of Fmoc chloride at low temperature. The resulting hydroxyl-functionalized solid product was reacted with cinnamoyl chloride again at low temperatures to control the heat generated from the reaction. The addition was done in the presence of an excess of triethylamine which acts as a HCl scavenger and catalyzes the reaction. The final step was the deprotection by stirring in a piperidine/acetonitrile solution to cleave the Fmoc group and return the amino end group. This process was followed by ^{1}H-NMR, watching for the appearance of the α-methylene protons of the carbamate linkage at 3.26 ppm (N-CH_2) and

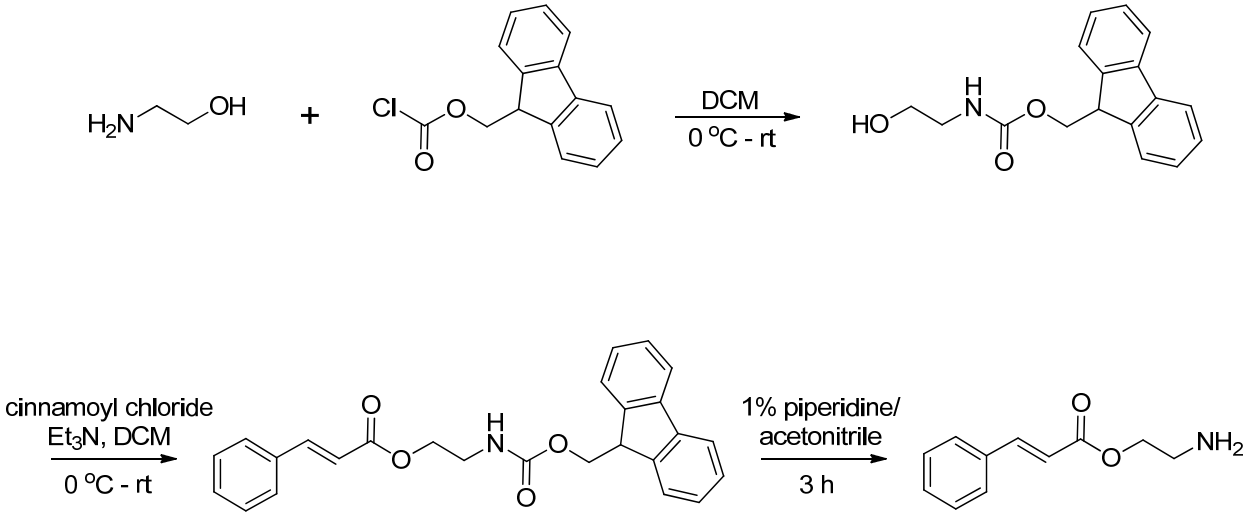

Scheme 4.2 Synthesis of functional amine monomer.

4.32 ppm (O-CH_2) for the protection step, the appearance of the vinylic proton of the cinnamate moiety at 6.55 ppm (CO-C*H*=CH) in the functionalization step, and the disappearance of the α-methylene protons corresponding to the carbamate. While the protection/deprotection method gave the desired compound, the three step synthesis resulted in poor overall yield as well as poor atom economy using the large Fmoc protecting group. In addition, the resulting PBAEs using 2-aminoethyl cinnmate are the same that result through the post-functionalization method where ethanolamine is used as the starting amine monomer (EC-BD, EC-HD). This directed further efforts towards the functional diacrylate monomer.

4.3.1.2 Diacrylate Monomer

The functional diacrylate monomer, CAD-DA (*5*) containing a photo-responsive cinnamamide group was realized by acrylation of the cinnamamide diol (CAD) used in the step-growth polycondensation of photo-responsive poly(ester urethane)s presented in Chapter II. As discussed, CAD was synthesized by reacting diethanolamine with cinnamoyl chloride

in the presence of triethylamine at low temperatures. In order to synthesize a diacrylate, the diol was further reacted with an excess of acrylol chloride in the presence of pyridine (Scheme 4.3). Pyridine was employed because it is less nucleophilic then triethylamine, as discussed in Chapter II has the ability to inhibit the reaction between the acyl chloride and less nucleophilic alcohol groups. ^{1}H-NMR shows the appearance of α-methylene peaks to the ester bond (4.37 ppm) and the vinylic protons (6.37, 6.08, 5.81 ppm) of the acrylate group, as well as the disappearance of the α-methylene peaks correlating to the original hydroxyl groups (3.66 ppm).

4.3.2 Polymer Synthesis

The synthesis of crosslinkable PBAE prepolymers was achieved through step growth polymerization and stoichiometric control of the monomer feed using an excess of diacrylate monomer, resulting in acrylate end groups. The general polymerization method could be run in bulk or with the addition of a small amount of solvent ($CHCl_3$) to help with the viscosity

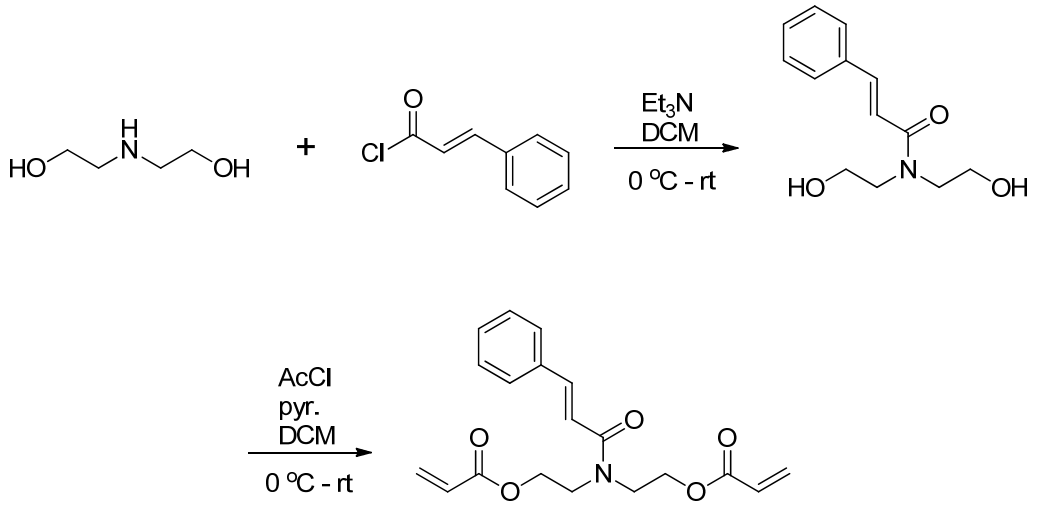

Scheme 4.3 Synthesis of functional diacrylate monomer.

and stirring of the reaction mixture. Unlike the polycondensation of polyesters discussed in Chapter II, PBAE polymerizations required no catalyst, and the reaction temperature was only 80 ^{o}C. Higher temperatures caused the initial gelation of the bulk melt after only a few hours which was attributed to the thermal initiation of the acrylate groups reacting with each other. After purification by precipitation, the diacrylate prepolymers can be thermally initiated by a free radical initiator AIBN, reacted with a thiol crosslinker through a thiol-ene method, or photo-initiated using an applicable photoinitiator; however, there is the likelihood of the latter affecting the photo-responsive moieties in an undesired manner. Therefore, only the two thermal methods were utilized to form thermoset networks.

4.3.2.1 Post-Polymerization Route

Four variations of hydroxyl pendant PBAEs were successfully synthesized using the general method discussed above, followed by post-functionalization to afford cinnamate pendant groups (Scheme 4.4). The choice of amino alcohol and diacrylate combination utilized ethanolamine (EO) or butanolamine (BO) with 1,4-butanediol diacrylate (BD) or 1,6-hexanediol diacrylate (HD). These starting materials were chosen to sequentially probe the structure property relationships in the resulting prepolymers and subsequent thermoset elastomers by examining the effects of the repeat unit (RU) chain length and pendant chain length on the thermal and mechanical properties. The different side chain lengths were also chosen to design polymers possessing chain spacers of differing length in between the polymer backbone and the photo-group functionality which is integrated during the post-functionalization step.

Conversion of alcohol pendant side chains to cinnamate moieties was achieved by reaction of an excess of cinnamoyl chloride in a dilute prepolymer solution at low

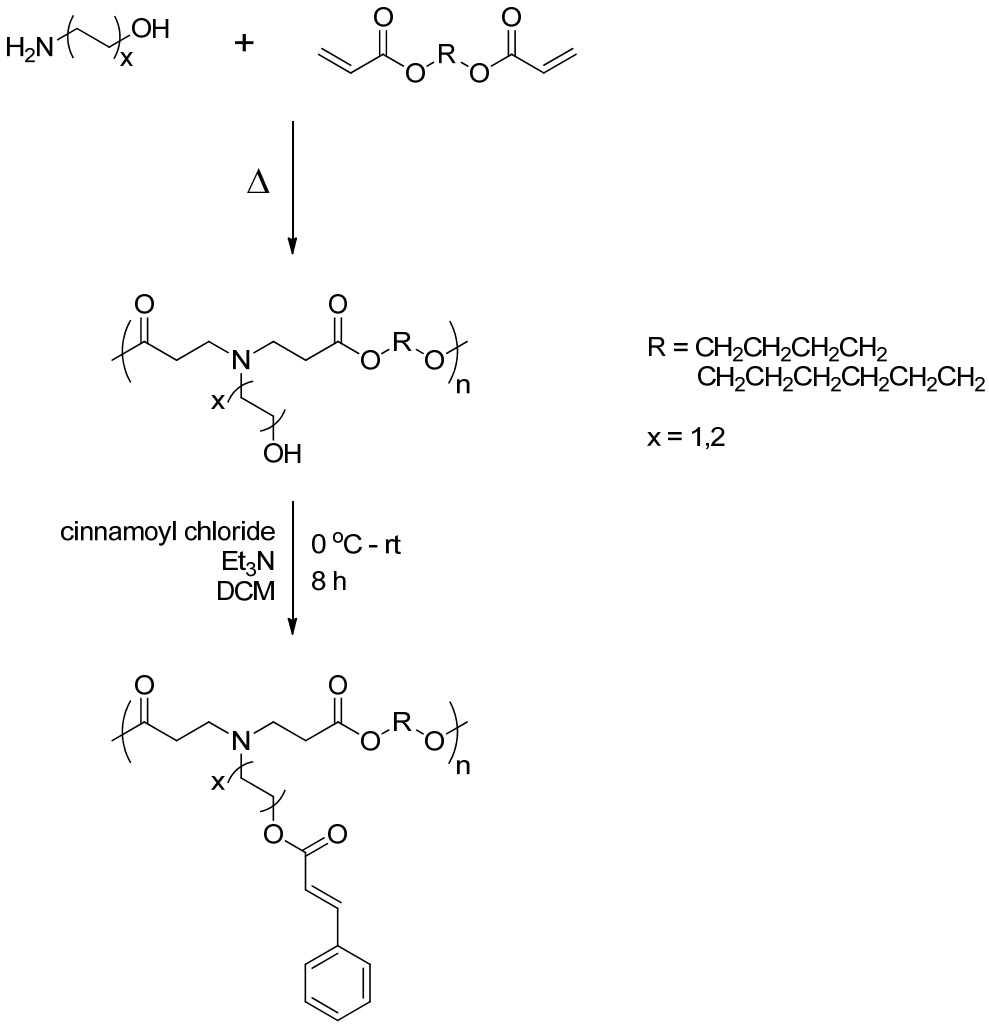

Scheme 4.4 Polymerization of alcohol and subsequent cinnamate pendant PBAE series.

temperatures in the presence of pyridine. The pyridine was used to scavenge the HCl produced in the reaction of the acyl chloride and alcohol, which could have been problematic had acid hydrolysis of the ester backbone occurred. By employing a slight excess of the pyridine, all free HCl was consumed to give the salt precipitate and no polymer backbone degradation was observed. This can be verified by the GPC analysis of the starting hydroxyl prepolymer and the resulting photo-responsive prepolymer. The GPC trace of EC-HD seen in Figure 4.3 shows the alcohol pendant prepolymer (blue) and the shifted cinnamate

functionalized polymer (orange). The corresponding M_n for each trace is 8,100 g/mol and 13,200 g/mol, respectively, and the slight decrease in PDI may be related to some fractionation in the purification process. If there was backbone degradation, the PDI would be expected to increase dramatically.

The GPC results can also confirm the conversion of alcohol groups to cinnamate groups by comparing the measured increase in MW to the theoretical increase. Full conversion of alcohol side chains would result in the addition of 4700 g/mol, with the GPC showing an increase of 5100 g/mol which exceeds the theoretical value by less than one repeat unit. Because GPC is a relative analysis technique and the structure of the different polymers can affect how they travel through the columns, ^{1}H-NMR was utilized to measure

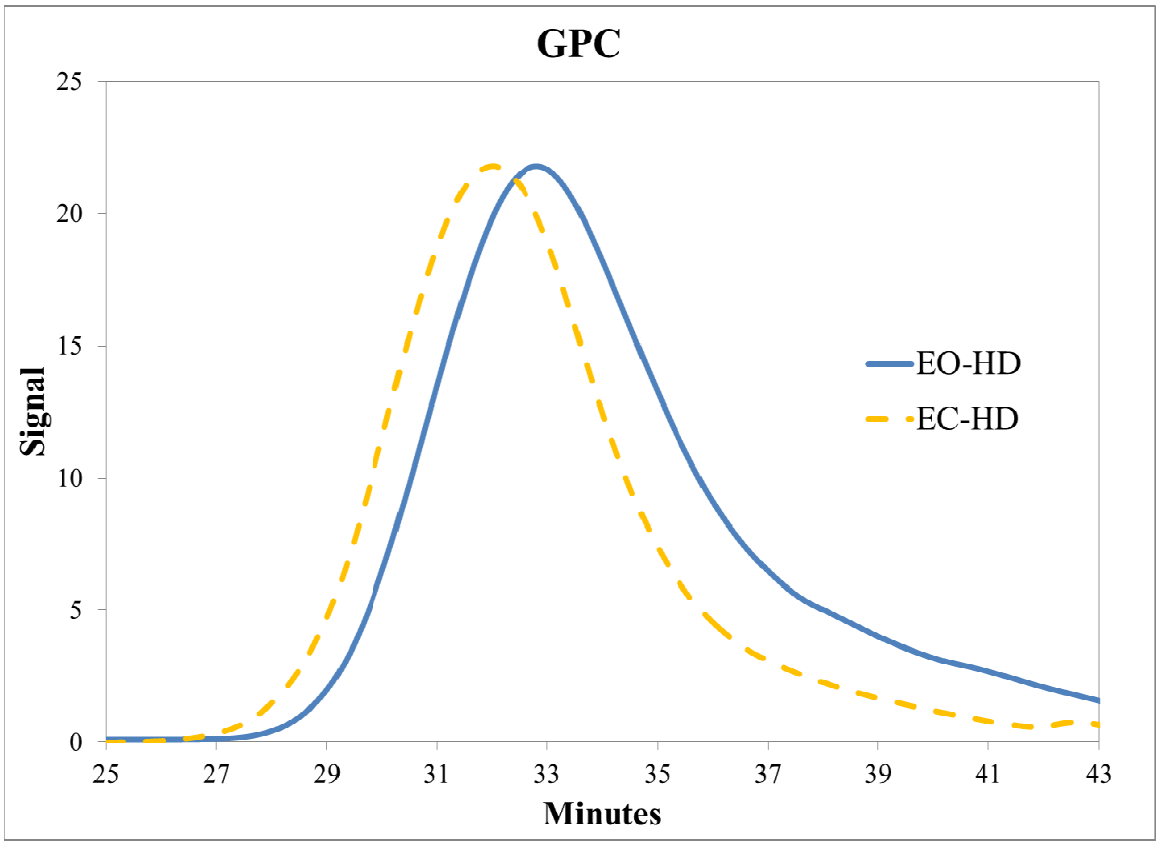

Figure 4.3 GPC chromatogram of EO-HD (blue) and EC-HD (orange).

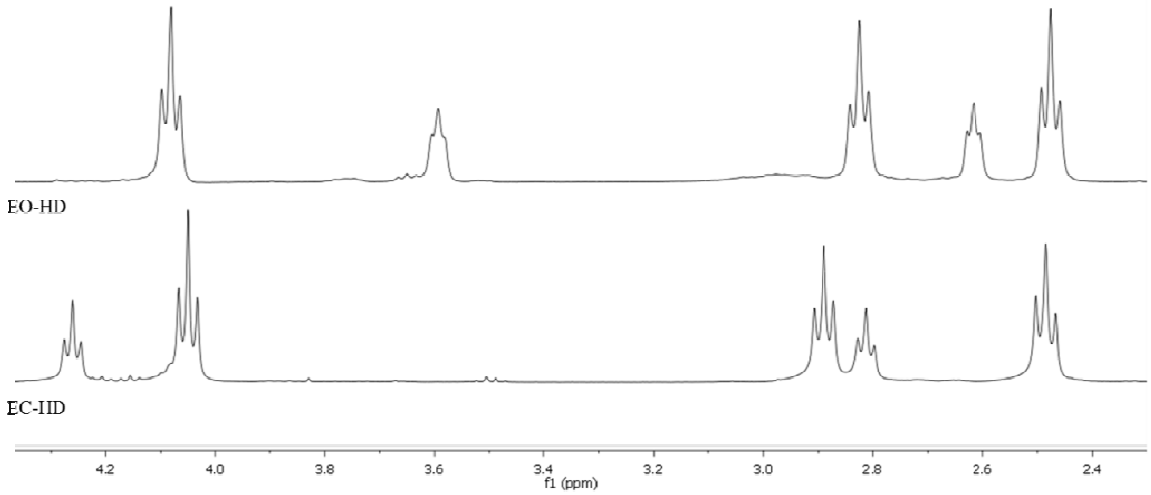

Figure 4.4 ^{1}H-NMR spectra of the methylene region of EO-HD (top) and EC-HD (bottom).

the absolute conversion. Evaluating the spectra of EO-HD (Figure 4.4, top) and EC-HD (Figure 4.4, bottom), the complete disappearance of peaks corresponding to the methylene protons of the side chain at 3.57 ppm, (-CH_2OH) and 2.59 ppm, (-CH_2N-) seen in the EO-HD spectrum was observed in the EC-HD spectrum. The appearance of the methylene protons at 4.23 ppm in the EC-HD spectrum was consistent with the formation of the new ester linkages within the polymer side-chains, as well as the shift of the methylene protons (-CH_2N-) downfield from 2.59 ppm to 2.79 ppm.

4.3.2.2 Functional Diacrylate Route

The synthesis of multifunctional PBAEs was accomplished by the 1,4-conjugate addition polymerization of the functional diacrylate monomer, CAD-DA with either ethanolamine or propargyl amine (Scheme 4.5). The resulting prepolymers contained the photo-group functionality in each repeat unit as well as an additional chemical handle. CAD-OH prepolymer possesses additional pendant hydroxyl groups much like the PBAE prepolymers used in the post-polymerization method, allowing for the possibility of further functionalization with carboxylic acids or acyl chlorides to attach other desirable moieties.

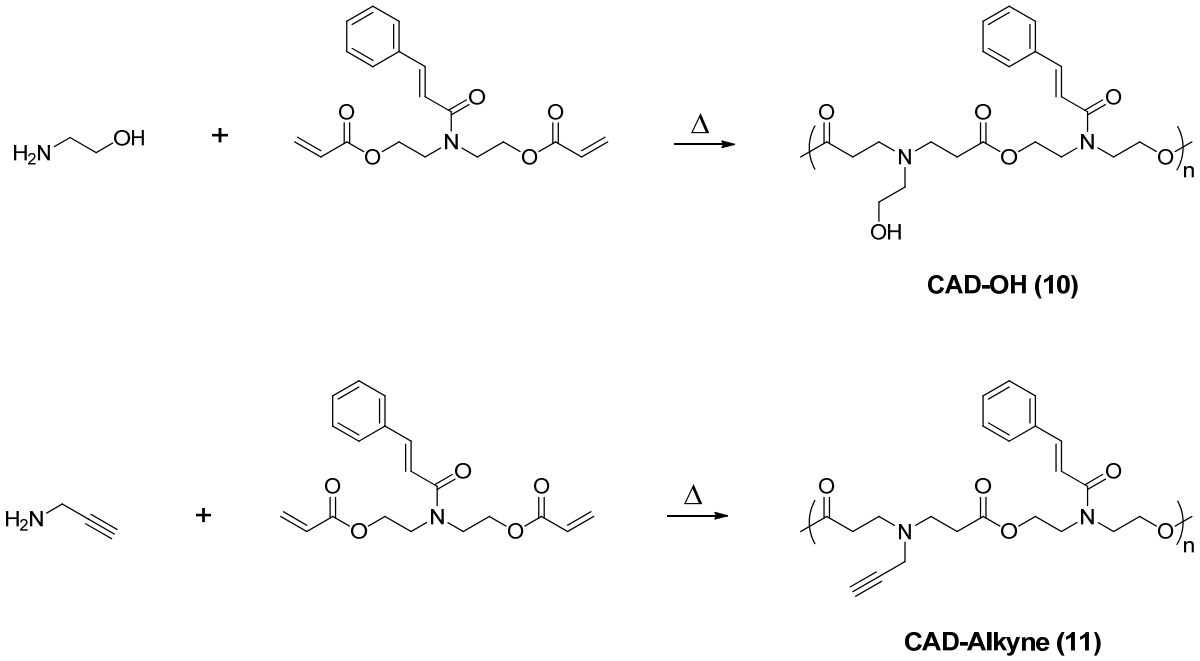

Scheme 4.5 Polymerization of multifunctional PBAEs reacting the functional diacrylate monomer CAD-DA with ethanolamine or propargyl amine.

The alcohol functionality also leads to a more hydrophilic material which should increase the rate of hydrolytic degradation. CAD-Alkyne prepolymers contain alkyne pendant groups in addition to the photo-responsive cinnamate functional groups. Alkyne functionality can be utilized in copper click chemistry with organic azide compounds to form the 1,3,5 triazole linkages between the polymer backbone and desired pendant group. The synthesis of both prepolymers used a stoichiometric imbalance, with an excess of the diacrylate monomer to produce crosslinkable endgroups. As can be seen in Table 4.2, the resulting prepolymers have low MW relating to short prepolymers although they were targeted for higher MW. This low reactivity could be due to the large pendant group of the CAD-DA monomer as well as the nearby side group which is incorporated by the amine monomer. Steric hindrance could inhibit the reaction of a second diacrylate monomer with an amine monomer that has already reacted once.

4.3.3 Thermal and Mechanical Analysis

4.3.3.1 Post-Polymerization Route

The thermal properties of the PBAE prepolymers and subsequent elastomeric films were measured using DSC and TGA (Table 4.1). The PBAE prepolymers synthesized through the post-functionalization route possess glass transition temperatures well below 0 ^{o}C, making them liquid prepolymers at room temperature. Varying the diacrylate and amino-alcohol monomers influenced the resulting T_g with changes to the side chain and polymer backbone having different impacts towards the magnitude of variation in transition temperature. In the four alcohol pendant PBAEs, the T_g ranged from -66 ^{o}C to -50 ^{o}C. Comparing prepolymers with the same diacrylate component, the T_g increased by ~5 ^{o}C when butanolamine (BO) was incorporated instead of ethanolamine (EO). Here the longer pendant group increases the rotational barrier for the polymer chains requiring higher temperatures to change from the glassy state to the amorphous phase. Examining the effect of the polymer backbone, within prepolymers composed of the same amino-alcohol monomer, the use of 1,4-butanediol diacrylate (BD) or 1,6-hexanediol diacrylate (HD) led to a variation of approximately 10 ^{o}C with the shorter backbone segment exhibiting the higher thermal transition. This is the inverse effect of the side group trend where the longer component increased the T_g. Within the polymer backbone, the longer diacrylate component led to larger flexibility and therefore a decreased thermal transition; the shorter BD segment restricted the resulting polymer chains to a larger extent therefore increasing the thermal energy required to transition. These results indicate that the dependence of the glass transition on the backbone segment is close to double the magnitude of the side group. Combining these two trends led to the very different thermal properties seen in EO-HD (-

Table 4.1 Molecular weight and thermal characterization of PBAE prepolymers.

Polymer Sample	$\overline{M}_n$ [a] (g/mol x 10^{-3})	$\overline{M}_w / \overline{M}_n$ [a]	Decomposition Temp.[b] 5% (^oC)	10% (^oC)	T_g (^oC)[c]
EO-BD	6.0	1.4	203	253	-54.0
EO-HD	8.1	2.3	197	219	-65.9
BO-BD	3.6	1.7	206	266	-49.6
BO-HD	5.3	1.9	205	223	-60.2
EC-BD	12.9	1.5	214	263	-31.7
EC-HD	13.2	2.1	207	308	-38.6
BC-BD	6.8	1.6	240	271	-26.7
BC-HD	11.3	2.0	225	258	-32.0

[a]GPC- PS Stds. [b]TGA. [c]DSC.

65.9 ^oC) and BO-BD (-49.6 ^oC) which have the same repeat unit MW. Although the magnitude may be different if both prepolymers were the same MW, for the results given, the lower MW BO-BD possesses the higher T_g which normally increases with MW so the trends would still hold, only to a greater magnitude.

After the post-functionalization of the alcohol pendant PBAEs to synthesize the cinnamate pendant PBAEs, there was an increase in the T_g for each of the prepolymers (-39 ^oC to -27 ^oC). When examining the same sets of prepolymers in order to understand the structure/property relationships as a result of the different diacrylate (BD versus HD) or side-chain components, it was apparent that the larger impact of the diacrylate component was diluted after functionalization of the pendant alcohol groups to afford the much

larger cinnamate moieties. Whether switching from the longer to shorter diacrylate or the shorter to longer side chain, the T_g difference was nearly 6 ^oC. The trends seen in the alcohol pendant PBAEs were still consistent but now both were of the same magnitude. The decomposition temperatures also followed this same relative trend.

Another interesting trend was seen in the increase of the T_g after functionalization of the prepolymers. For EC-BD and BC-BD, there was an increase of close to 22 ^oC from EO-BD and BO-BD, respectively. On the other hand, for the longer backbone segment PBAEs (EC-HD and BC-HD), the increase was close to 28 ^oC. There was minimal variation observed between different side groups. It was expected that the conversion of the side chain alcohols to cinnamates would induce the same shift in transition temperature, no matter which diacrylate component was utilized, however this was not the case. The explanation for this is not known but could be related to the possible interactions between the conjugated pendant groups, where the longer hexanediol backbone unit might allow them to interact in a greater number of conformations than with the shorter butanediol segment.

4.3.3.2 Functional Diacrylate Route

The multifunctional PBAEs produced via the functional diacrylate route exhibited glass transition temperatures an order of magnitude higher than the post-functionalized PBAEs. CAD-OH had a T_g of -6.0 ^oC while CAD-Alkyne (4.5 ^oC) had the only T_g above 0 ^oC for any of the PBAE materials. These higher thermal transitions are due to both the large side groups as was the case when the alcohol pendant PBAEs were functionalized to give cinnamate groups, as well as the shorter and less flexible polymer backbone. In comparison to EC-BD (-31.7 ^oC) which has the shortest polymer backbone in combination with the ethanolamine based pendant group, CAD-OH has a T_g that is 25 ^oC higher, even though it is

Table 4.2 Molecular weight and thermal characterization of CAD-OH and CAD-Alkyne prepolymers

Polymer Sample	$\overline{M}_n$ [a] (g/mol x 10^{-3})	$\overline{M}_w$ / $\overline{M}_n$ [a]	Decomposition Temp.[b] 5% (^oC)	10% (^oC)	T_g (^oC)[c]
CAD-OH	1.3	1.9	238	297	-6.0
CAD-Alkyne	1.0	1.4	223	293	4.5

[a]GPC- PS Stds. [b]TGA. [c]DSC.

also smaller in MW. Along the polymer backbone of both multifunctional PBAEs the longest methyl chain spacer is an ethyl segment which leads to less flexibility, and combination with multiple pendant groups leads to the higher thermal transitions. The difference between CAD-OH and CAD-Alkyne can be attributed to the difference in flexibility of the pendant groups. Although the ethanol side chain of CAD-OH is slightly higher MW, the rotational barrier of the ethyl chain spacer is less than that of the planar, rigid alkyne which allows CAD-OH a higher degree of freedom resulting in the lower transition temperature compared to CAD-Alkyne.

4.3.3.3 PBAE Elastomers

The amorphous nature and low glass transition temperatures of the PBAE prepolymers allowed for easier processing to form permanent networks of desired size and shape by molding or solvent casting. Curing of the prepolymers to produce the subsequent elastomers increased the T_g by 12-15 ^oC, which was expected as the netpoints further restrict movement of the polymer chains. Table 4.3 shows the thermal and mechanical properties of the resulting thermoset elastomers. The low glass transition temperatures of all of the PBAE elastomers (-23.1 to -14.5 ^oC) led to soft elastomeric materials at room temperature (23 ^oC), as measured by Instron. As expected the highest T_g material, the BC-BD film, had the

Table 4.3 Thermal and mechanical properties of PBAE thermoset elastomers.

Series	Decomposition[a] 5% (°C)	10% (°C)	T_g (°C)[b]	*E* (MPa)[c]	Break[c]
EC-BD	227	275	-19.2	0.7	78%
EC-HD	301	321	-23.1	0.3	135%
BC-BD	251	286	-14.5	1.1	68%
BC-HD	270	286	-20.4	0.4	85%

[a]TGA, [b]DSC, [c]Instron

highest modulus at 1.1 MPa and the trend continued for the other three elastomers. The extent of elongation followed the opposite general trend where the lower modulus materials are able to stretch to a greater magnitude. The decomposition temperatures of the elastomer materials also increased from the related prepolymers as was anticipated.

4.4 General Conclusions

The first example of photo-responsive PBAEs were synthesized through a post-polymerization route which afforded a series of soft PBAE elastomers with thermal and mechanical properties that were predictably tuned based on the structure/property relationships examined within this chapter. The incorporation of other amino-alcohol monomers or diacrylate monomers would be expected to follow the same trends and allow for further tailoring of properties. By employing a functional monomer route where a photo-responsive diacrylate monomer was synthesized and then polymerized with different primary amine monomers, multifunctional photo-responsive PBAEs were developed. The additional functionality, not limited to the alcohol or alkyne moieties used in this work, affords a chemical handle which can be used for attachment of supplementary chemical or biological

moieties. Furthermore, the bulk physical and chemical properties can modified in the polymer or after elastomer formation, as well as, the possibility of localized surface modification. These soft PBAE elastomers also fall within the range of soft tissue which renders these as promising multifunctional materials for biomedical devices such as tissue scaffolds.

4.5 Acknowledgments

The author would like to cite funding support for this work from the National Science Foundation (Division of Materials Research) under Grant 0418499.

References

1) Akinc, A.; Anderson, D.G.; Lynn, D.M.; Langer, R. *Bioconjugate Chem* 2003, *14*, 979.

2) Akinc, A.; Lynn, D.M.; Anderson, D.G.; Langer, R. *J Am Chem Soc* 2003, *125*, 5316.

3) Brey, D.M.; Erickson, I.; Burdick, J. *J Biomed Mater Res Part A* 2008, *85A*, 731.

4) Brey, D.M.; Ifkovits, J.L.; Mozia, R.I.; Katz, J.S.; Burdick, J. *Acta Biomater* 2008, *4*, 207.

5) Jere, D.; Yoo, M.; Arote, R.; Kim, T.; Cho, M.; Nah, J. *Pharm Res* 2007, *25*, 875.

6) Lynn, D.M.; Langer, R. *J Am Chem Soc* 2000, *122*, 10761.

7) Anderson, D.G.; Lynn, D.M.; Langer, R. *Angew Chem Int Ed* 2003, *42*, 3153.

8) Lynn, D.M.; Anderson, D.G.; Putnam, D.; Langer, R. *J Am Chem Soc* 2001, *123*, 8155.

9) Anderson, D.G.; Tweedie, C.A.; Hossain, N.; Navarro, S.M.; Brey, D.M.; Van Vliet, K.J.; Langer, R.; Burdick, J.A. *Adv Mater* 2006, *18*, 2614.

10) Wu, D.C.; Liu, Y.; He, C.B. *Macromolecules* 2008, *41*, 18.

11) Huynh, C.T.; Lee, D.S. *Colloid Polym Sci* 2012, DOI: 10.1007/s00396-012-2624-z

12) Lakhera, N.; Laursen, C.M.; Safranski, D.L.; Frick, C.P. *J Polym Sci Part B Polym Phys* 2012, *50*, 777.

13) Zugates, G.T.; Anderson, D.G.; Little, S.R.; Lawhorn, I.E.B.; Langer, R. *J Am Chem Soc* 2006, *128*, 12726.

Chapter V

GENERAL CONCLUSIONS AND FUTURE RESEARCH DIRECTIONS

5.1 General Conclusions

This dissertation focused on two versatile platforms for the development of photo-responsive biomaterials with the ability to perform light-induced shape memory. The synthesis and characterization of a library of novel poly(ester urethane)s containing photo-responsive groups uniformly along the polymer backbone is discussed in Chapter II. The incorporation of one of three bifunctional photo-monomers (DCA, DCE, CAD) with complimentary cyclic/linear diols or diacids resulted in amorphous prepolymers whose subsequent thermoset elastomers possessed thermal transitions ranging from -10 – 50 ^{o}C and modulus ranging from 0.4 – 60 MPa. Macroscopic light-induced shape memory was realized by increasing the crosslink density of the thermoset elastomer through the reversible photo-induced [2+2] cycloaddition of the photo groups along the polymer backbone. The system's ability to trigger at ambient temperature avoids the limitation of a narrow temperature range available for biomedical applications, and light triggering is more discriminate. Elastomers also boasted negligible cytotoxicity and degradation under physiological conditions.

Chapter III examines the additional thermal shape memory properties in the DCA poly(ester urethane) series along with programming methods used to address the need for discrete mechanisms of triggering a triple shape effect within one temperature range by

combining a light and thermally triggered shape memory effect. The DCA series showed thermal strain fixity and strain recovery as high as 99% and 96%, respectively. Sequential programming by photo-fixing and thermal fixing resulted in triple shape memory which could be performed on macroscopic and microscopoic scales. The ability to change macroscopic shape or dimensions combined with dynamic surfaces make these materials multifunctional and advantageous for a variety of biomaterials applications.

Chapter IV discusses the synthesis and characterization of novel photo-responsive poly(β-aminoester)s as a versatile platform to introduce additional reactive functionality and tune properties. Post-polymerization of alcohol pendant PBAEs with cinnamoyl chloride afforded a library of soft elastomeric materials with thermal and mechanical properties that can be predictably tuned. Utilizing a novel diacrylate photo-monomer and polymerization with different primary amine monomers, multifunctional photo-responsive PBAEs were developed to which supplementary chemical or biological moieties could be attached, or polymer properties modified.

5.2 Directions

As introduced in the review of shape memory polymers in Chapter I, there is significant interest in use of SMPs for biomedical applications, some of which have been realized. The application of *in vivo* light responsive shape memory materials requires model *in vitro* studies to examine the viability of surrounding cells and tissue during the photo-recovery of macroscopic shapes in both the PEU and PBAE systems. Such tests will need to also focus on optimization with available surgical scopes which can irradiate a material once within the body in order to negate bulk tissue irradiation.

Investigation of the DCA PEU system as a multifunctional smart tissue scaffold should be performed due to its ability to perform a triple shape effect at one targeted temperature on multiple size scales. Interactions between the shape memory surface and surrounding tissue in the temporary form and during surface switching should elicit interesting responses such as adhesion, migration, and proliferation[1,2] that can be used in combination with macroscopic shape changing employed for easier implantation and removal. *In vivo* degradation and cytotoxicity studies are also required to fully evaluate these materials for biomaterials applications. In addition, *in vitro* model studies would be necessary to show that the macroscopic shape change showed the mechanical force to recover in environments of possible applications. Multifunctional PBAEs via the functional diacrylate route could be similarly studied as smart scaffolds where rather than changing physical surface topography, the chemical nature of the surface could be functionalized with relevant chemical or biological compounds.

Lastly, the combination of macroscopic light-induced shape memory and macroscopic/microscopic thermal shape memory leads to probing the feasibility of microscopic light-induced shape memory. An alternate method of programming microscopic features would be required so that the PRINT™ mold was uniformly compressed while the film surface was also visible during irradiation. This could be possible with the fabrication of a transparent compression device or the design of a press with attached light source. Practical sizes, aspect ratio, and shapes of the surface arrays would also need to be investigated.

References

1) Yim, E.K.F.; Leong, K.W. *Nanomedicine* 2005, *1*, 10.

2) McNamara, L.E.; McMurray, R.J.; Biggs, M.J.P.; Kantawong, F.; Oreffo, R.O.C.; Dalby, M.J. *J Tissue Eng* 2010, *2010*, 120623.

Appendix A

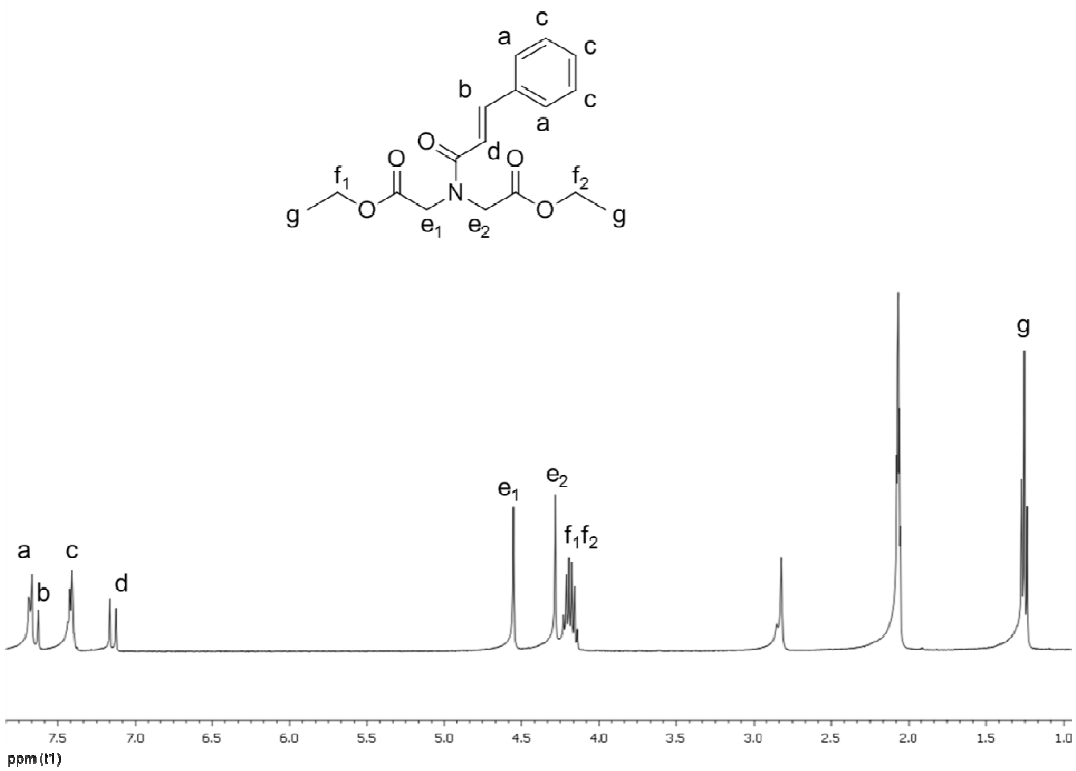

^{1}H-NMR of DCA monomer

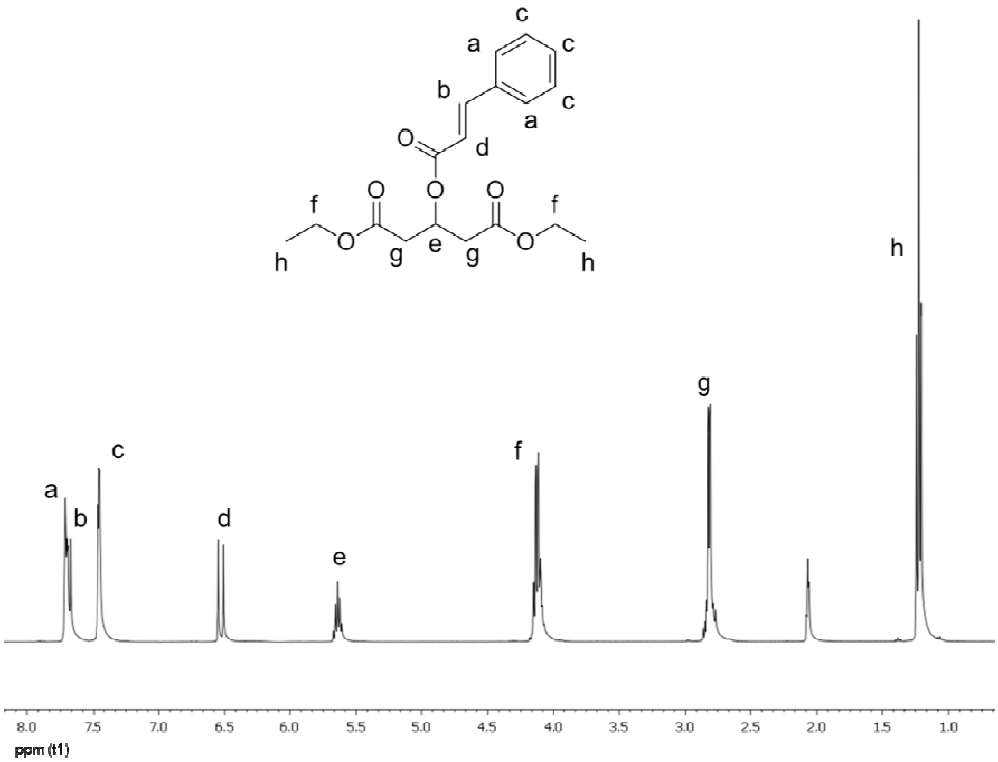

^{1}H-NMR of DCE monomer

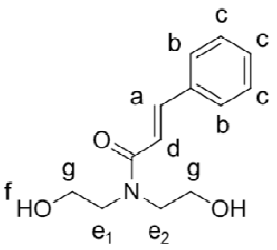

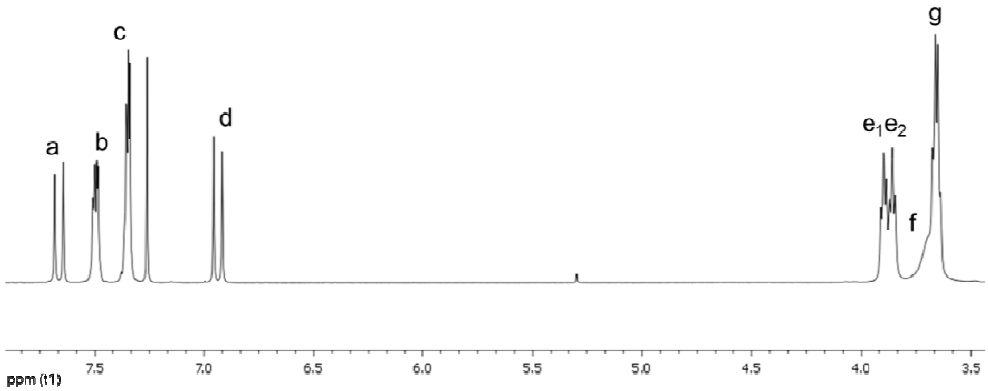

^{1}H-NMR CAD monomer

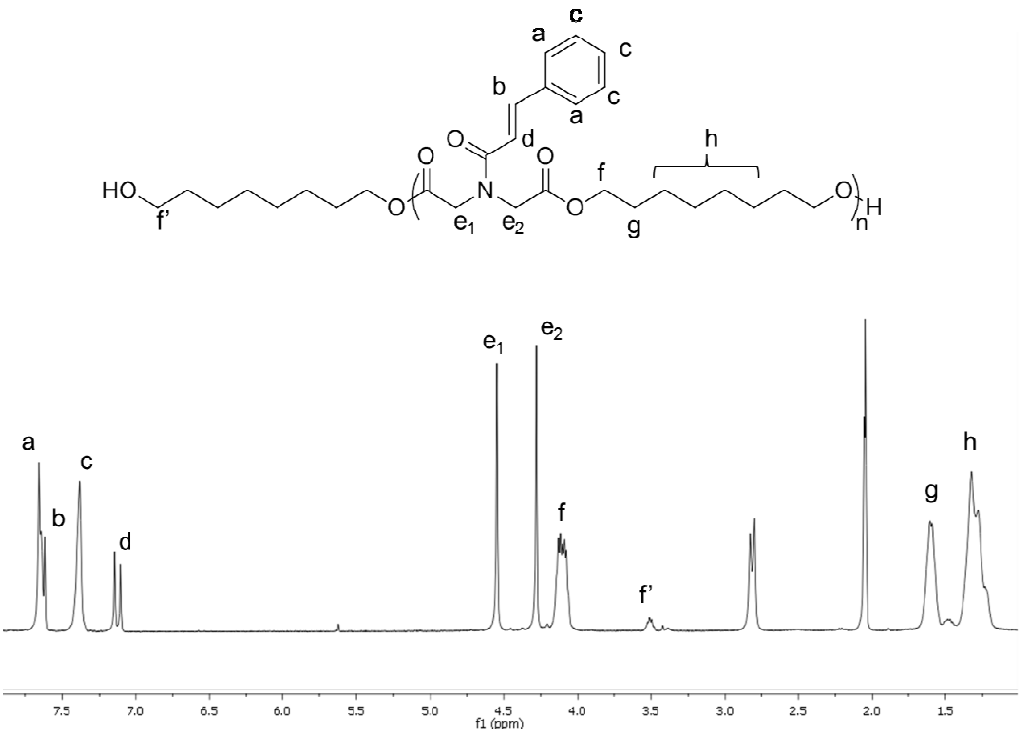

^{1}H-NMR of DCA-OD prepolymer

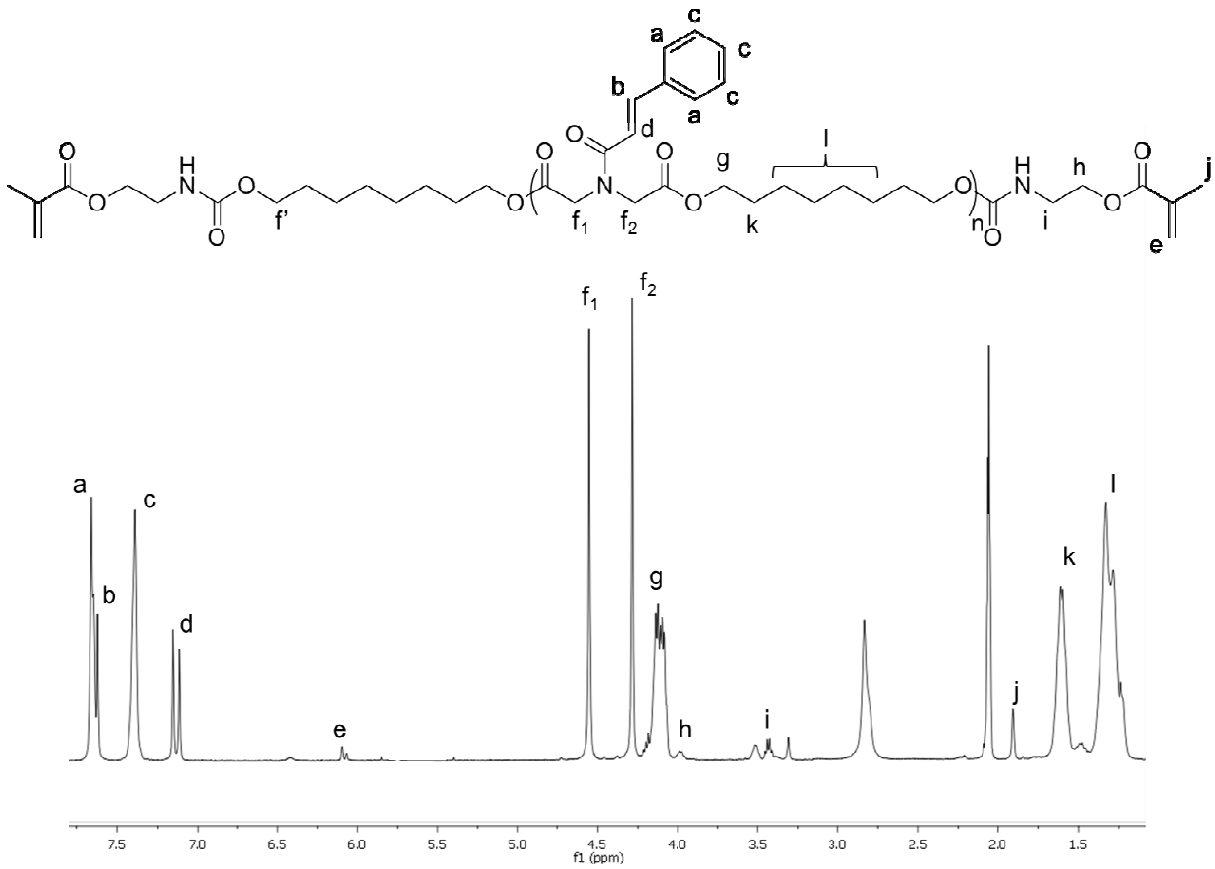

^{1}H-NMR of DCA-OD endcapped prepolymer

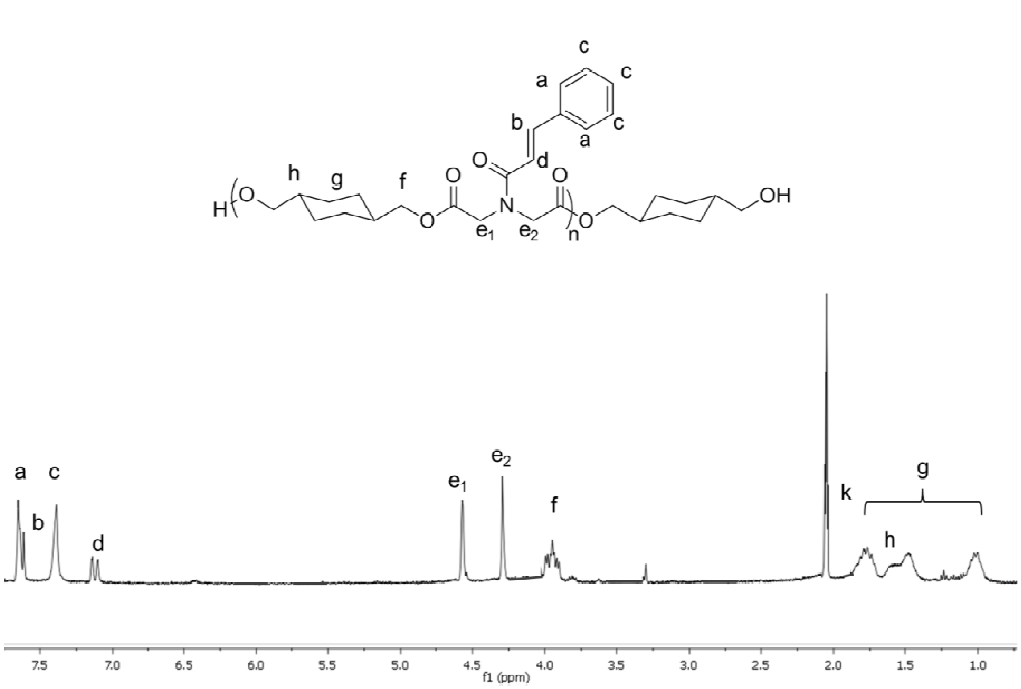

^{1}H-NMR of DCA-CHDM prepolymer

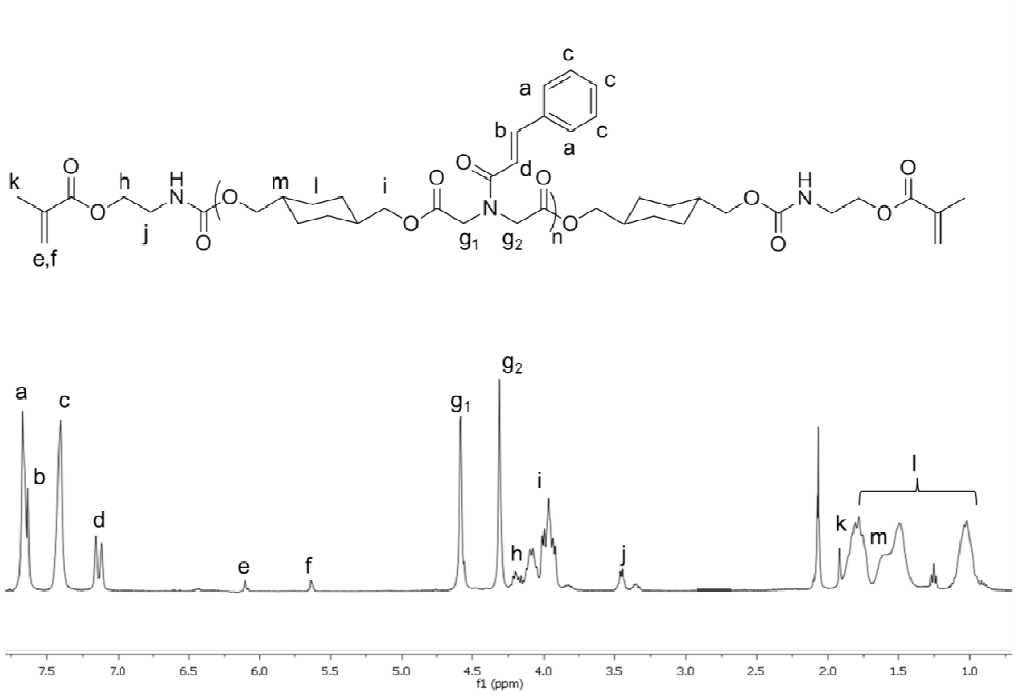

^{1}H-NMR of DCA-CHDM endcapped prepolymer

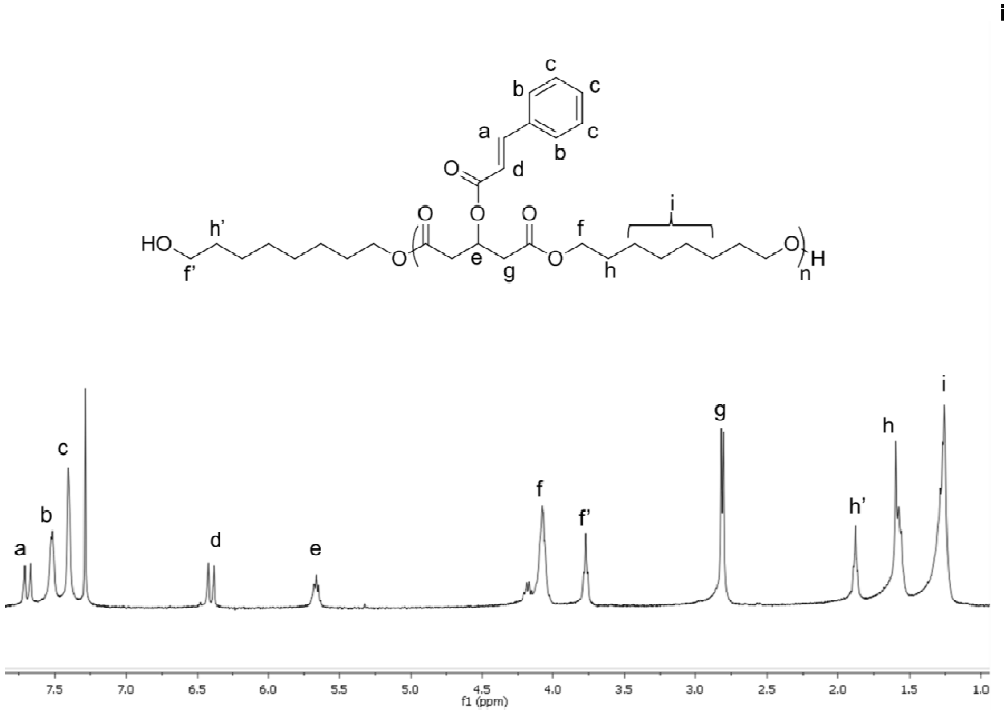

^{1}H-NMR of DCE-OD prepolymer

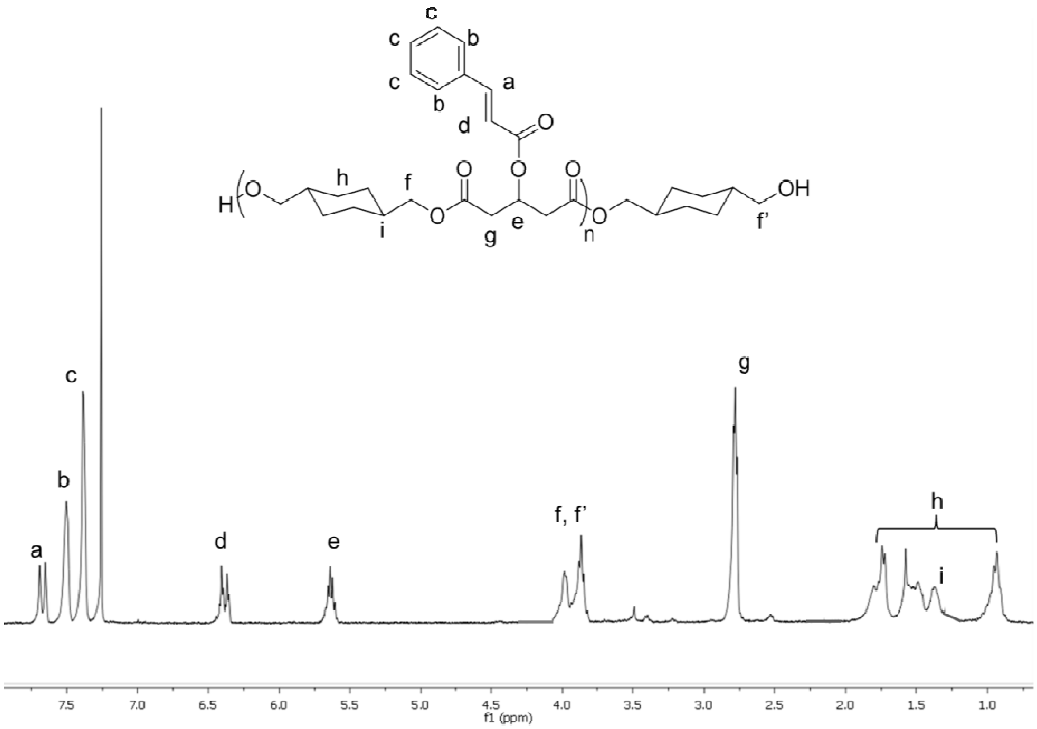

^{1}H-NMR of DCE-CHDM prepolymer

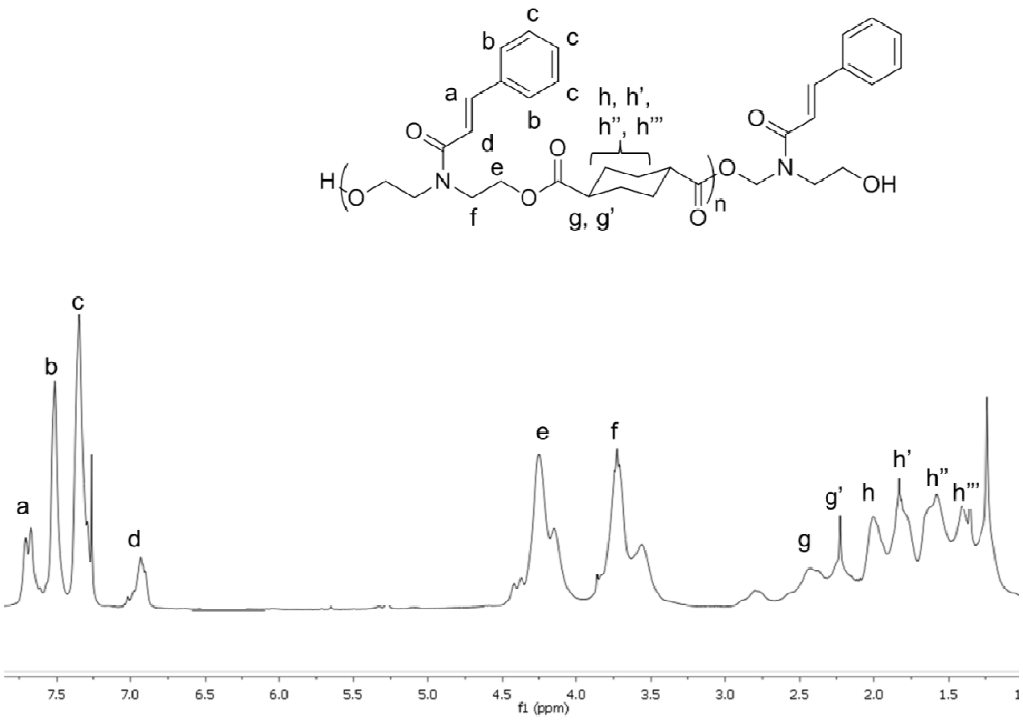

^{1}H-NMR of CAD-CHDCA

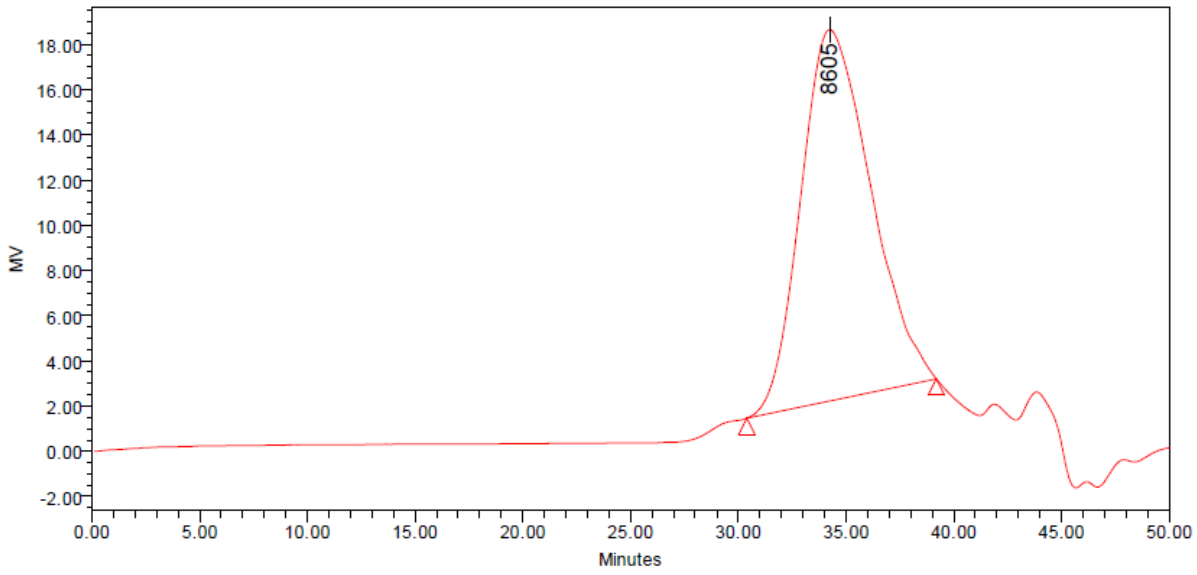

GPC Results

	Dist Name	Mn	Mw	Mv	MP	Mz	Mz+1	Poly dispersity	K	alpha
1		5502	8575		8605	12057	15622	1.558549		

GPC Chromatogram of DCA-OD-5

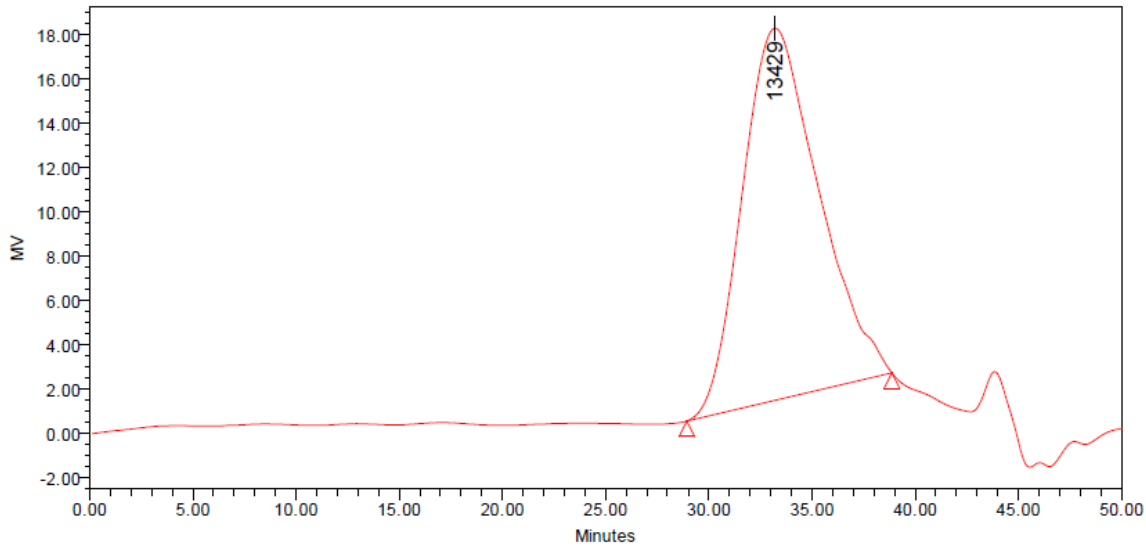

GPC Results

	Dist Name	Mn	Mw	Mv	MP	Mz	Mz+1	Poly dispersity	K	alpha
1		7935	14183		13429	21583	29196	1.787429		

GPC Chromatogram of DCA-OD-8

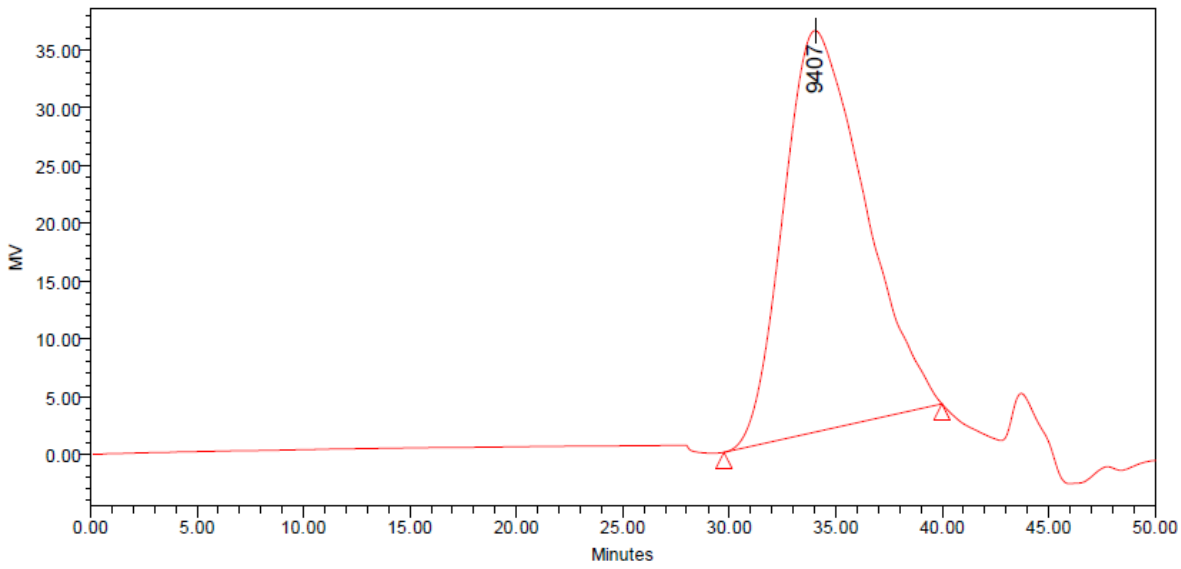

GPC Results

	Dist Name	Mn	Mw	Mv	MP	Mz	Mz+1	Poly dispersity	K	alpha
1		4903	9175		9407	14099	18966	1.871272		

GPC Chromatogram of DCA-CHDM-5

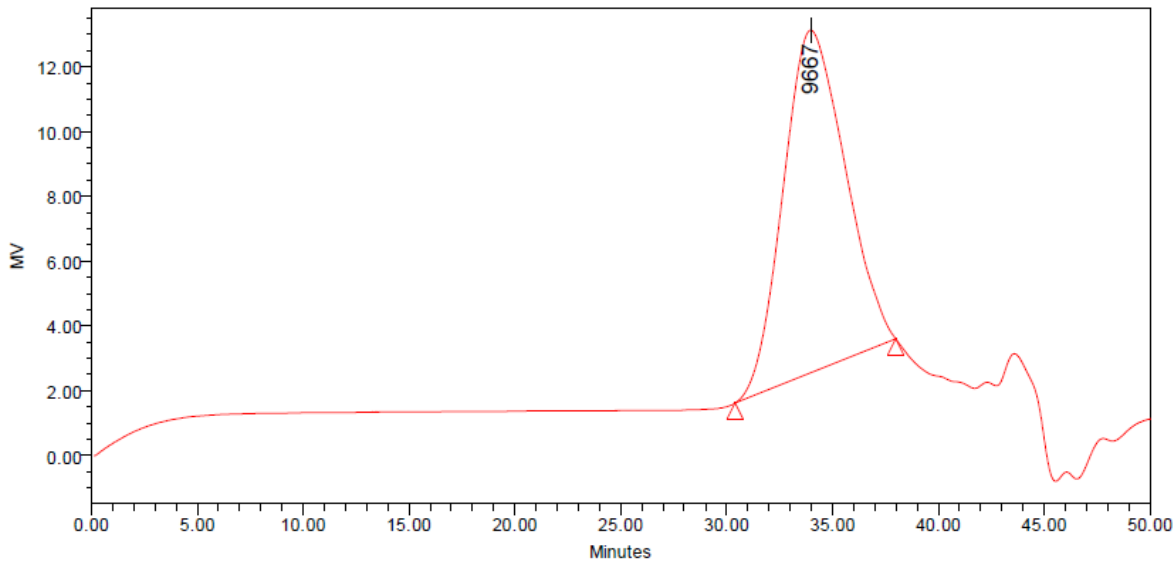

GPC Results

	Dist Name	Mn	Mw	Mv	MP	Mz	Mz+1	Poly dispersity	K	alpha
1		7219	10105		9667	13443	16915	1.399799		

GPC Chromatogram of DCA-CHDM-8

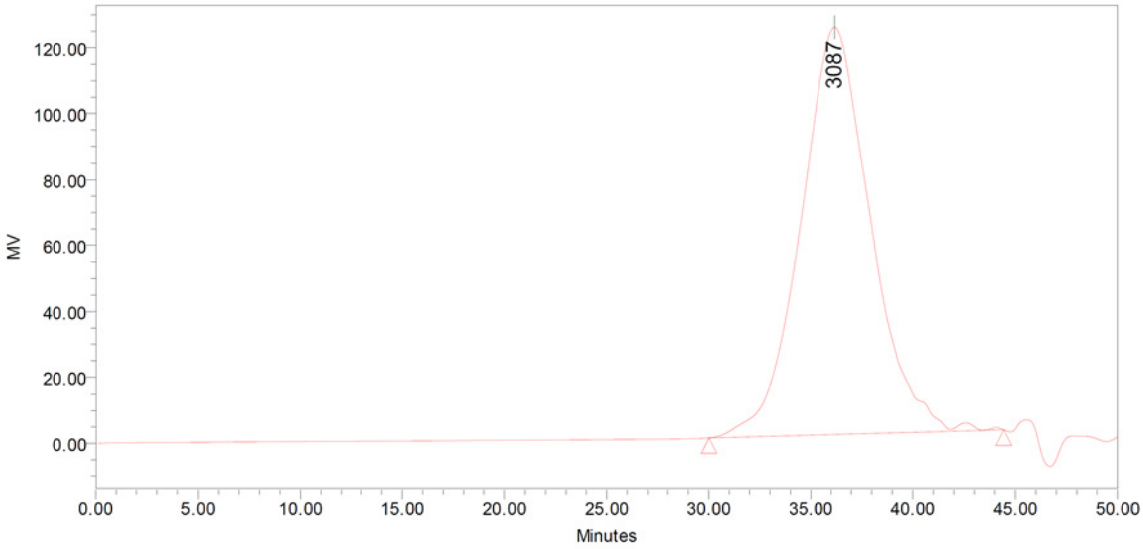

GPC Results

	Dist Name	Mn	Mw	Mv	MP	Mz	Mz+1	Poly dispersity	K	alpha
1		1944	4051		3087	7880	14762	2.083307		

GPC Chromatogram of DCE-OD

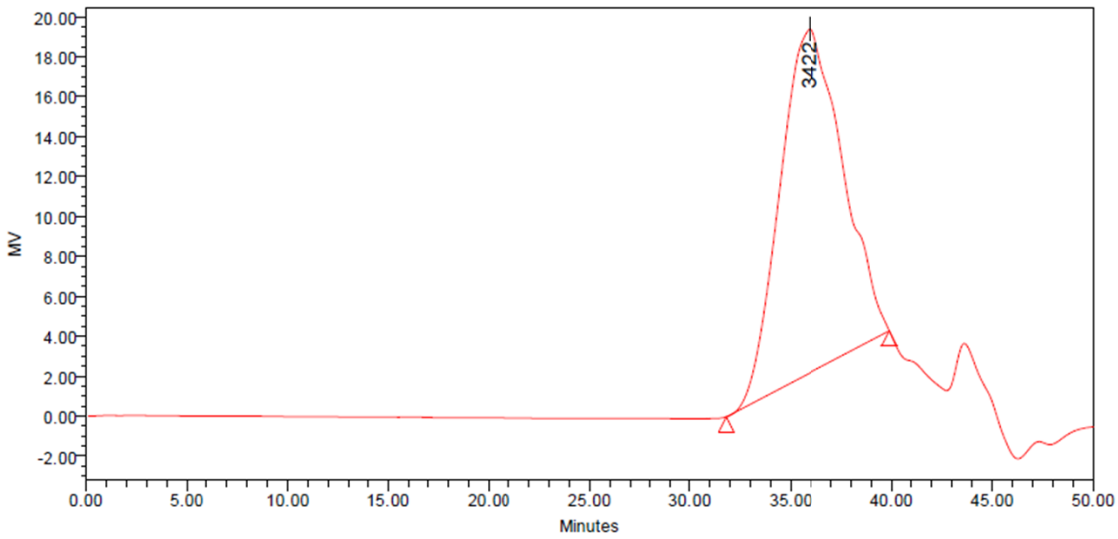

GPC Results

	Dist Name	Mn	Mw	Mv	MP	Mz	Mz+1	Poly dispersity	K	alpha
1		2574	3929		3422	5604	7345	1.526089		

GPC Chromatogram of DCE-CHDM

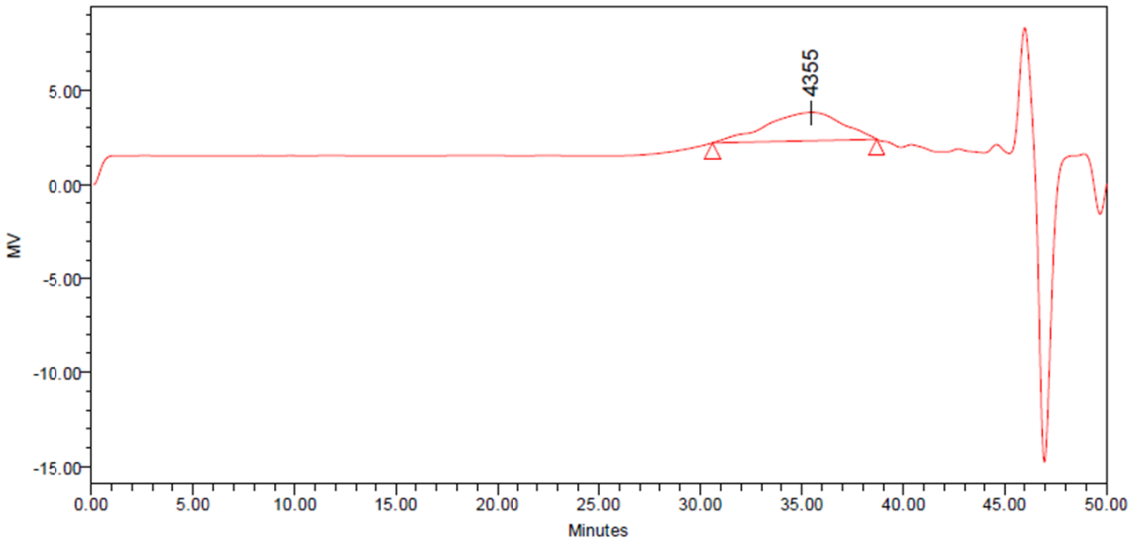

GPC Results

	Dist Name	Mn	Mw	Mv	MP	Mz	Mz+1	Poly dispersity	K	alpha
1		4097	7381		4355	13057	19379	1.801530		

GPC Chromatogram of CAD-CHDCA

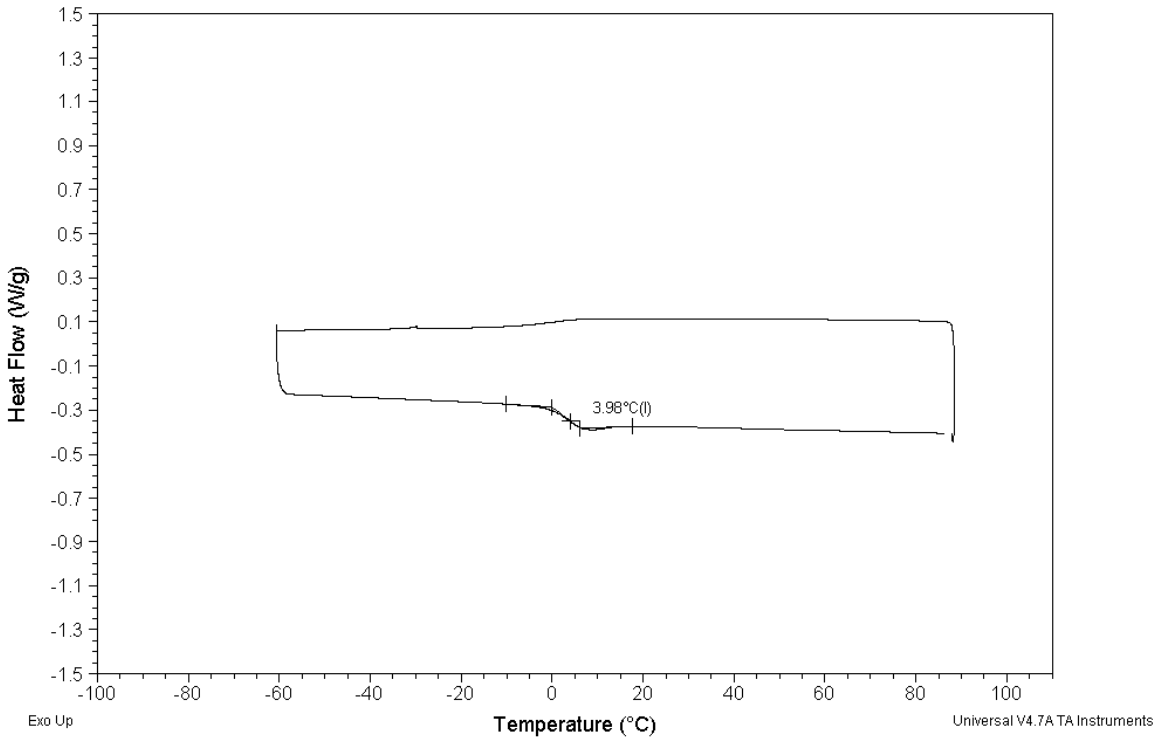

DSC of DCA-OD-5

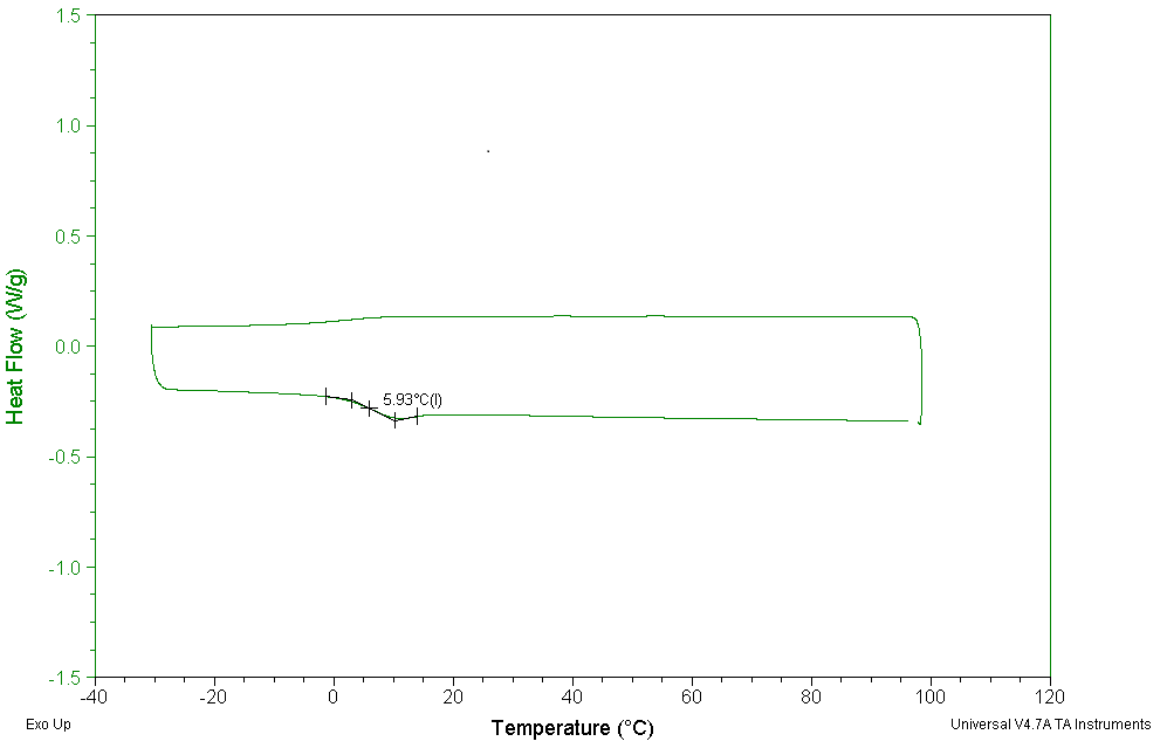

DSC of DCA-OD-8

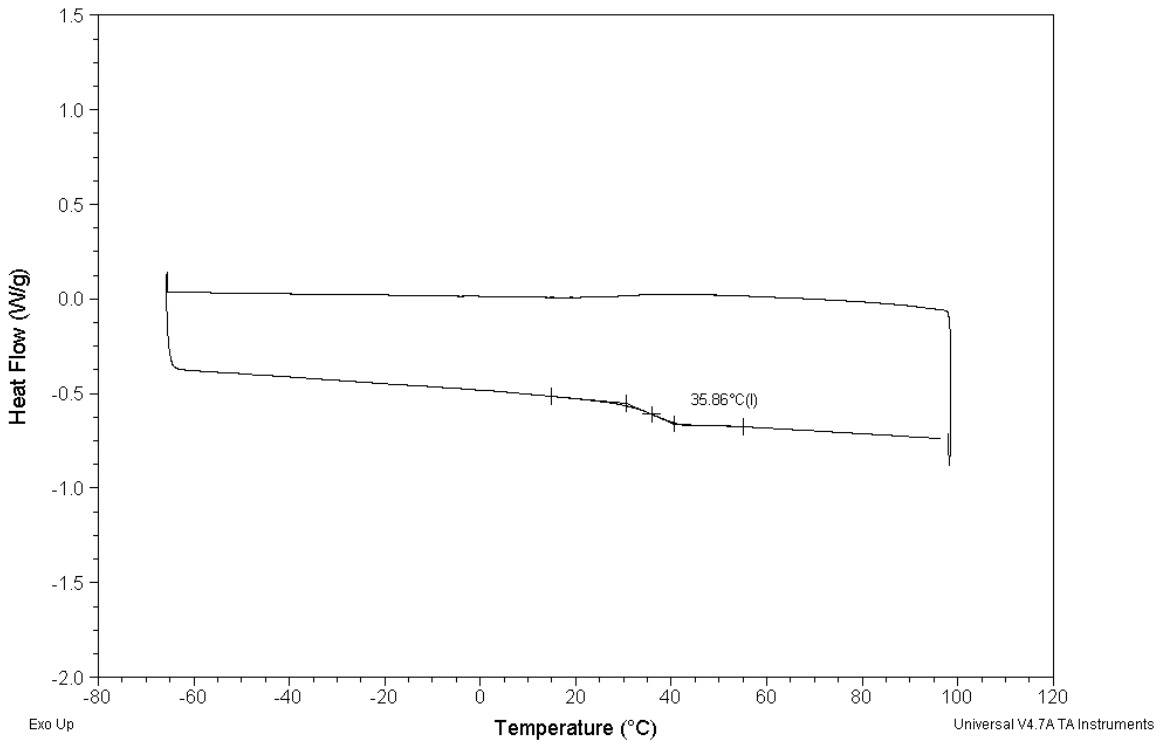

DSC of DCA-CHDM-5

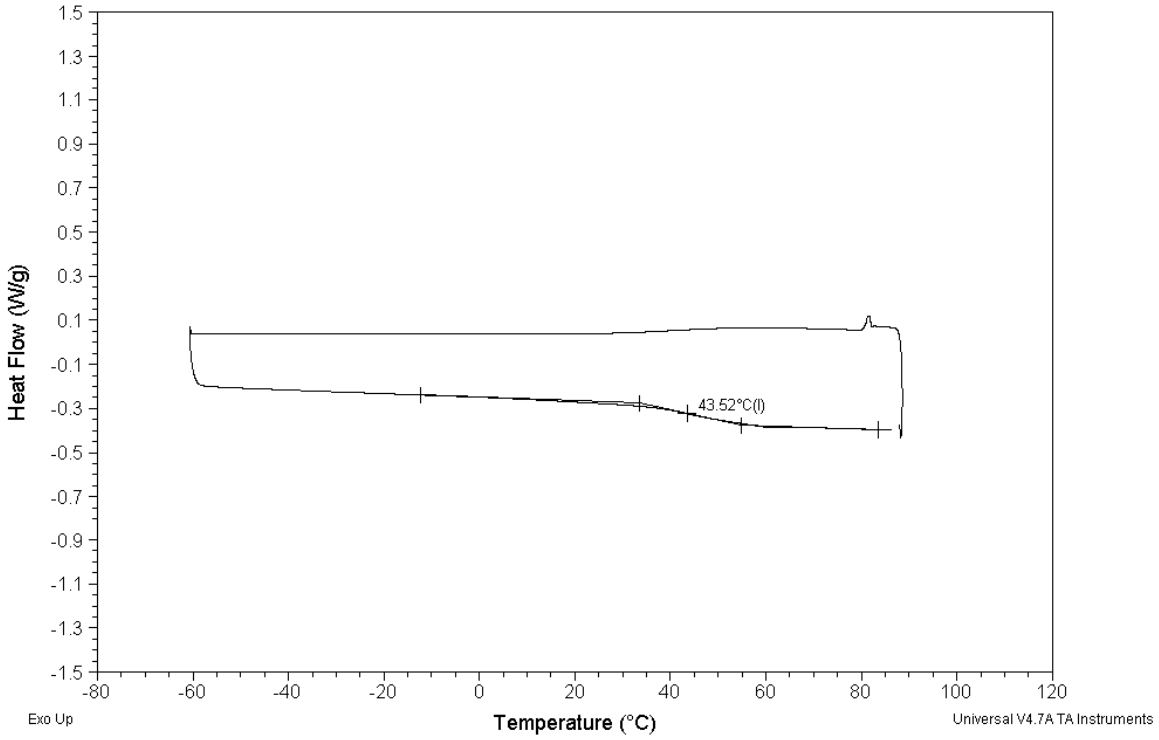

DSC of DCA-CHDM-8

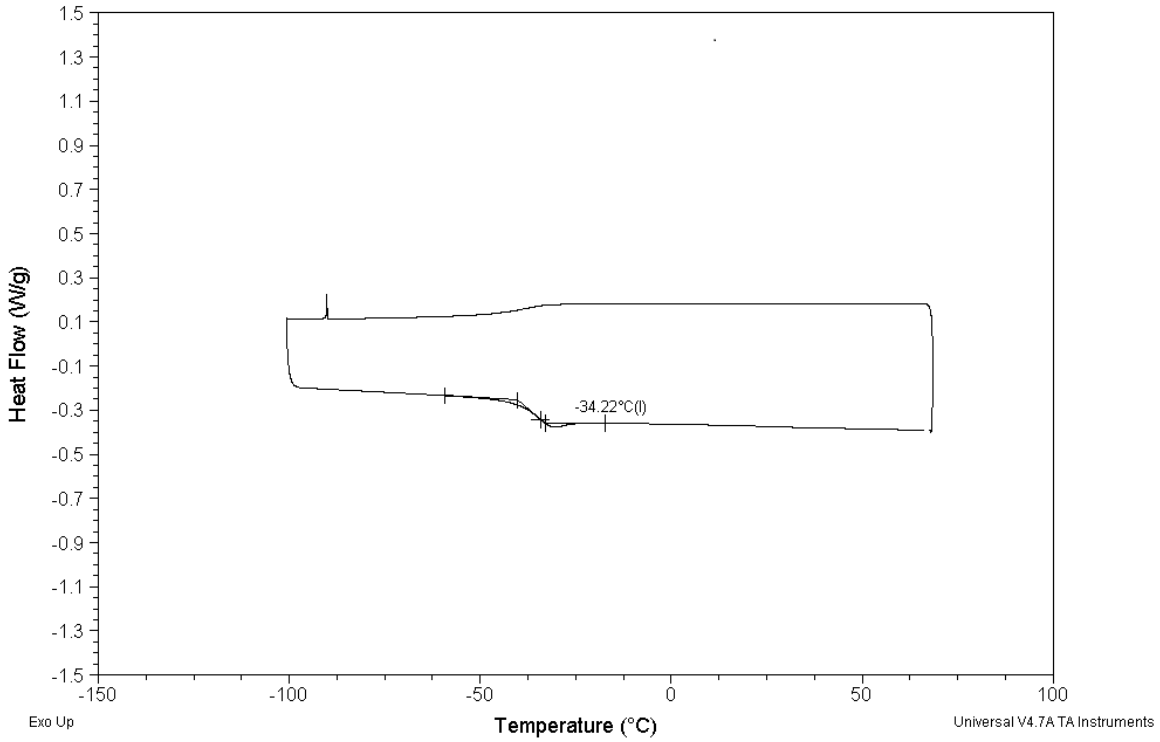
Heat Flow (W/g)
1.5
1.3
1.1
0.9
0.7
0.5
0.3
0.1
-0.1
-0.3
-0.5
-0.7
-0.9
-1.1
-1.3
-1.5
-34.22°C(I)
-150
-100
-50
0
50
100
Exo Up
Temperature (°C)
Universal V4.7A TA Instruments

DSC of DCE-OD

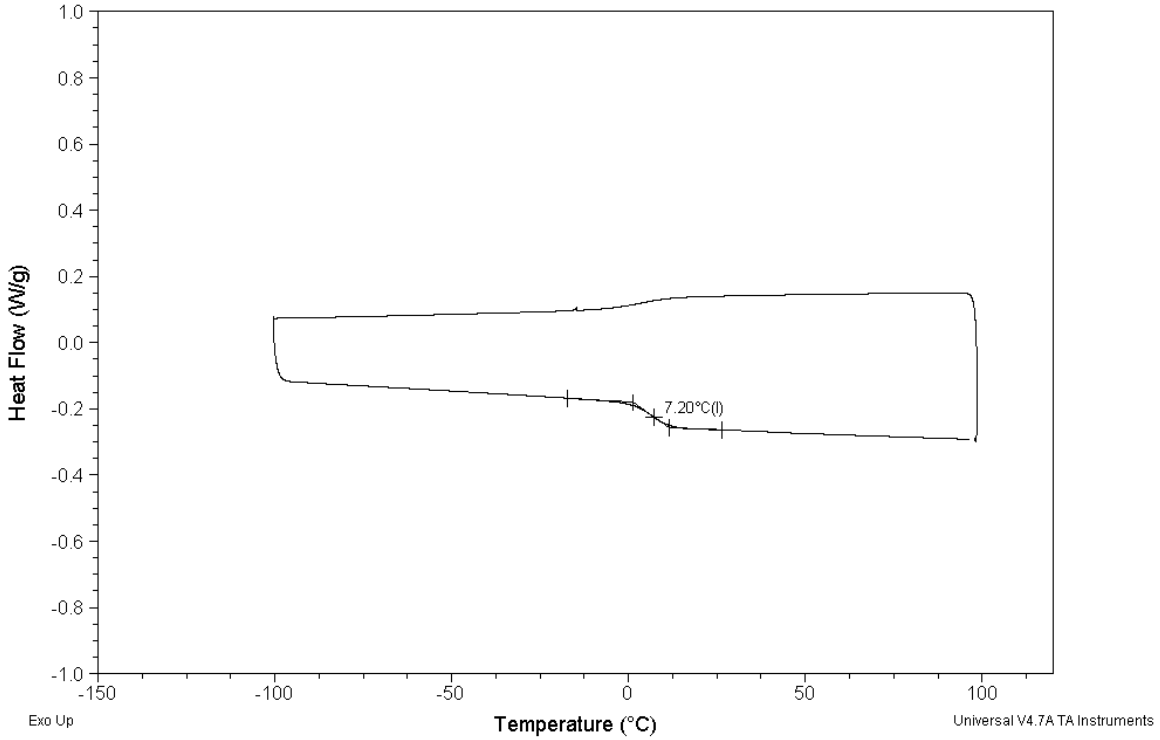

DSC of DCE-CHDM

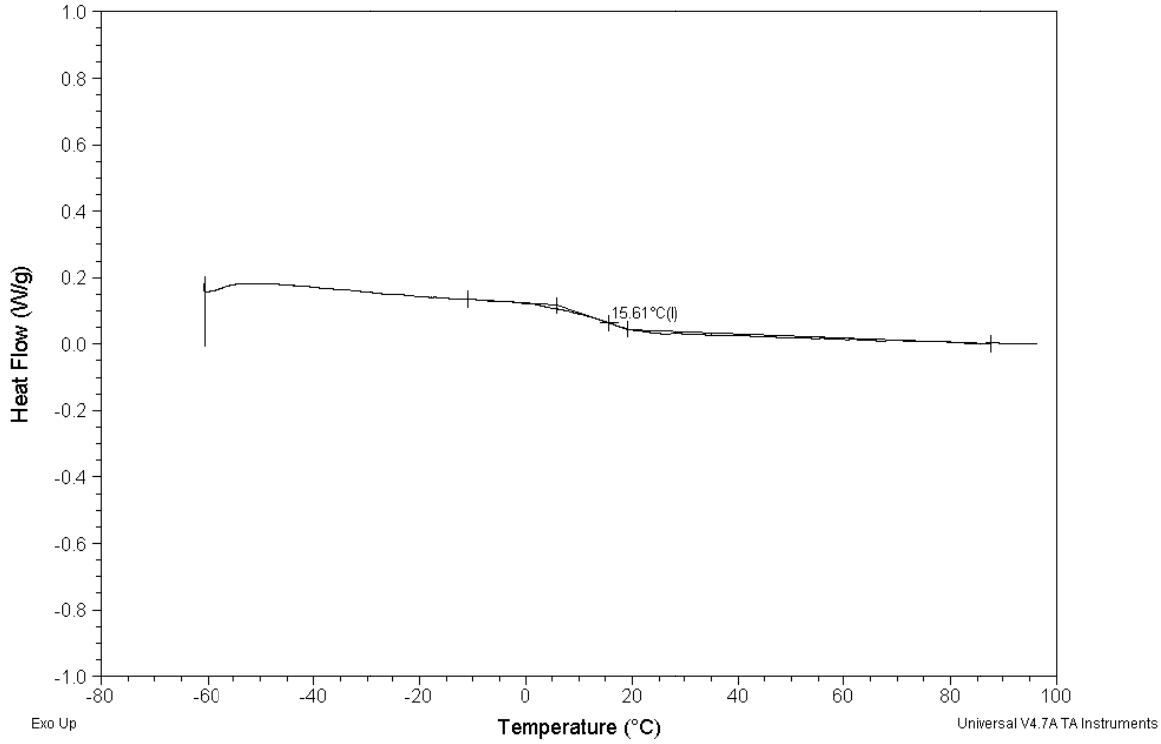

DSC of CAD-CHDCA

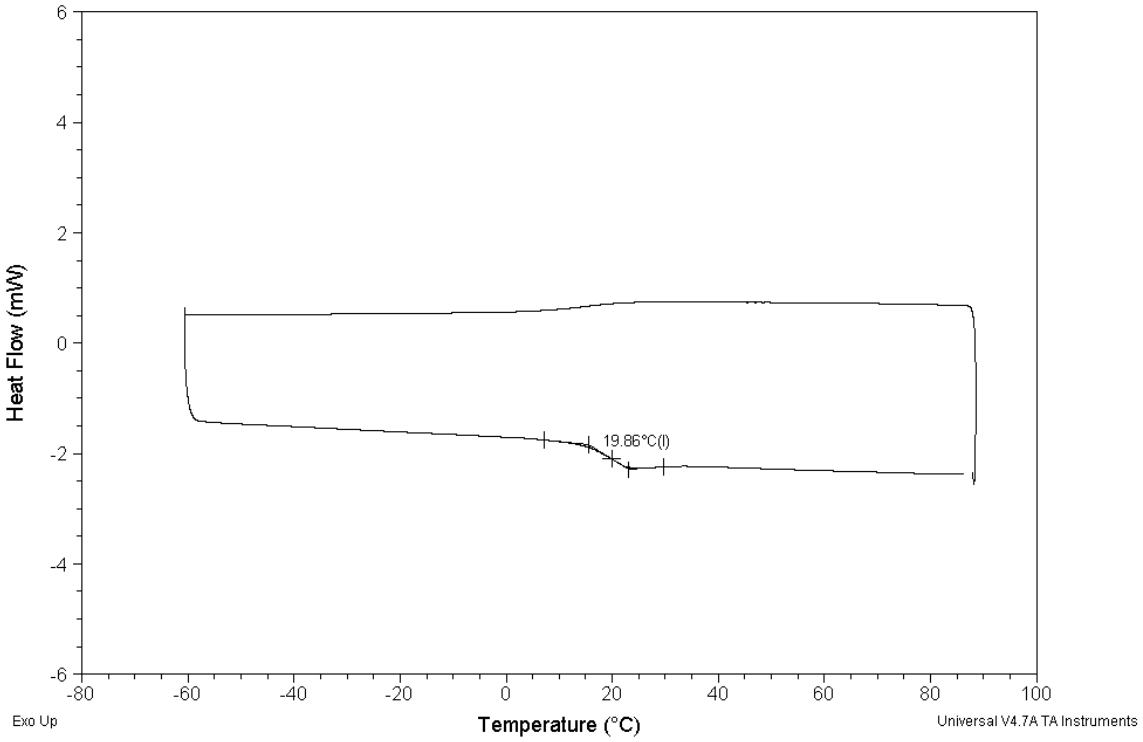

DSC of DCA-OD Film

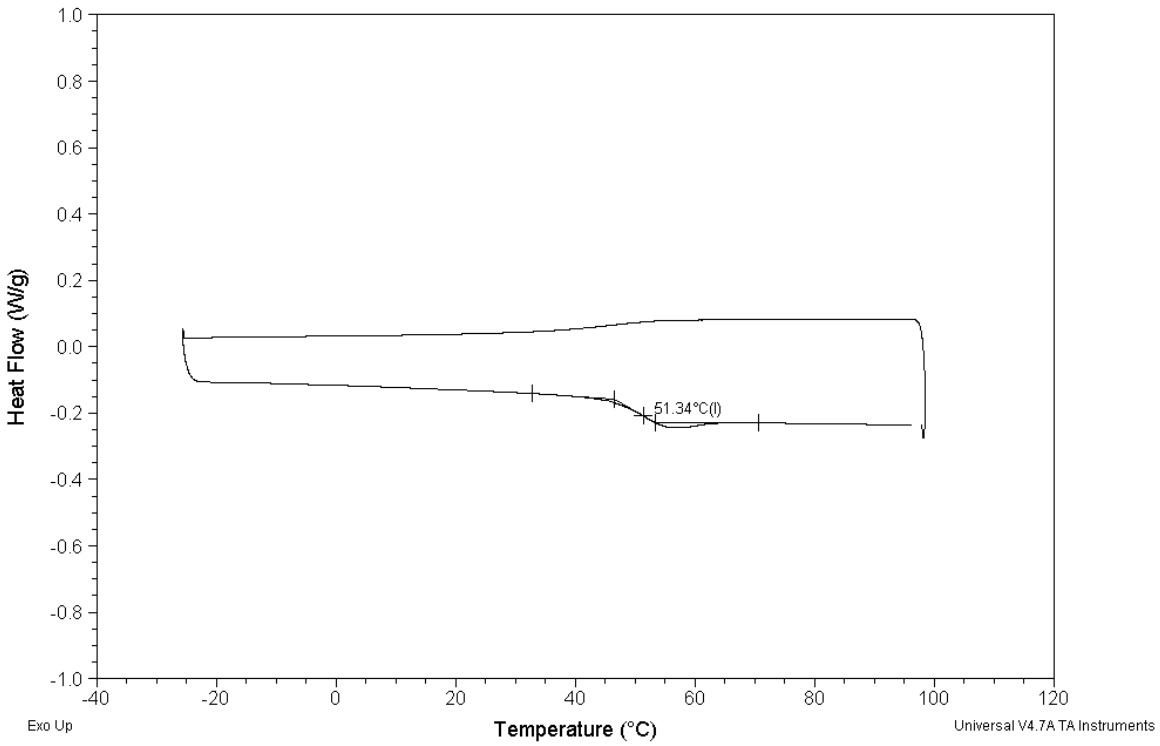

DSC of DCA-CHDM Film

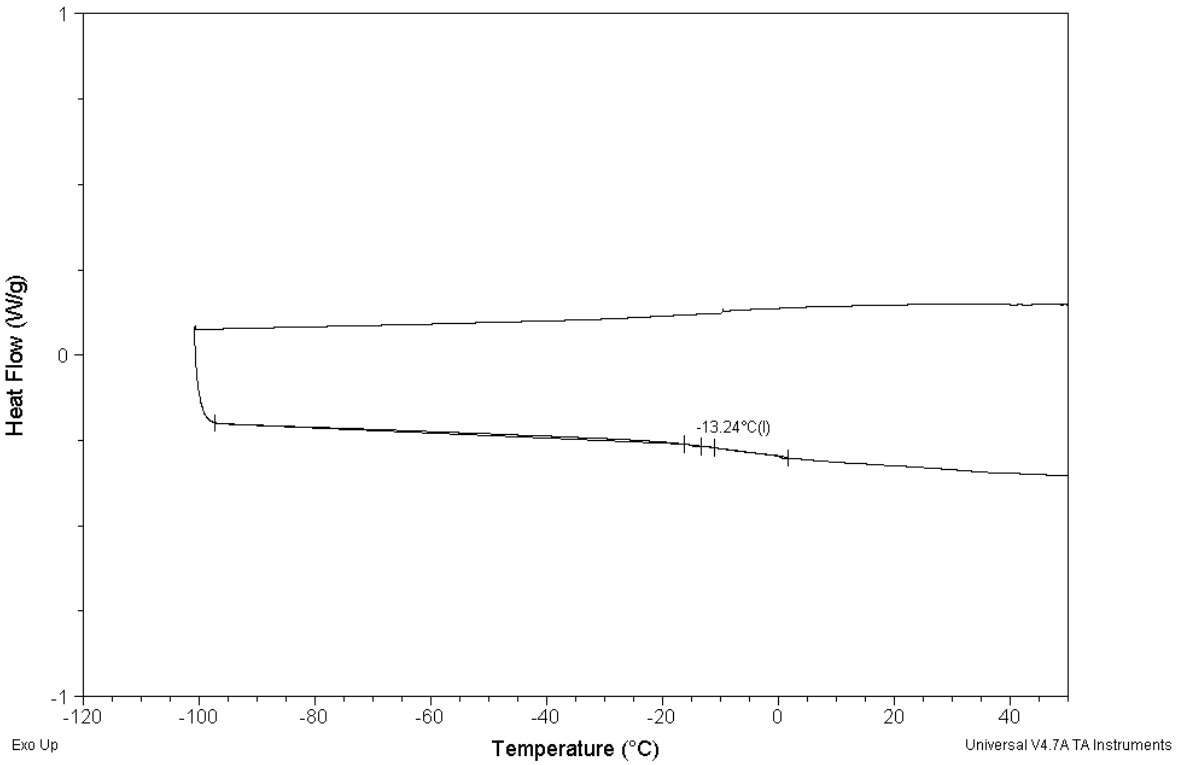

DSC of DCE-OD Film

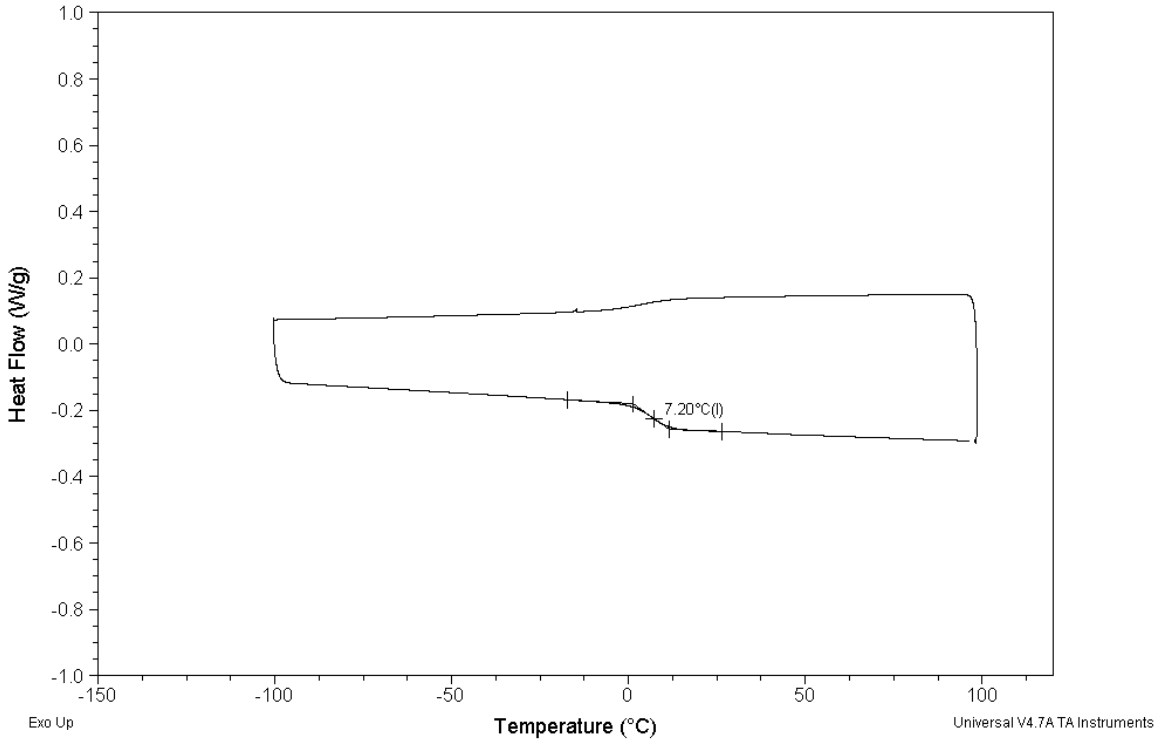

DSC of DCE-CHDM Film

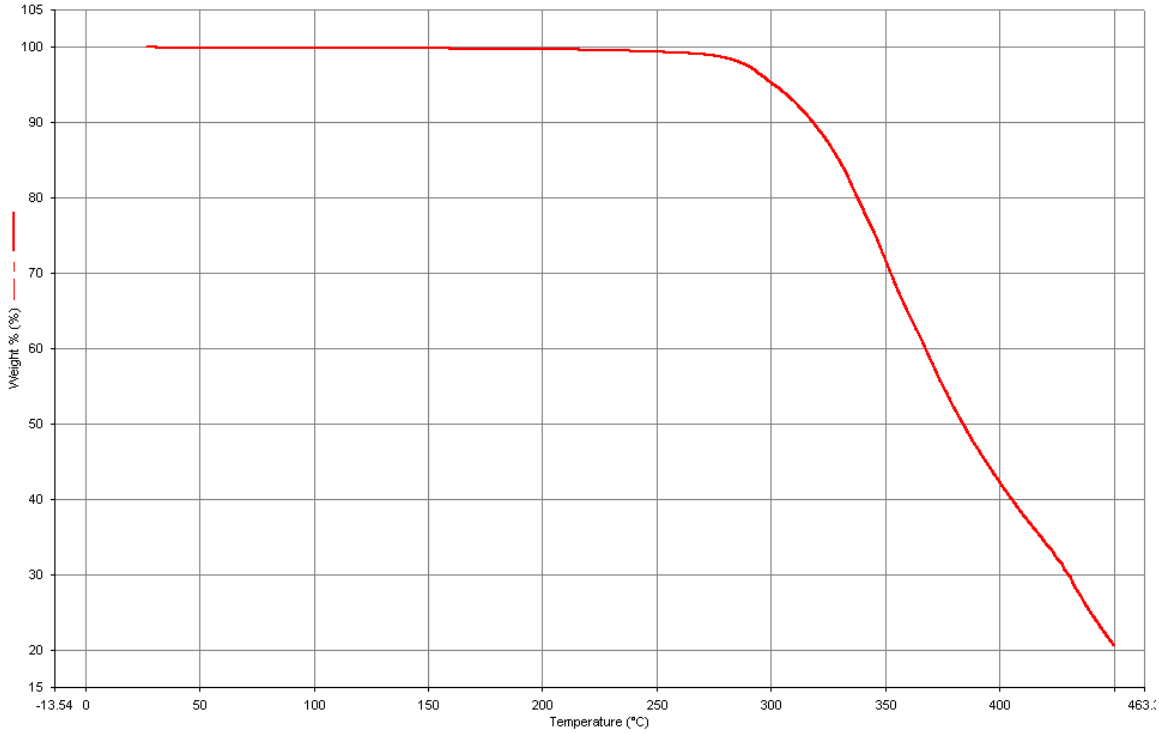

TGA of DCA-OD-5

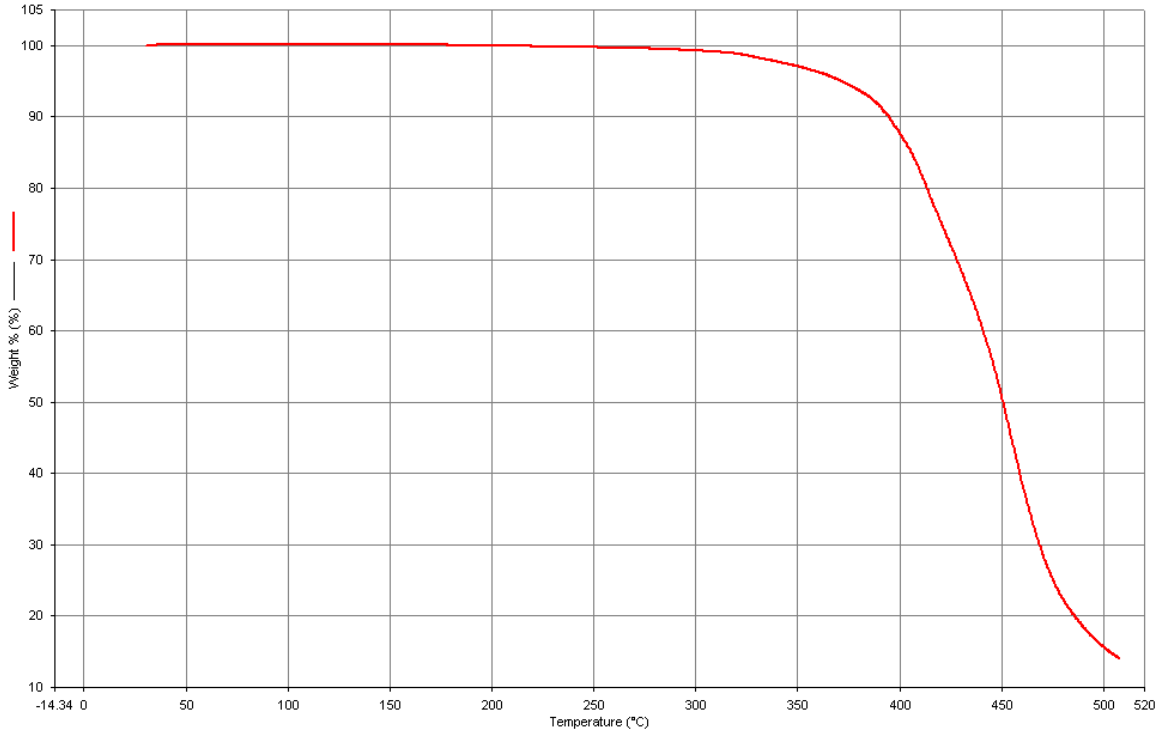

TGA of DCA-OD-8

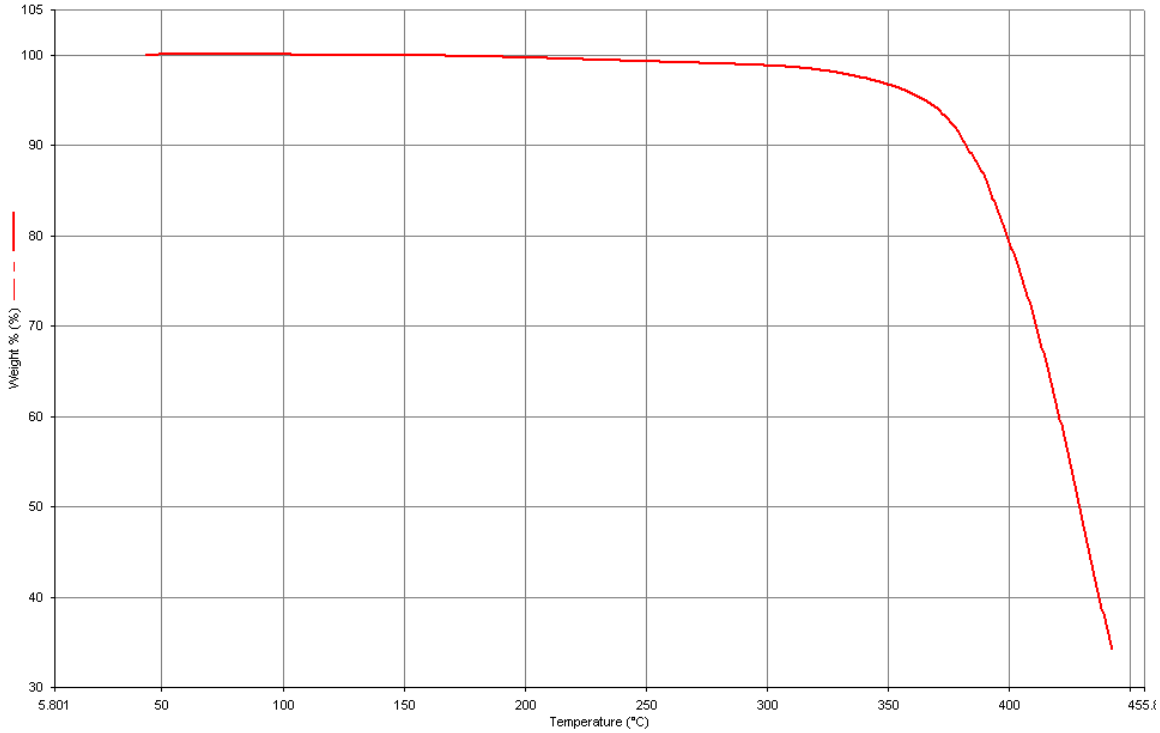

TGA of DCA-CHDM-5

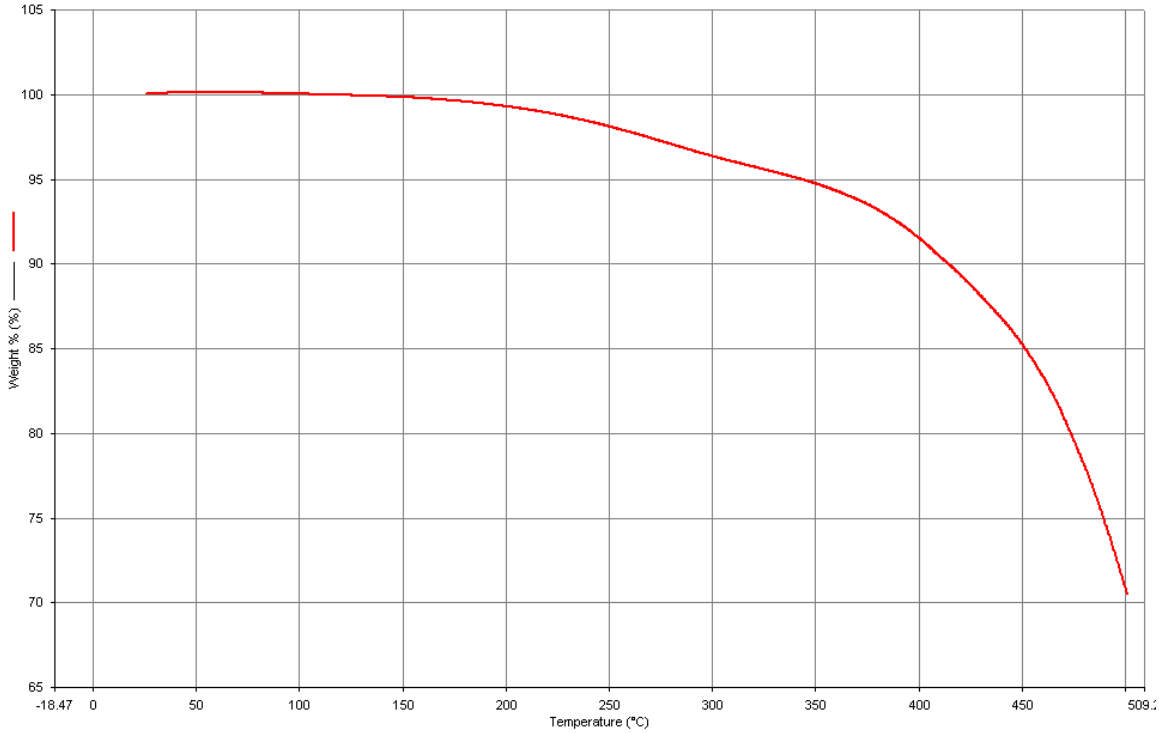

TGA of DCA-CHDM-8

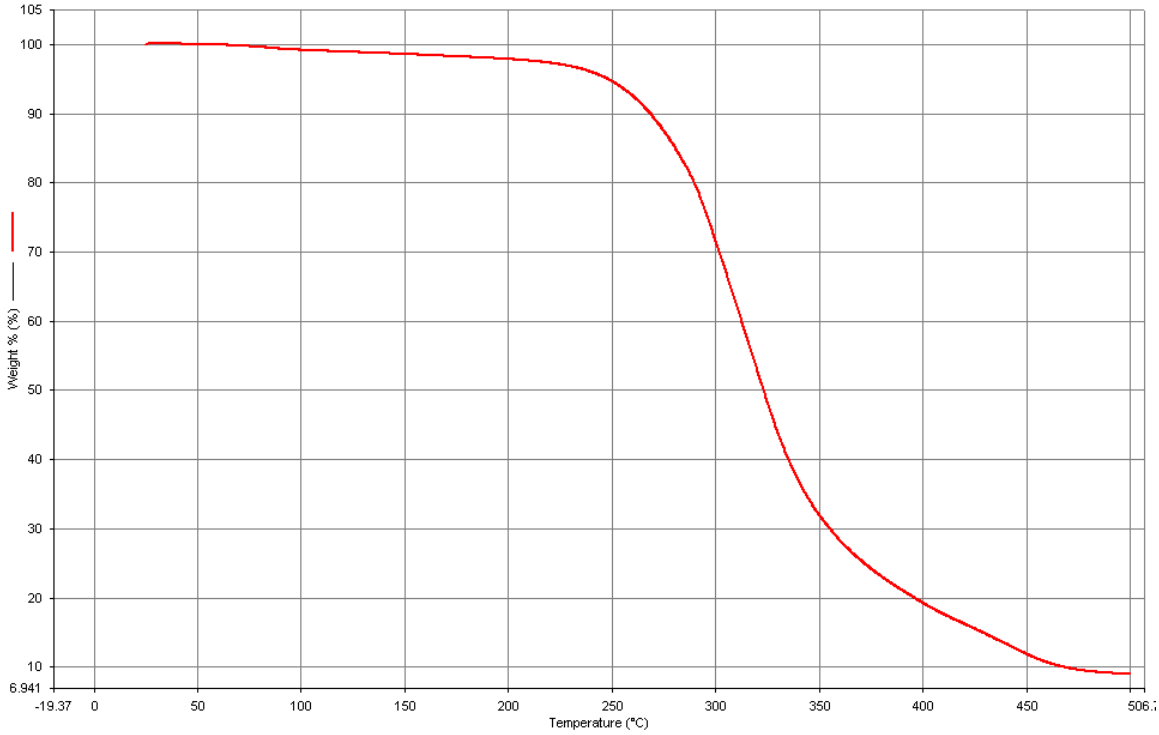
105
100
90
80
70
60
50
40
30
20
10
6.941
Weight % (%)
-19.37
0
50
100
150
200
250
300
350
400
450
Temperature (°C)

TGA of DCE-OD

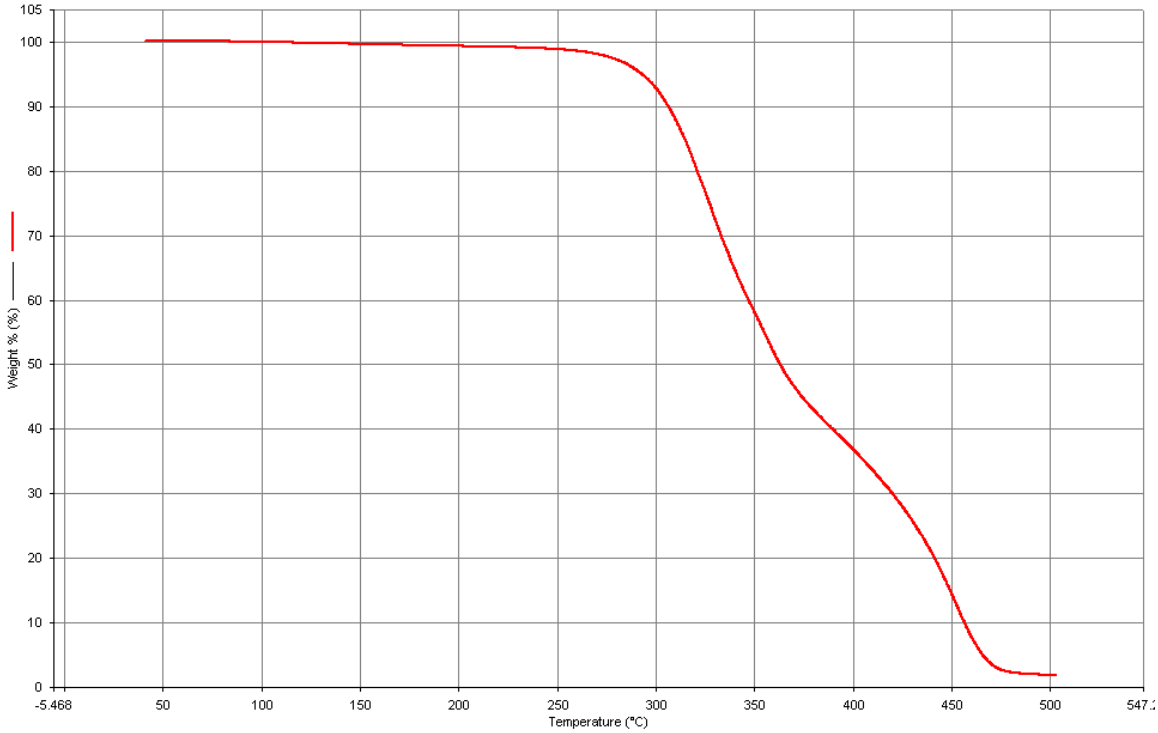

TGA of DCE-CHDM

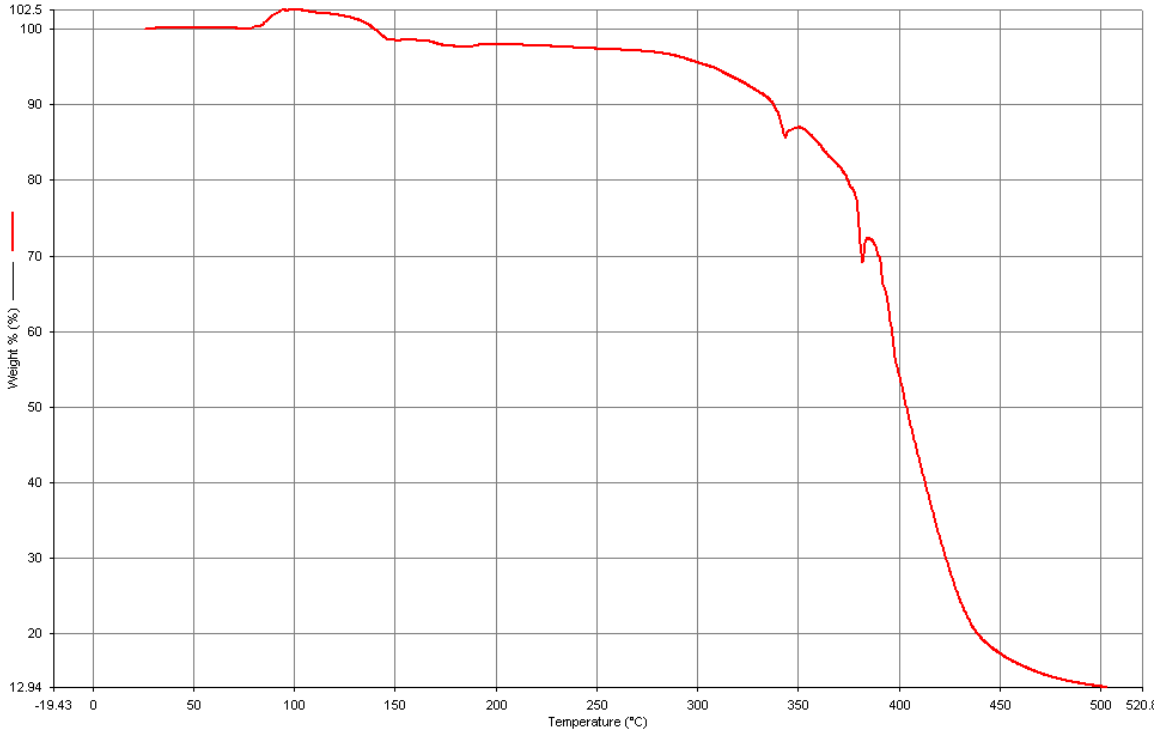

TGA of CAD-CHDCA

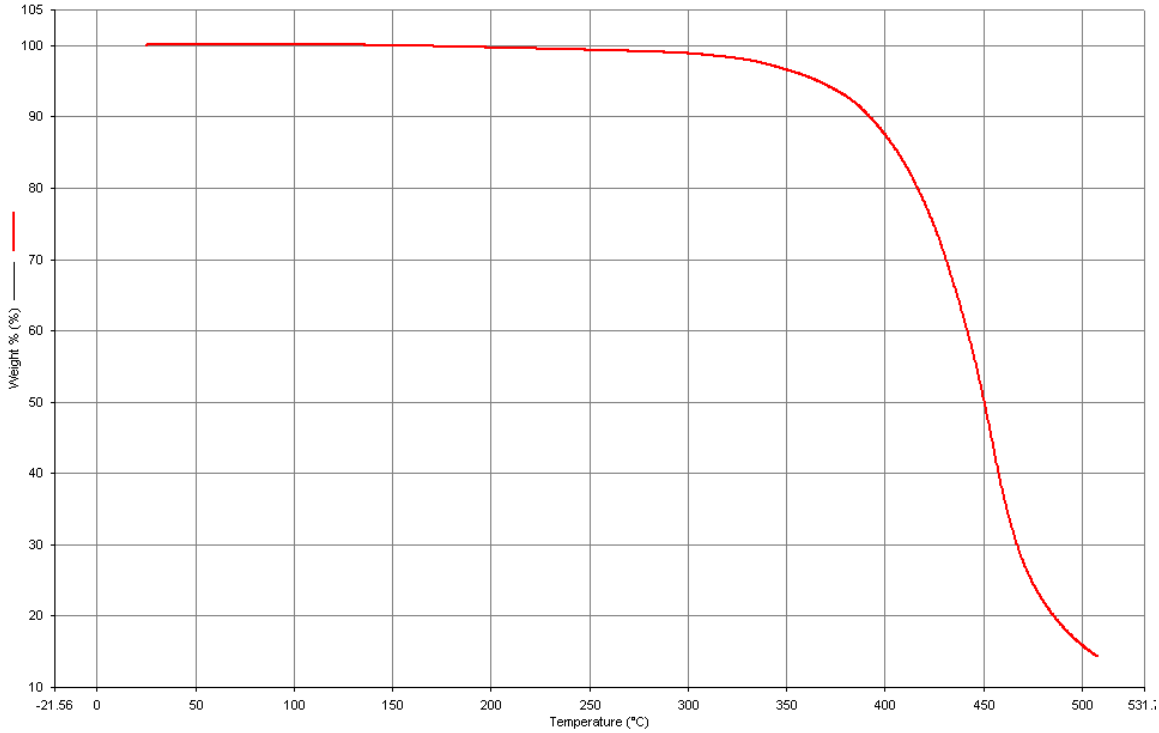

TGA of DCA-OD Film

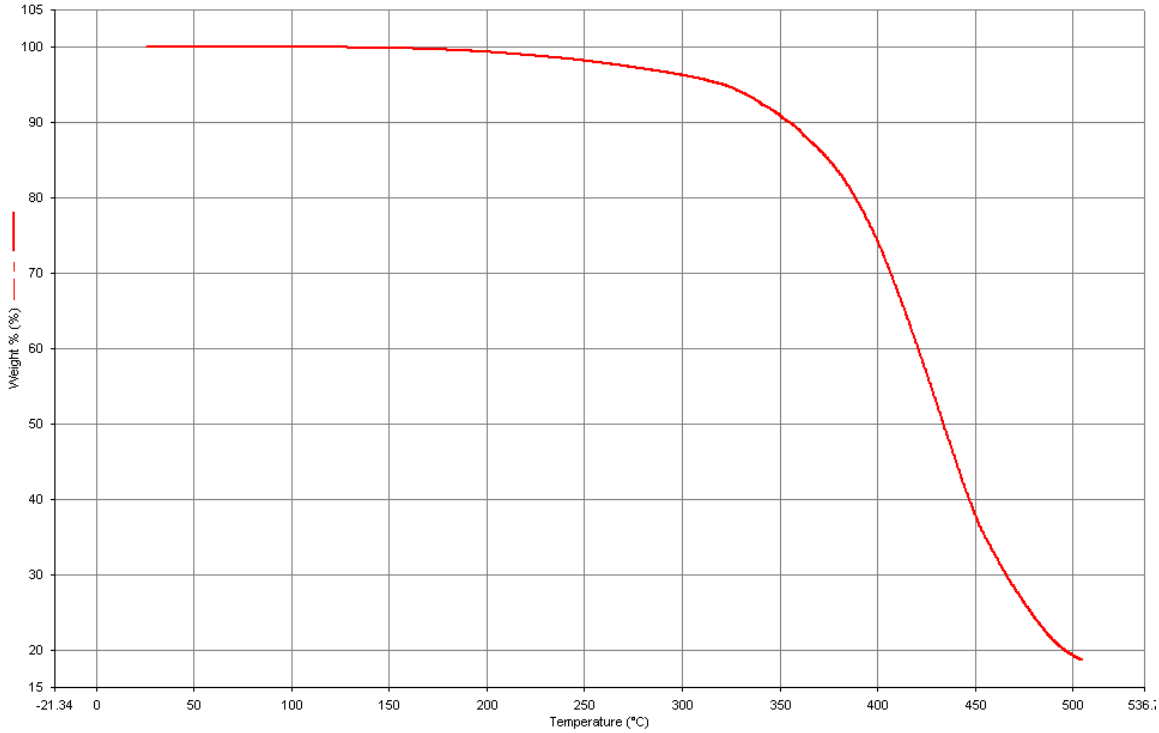

TGA of DCA-CHDM Film

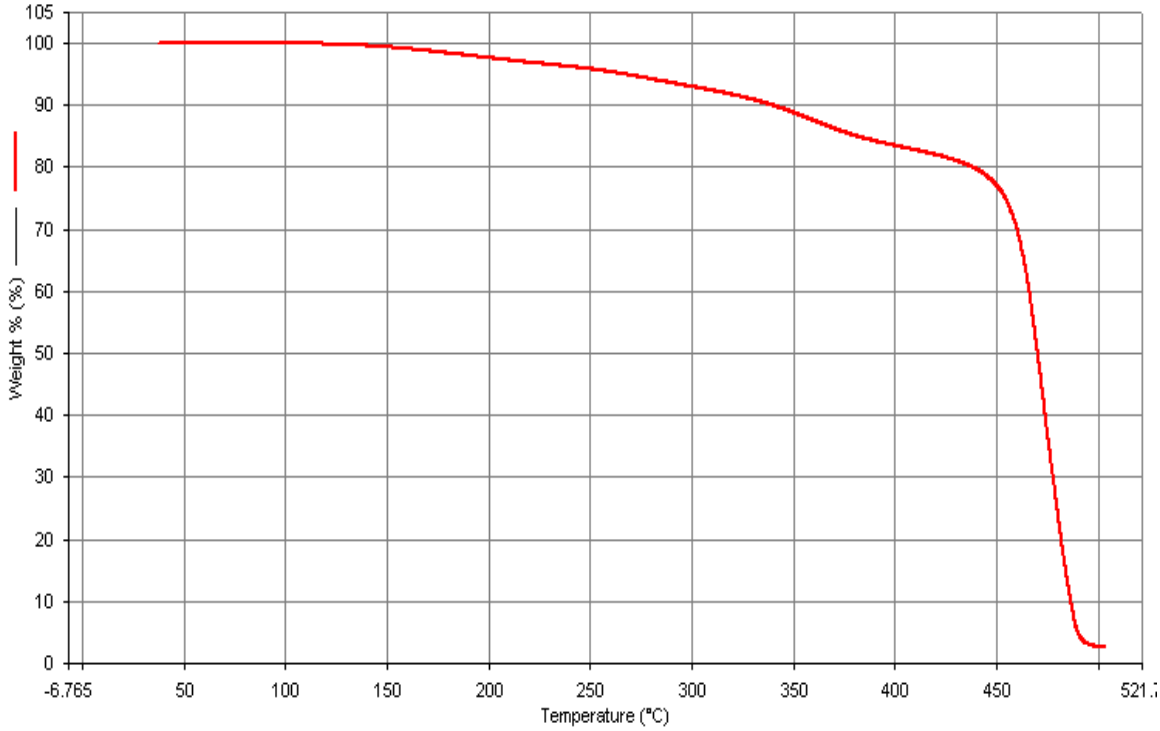

TGA of DCE-OD Film

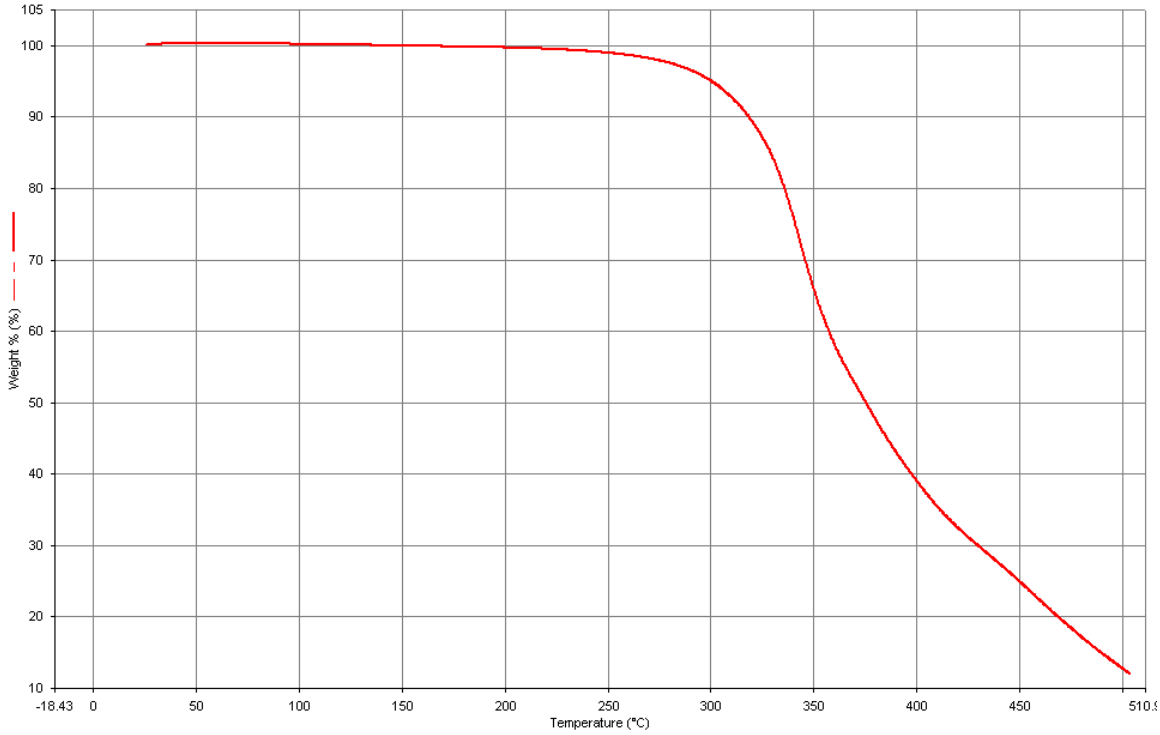

TGA of DCE-CHDM Film

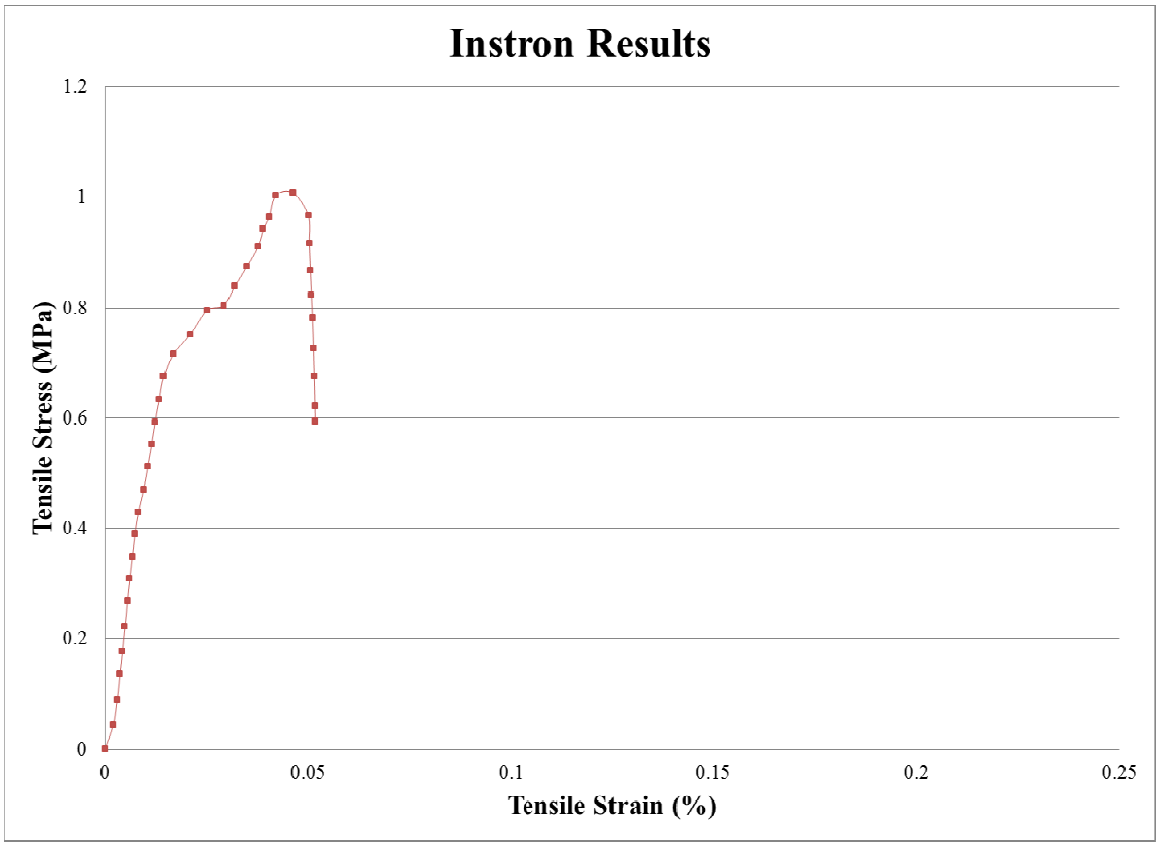

Instron results for DCA-CHDM elastomer

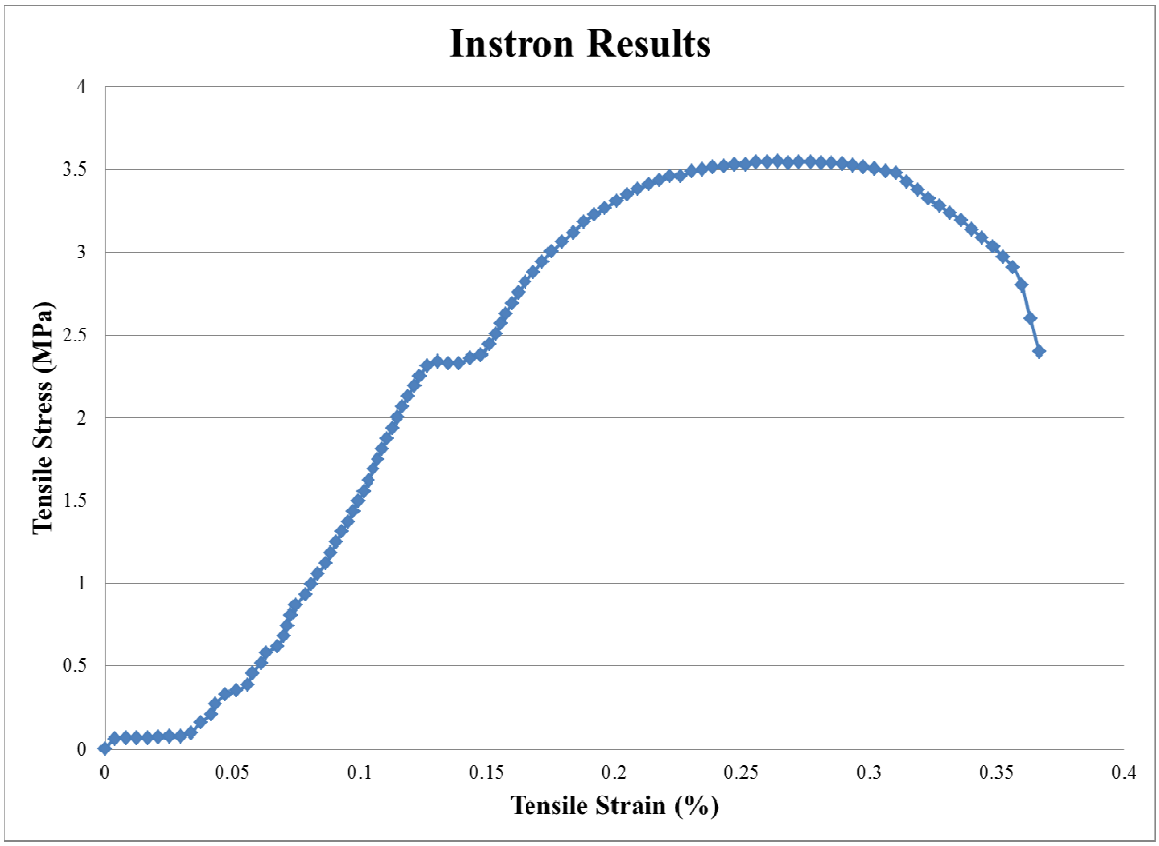

Instron results for DCA-OD

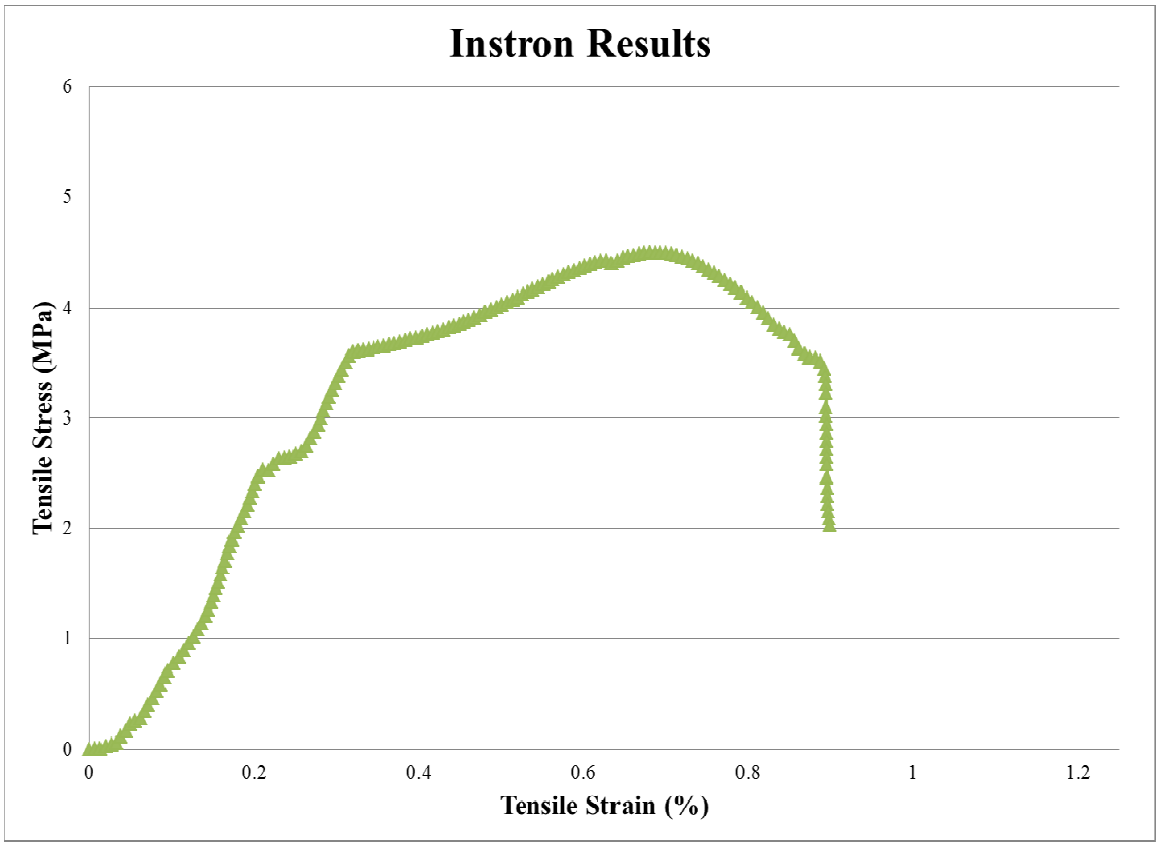

Instron results for DCE-CHDM

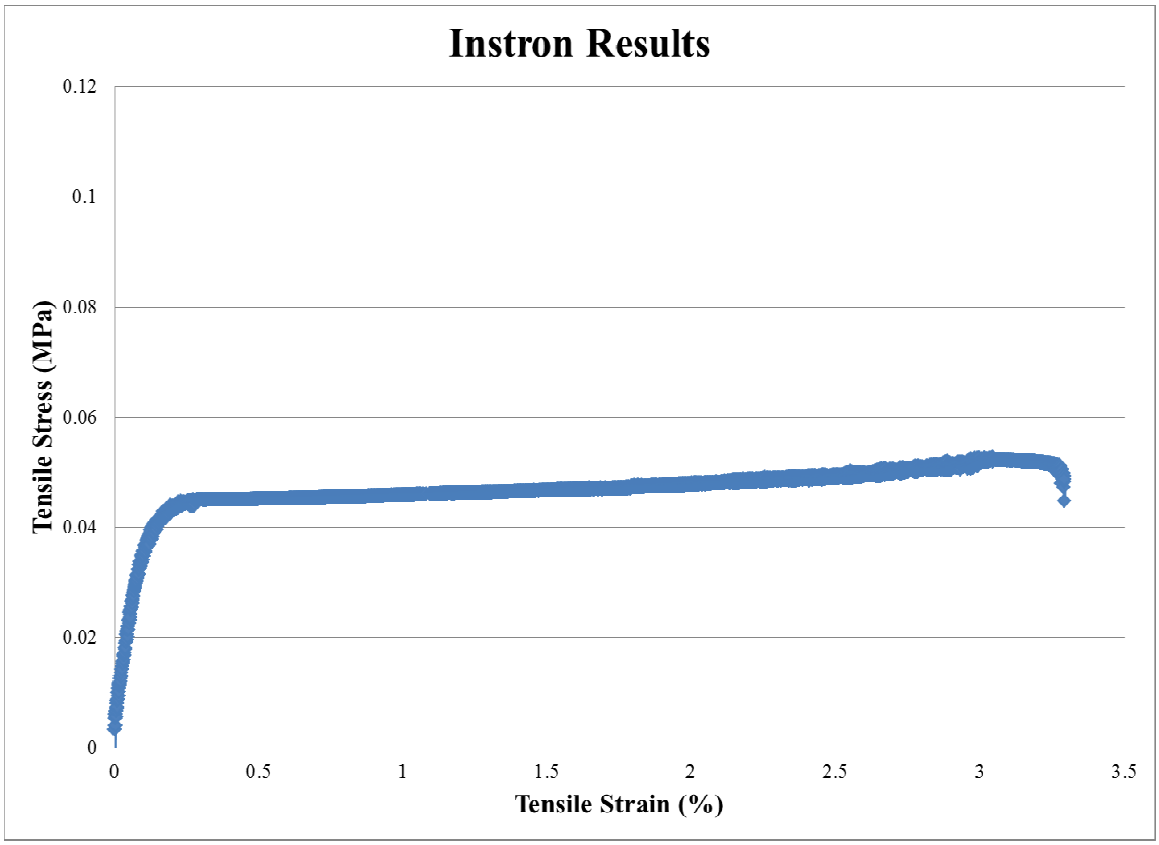

Instron results for DCE-OD elastomer

Appendix B

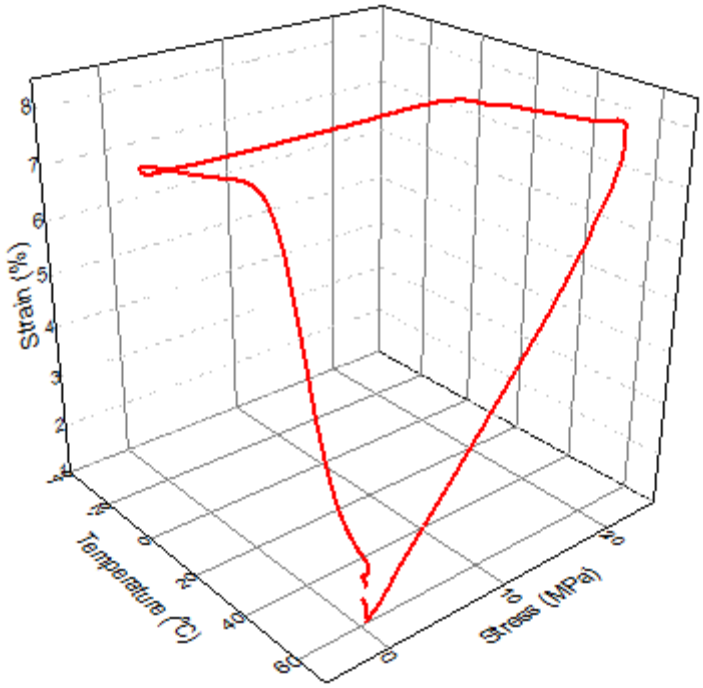

DMA Curve for DCA-OD SMP Film

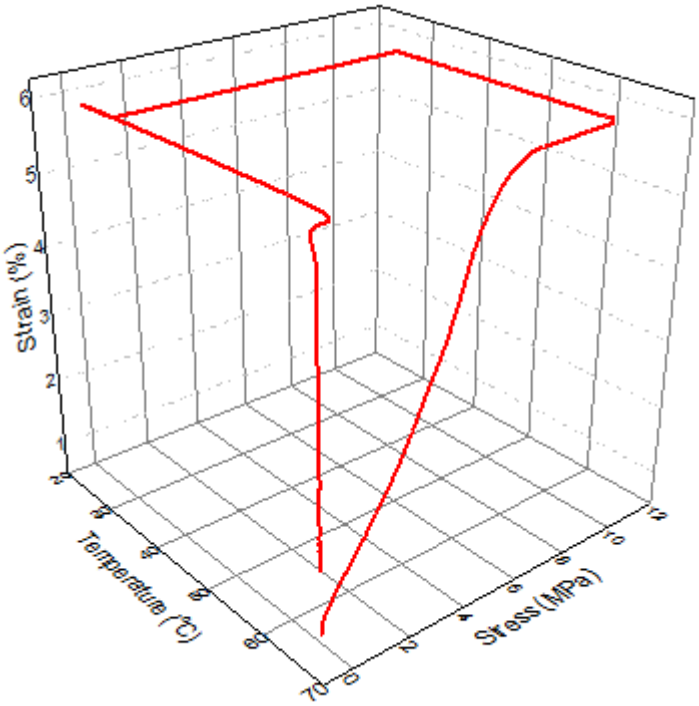

DMA Curve for DCE-CHDM SMP Film

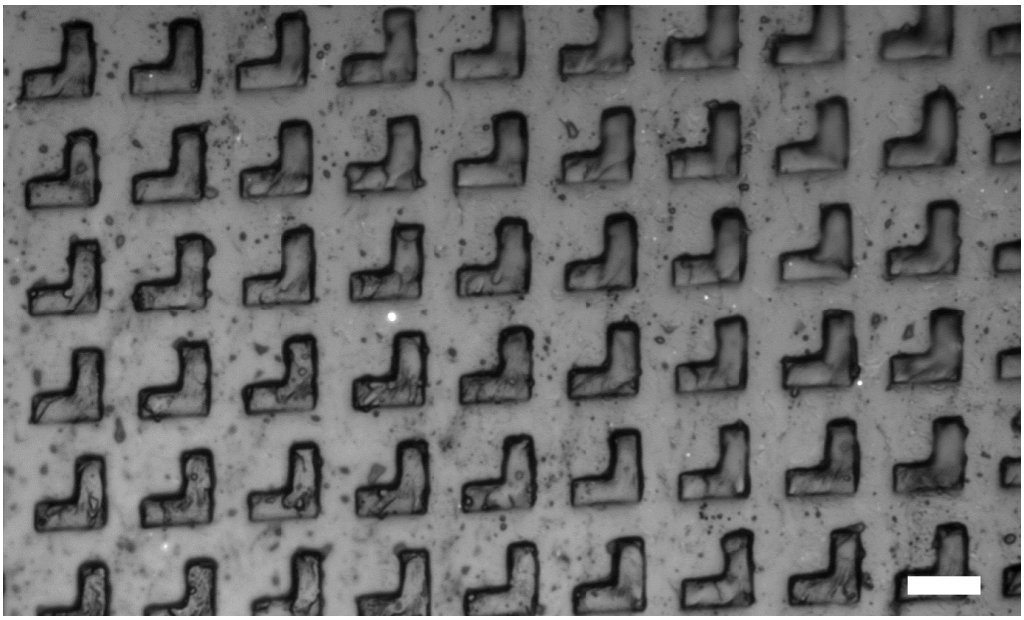

DCA-CHDM: 10 micron boomerangs (scale bar = 10 μm)

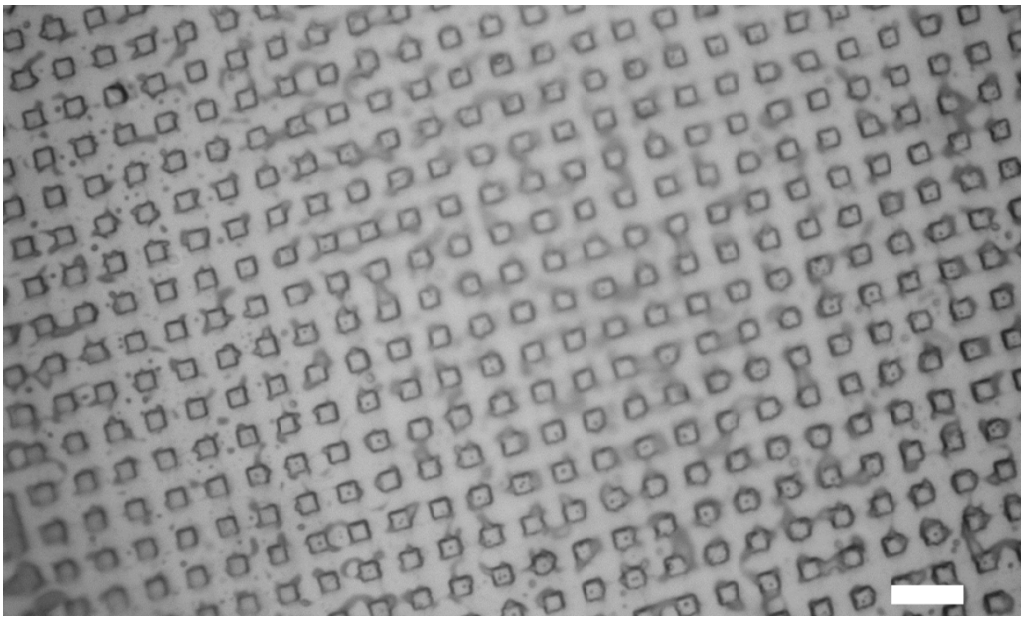

DCA-OD: 6 micron cubes (scale bar = 20 μm)

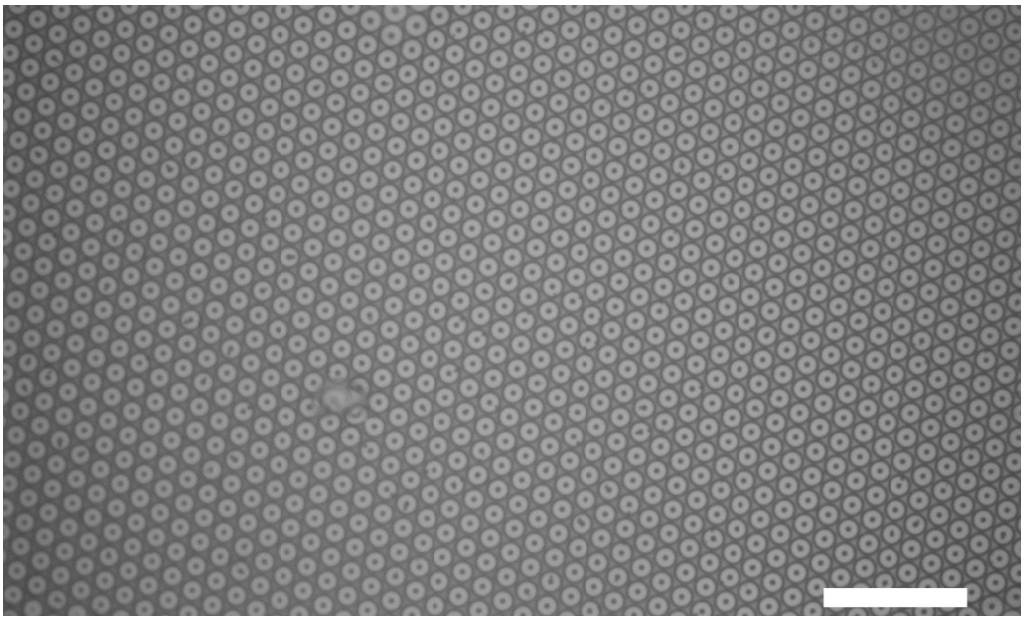

DCA-OD: 3 micron donuts (scale bar = 10 μm)

Appendix C

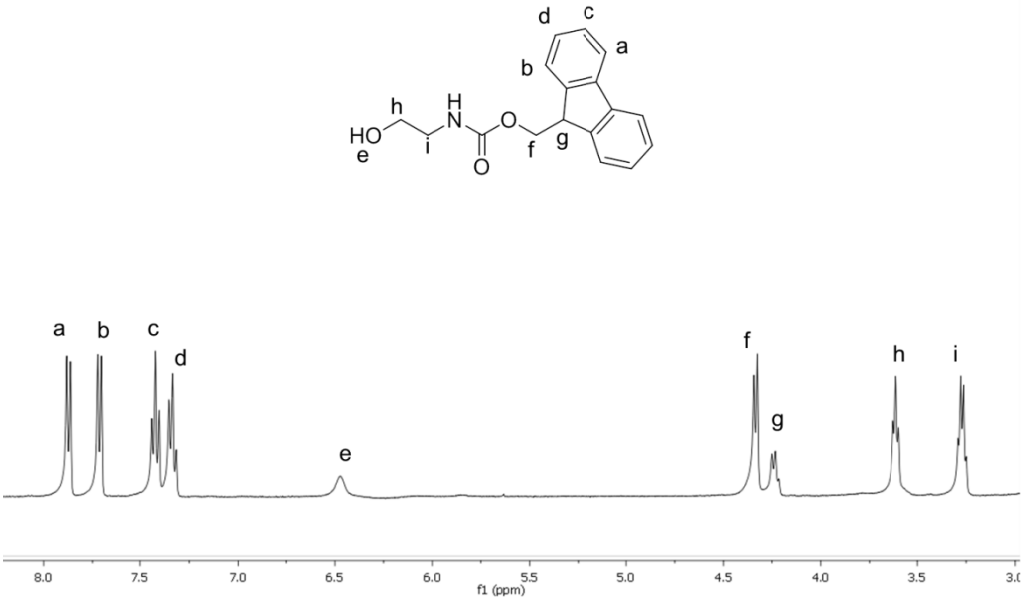

^{1}H-NMR of Fmoc-protected ethanolamine

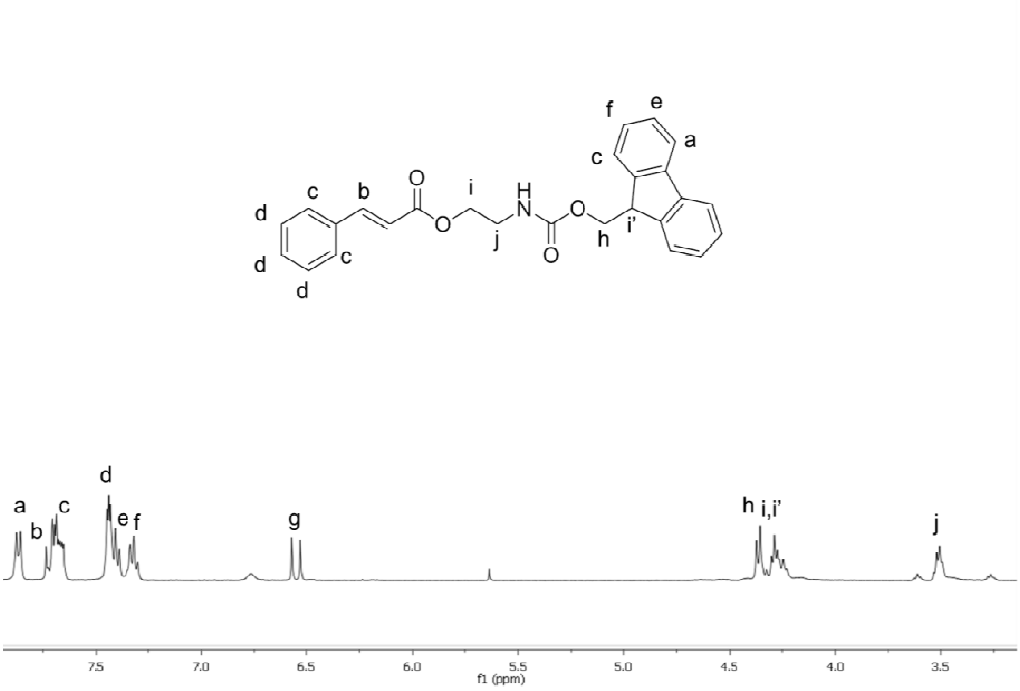

^{1}H-NMR of Fmoc-protected cinnamate compound

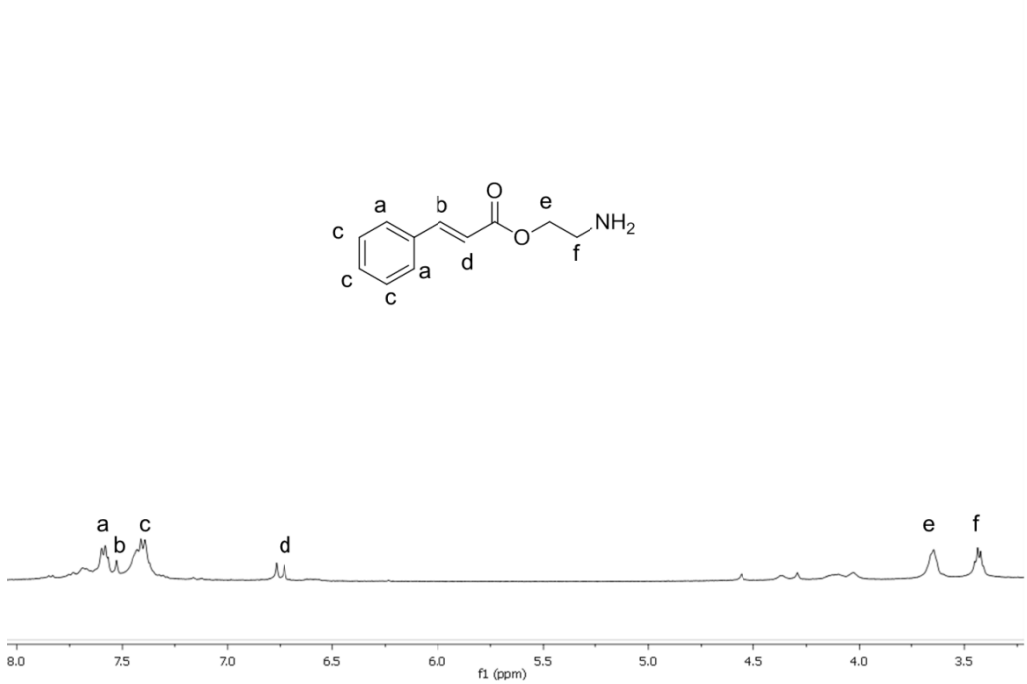

^{1}H-NMR of 2-aminoethyl cinnamate monomer

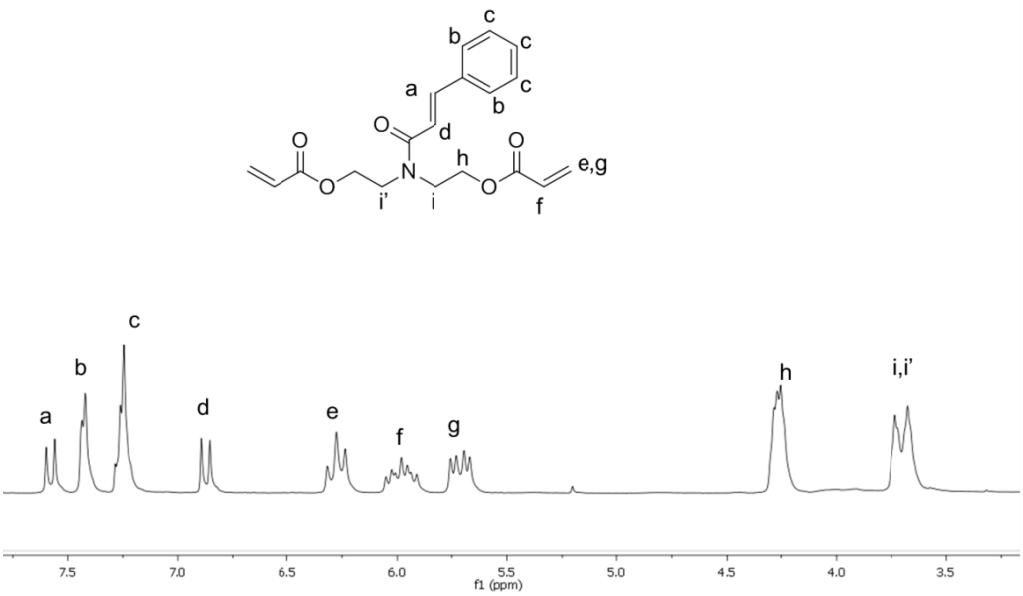

^{1}H-NMR of CAD-DA Monomer

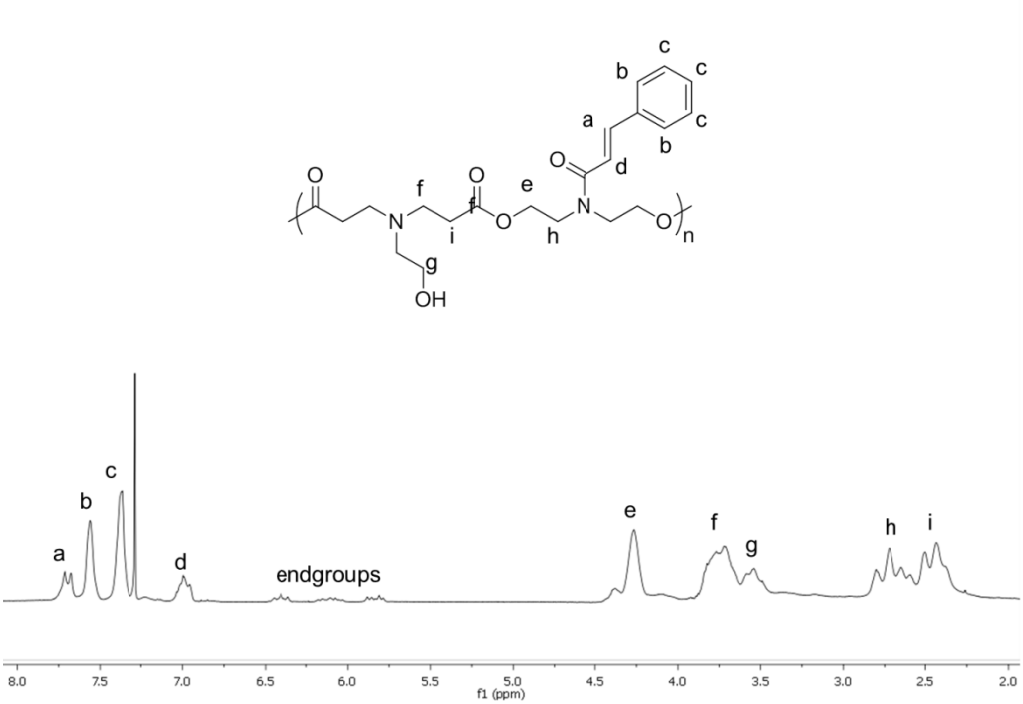

^{1}H-NMR of CAD-OH prepolymer

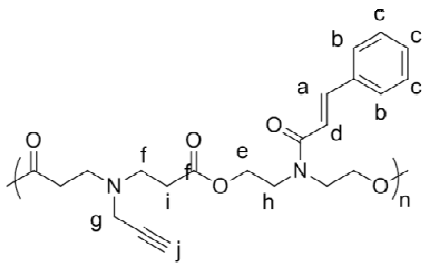

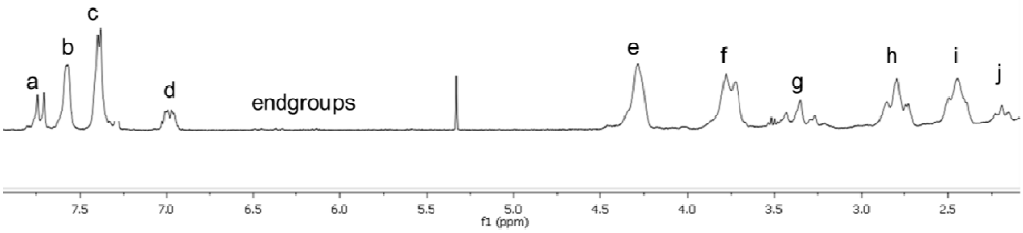

^{1}H-NMR of CAD-Alkyne prepolymer

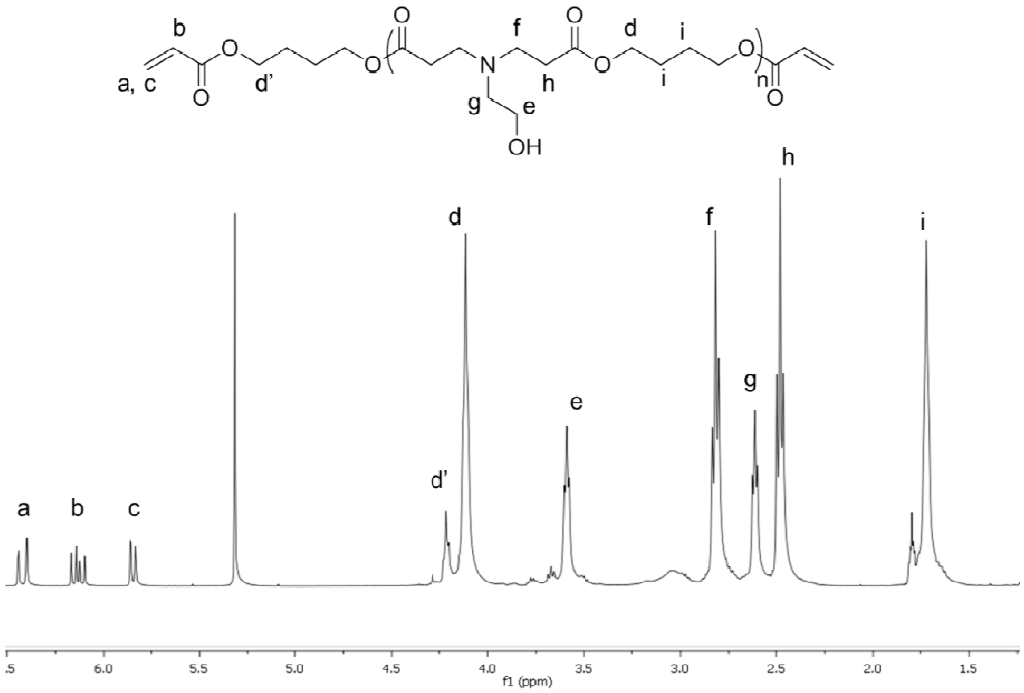

^{1}H-NMR of EO-BD

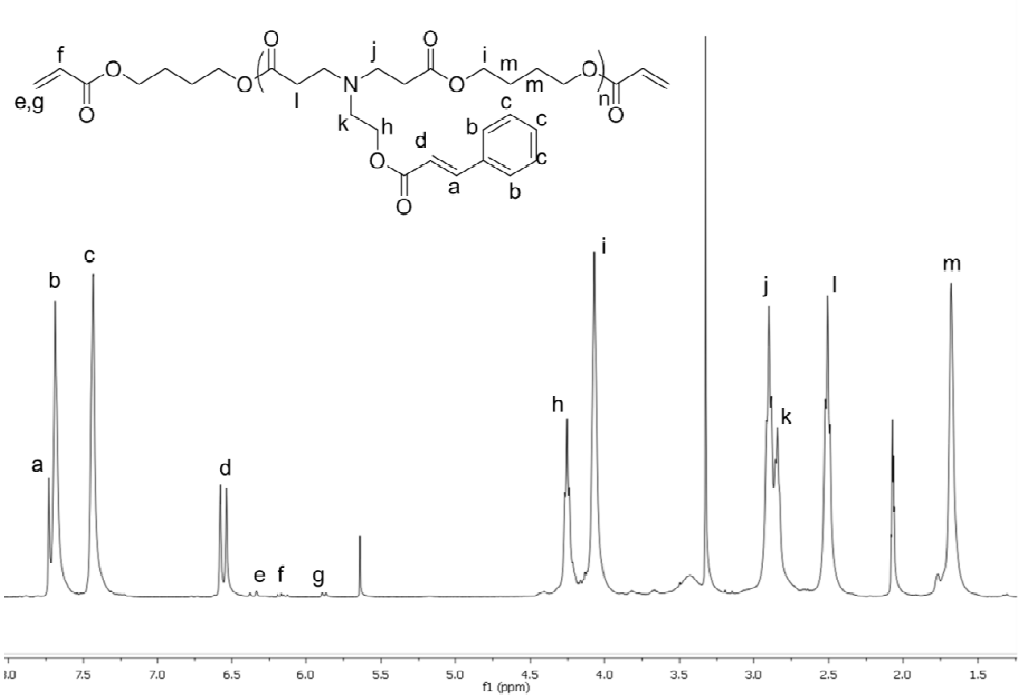

^{1}H-NMR of EC-BD

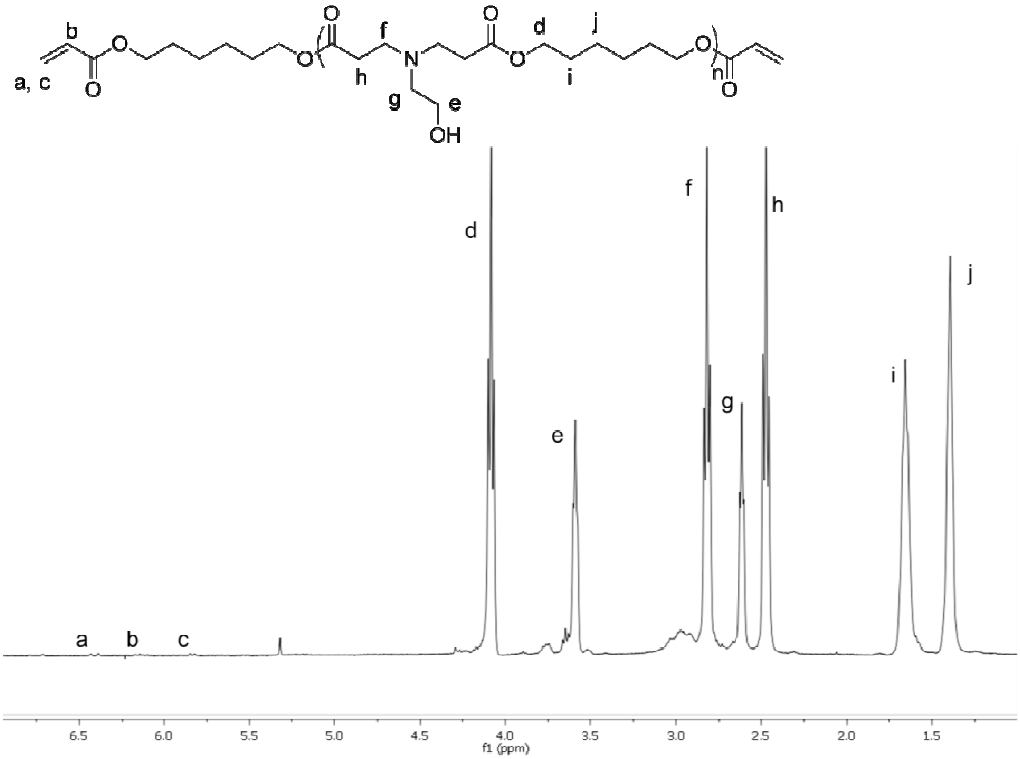

^{1}H-NMR of EO-HD

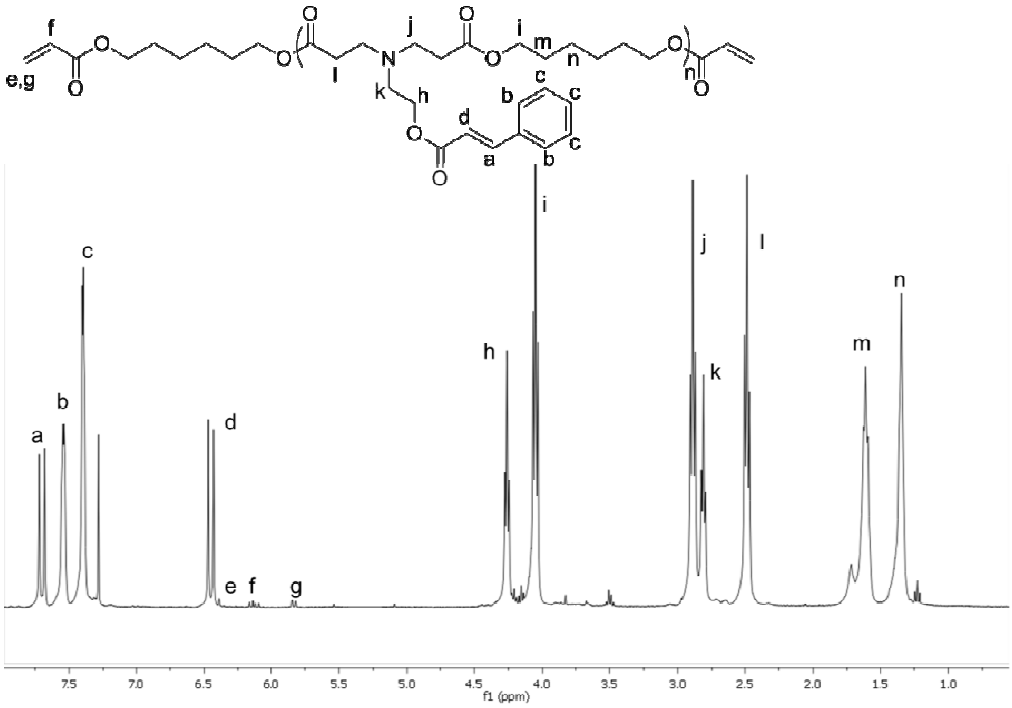

^{1}H-NMR of EC-HD

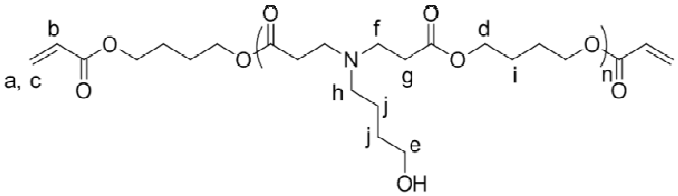

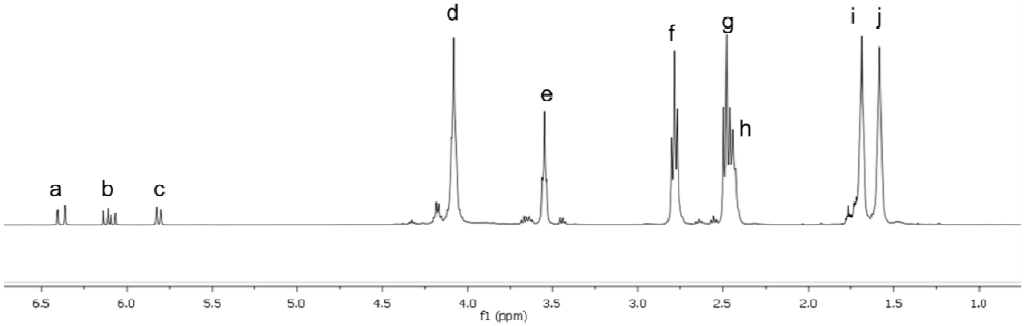

^{1}H-NMR of BO-BD

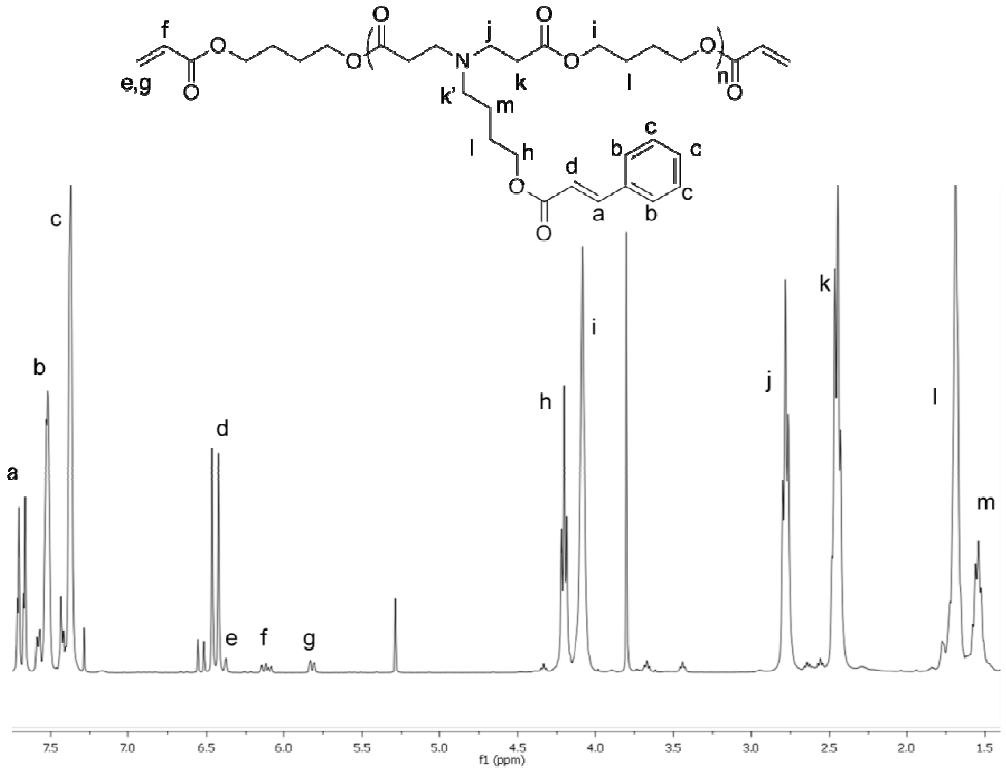

^{1}H-NMR of BC-BD

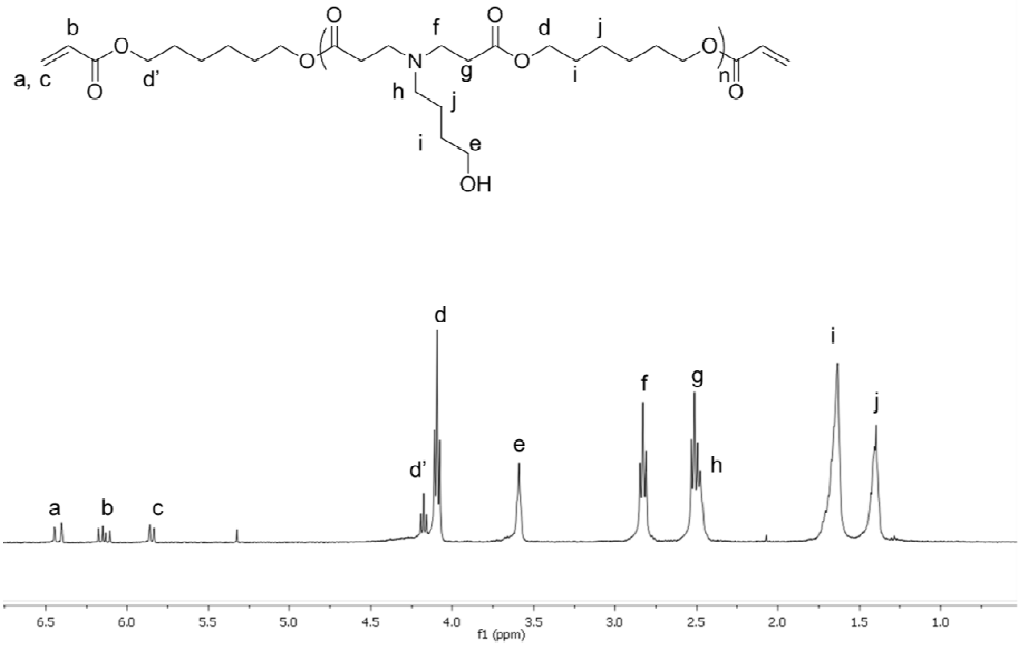

^{1}H-NMR of BO-HD

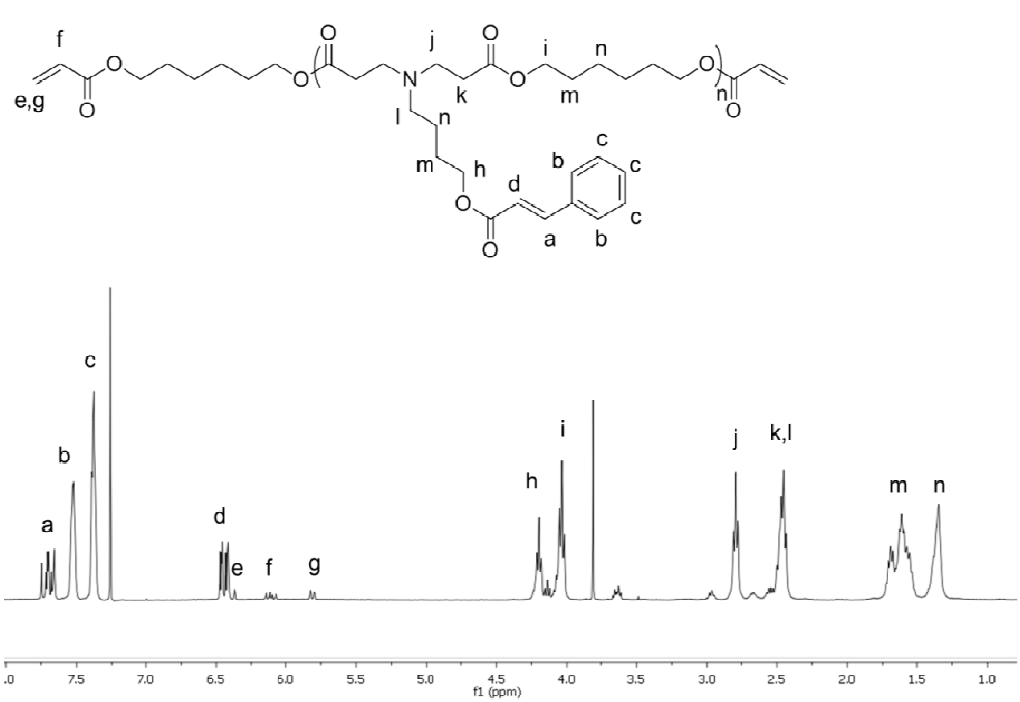

^{1}H-NMR of BC-HD

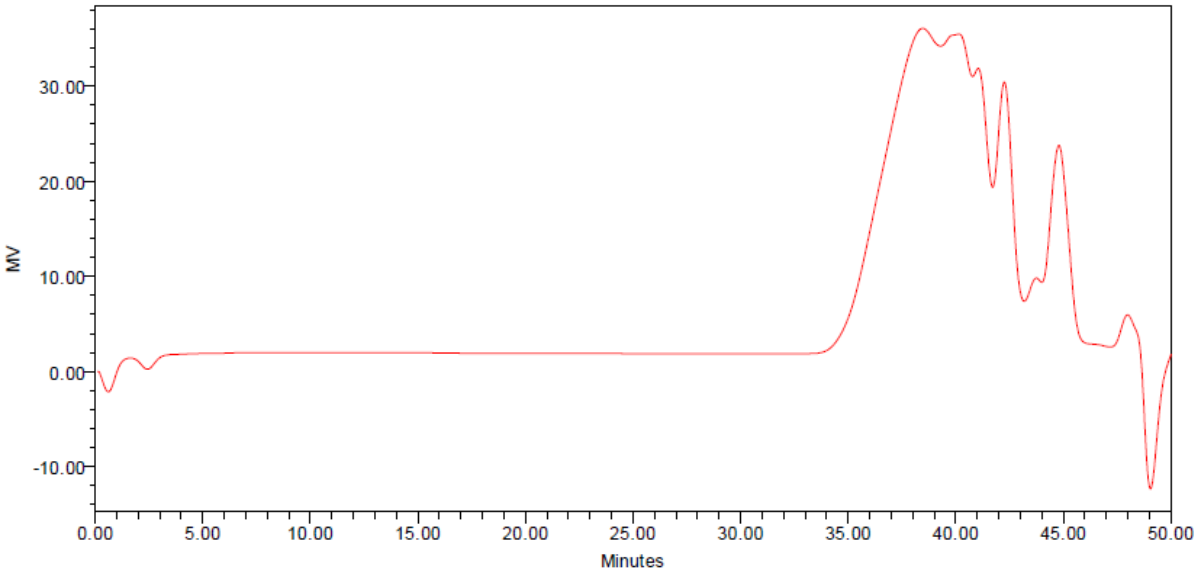

GPC of CAD-OH polymer

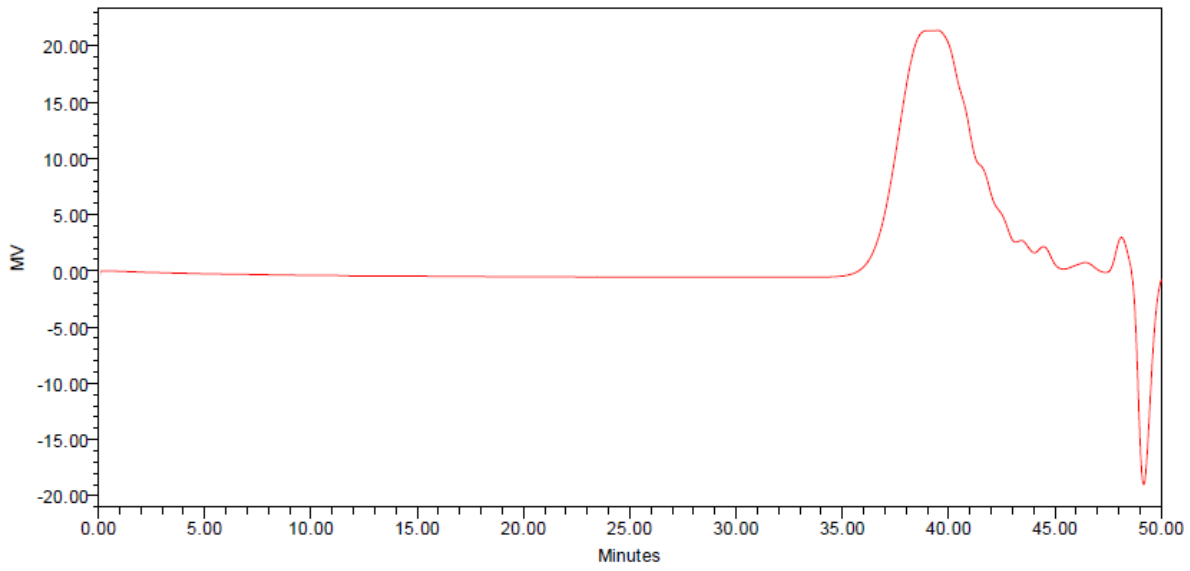

GPC of CAD-Alkyne polymer

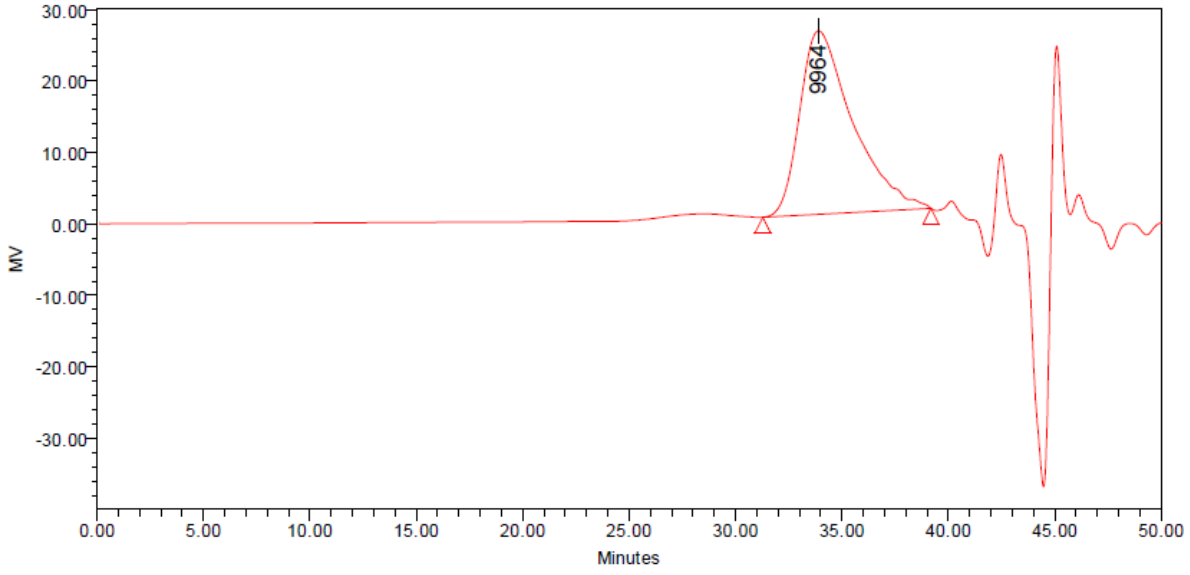

GPC Results

	Dist Name	Mn	Mw	Mv	MP	Mz	Mz+1	Poly dispersity	K	alpha
1		6022	8574		9964	10731	12519	1.423803		

GPC of EO-BD prepolymer

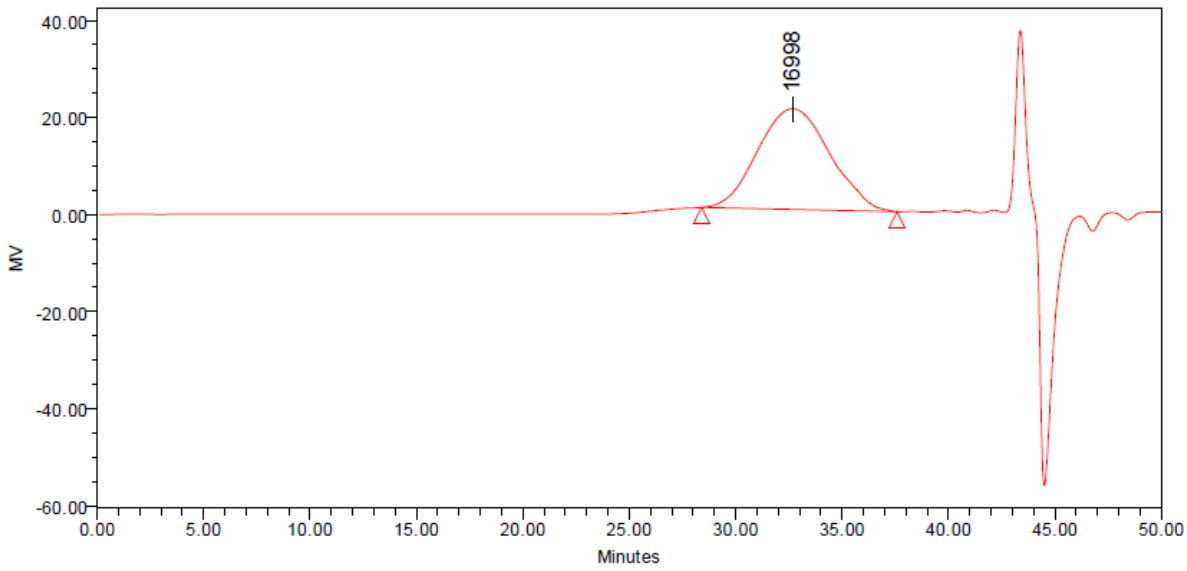

GPC Results

	Dist Name	Mn	Mw	Mv	MP	Mz	Mz+1	Poly dispersity	K	alpha
1		12868	19762		16998	28769	38975	1.535783		

GPC of EC-BD prepolymer

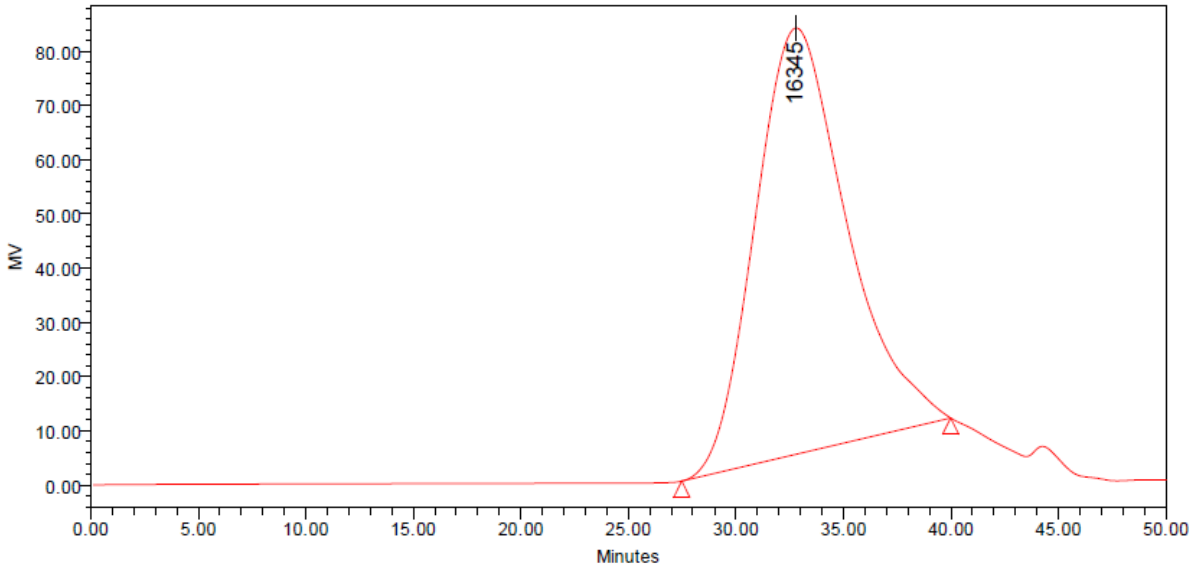

GPC Results

	Dist Name	Mn	Mw	Mv	MP	Mz	Mz+1	Poly dispersity	K	alpha
1		8109	18703		16345	32775	48905	2.306444		

GPC of EO-HD prepolymer

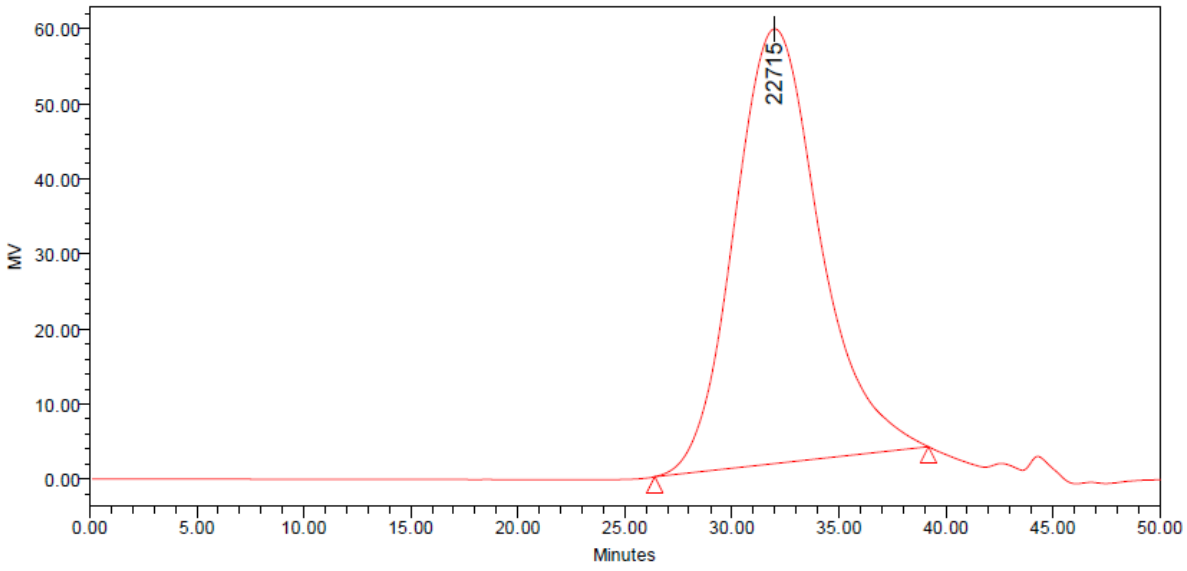

GPC Results

	Dist Name	Mn	Mw	Mv	MP	Mz	Mz+1	Poly dispersity	K	alpha
1		13208	27924		22715	49387	78671	2.114127		

GPC of EC-HD prepolymer

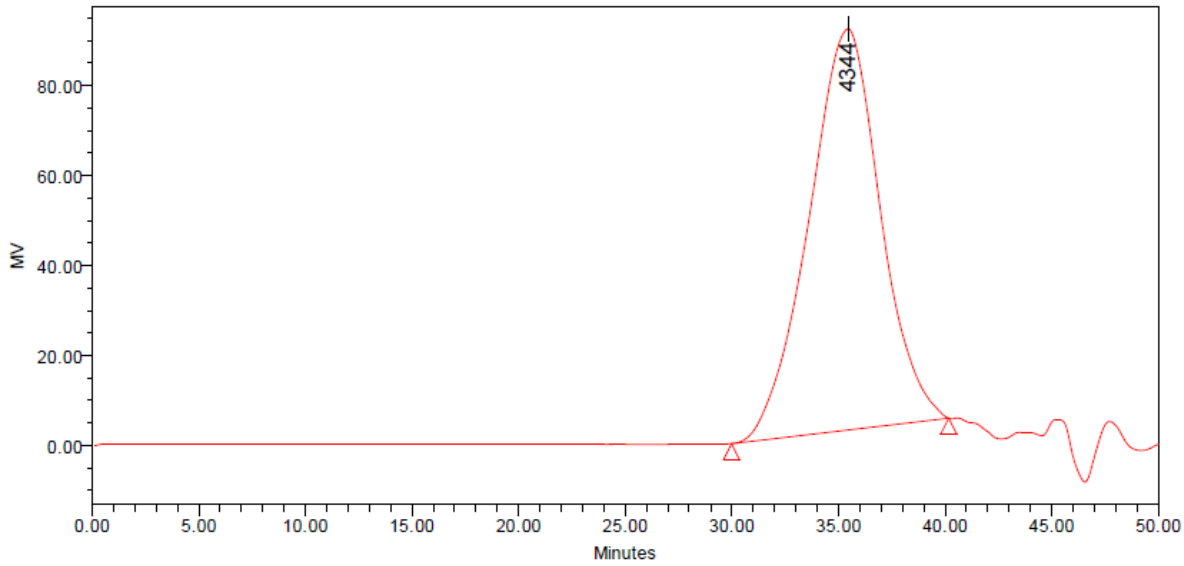

GPC Results

	Dist Name	Mn	Mw	Mv	MP	Mz	Mz+1	Poly dispersity	K	alpha
1		3584	6237		4344	10549	16144	1.740095		

GPC of BO-BD prepolymer

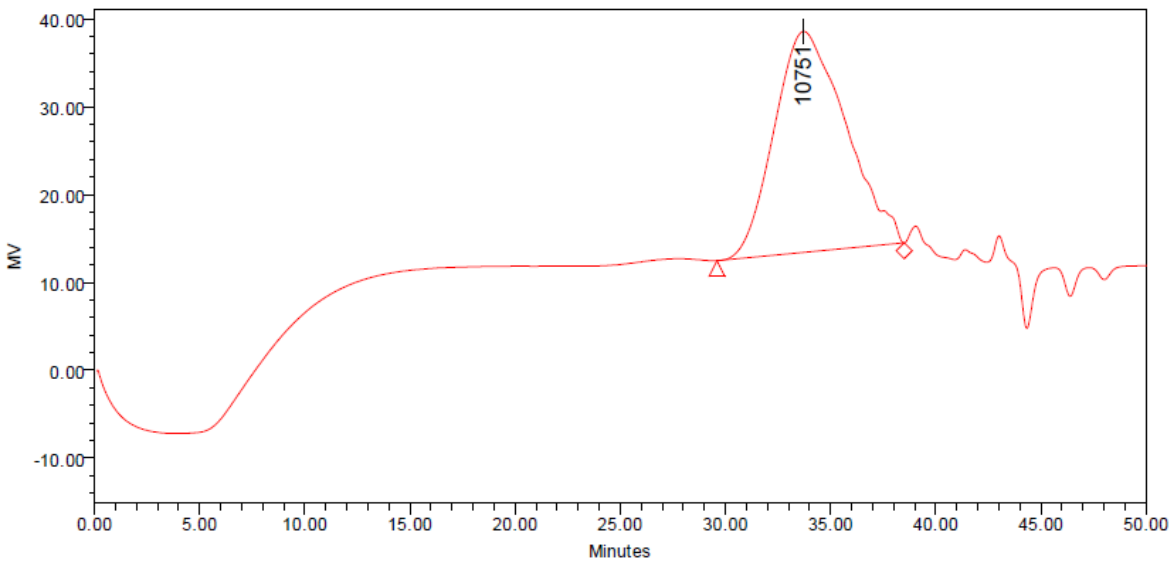

GPC Results

	Dist Name	Mn	Mw	Mv	MP	Mz	Mz+1	Poly dispersity	K	alpha
1		6794	10848		10751	15577	20356	1.596830		

GPC of BC-BD prepolymer

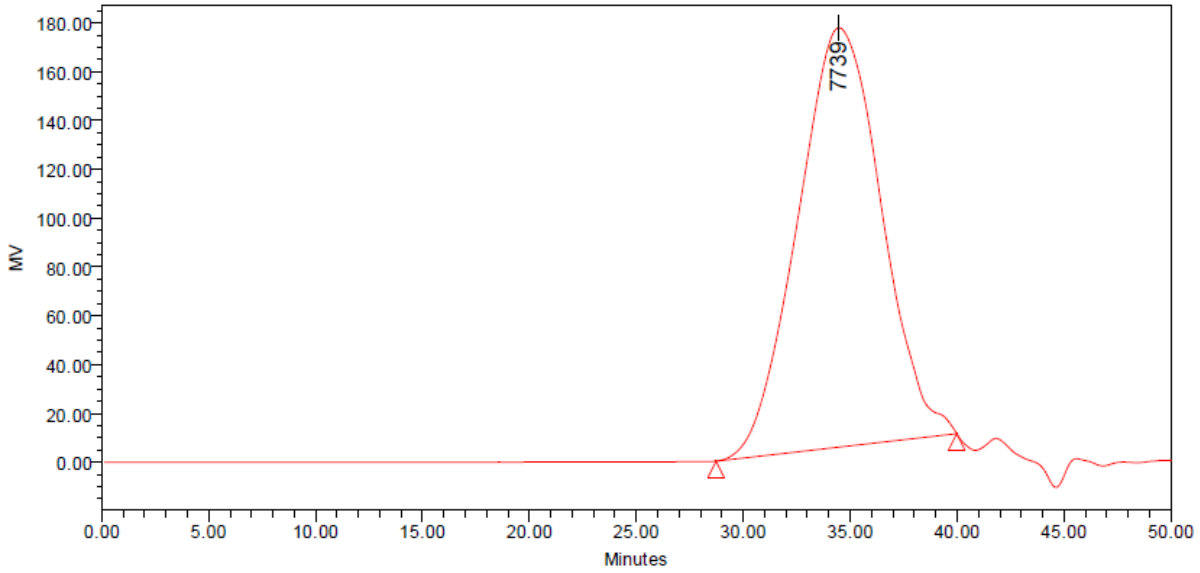

GPC Results

	Dist Name	Mn	Mw	Mv	MP	Mz	Mz+1	Poly dispersity	K	alpha
1		5326	10090		7739	17352	26438	1.894612		

GPC of BO-HD prepolymer

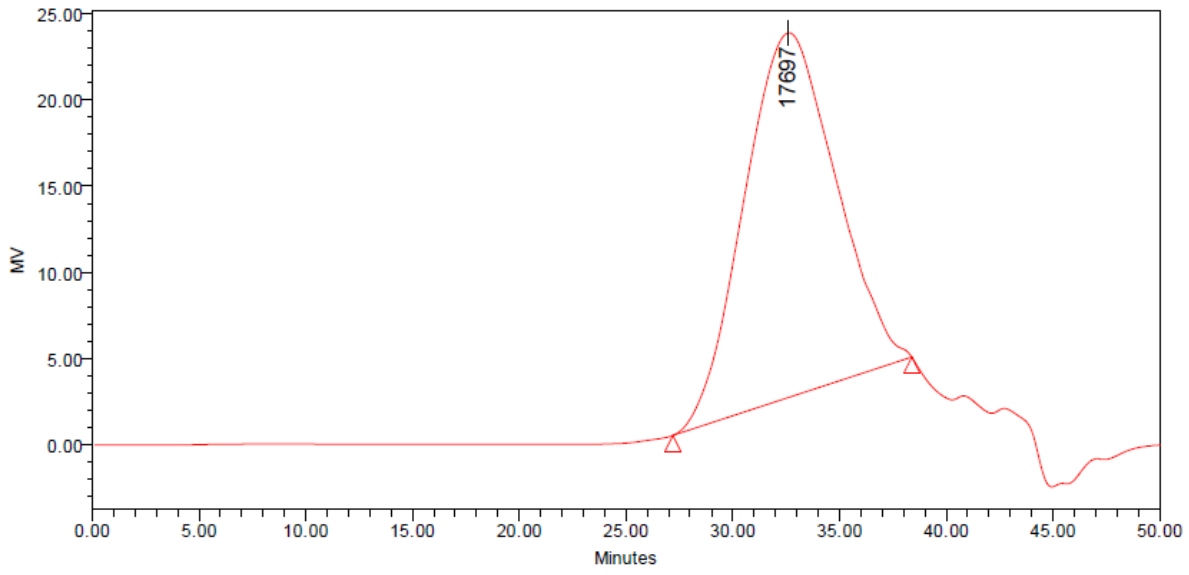

GPC Results

	Dist Name	Mn	Mw	Mv	MP	Mz	Mz+1	Poly dispersity	K	alpha
1		11310	22974		17697	41085	62815	2.031240		

GPC of BC-HD prepolymer

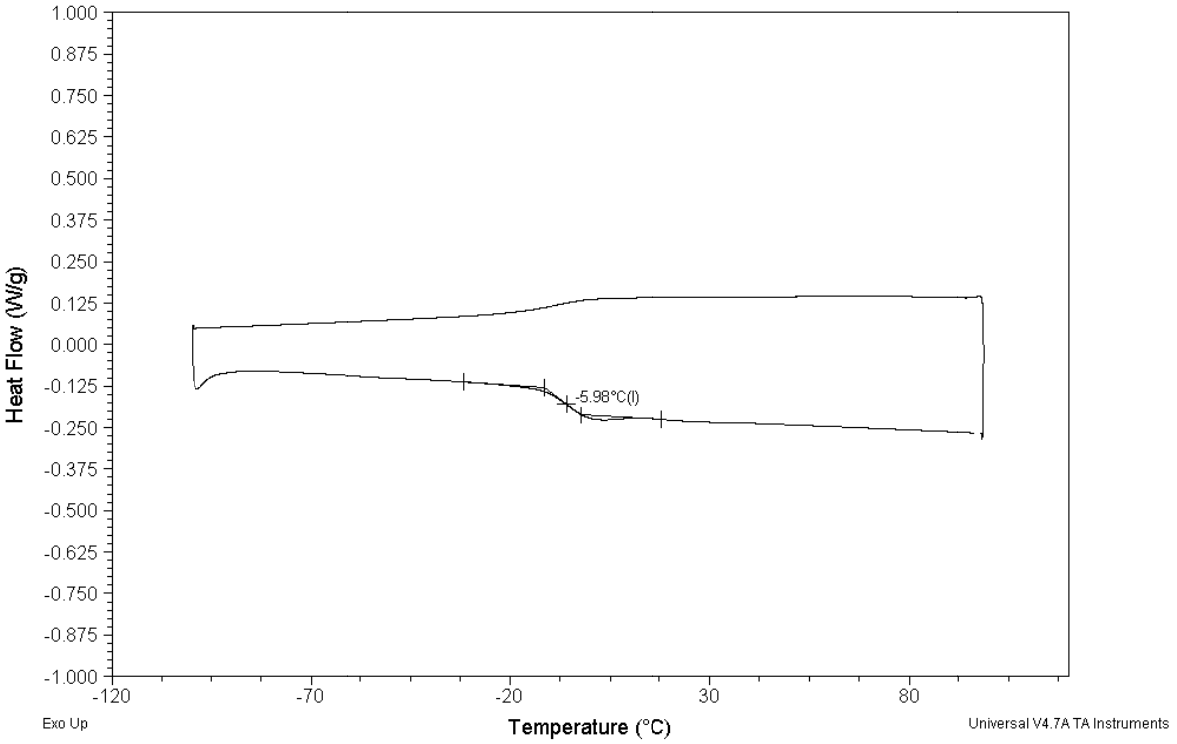

DSC of CAD-OH polymer

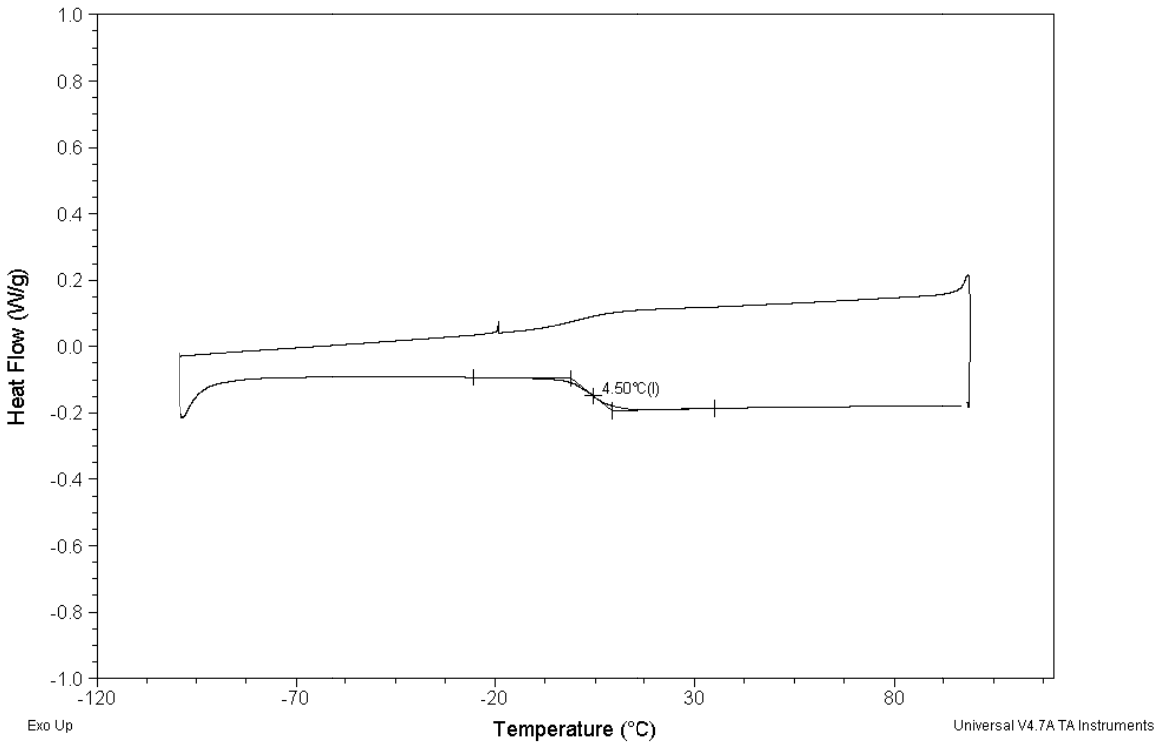

DSC of CAD-Alkyne polymer

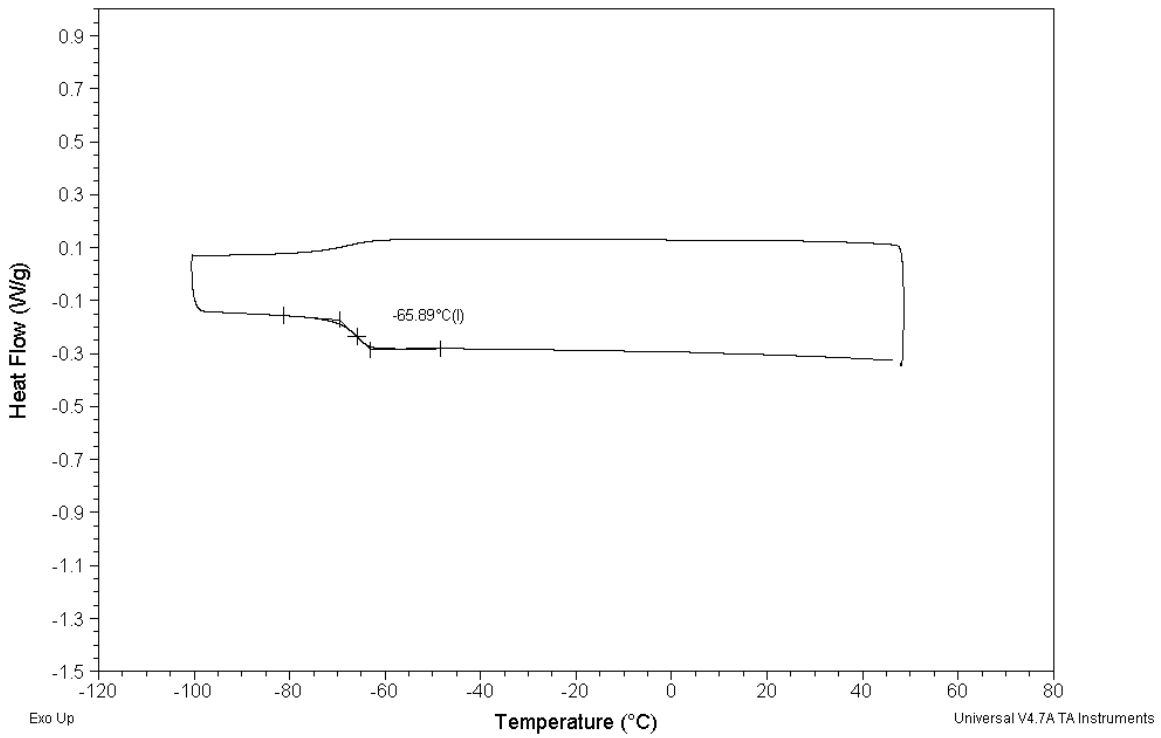

DSC of EO-HD prepolymer

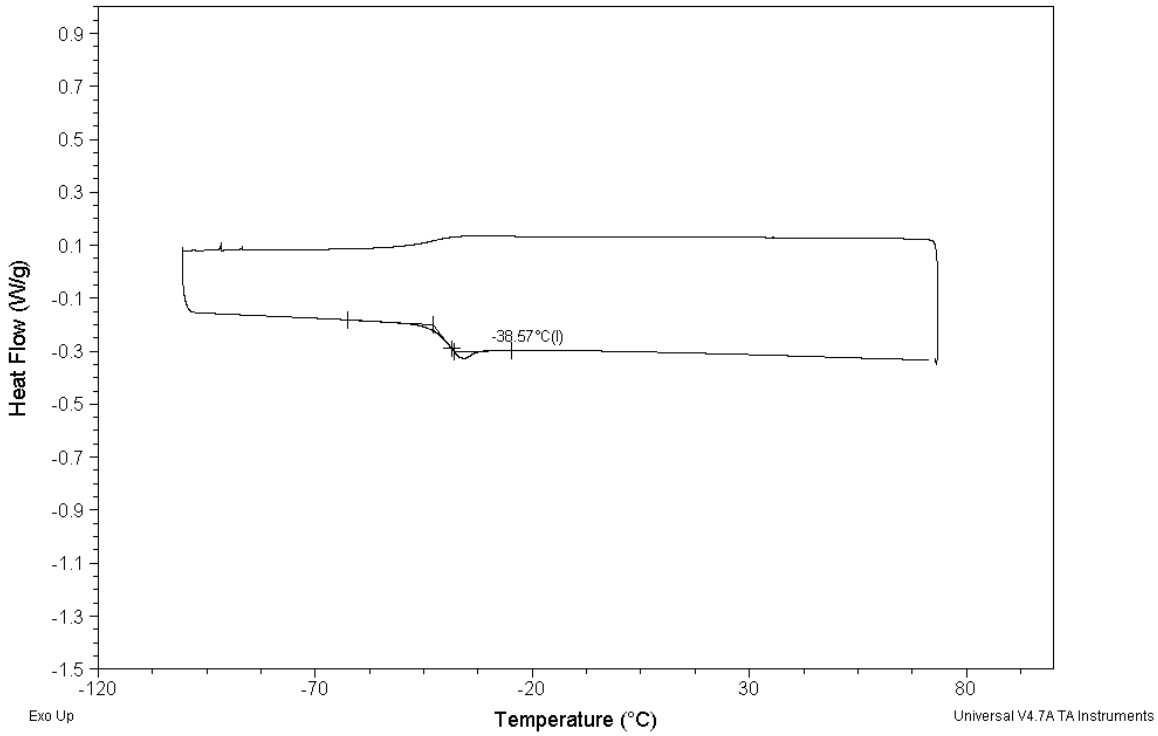
0.9
0.7
0.5
0.3
0.1
-0.1
-0.3
-0.5
-0.7
-0.9
-1.1
-1.3
-1.5
Heat Flow (W/g)
-38.57°C(I)
-120
-70
-20
30
80
Exo Up
Temperature (°C)
Universal V4.7A TA Instruments

DSC of EC-HD

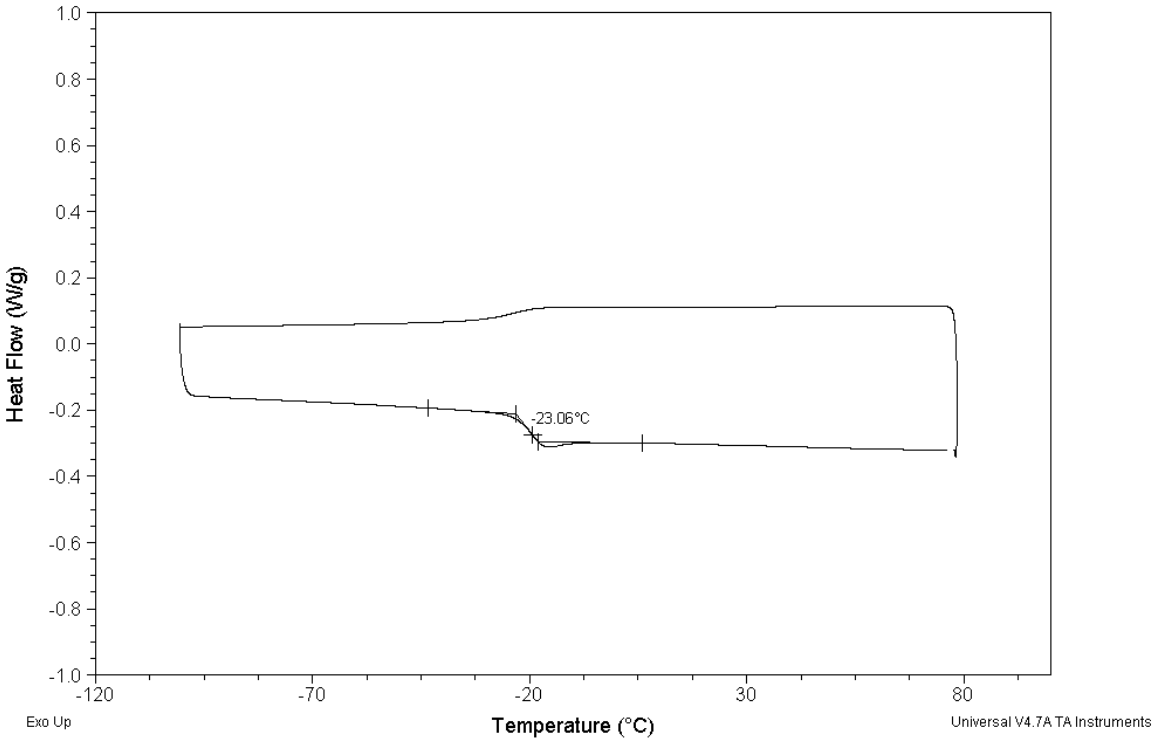

DSC of EC-HD Film

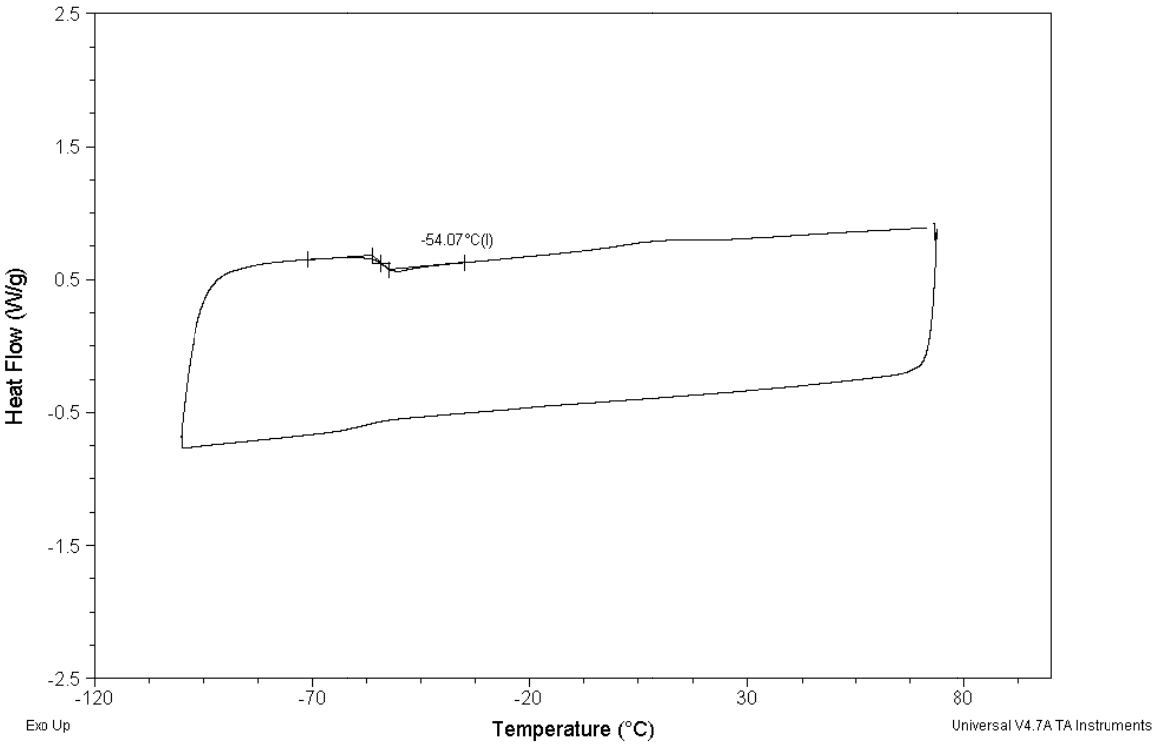
2.5
1.5
0.5
-0.5
-1.5
-2.5
Heat Flow (W/g)
-54.07°C(I)
-120
-70
-20
30
80
Exo Up
Temperature (°C)
Universal V4.7A TA Instruments

DSC of EO-BD

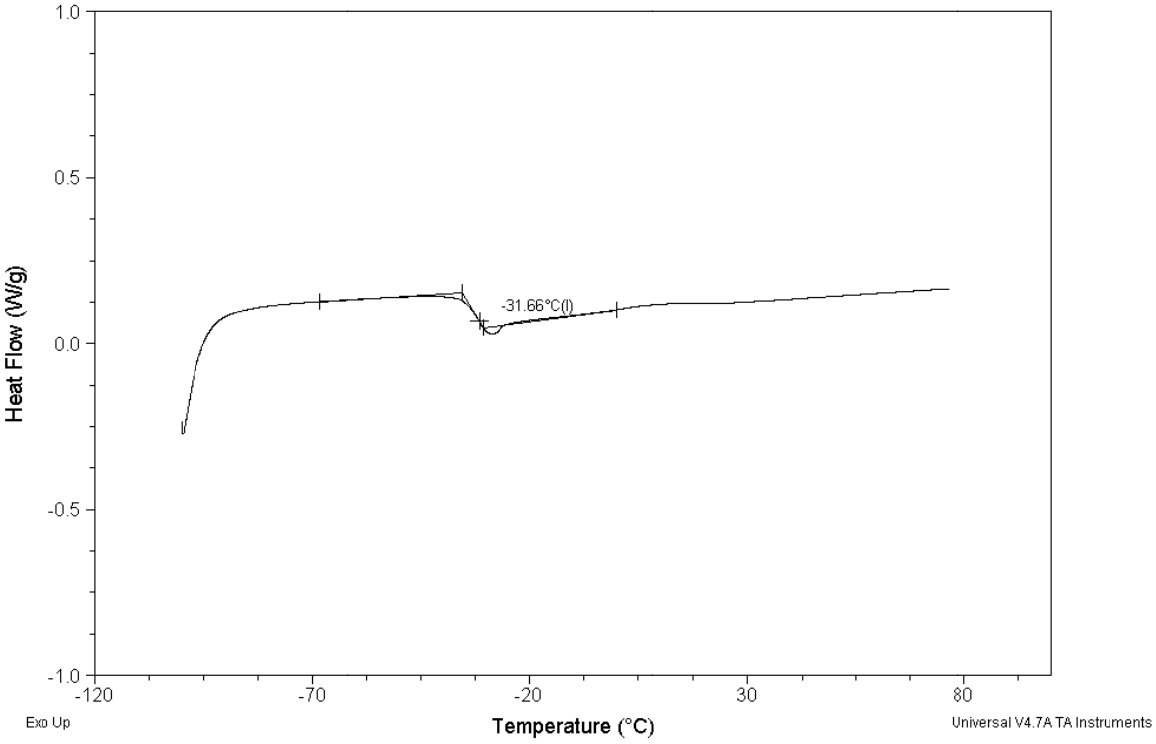
1.0
0.5
0.0
-0.5
-1.0
Heat Flow (W/g)
-31.66°C(I)
-120
-70
-20
30
80
Exo Up
Temperature (°C)
Universal V4.7A TA Instruments

DSC of EC-BD

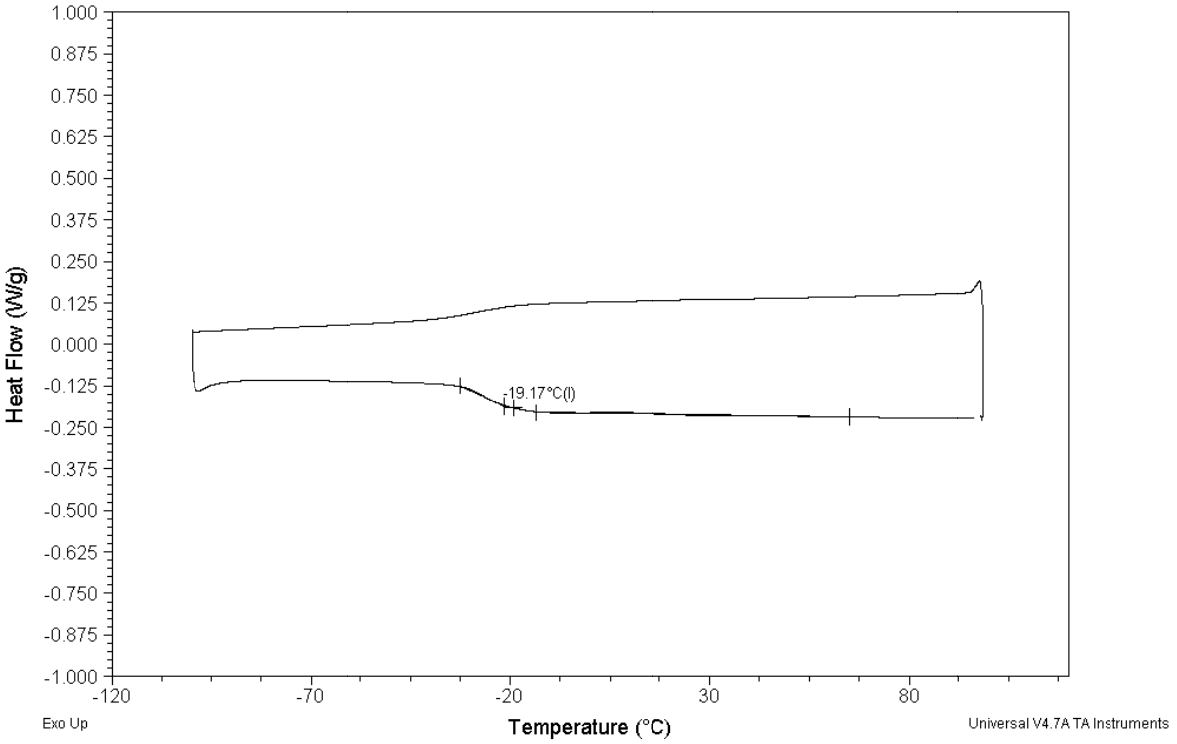

DSC of EC-BD Film

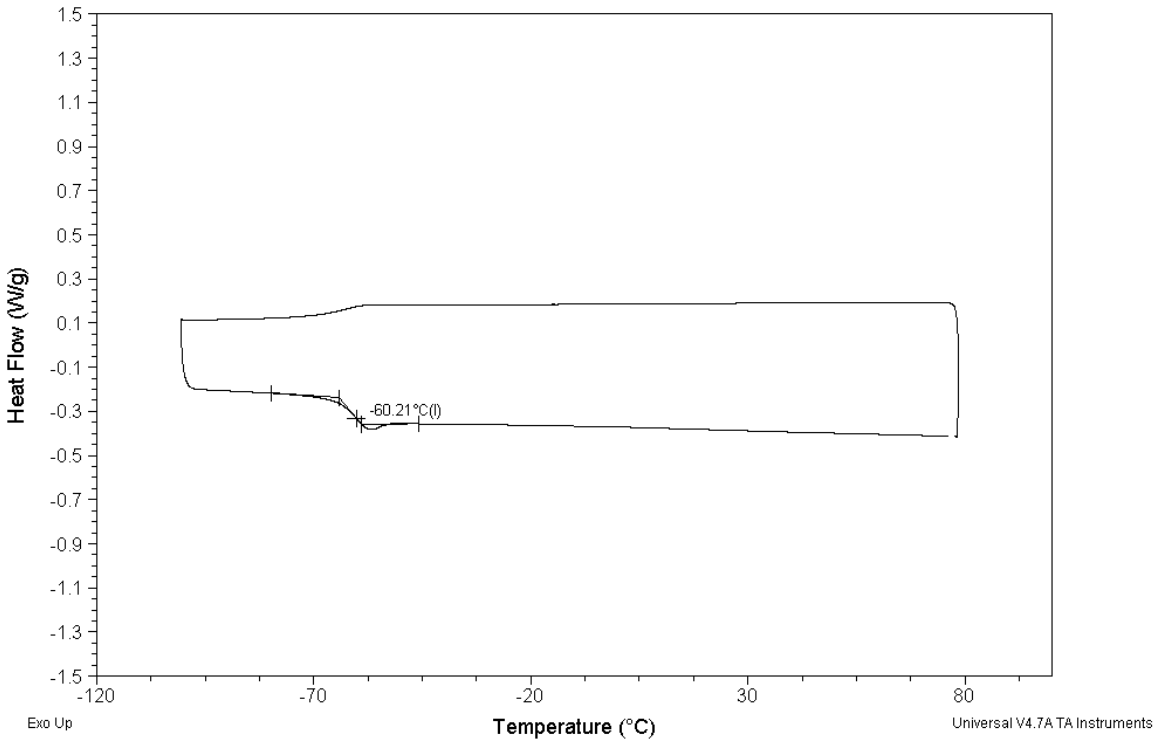
1.5
1.3
1.1
0.9
0.7
0.5
0.3
0.1
-0.1
-0.3
-0.5
-0.7
-0.9
-1.1
-1.3
-1.5
Heat Flow (W/g)
-60.21°C(I)
-120
-70
-20
30
80
Exo Up
Temperature (°C)
Universal V4.7A TA Instruments

DSC of BO-HD

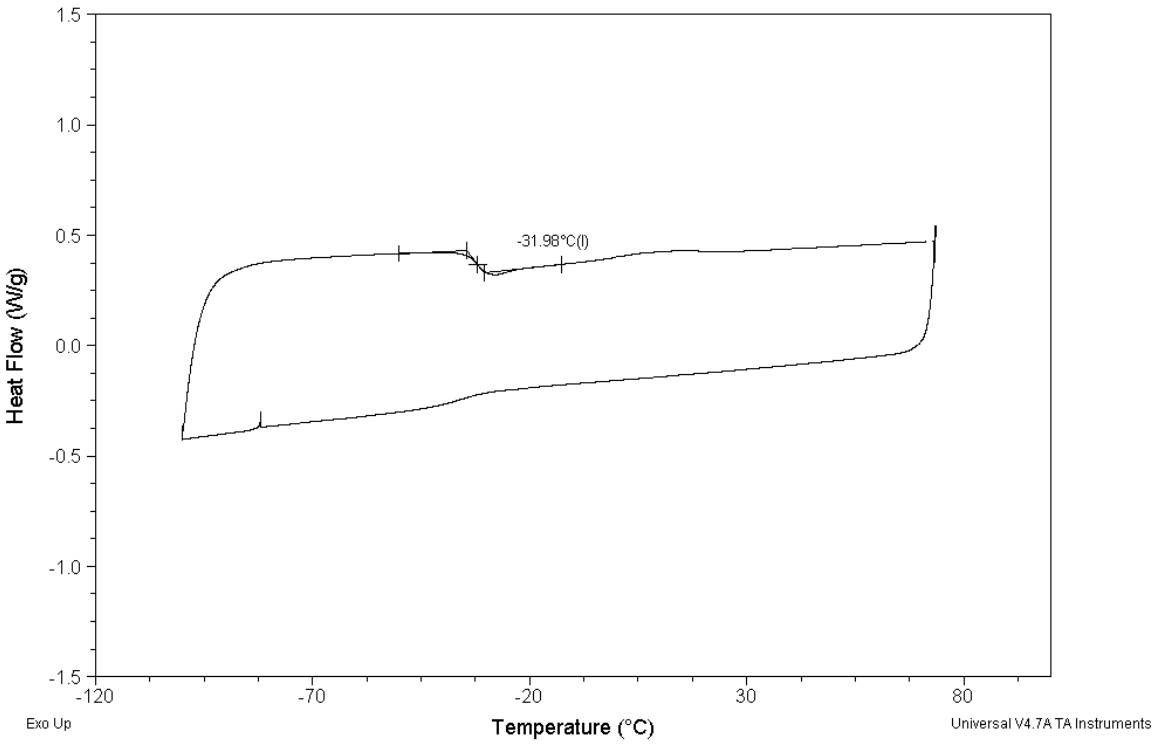
1.5
1.0
0.5
0.0
-0.5
-1.0
-1.5
Heat Flow (W/g)
-31.98°C(I)
-120
-70
-20
30
80
Exo Up
Temperature (°C)
Universal V4.7A TA Instruments

DSC of BC-HD

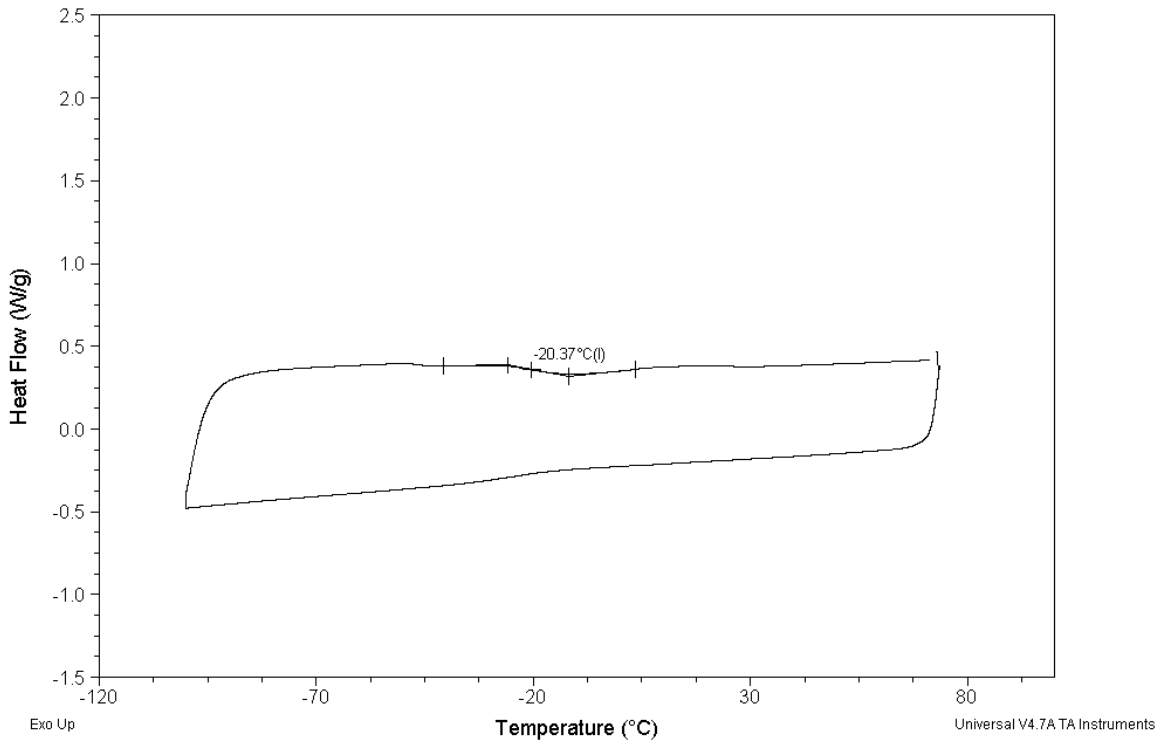

DSC of BC-HD Film

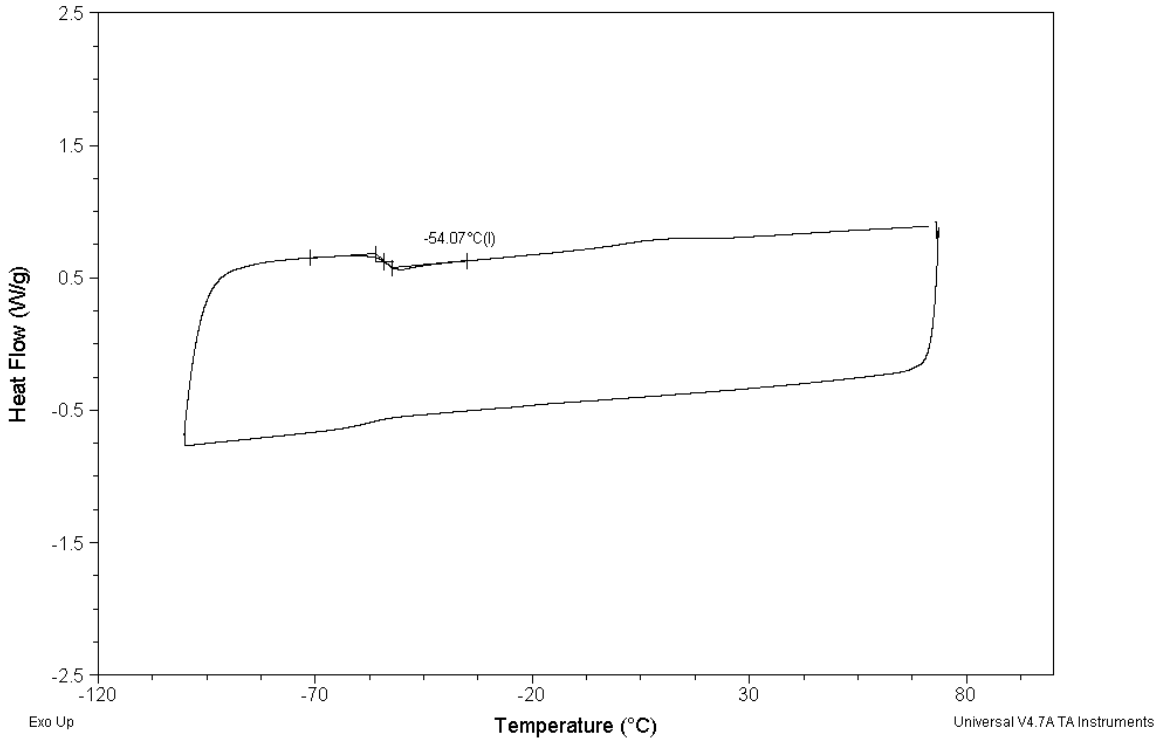
2.5
1.5
0.5
-0.5
-1.5
-2.5
Heat Flow (W/g)
-54.07°C(I)
-120
-70
-20
30
80
Exo Up
Temperature (°C)
Universal V4.7A TA Instruments

DSC of BO-BD

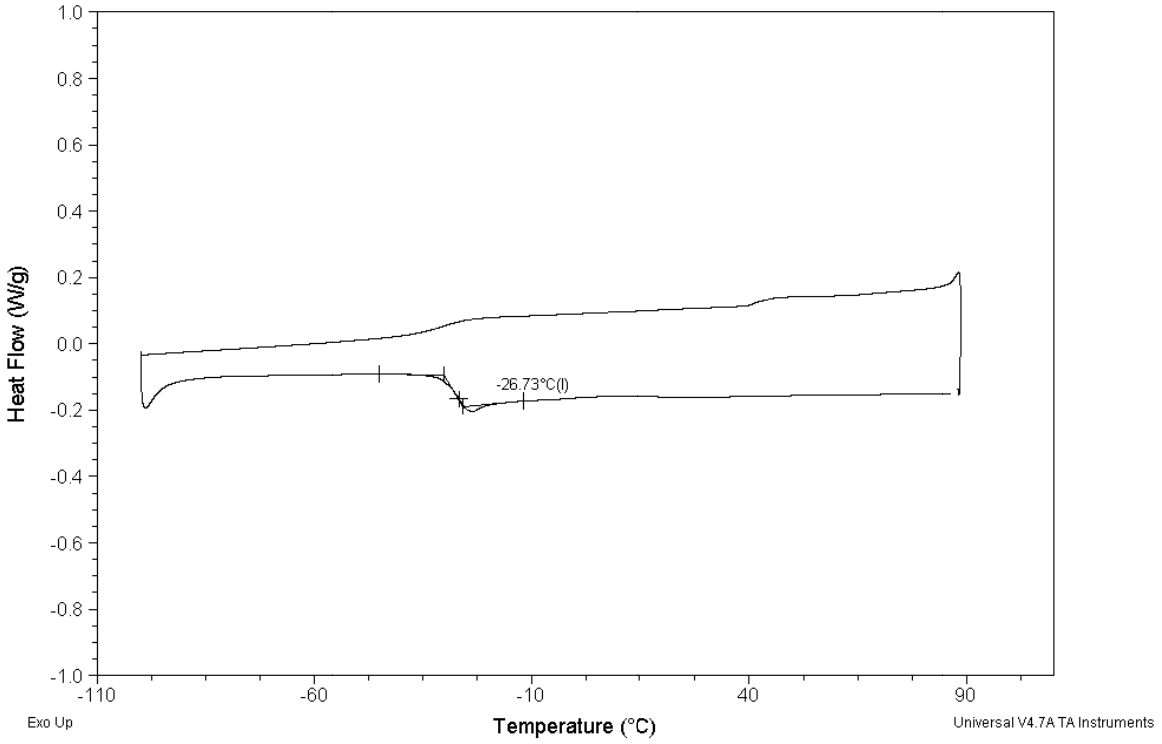
1.0
0.8
0.6
0.4
0.2
0.0
-0.2
-0.4
-0.6
-0.8
-1.0
Heat Flow (W/g)
-26.73°C(I)
-110
-60
-10
40
90
Exo Up
Temperature (°C)
Universal V4.7A TA Instruments

DSC of BC-BD

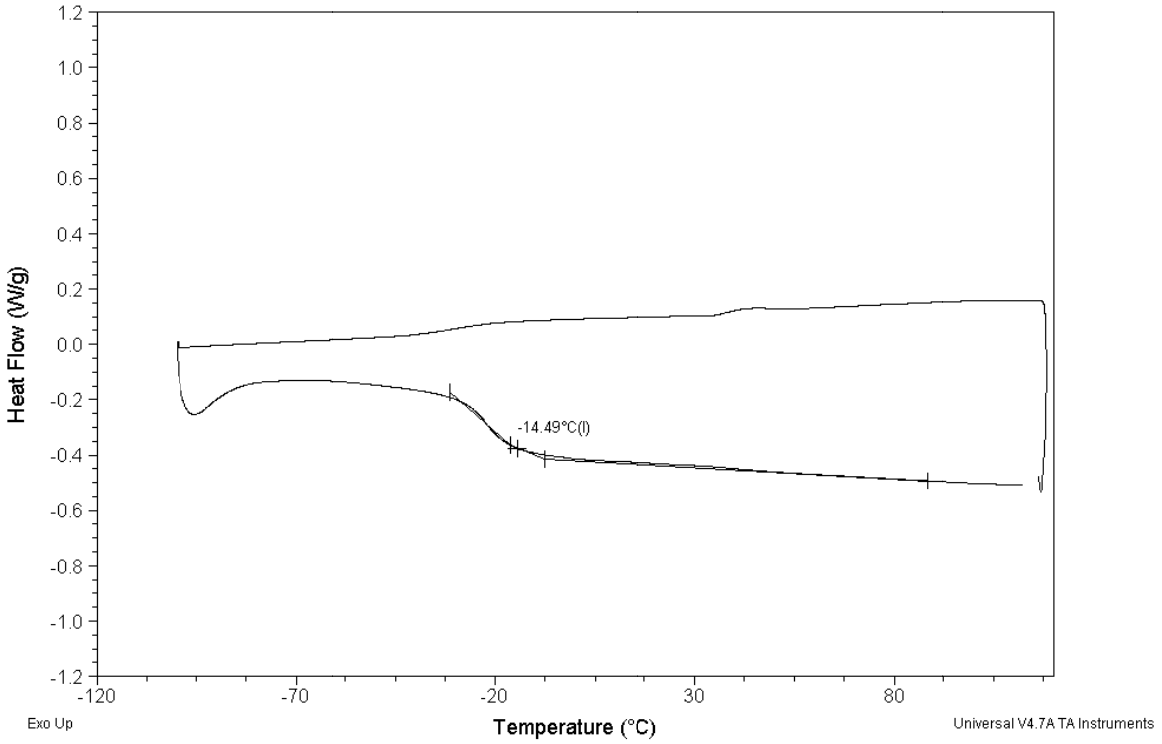

DSC of BC-BD Film

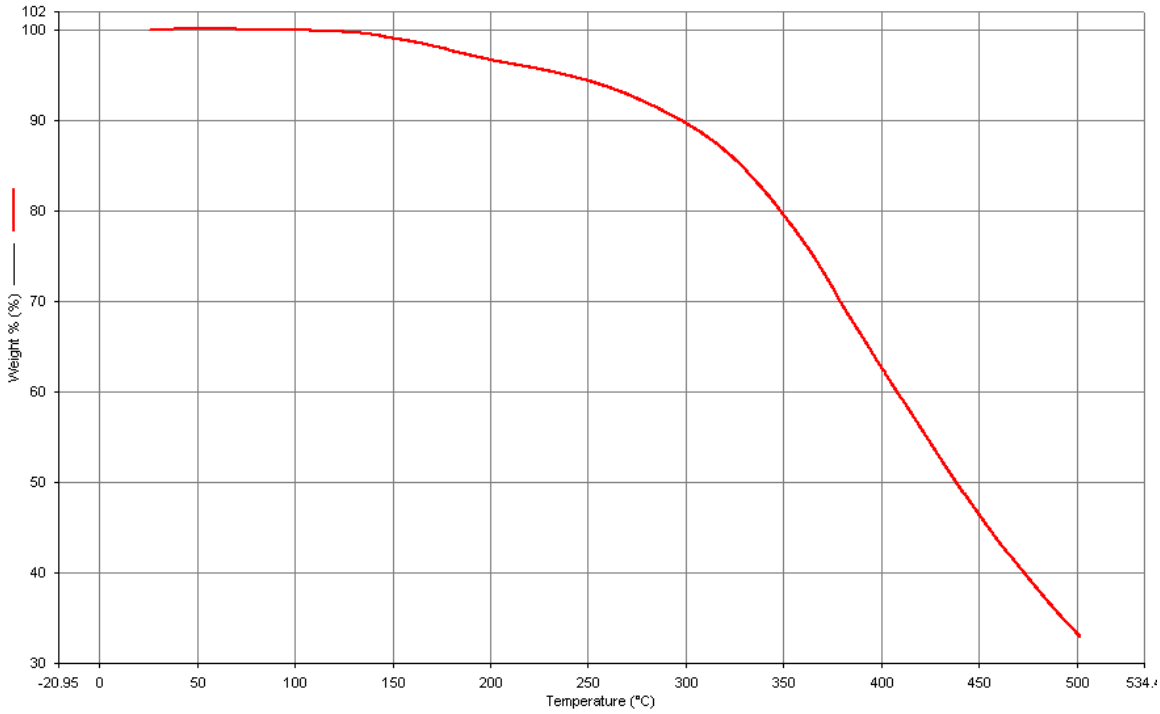

TGA of CAD-OH polymer

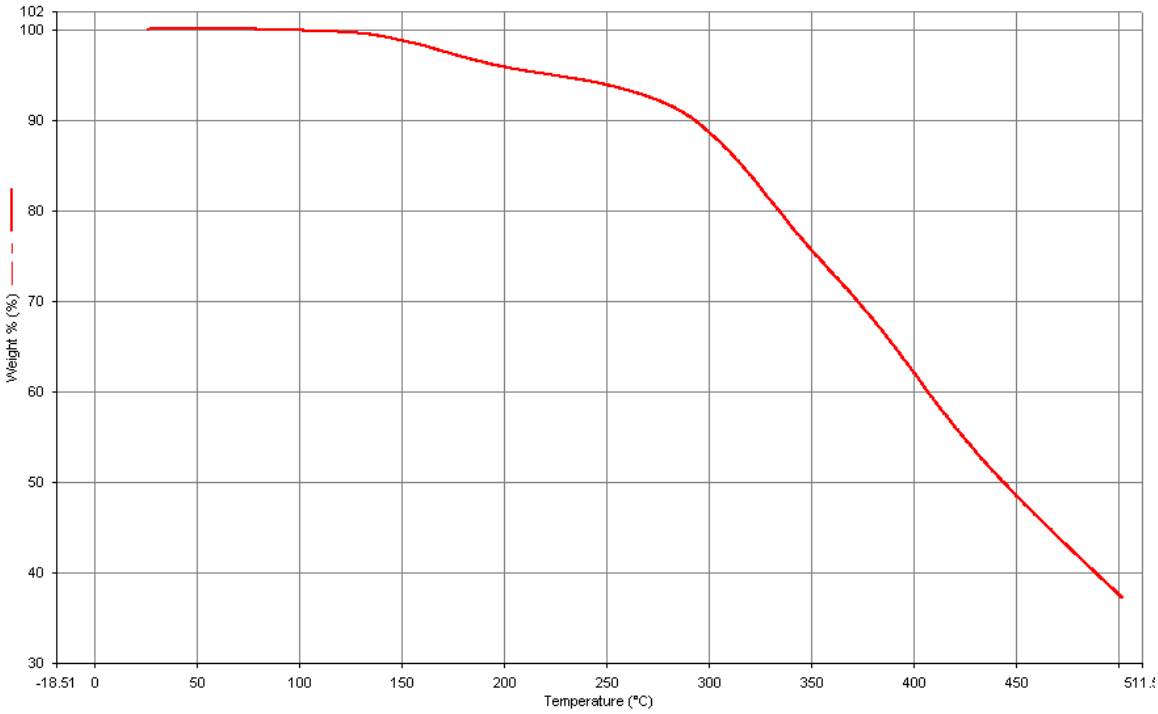

TGA of CAD-Alkyne polymer

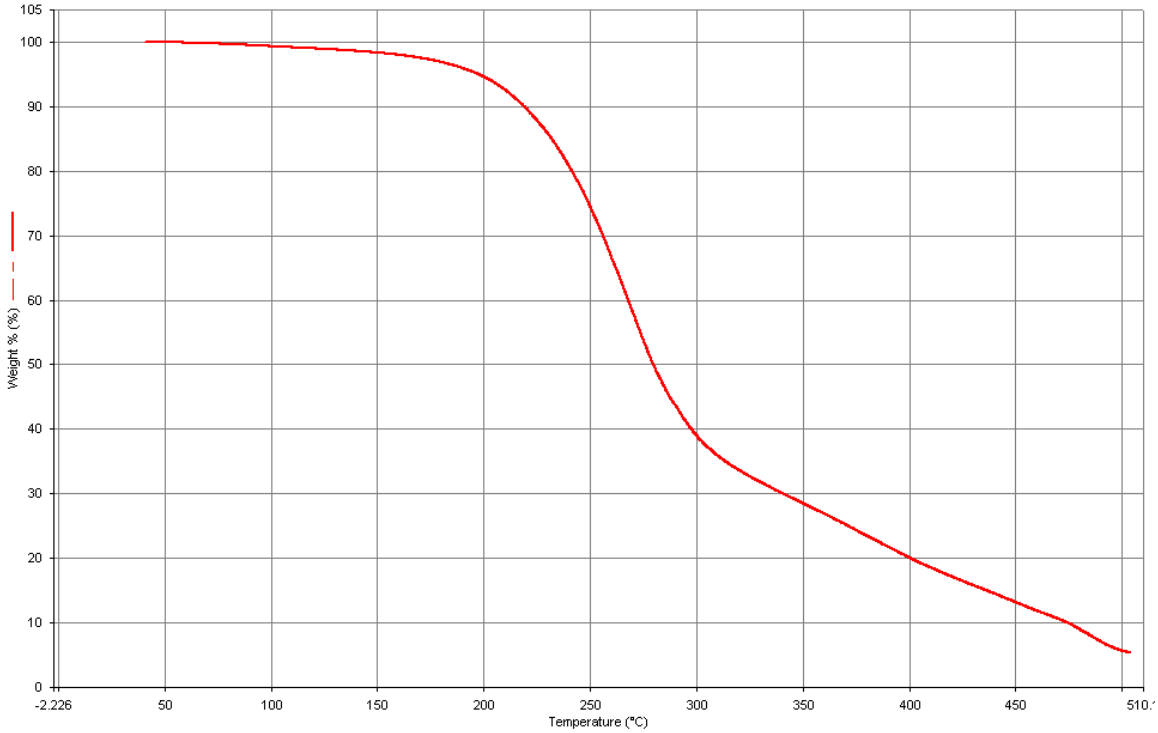
105
100
90
80
70
60
50
40
30
20
10
0
Weight % (%)
-2.226
50
100
150
200
250
300
350
400
450
Temperature (°C)

TGA of EO-HD

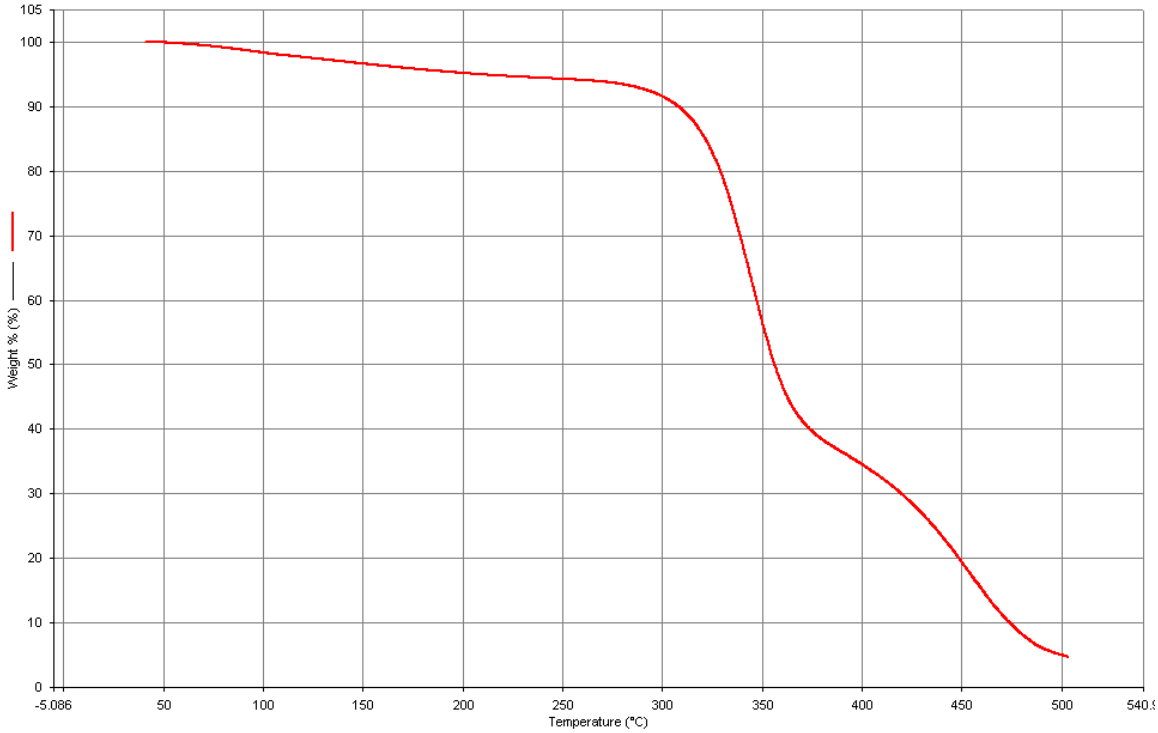
105
100
90
80
70
60
50
40
30
20
10
0
Weight % (%)
-5.086
50
100
150
200
250
300
350
400
450
500
Temperature (°C)

TGA of EC-HD

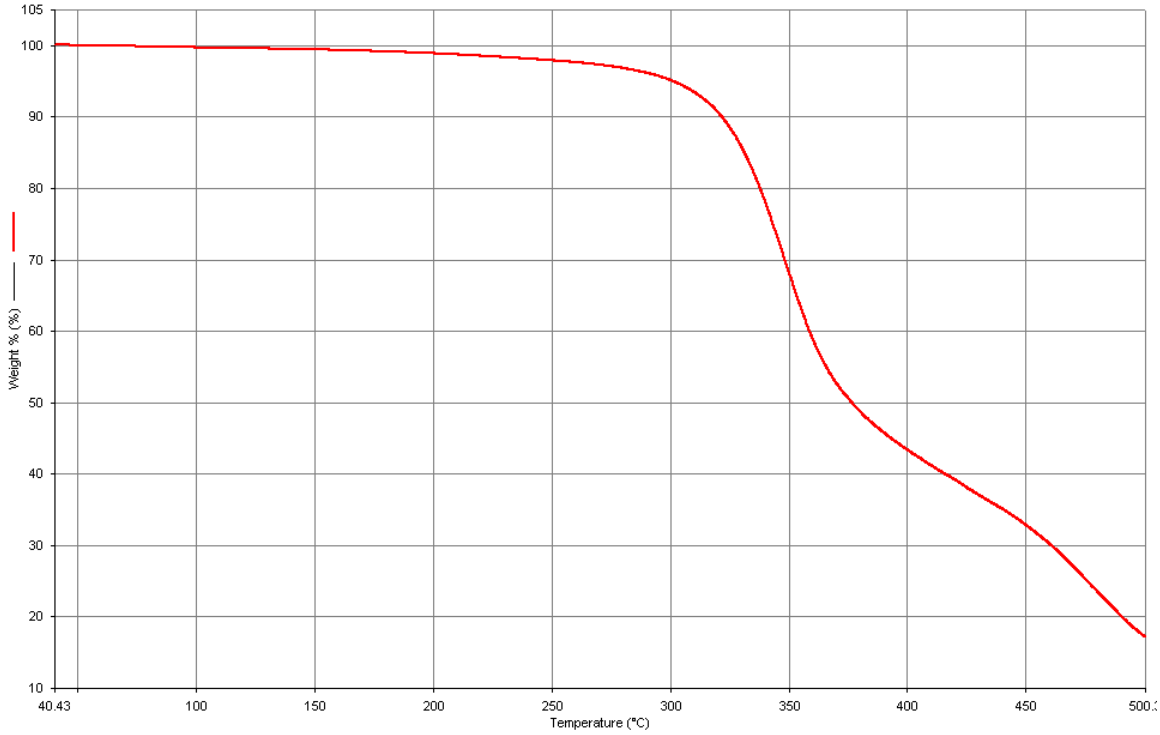

TGA of EC-HD Film

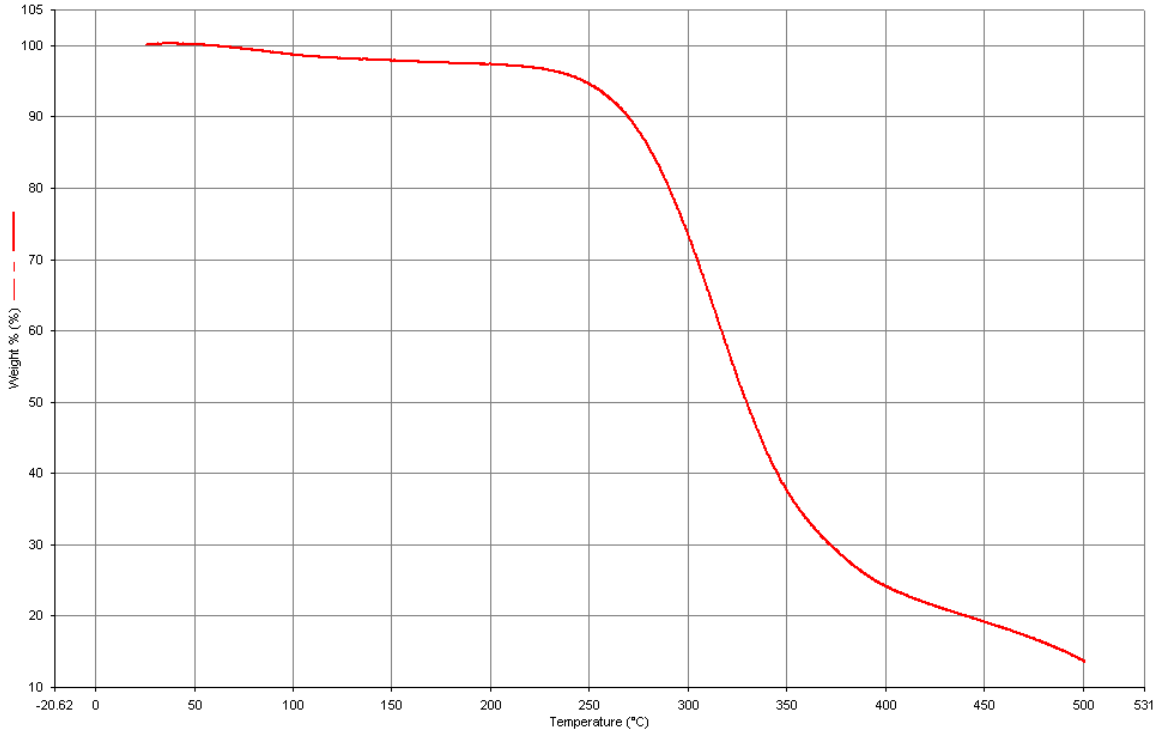
105
100
90
80
70
60
50
40
30
20
10
Weight % (%)
-20.62
0
50
100
150
200
250
300
350
400
450
500
531
Temperature (°C)

TGA of EO-BD

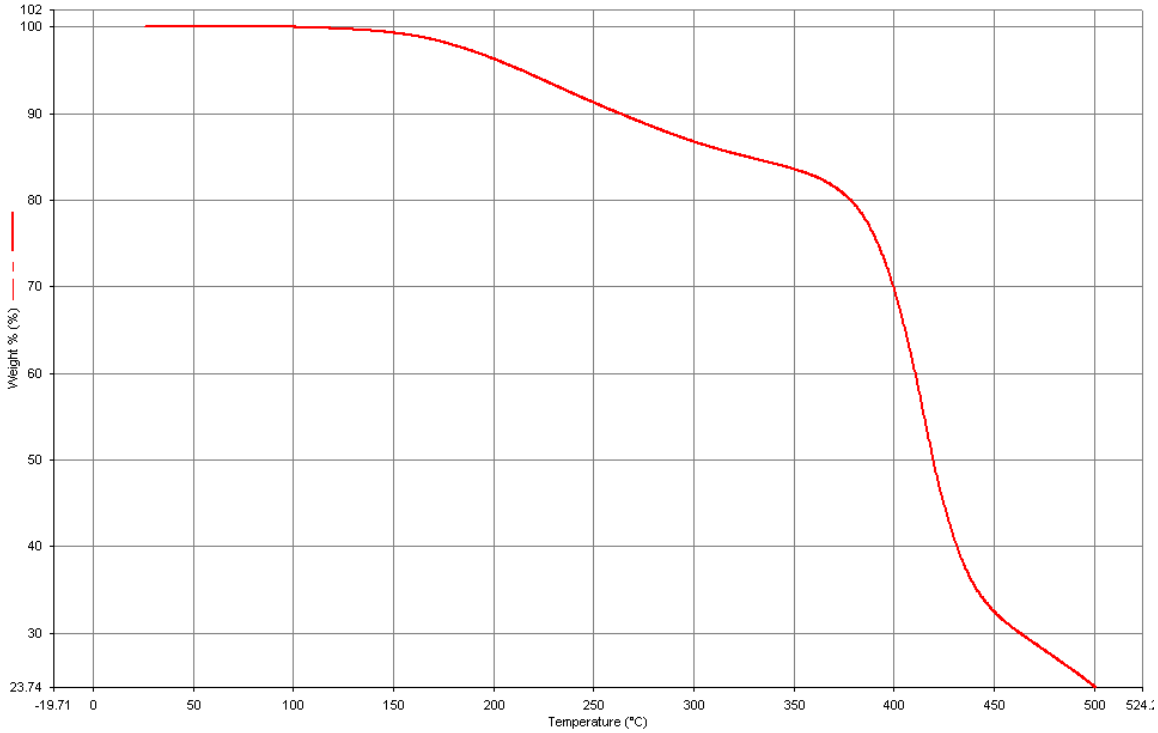
102
100
90
80
70
60
50
40
30
23.74
Weight % (%)
-19.71
0
50
100
150
200
250
300
350
400
450
500
Temperature (°C)

TGA of EC-BD

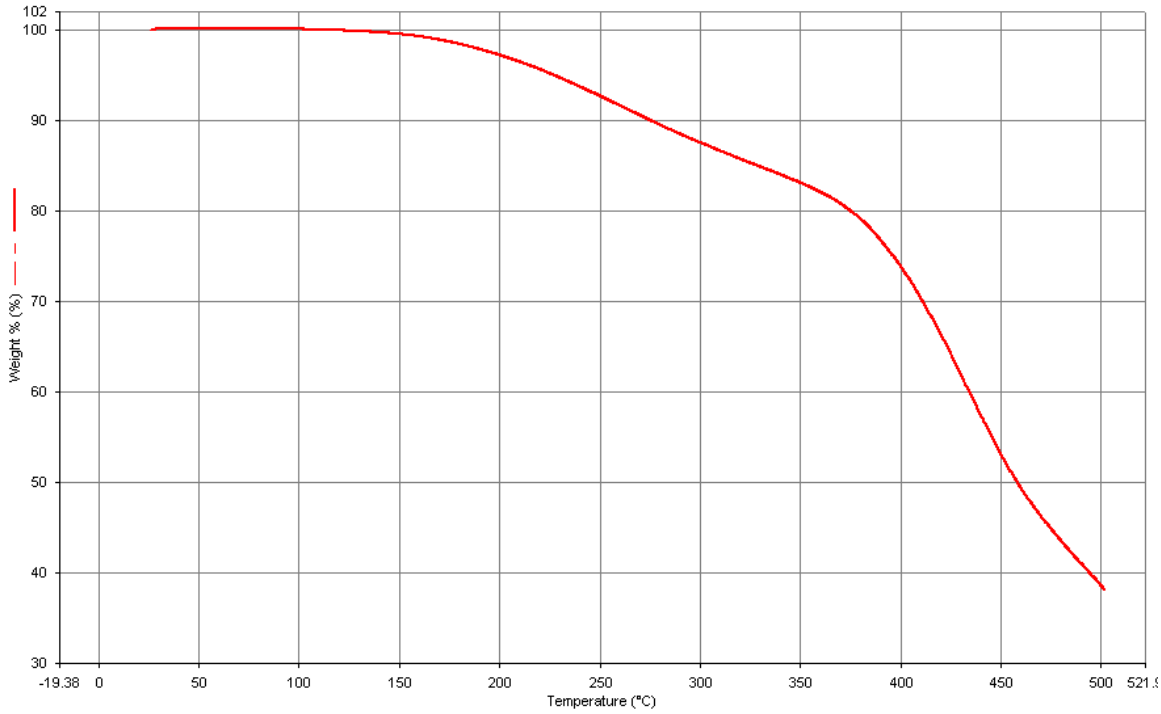

TGA of EC-BD Film

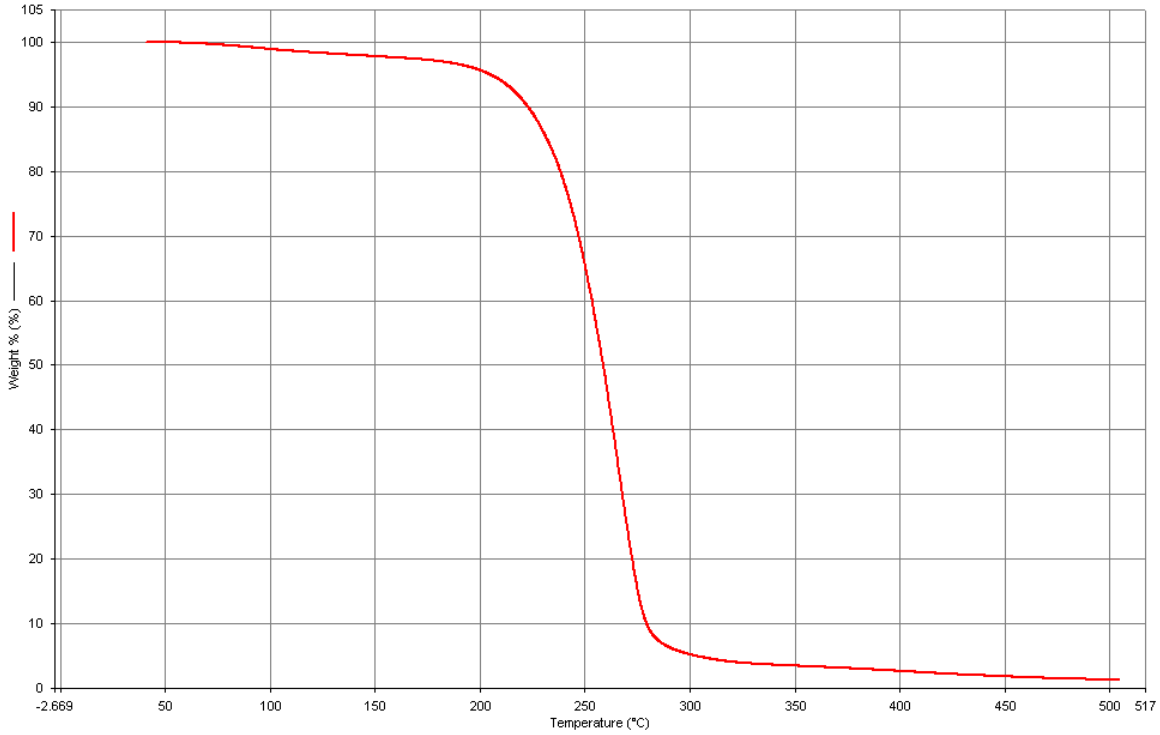
105
100
90
80
70
60
50
40
30
20
10
0
Weight % (%)
-2.669
50
100
150
200
250
300
350
400
450
500
517
Temperature (°C)

TGA of BO-HD

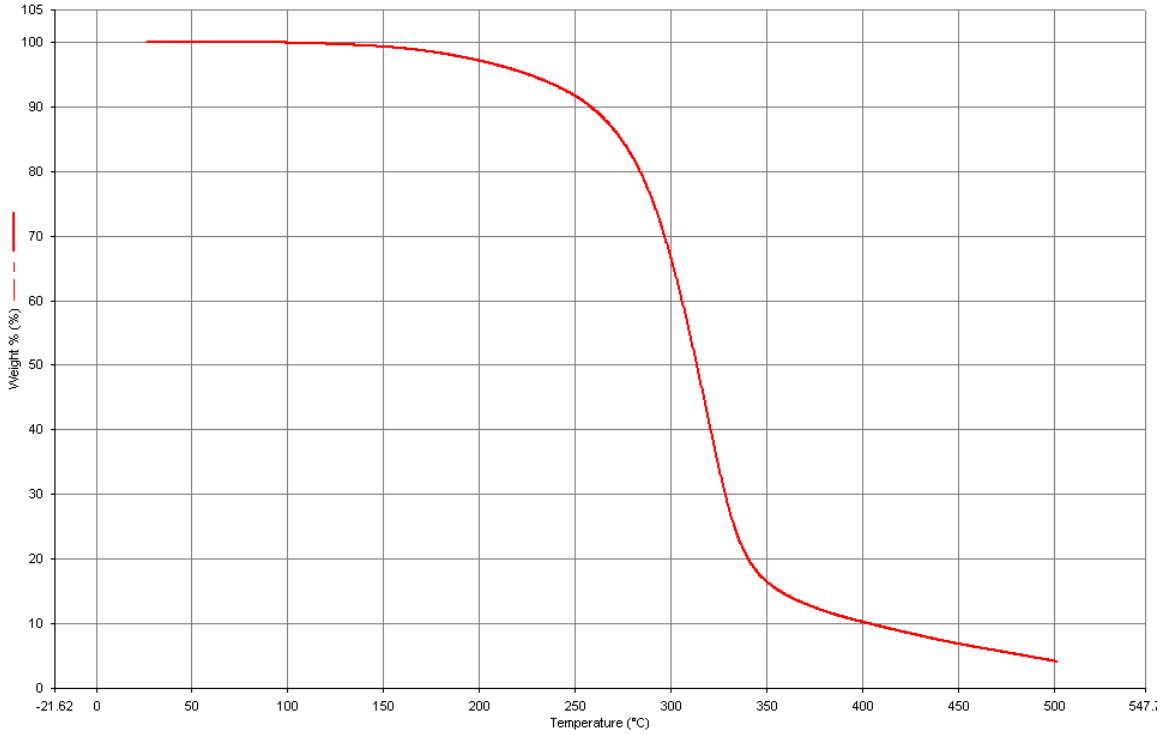
105
100
90
80
70
60
50
40
30
20
10
0
Weight % (%)
-21.62
0
50
100
150
200
250
300
350
400
450
500
547.
Temperature (°C)

TGA of BC-HD

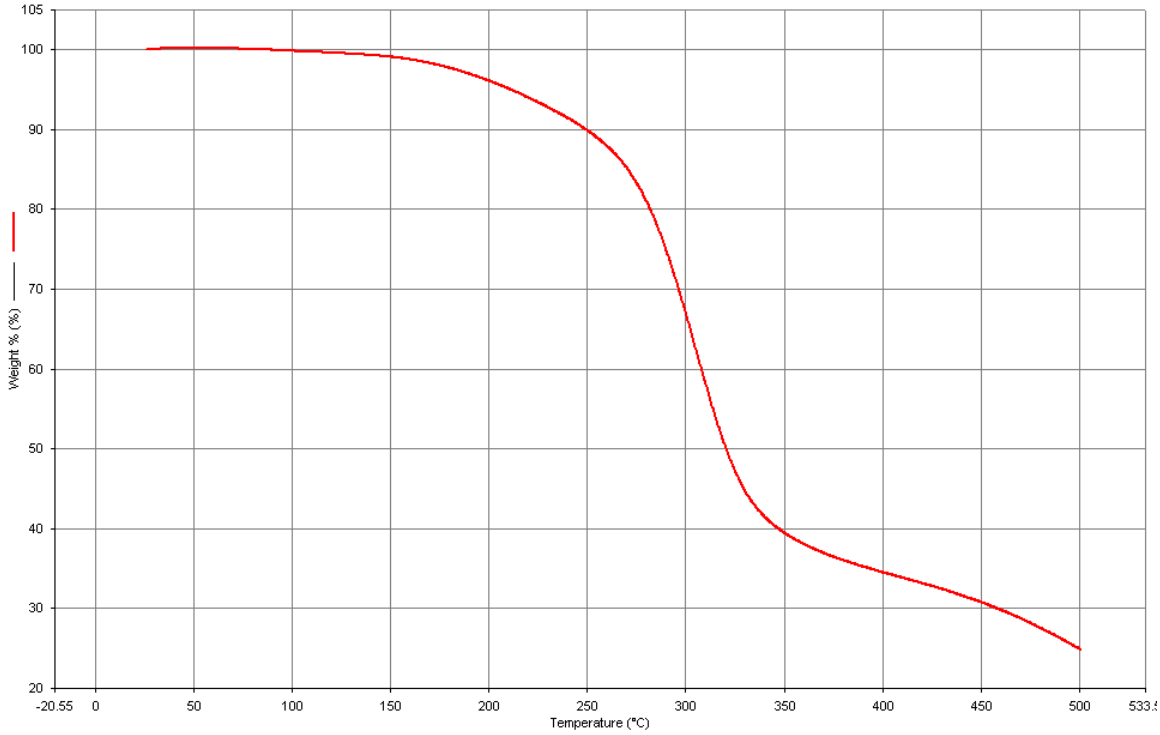

TGA of BC-HD Film

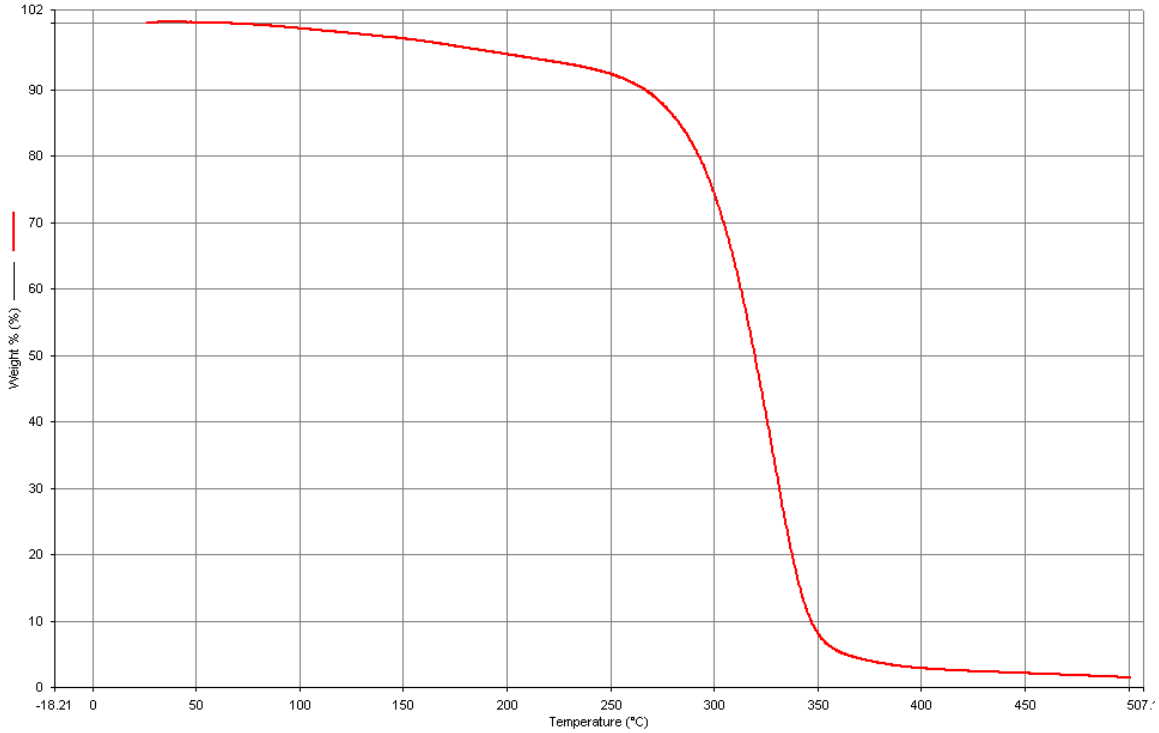
102
90
80
70
60
50
40
30
20
10
0
Weight % (%)
-18.21
0
50
100
150
200
250
300
350
400
450
Temperature (°C)

TGA of BO-BD

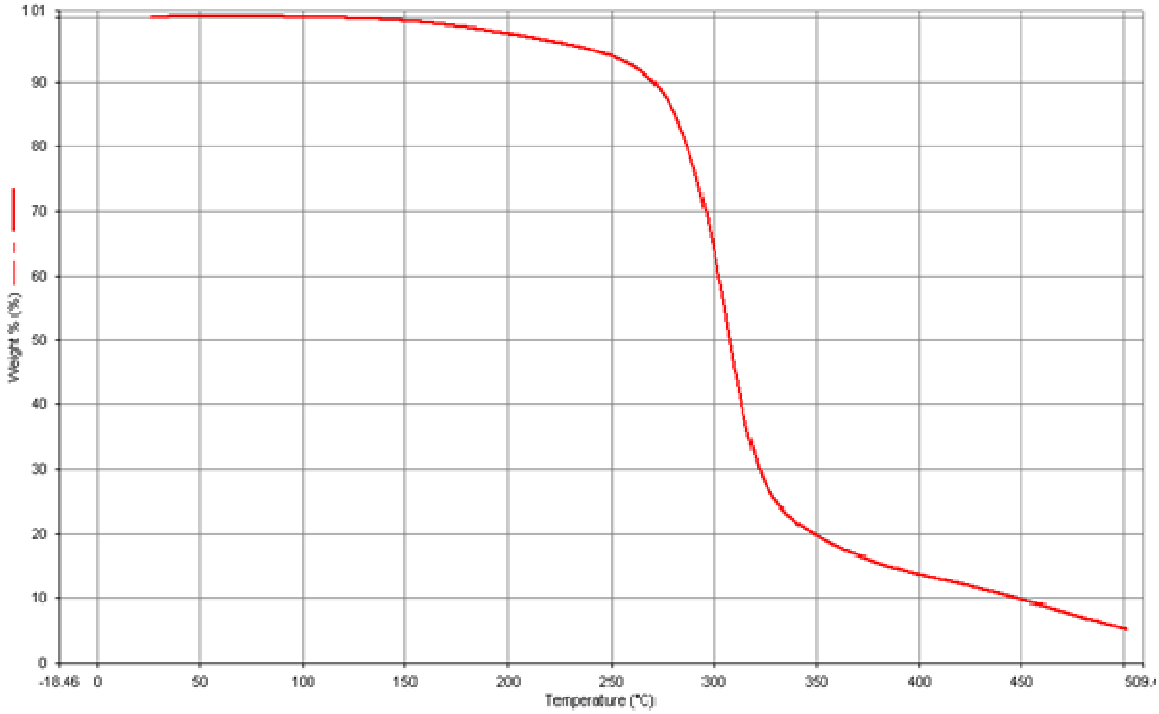
101
90
80
70
60
50
40
30
20
10
0
Weight % (%)
-18.46
0
50
100
150
200
250
300
350
400
450
509.
Temperature (°C)

TGA of BC-BD

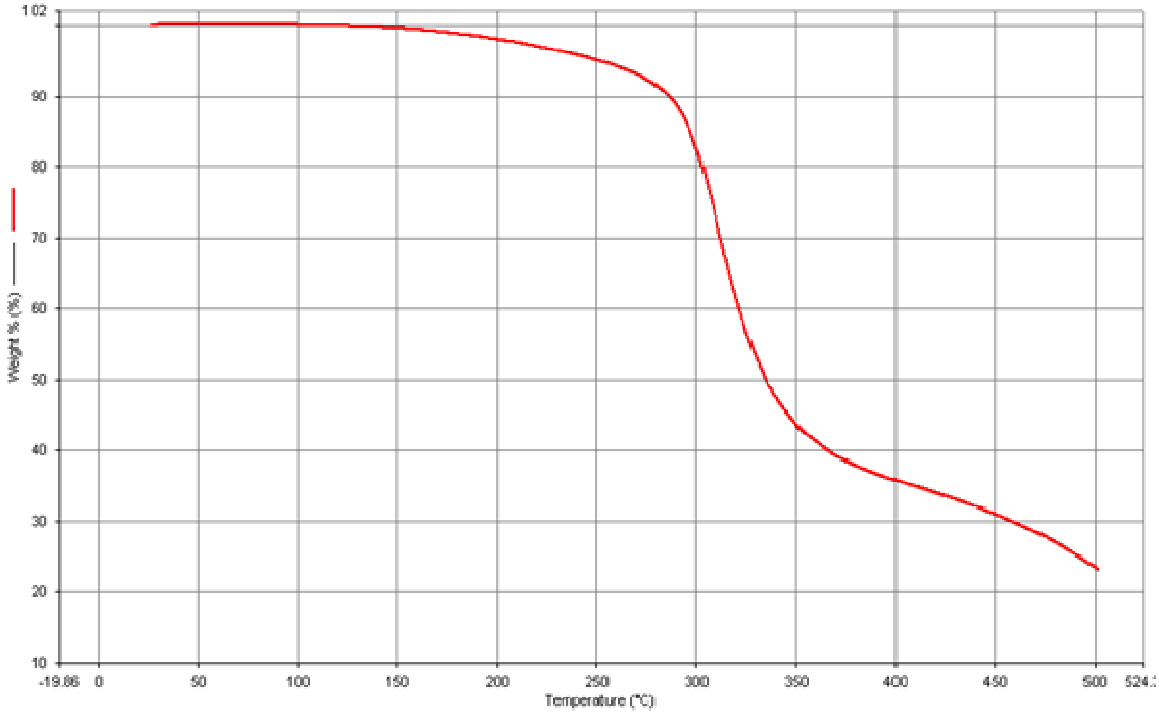

TGA of BC-BD Film

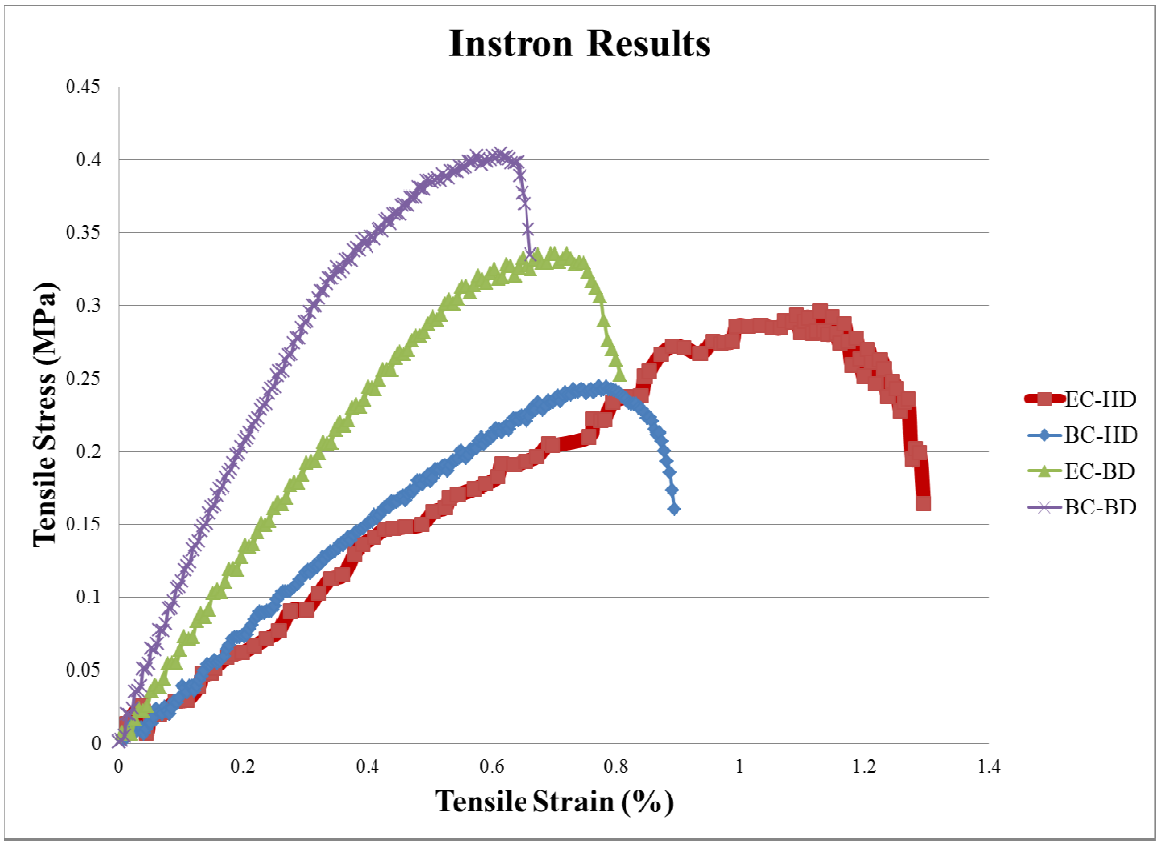

Instron results for PBAE elastomers

Appendix D

The following appendix contains the synthesis and characterization of initial thiol pendant copolyesters used as functional thermal shape memory materials. Currently, the most common SMPs for biomedical application are based on PCL, PLGA, and PLLA, as well as various copolymers of the three.[1,2] These materials are degradable and can be targeted for specific transition temperatures, however, there is no additional functionality available for tailoring properties or incorporating chemical and biological moieties of interest for different applications. Recently, Brosnan *et al*. developed poly(ester urethane) copolymers with pendant azide groups along the polymer backbone which possessed thermal shape memory and could be further functionalized via copper click chemistry to tailor the chemical and physical properties of the materials in the bulk and on the surface.[3] The shape memory properties of the system were based on the incorporation of adipic acid (AA) which as a homopolymer is a semicrystalline material. Within copolymers, the adipic acid affords a melting transition which can be tuned by altering the concentration of AA in the melt.

Thiol-ene reactions are another form of click chemistry that have been recently examined as synthetic tools due to the relative ease of reaction and lack of side reactions/products.[4,5,6] The incorporation of free mercapto groups along a polymer chain was first reported in 1960 using a protection/deprotection method for polyurethanes and polyamides.[7,8] The synthesis of degradable polyesters was not available through this method due to the harsh conditions of the deprotection process, however, recently polycondensation methods utilizing HCl[9], enzymes[10], or scandium trifluoromethanesulfonate [$Sc(OTf)_3$][11] have resulted in thiol pendant polyesters without requiring protection/deprotection steps.

Herein, we present the synthesis of thiol containing copolyesters using $Sc(OTf)_3$ catalyst, which possess thermal shape memory due to the incorporation of AA. The pendant thiol groups are utilized for crosslinking and functionalization through thiol-ene click chemistry. Varying the incorporation and MW, the transition temperature can be tuned and the concentration of free thiol groups adjusted. The shape memory effect can be utilized for macroscopic and microscopic shape changes through various bulk or soft lithography programming techniques. Furthermore, in comparison to copper click chemistry involving potentially dangerous azide containing materials, the thiol containing materials offer a safer route to functional shape memory materials, as well as do not require the need for metal catalyst.

Experimental

Materials. 1,8-octanediol, mercaptosuccinic acid (MSA), and scandium triflate were purchased from VWR and used without further purification. All other reagents were purchased from Sigma Aldrich and used without further purification unless otherwise noted. Trimethylolpropane triacrylate was deinhibited by filtering through basic alumina.

Instrumentation. Gel permeation chromatography was used to determine molecular weights and molecular weight distributions, M_w/M_n, of polymer samples using a Waters Alliance 2695 and Waters 2414 Refractive Index detector. Molecular weights were calculated using a calibration plot constructed from polystyrene standards (Polyscience Corp.). The measurements were taken at 35 °C with THF as the mobile phase on three columns (Waters Styragel HR5, HR4, and HR2). ^{1}H NMR spectra of the monomers and polymers were obtained on a Bruker 400 ADVANCE spectrometer. Thermal transitions were analyzed using TA Differential Scanning Calorimeter Q200 with liquid N_2 cooling unit

at a cooling rate of 5 ^{o}C/min and heating rate of 10 ^{o}C/min. A Pyris I Thermogravimetric Analyzer was used to collect 5% and 10% decomposition temperature data from 25 ^{o}C to 500 ^{o}C at a heating rate of 20 ^{o}C/min in N_2 atmosphere. Stress-strain data for thermal shape memory transitions was collected on a Pyris Diamond Dynamic Mechanical Analyzer with liquid N_2 cooling unit.

Polymer Synthesis. An example of a typical polymerization is given. A round-bottom flask was charged with mercaptosuccinic acid (0.407 g, 2.71 mmol) adipic acid (1.583 g, 10.83 mmol), 1,8-octanediol (2.00 g, 13.68 mmol), and scandium triflate catalyst (0.069, 0.14 mmol), after which it was evacuated and filled with N_2. The mixture of monomers was heated to a melt at 80 ^{o}C and stirred for 2 h. The pressure was slowly reduced to 0.01-2.0 torr after this initial reaction period. The mixture continued to stir under reduced pressure for another 24 hours. The reaction was removed from heat and atmospheric pressure was re-established before the polymer was dissolved in 5 mL of chloroform and precipitated into cold stirring methanol (-78 ^{o}C). The polymer was then dried under vacuum for 24 hours. ^{1}H-NMR: δ (ppm) = 4.15 (dt, 1H, J_1 = 4 Hz, J_2 = 8 Hz), 4.05 (t, 4H, J = 6 Hz), 3.74 (t, endgroup, J = 8 Hz), 3.00 (dd, 1H, J_1 = 8 Hz, J_2 = 16 Hz), 2.75 (dd, 1H, J_1 = 6 Hz, J_2 = 18 Hz), 2.32(t, 4H, J = 6 Hz), 2.20 (d, 1H, J = 12 Hz), 1.66 (qn, 4H, J = 4 Hz), 1.61 (t, 4H, J = 6 Hz), 1.32 (m, 8H).

Crosslinking. Prepolymers were crosslinked without further functionalization or endcapping by reacting with a trifunctional crosslinking agent. To a 50 wt % polymer solution in $CHCl_3$ was added trimethylolpropane triacrylate (0.01 g, 0.033 mmol) and diethoxyacetophenone (0.008 g, 0.038 mmol). The solution was cast onto a glass slide or

into Teflon molds followed by irradiation in an ELC-500 UV crosslinking chamber for 20 minutes.

Characterization

Macroscale Shape Memory. Dynamic mechanical analysis (DMA) was used to measure strain fixity and strain recovery for macroscopic thermal shape memory. The DMA programming/recovery cycle method was as follows: sample was heated to 20 ^{o}C above T_m at a rate of 5 ^{o}C/min; stress was applied to the prescribed magnitude of force at a rate of 100 mN/min; sample under stress was cooled below 0 ^{o}C at a rate of 20 ^{o}C/min; stress was removed; sample was heated to 20 ^{o}C above T_m at a rate of 5 ^{o}C/min. Using the resulting data, the strain fixity (R_f) and strain recovery (R_r) were calculated.

For programming a variety of shapes (bending, twisting, coiling) the following general procedure was used. Samples were heated in an oven at 20 ^{o}C above the T_m for ~15 min and then deformed and cooled to 2 ^{o}C to fix the temporary shape. Temporary shapes were persistent at room temperature and recovery occurred when placing the temporary shape into an oven or water bath above T_{trans}.

Microscale Surface Shape Memory. Shape programming on a microscopic level was possible utilizing PRINT^{TM} (particle replication in non-wetting templates) technology[15] to emboss the surface of films using a previously determined method.[9] Polymer films were heated above T_{trans} and the PRINT^{TM} mold was placed onto the film surface, which was then placed between glass slides in a press. The press containing the molded film was placed in an oven above T_{trans} for 30 min and then cooled at 2 ^{o}C for 1 h. Recovery of the permanent surface topography was accomplished by heating above T_{trans} for 30-60 min. Flat surfaces and embossed surfaces with microscopic features were imaged using a Zeiss Imager D.1m

microscope with AxioCam. A halogen bulb source was used for brightfield imaging under 100x magnification.

Results and Discussion

Polymer Synthesis. Linear semi-crystalline thiol pendant copolyesters (TPEs) were successful synthesized by reaction of mercaptosuccinic acid and adipic acid with 1,8-octanediol. The monomer feed was used to control the incorporation of thiol side chains, target MW, and give hydroxyl chain ends. The use of scandium triflate catalyst at 80 ^{o}C prohibited the reaction between diacid and thiol group to form thioesters which would have resulted in unwanted branching/gelling.

Two different TPE prepolymers were synthesized, varying the incorporation of thiol and adipic acid. TPE-1 used a monomer feed for 80:20 adipic acid/mercaptosuccinic acid and in TPE-2 the thiol monomer incorporation was doubled by employing a 60:40 ratio. The

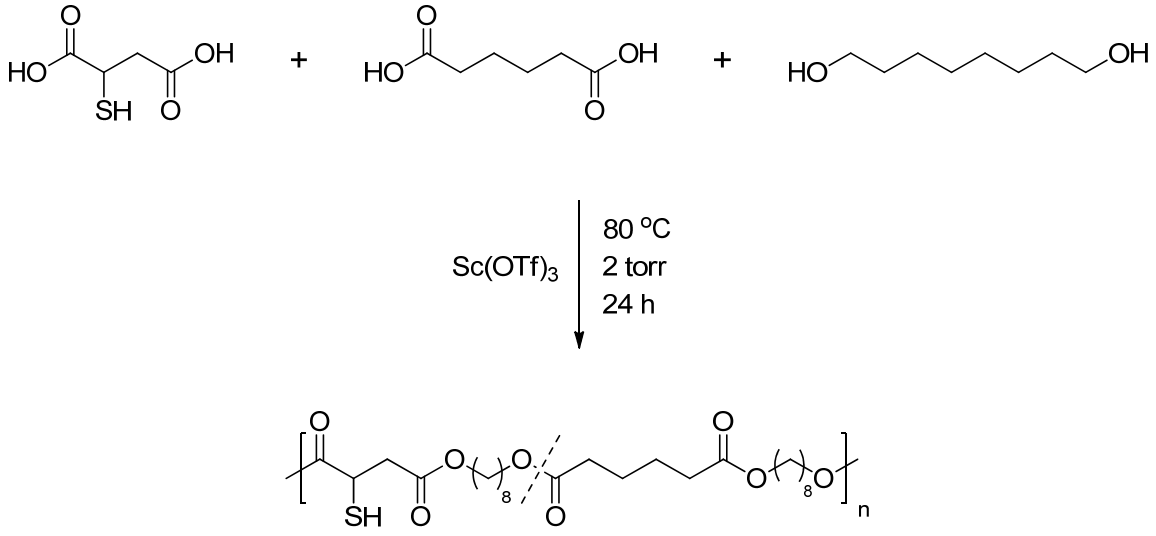

Scheme 1. Polymerization of thiol-pendant copolyesters (TPEs).

resulting polymers had an overall thiol incorporation of 10% (TPE-1) and 20% (TPE-2). The incorporation of thiol monomer was followed by ^{1}H-NMR comparing the thiol proton at 2.20 ppm and the methylene protons corresponding to the adipate repeat unit at 2.32 ppm (-CH_2COOCH_2-), and the incorporation shows good agreement with the feed ratio. The MW control for TPE-1 also showed good agreement with the targeted stoichiometric imbalance, however when the incorporation of thiol monomer increased in TPE-2, there was a large difference in the target and actual MWs. This could be due to a reactivity difference between the adipic acid and mercaptosuccinic acid monomers being more prevalent when a more equal feed ratio is used.

Thermoset Network Formation. Copolyester prepolymers were targeted for hydroxyl end groups by controlling the monomer stoichiometry. This was to afford a reactive functional group for a post-polymerization functionalization step to attach crosslinkable end groups through the reaction of alcohol end and 2-isocyanatoethyl methacrylate. During the reaction between alcohol and isocyanate, however, the reaction between thiol and methacrylate also occurs even at room temperature due to the high concentration and reactivity of thiol groups with the methacrylate compound. This led to undesirable gelation during the end-capping step. Therefore, instead of end-capping the prepolymers the photo-initiated reaction between a small percentage of thiol pendant groups and a trifunctional acrylate crosslinking agent was utilized to form thermoset semi-crystalline elastomers. The photo-initiator, diethoxyacetphenone, was added to a solution of prepolymer and crosslinking agent in chloroform, vortexed and then molded or cast. After UV curing for 10-20 minutes,

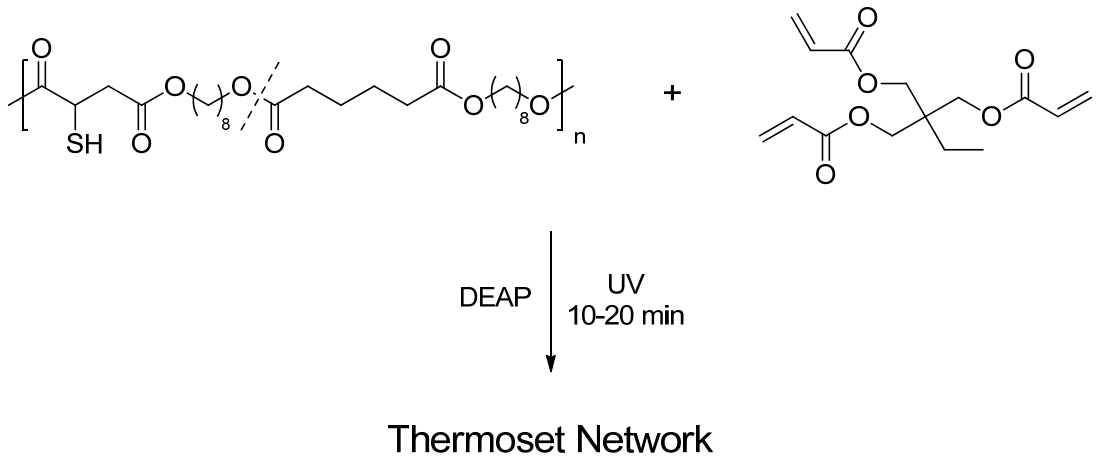

Scheme 2. Thermoset elastomer formation.

semi-crystalline elastomers were generated. By varying the crosslinking agent concentration, the crosslink density, as well as the amount of free thiol pendant groups remaining after curing could be tailored.

Based on the incorporation of thiol monomer, the amount of thiol pendant groups was calculated according to the average degree of polymerization (DP). The crosslinker was then added in quantities which would leave a known percentage of free thiol groups after photo-initiated thiol-ene crosslinking. Table 2 shows the value for both crosslinker concentration with respect to thiol groups and the theoretical concentration of thiol groups remaining after curing. For both TPE-1 and TPE-2, one elastomer was fabricated using ~10 % crosslinker, while the other used ~1% which leads to free thiol concentrations of ~70% and ~95% , respectively.

Thermal Characterization. The thermal properties of TPE-1 and TPE-2 were analyzed using DSC and TGA. The results for thermal transitions and decomposition temperatures can be seen in Table 1. DSC curves of both polymers showed melt and crystallization transitions, however the glass transition temperature was not discernible. The

Table 1. Characterization of polymer properties.

Sample	MSA: AA	MW (g x mol^{-1})[a]	PDI[a]	Decomposition (°C)[b]		T_C (°C)[c]	T_m (°C)[c]
				5%	10%		
TPE-1	20:80	12,100	1.97	333	347	35.5	50.7/52.8
TPE-2	40:60	6,800	1.71	432	458	18.9	33.3/39.7

[a]GPC – PS Stds. [b]TGA. [c]DSC.

semi-crystalline nature of the TPEs is attributed to the incorporation of adipic acid. The higher the concentration of adipic acid in the copolyester, the higher the T_c and T_m as can be seen by comparing TPE-1 (T_c = 35.5 °C, T_m = 50.7 °C) and TPE-2 (T_c = 18.9 °C, T_m = 33.3 °C). Each polymer also has a secondary melting transition very close to the major melting transition although only one T_c is seen. This is an artifact of adipic acid which is known to have two melting transitions. During melting of the crystallites at the first transition temperature, there is a reorganization and formation of a small amount of crystallites with a higher T_m (TPE-1 T_{m2} = 52.8 °C, TPE-2 T_{m2} = 39.7 °C). The decomposition temperatures also vary with thiol monomer incorporation. For TPE-1, where only 10% of RUs contain thiol pendant groups had decomposition temperatures in the mid 300 °C range, while TPE-2 had increased decomposition temperatures in the mid 400 °C range.

TPE-1 elastomers exhibited a minor decrease in T_m due to the netpoints impeding crystallization a small degree with the amount of added crosslinking agent having a negligible impact. On the other hand, TPE-2 film A (11.2 % crosslinking agent) there was an almost 10 °C decrease in the T_m and 15 °C change in the materials T_c. TPE-2 film B (1% crosslinking agent) displayed only a small decrease, similar to both TPE-1 films (Table 2).

Table 2. Thermal properties of TPE elastomers.

Sample	Crosslinker Conc. (mol % of SH)	Free Thiol Conc. (mol % remaining)	Decomposition (^oC)[a]		T_C (^oC)[b]	T_m (^oC)[b]
			5%	10%		
TPE-1:A	8.7	73.8	346	363	33.1	52.8
TPE-1:B	2.0	94.0	397	434	31.9	51.7
TPE-2:A	11.2	66.4	428	471	2.0	25.3
TPE-2:B	1.0	97.0	440	476	13.2	32.5

[a]TGA. [b]DSC.

This can be attributed to the larger incorporation of thiol monomer reducing the crystallinity imparted by the adipic acid, which in turn makes the amount of crosslinker have a more prominent impact. The greater the crosslink density which corresponds to larger amount of crosslinker, the more crystallization is impeded. Table 3 shows the results of melting enthalpy and enthalpy of crystallization measured by DSC for each film and the corresponding prepolymers, as well as the percent crystallinity in comparison to an AA/OD homopolymer. As can be seen, the TPE-1 prepolymer and films showed very similar crystallinity (50-60% of the homopolymer). TPE-2 prepolymer, containing less incorporation of adipic acid, had an expected lower percent crystallinity (40%) compared to the AA/OD homopolymer and the subsequent films showed further decrease in % crystallinity with TPE-2 film A losing nearly half of the crystalline phases.

Table 3. Crystallinity of TPE prepolymers and elastomers.

Sample	ΔH_c (J/g)[a]	ΔH_m (J/g)[a]	% Crystallinity[b] (exothermic)	% Crystallinity[b] (endothermic)
TPE-1 Prepoly	60.1	57.8	62.6	59.6
TPE-1:A	57.0	58.5	59.3	60.3
TPE-1B	51.3	50.1	53.4	51.7
TPE-2 Prepoly	42.6	40.4	44.3	41.6
TPE-2:A	35.8	30.0	35.2	30.9
TPE-2:B	26.2	25.1	27.3	25.9

[a]DSC. [b]Compared to AA/OD homopolymer (96.0 J/g and 97.0 J/g).

Thermal Shape Memory. The potential for thermal shape memory was investigated using the T_m as the transition temperature for the semi-crystalline TPE elastomers.

Macroscopic Shape Memory. The macroscopic SME for TPE elastomers was realized by heating films above T_{trans} and applying a force or stress. Cooling below T_{trans} fixed the programmed shape and the original shape was recovered by again heating above T_{trans}. As is the case with most SMPs on the macroscale, the shape change is delocalized meaning it occurs throughout the entire material when heat is applied. Figure 1 shows a TPE-1 elastomer progressing through a SM cycle. The original flat film (left) was heated to 80 ^{o}C to melt the polymer crystallites and deformed into a helical structure (middle) followed

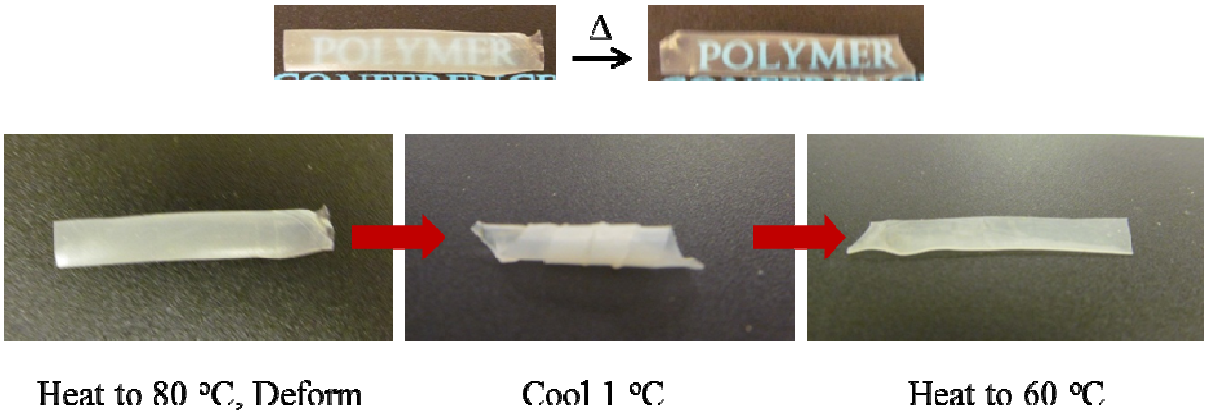

Figure 1. Macroscopic thermal shape memory of TPE-1 elastomer.

Table 4. Thermal shape memory characterization.

Series	T_m (°C)[a]	R_f (%)[b]	R_r(%)[b]
TPE-1 Elastomer	51.7	99	97
TPE-2 Elastomer	32.5	95	95

[a]DSC, [b]DMA

by cooling before removal of the external force. By heating to 60 °C, the recovery is triggered, restoring the permanent flat shape (right).

DMA testing was used to quantify the R_f and R_r of the systems (Table 4) using a cyclic programming/recovery method. Both TPE-1 and TPE-2 showed strain fixity > 95% with TPE-1 having near quantitative fixation (99%). Strain recovery was also slightly higher for TPE -1 (97%), but TPE-2 also shows outstanding recovery (95%). The slightly higher fixity and recovery in TPE-1 compared to TPE-2 is due to the larger percent crystallinity due to the greater concentration of adipic acid in the prepolymer.

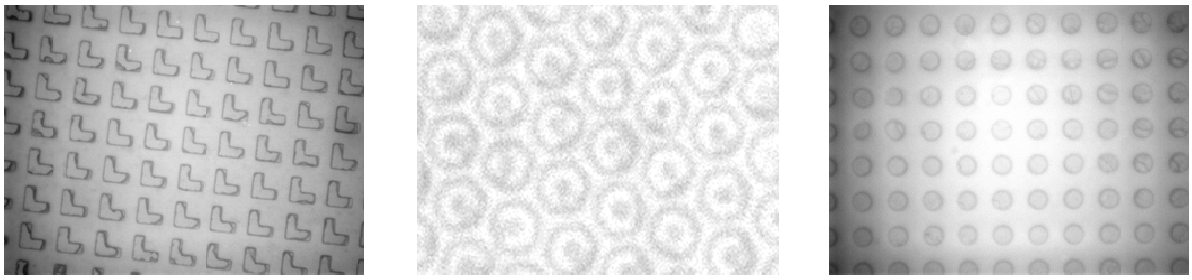

10 μm Boomerangs 3 μm Hexnuts 7 x 14 μm Posts

Figure 2. Bright-field microscope images of various microscopic surface patterns programmed on TPE-1 elastomer films.

Localized Surface Shape Memory. Reversible microscale surface features were successfully programmed into the surface of elastomer films using a soft lithography embossing method. A variety of shapes and sizes were patterned into the surface (Figure 2) by heating film samples and applying a perfluoropolyether (PFPE) mold under pressure by compressing between glass slides in a mechanical press. The elastomeric PFPE molds are replica molds of silicon master templates used to create reproducible pattern arrays on micro and nanoscales. The result is transfer of a repeatable surface pattern onto the surface of the polymer film. Heating is required to exceed T_{trans} and create a rubbery surface that can be deformed. A sufficient amount of consistent pressure is also needed to force the thermoset film surface into the mold. Additionally, permanent surface features can be built into the film by applying the mold in the crosslinking process. During heating of prepolymer solution, the mold can be placed on top of the casted film and capillary action allows filling of the mold. After thermosetting, removal of the mold leaves micro-features in the original shape, which can be programmed over with features of different sizes and shapes, but then recover the original pattern after triggering return. Figure 3 shows the original, temporary,

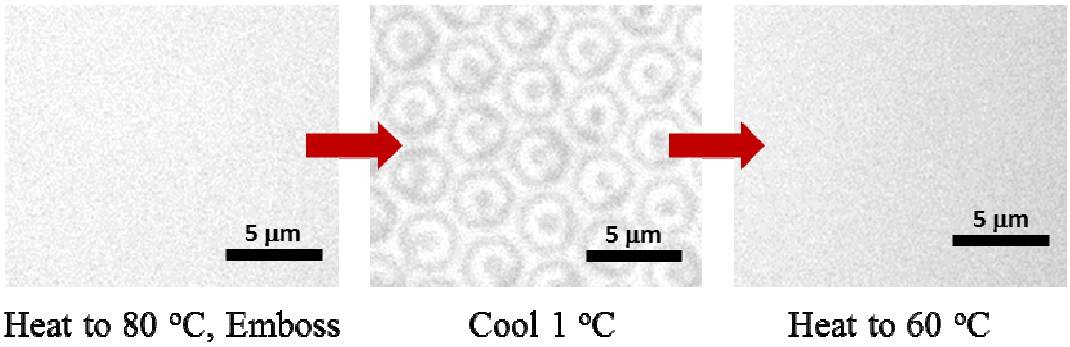

Figure 3. Bright-field images of microscopic thermal shape memory of TPE-1 elastomer.

and recovered shape memory surfaces for a TPE-1 film. Starting with a flat surface (left), the film was patterned with a 3 µm hexnut array (middle) through the embossing method, which was persistent for the time period it was kept below T_{trans} (52 ^{o}C). Heating the film above T_{trans} erased the micropattern and returned the flat surface (right) after 30 min with no noticeable change to the macroscopic dimensions of the film, showing the delocalized nature of the surface SME.

General Conclusions

Linear semi-crystalline thiol pendant copolyester elastomers exhibited excellent macroscopic and microscopic shape memory properties as well as tunable thermal properties by varying the thiol incorporation through the monomer feed ratio and the crosslink density of the elastomers by addition of different concentrations of crosslinking agent. The thiol pendant groups allow for the thiol-ene reaction between the polymer side-chains and the acrylates of the crosslinker, but also have the potential for use as chemical handles for further functionalization of the polymers and elastomers. This in combination with bulk and surface shape memory properties and degradable polyester backbone make these materials promising candidates for multifunctional materials for a variety of applications.

Acknowledgements

The authors would like to thank the DeSimone group for supplying PRINT™ molds used in surface embossing and use of the Zeiss Imager D.1m microscope. This research was funded by the National Science Foundation (Department of Materials Research) under Grant 1122483 (UNC MIRT).

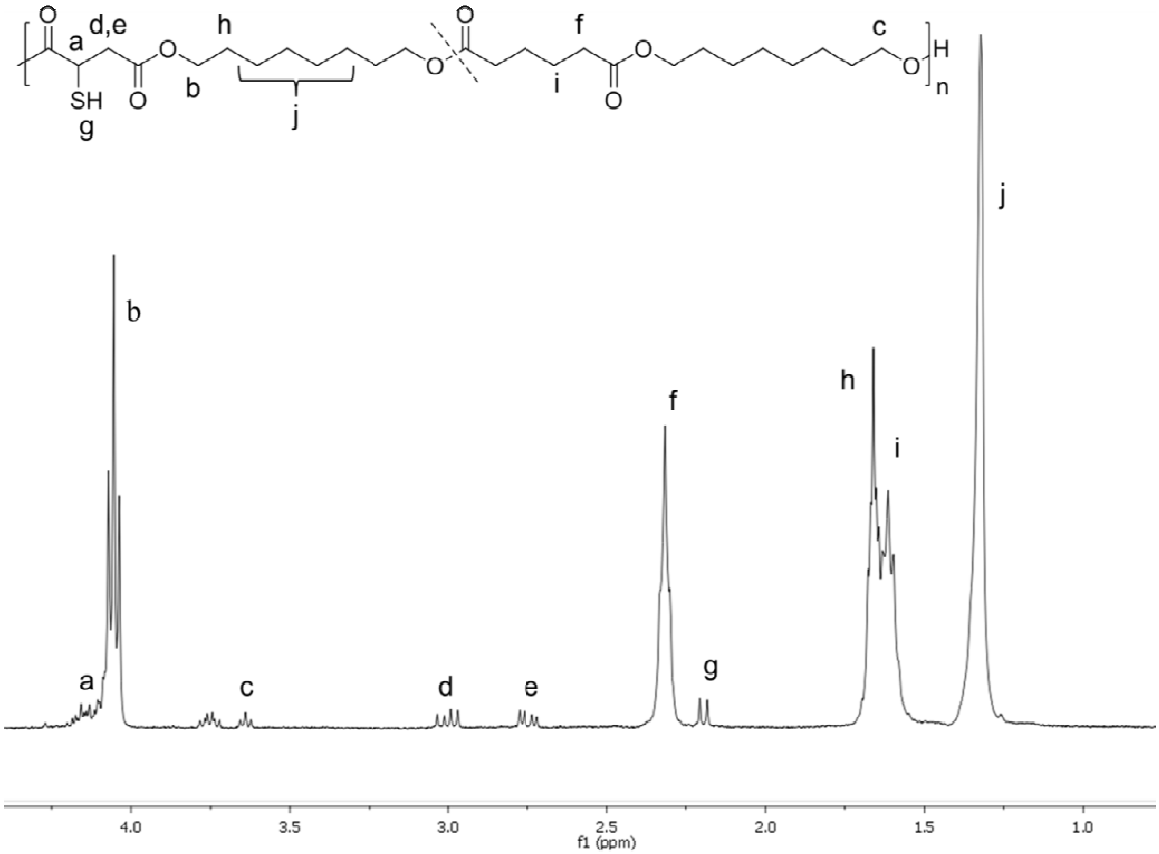

^{1}H-NMR of TPE-1

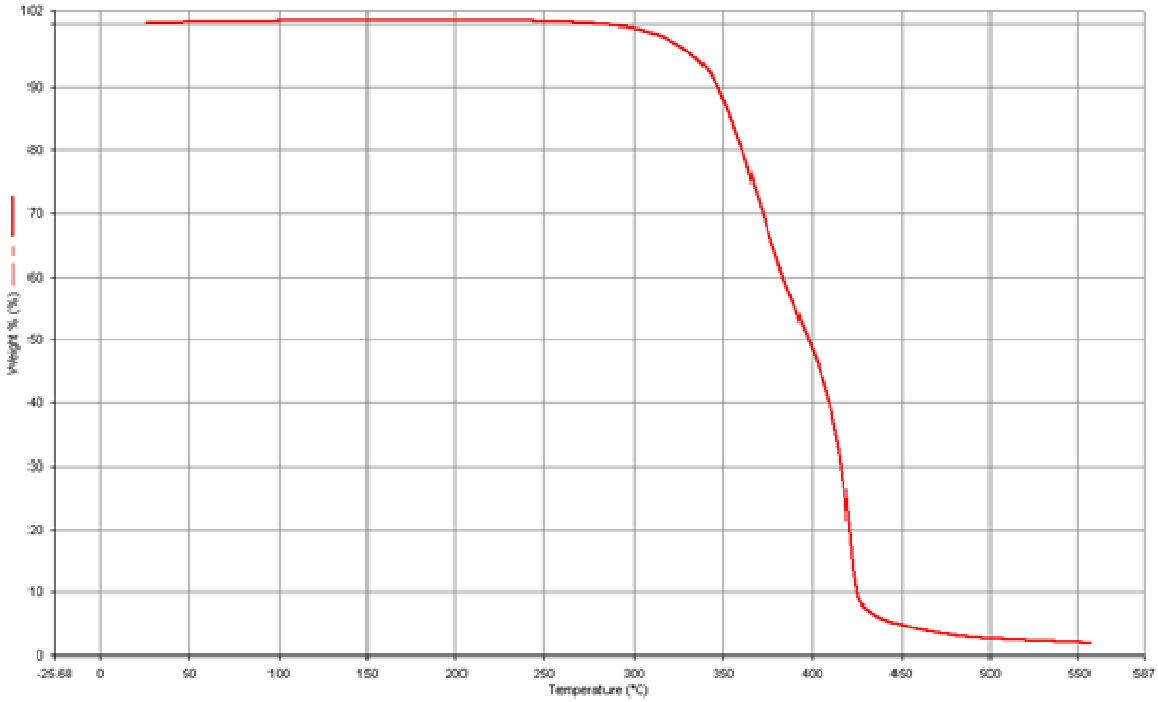

TGA of TPE-1 Prepolymer

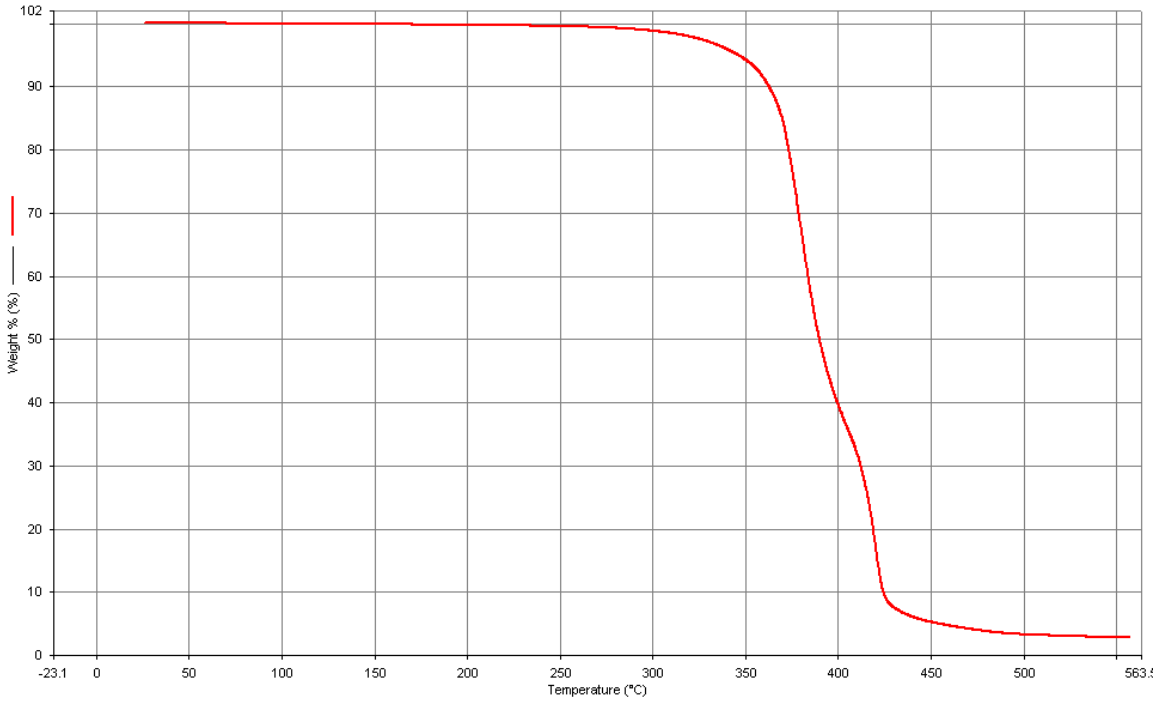

TGA of TPE-1 Film A

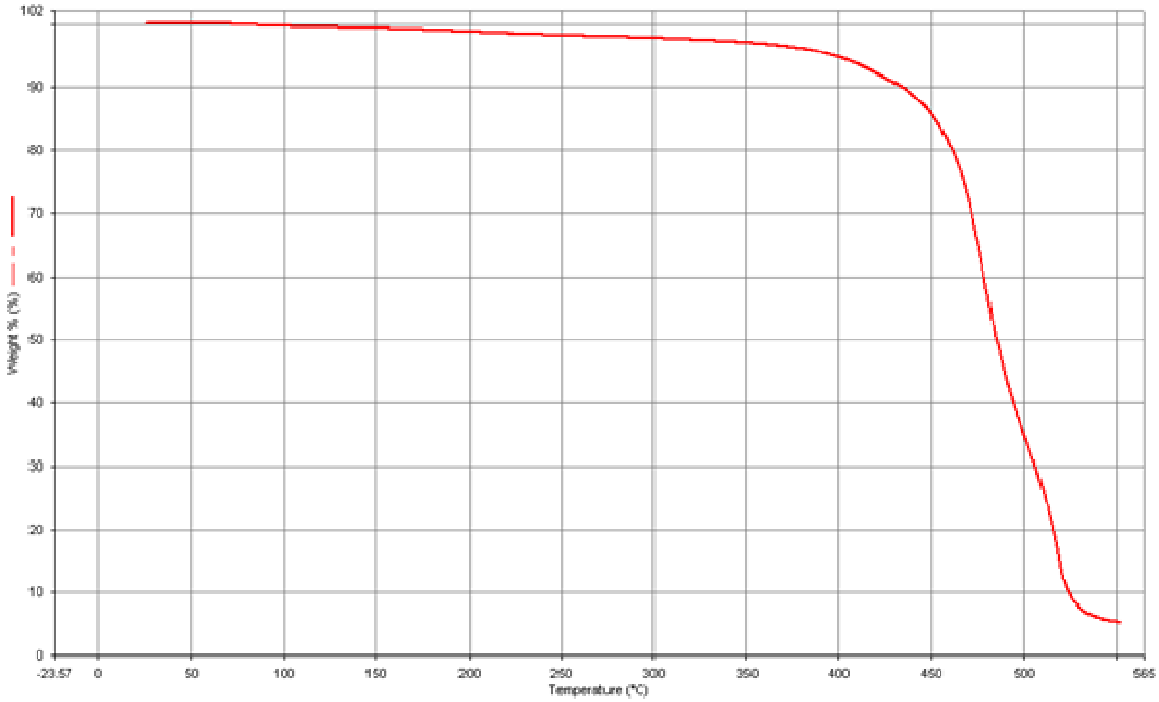

TGA of TPE-1 Film B

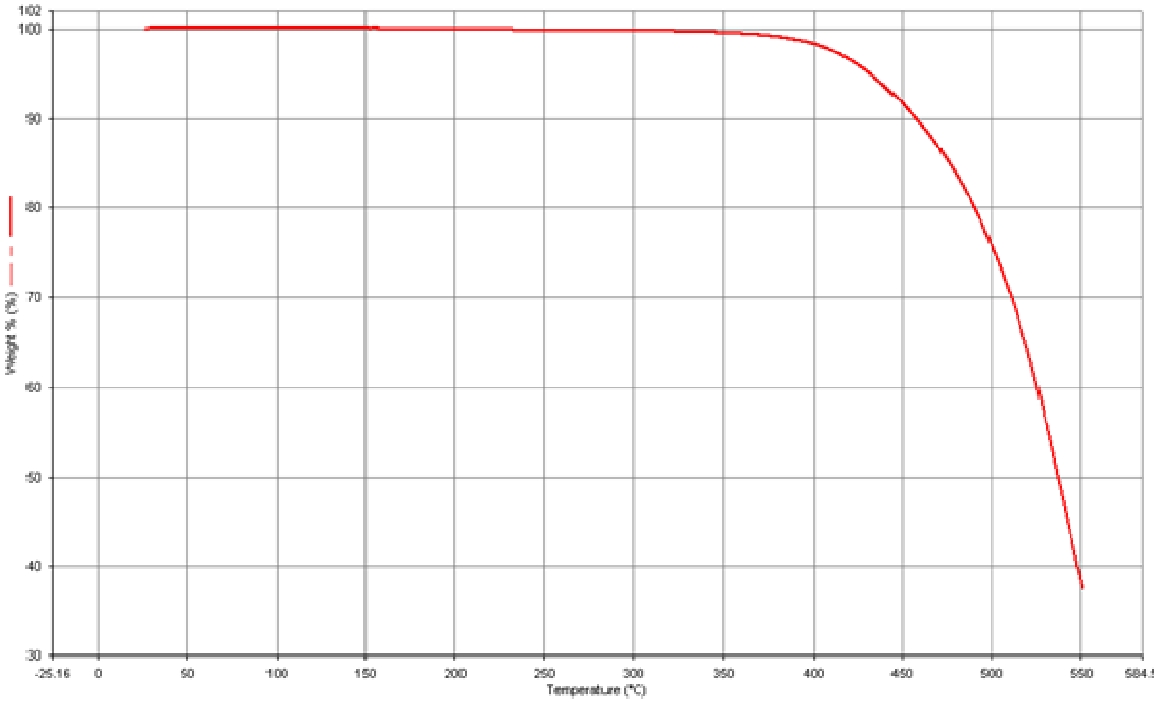

TGA of TPE-2 Prepolymer

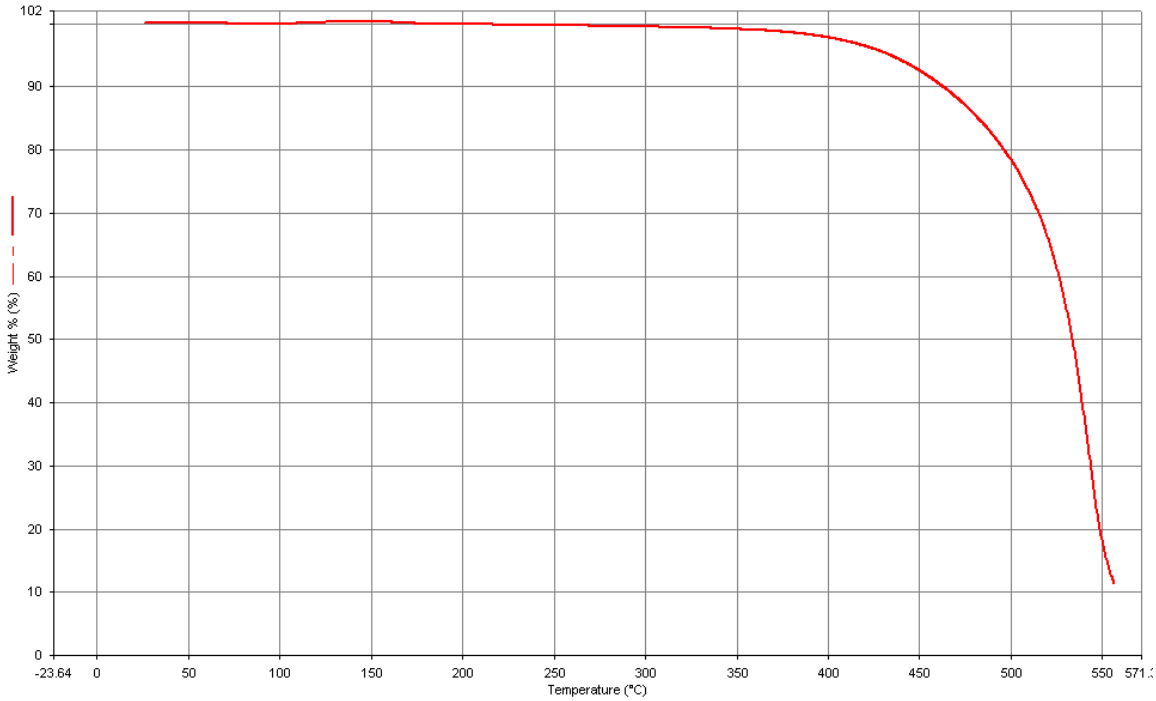

TGA of TPE-2 Film A

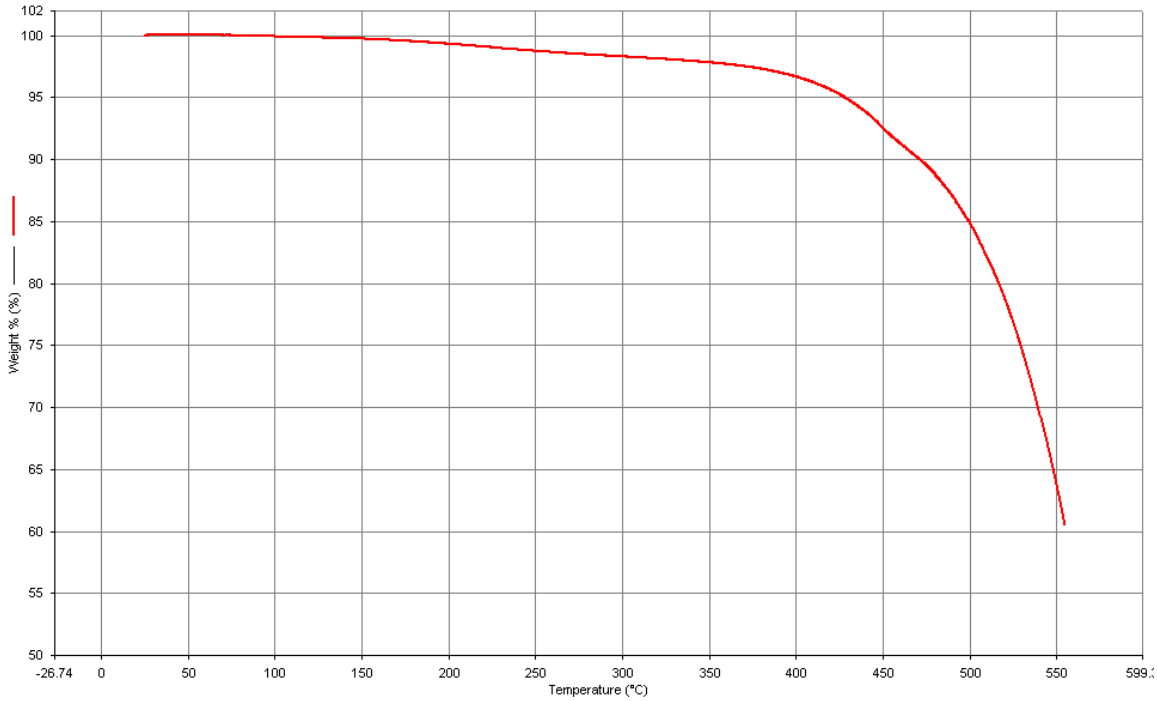

TGA of TPE-2 Film B

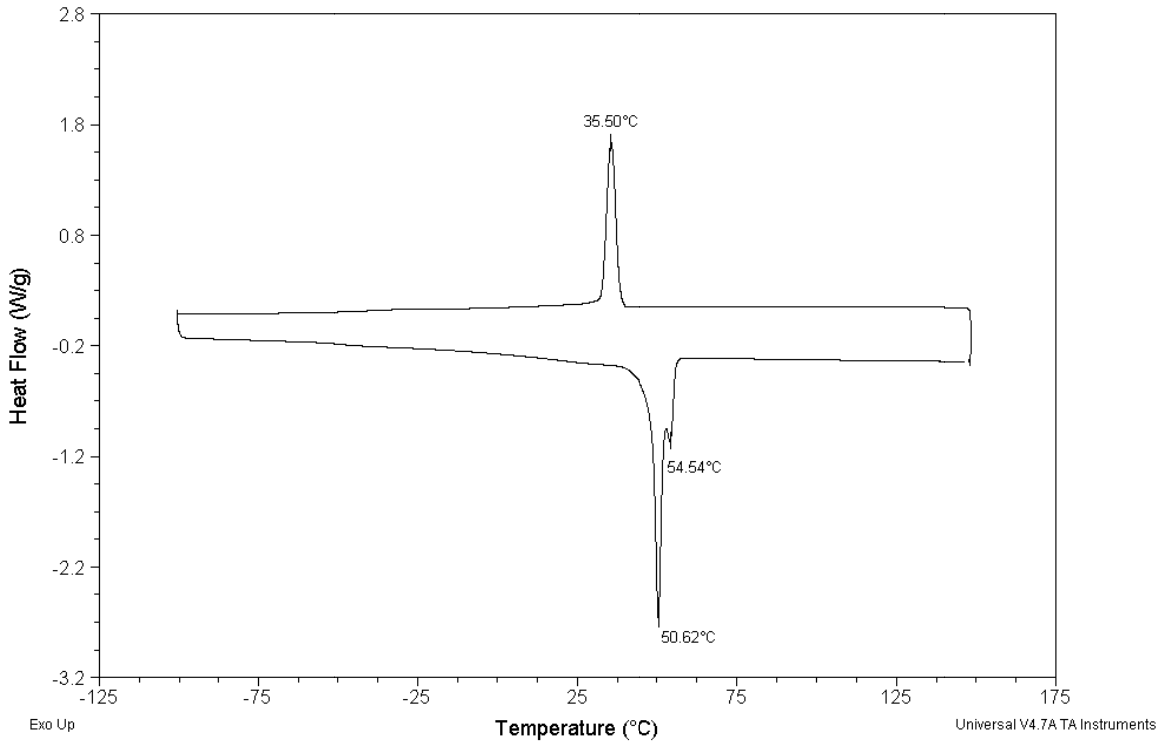

DSC of TPE-1 Prepolymer

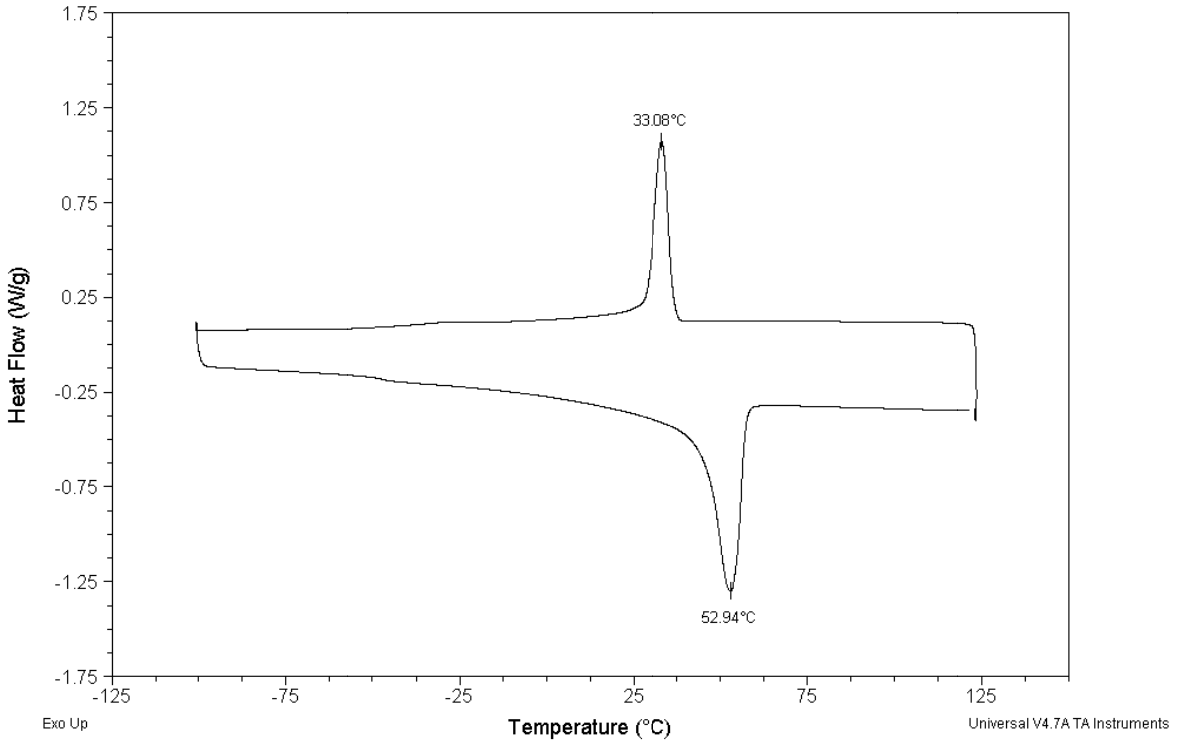

DSC of TPE-1 Film A

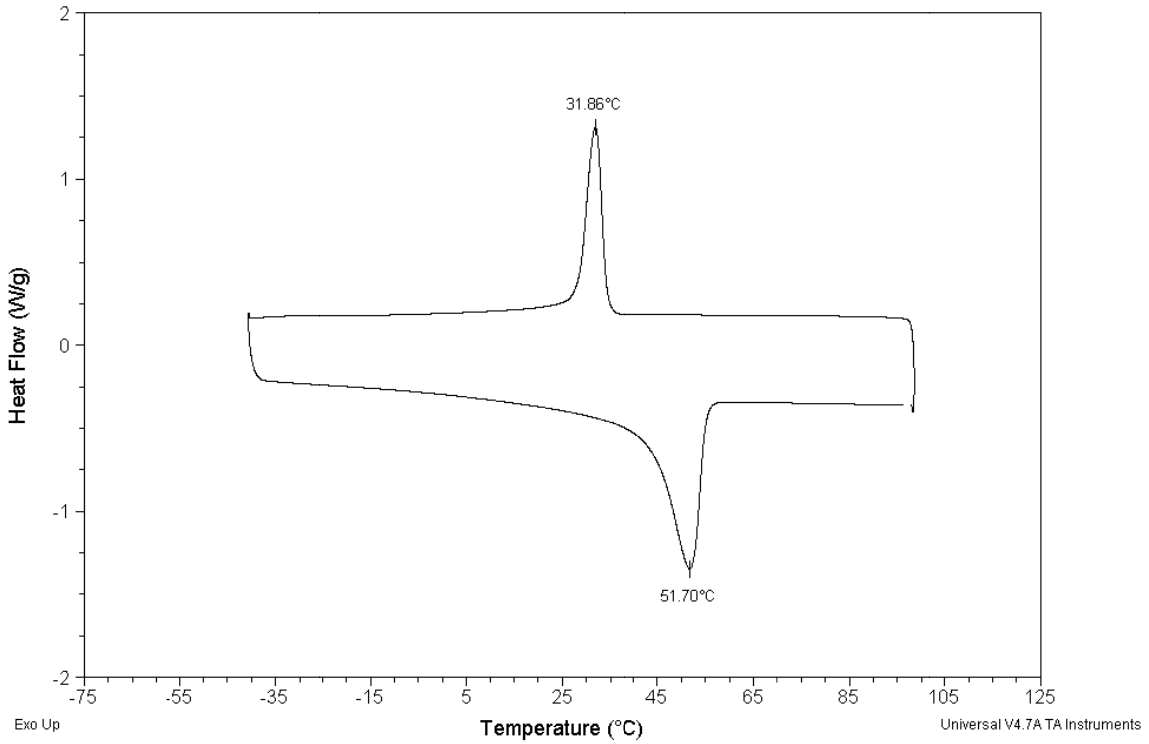

DSC of TPE-1 Film B

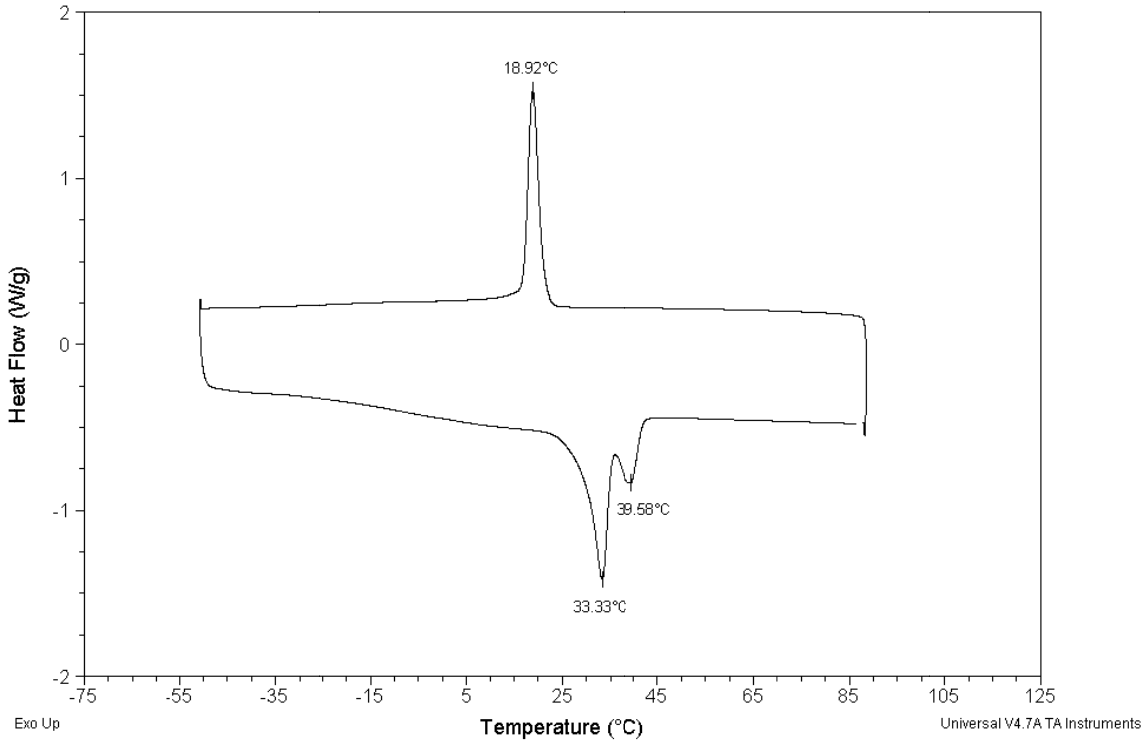

DSC of TPE-2 Prepolymer

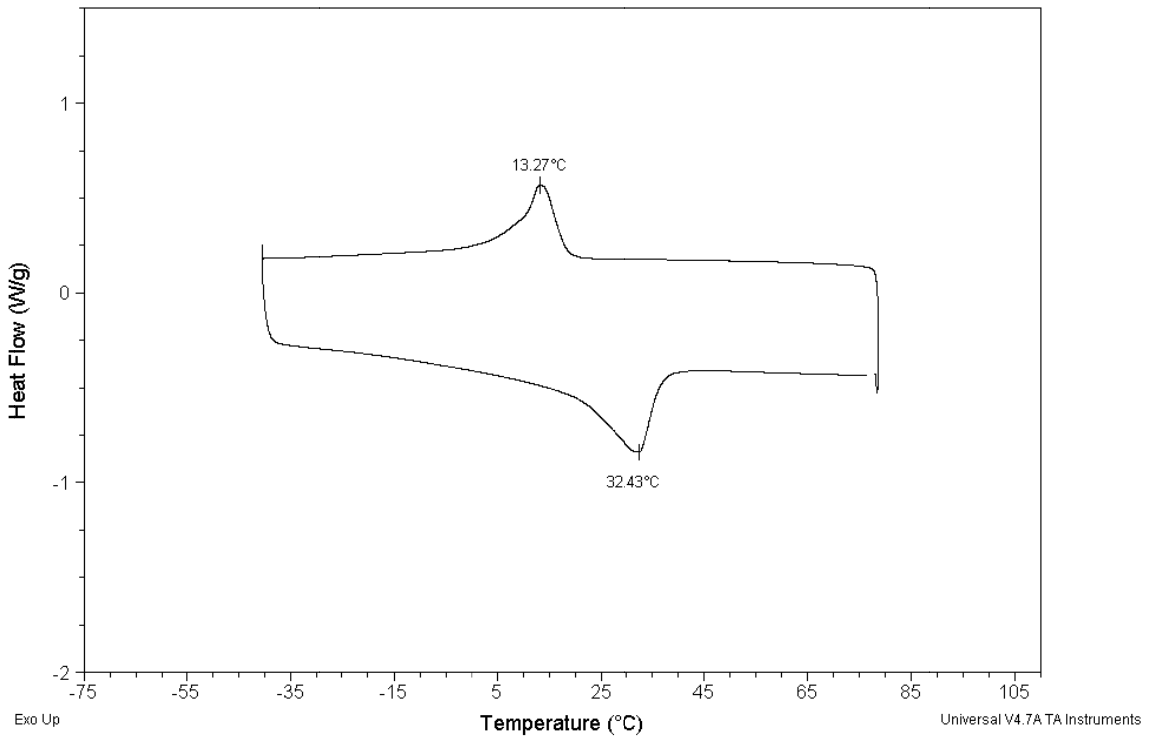

DSC of TPE-2 Film A

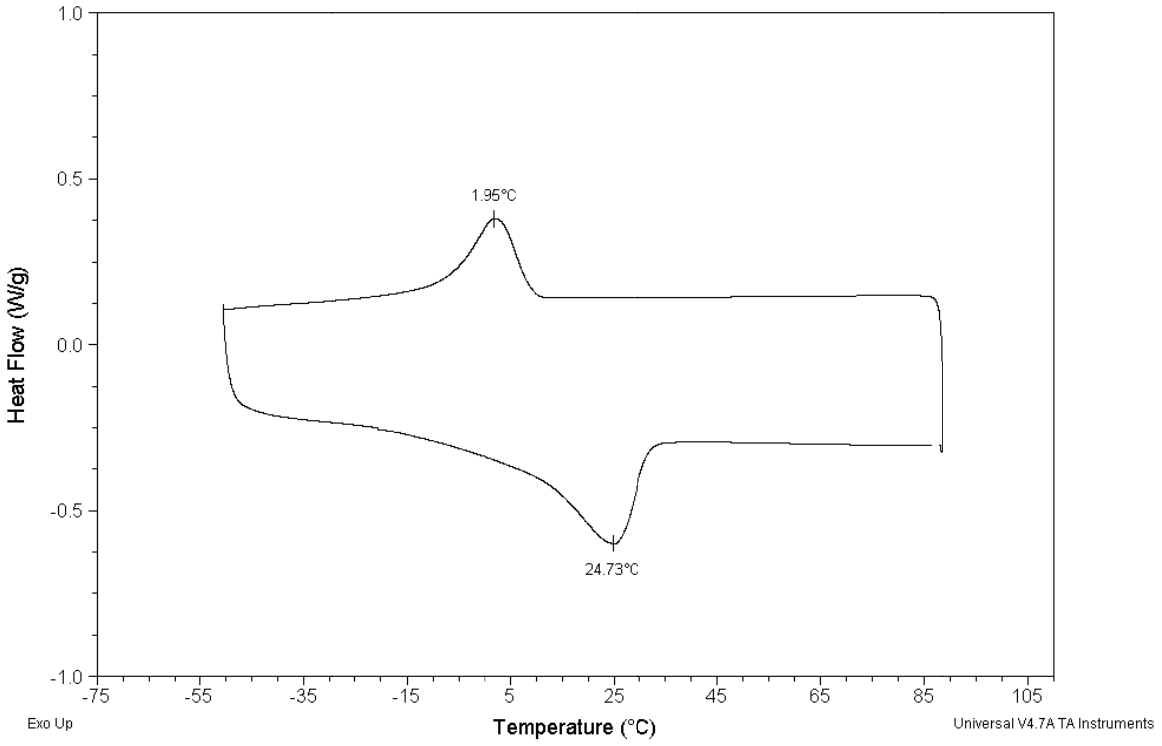

DSC of TPE-2 Film B

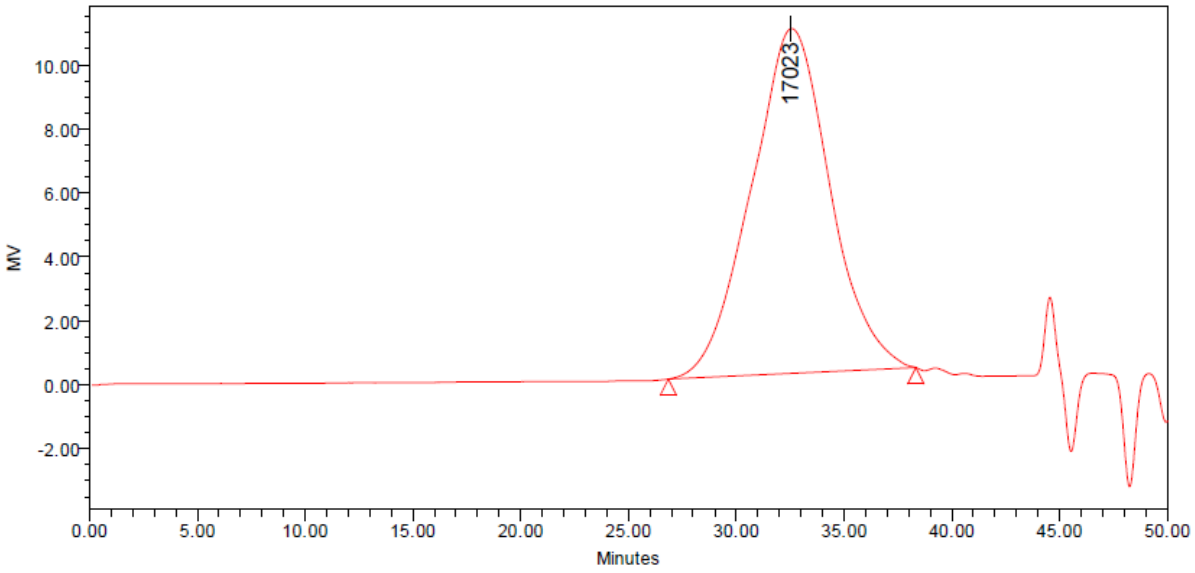

GPC Results

	Dist Name	Mn	Mw	Mv	MP	Mz	Mz+1	Poly dispersity	K	alpha
1		12135	23961		17023	44707	73400	1.974584		

GPC Chromatogram of TPE-1 Prepolymer

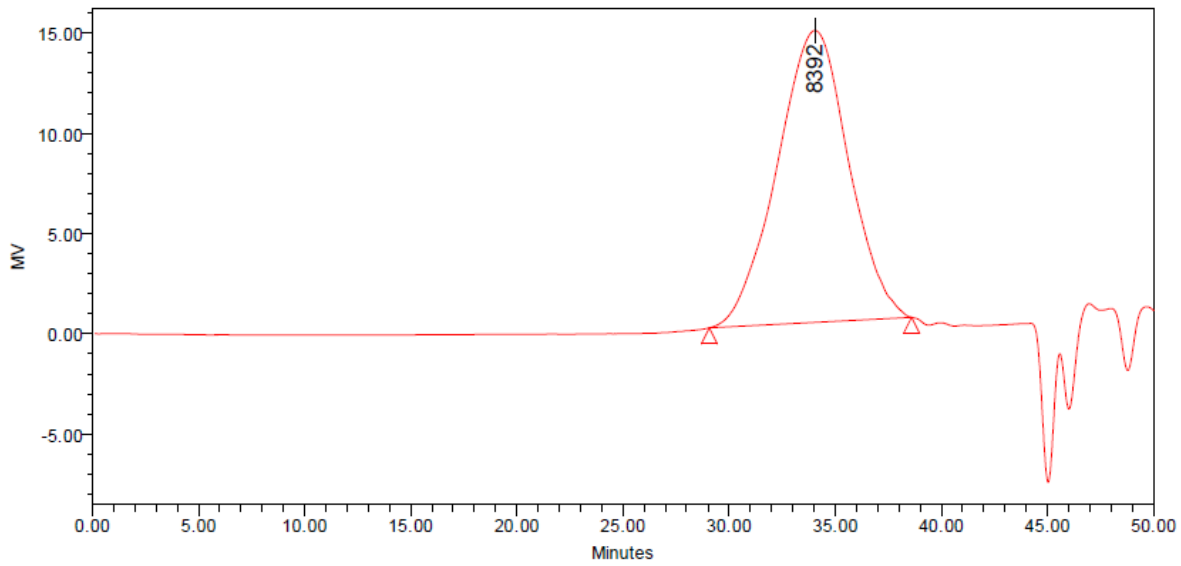

GPC Results

	Dist Name	Mn	Mw	Mv	MP	Mz	Mz+1	Poly dispersity	K	alpha
1		6823	11533		8392	19001	28469	1.690224		

GPC Chromatogram of TPE-2 Prepolymer

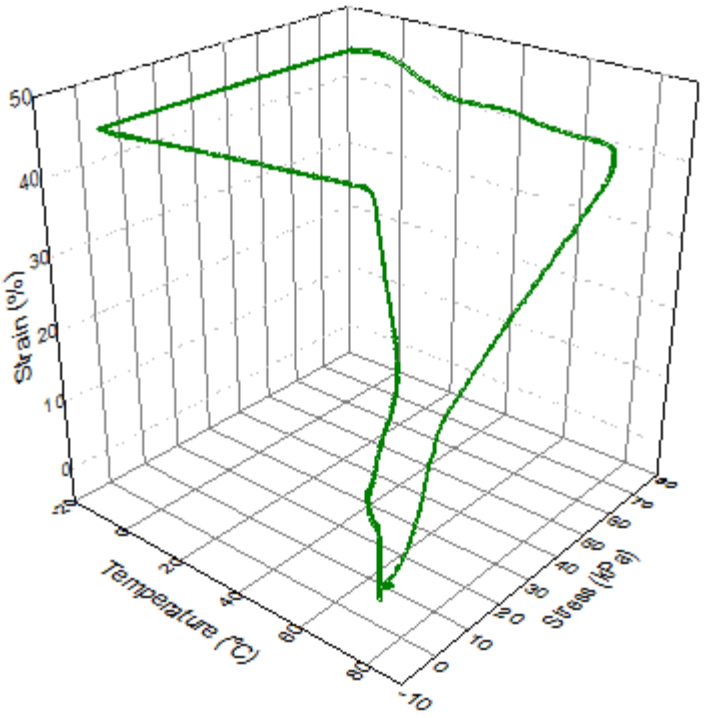

DMA Curve of TPE-1

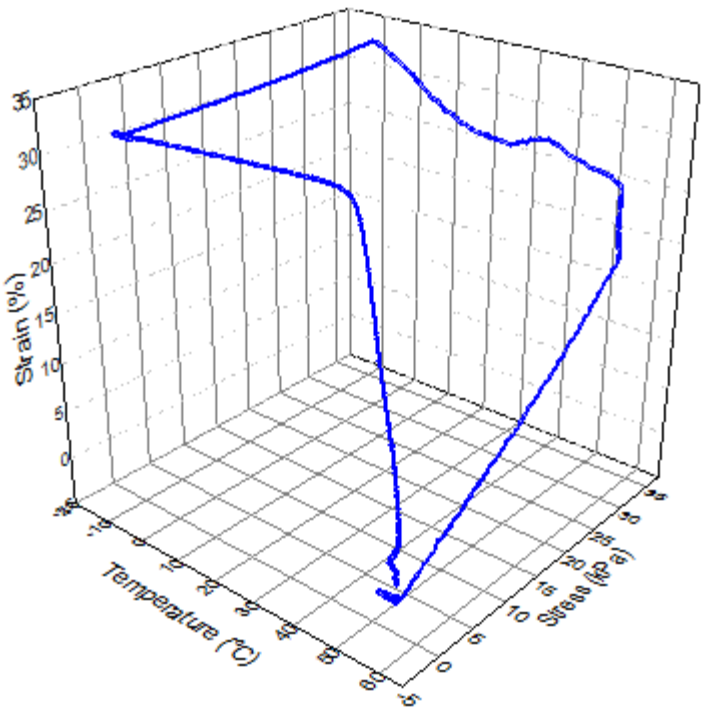

DMA curve of TPE-2, Cycle 1

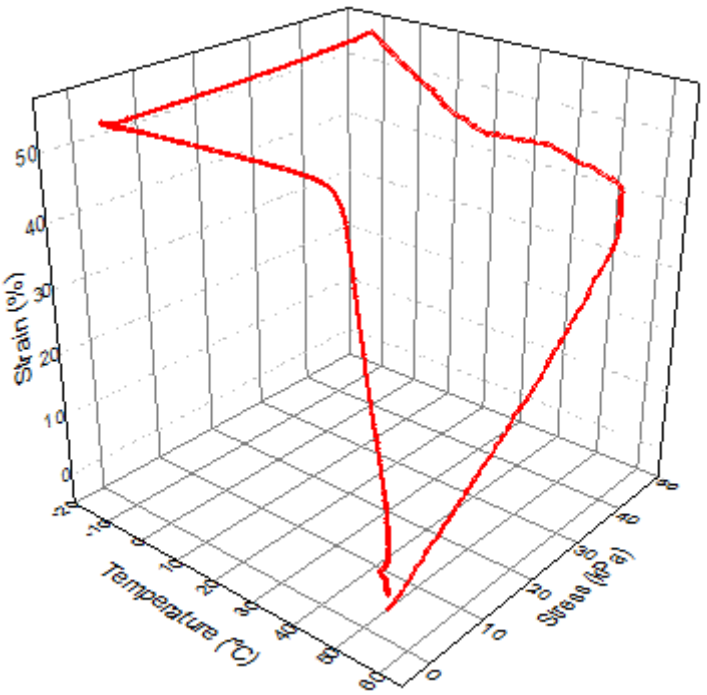

DMA curve of TPE-2, Cycle 2

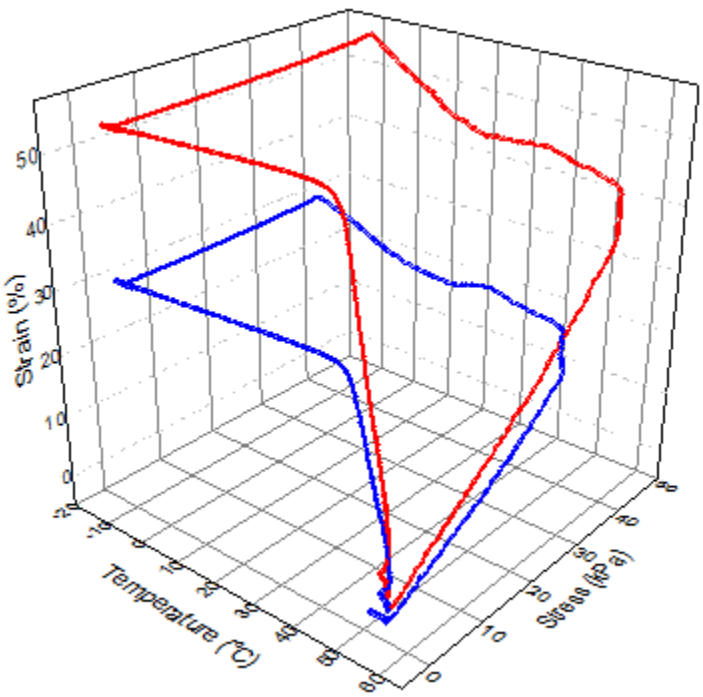

DMA curve of TPE-2, two cycles

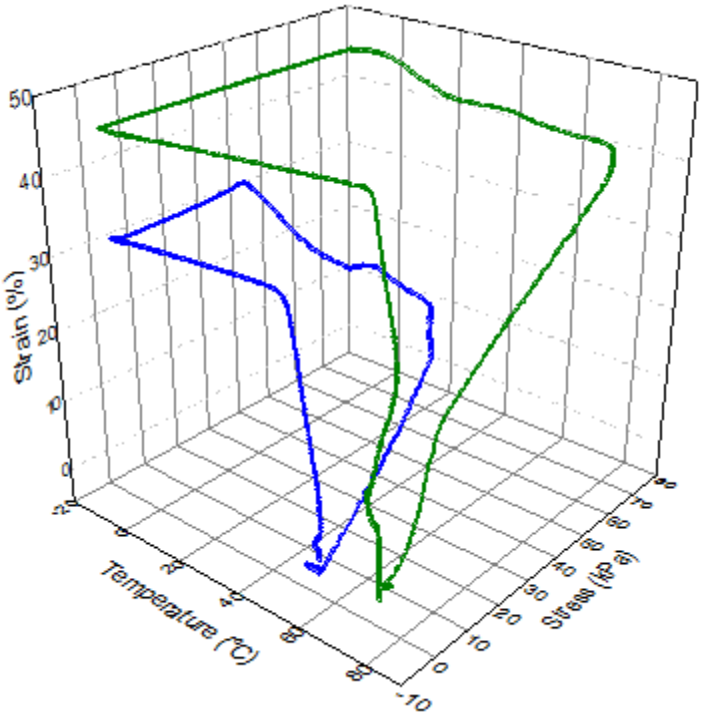

DMA curve of TPE-1 (green) and TPE-2 (blue)

References

1) Laurencin, C.T.; Sobrasua, I.E.M.; Langer, R.S. in *Biomedical Applications of Synthetic Biodegradable Polymers*, CRC Press, Boca Raton, 1995.

2) J.D. Bronzino *The Biodmedical Engineering Handbook*, CRC Press, Boca Raton, 1995.

3) Brosnan, S.; Brown, A.; Luft, J.C.; DeSimone, J.D.; Sheares Ashby, V. *Proc. Natl. Acad. Sci.* 2012*, Submitted 2012-05919*.

4) Hoyle, C.E.; Lee, T.Y.; Roper, T. *J Polym Sci, Part A:Polym Chem* 2004, *42*, 5301.

5) Campos, L.M.; Killops, K.L.; Sakai, R.; Paulusse, J.M.J.; Damiron, D.; Drockenmuller, E.; Messmore, B.W.; Hawker, C.J. *Macromolecules*, 2008, *41*, 7063.

6) Semsarilar, M.; Ladmiral, V.; Perrier, S. *Macromolecules* 2010, *43*, 1438.

7) Overberger, C.G.; Aschkenasy, H. *J Am Chem Soc* 1960, *82*, 4357.

8) Overberger, C.G.; Aschkenasy, H. *J Org Chem* 1960, *25*, 1648.

9) Seabra, A.B.; Silva, R.; Oliveira, M.G. *Biomacromolecules* 2005, *6*, 2521.

10) Kato, M.; Toshima, K.; Matsumura, S. *Biomacromolecules* 2009, *10*, 366.

11) Yamamoto, K.; Takasu, A. *Macromolecules* 2010, *43*, 8519.